Shelf architecture and submarine landsliding at Gela Basin (Strait of Sicily)

Dissertation zur Erlangung des Doktorgrades der Naturwissenschaften

Dr. rer. nat.

am Fachbereich Geowissenschaften

der Universität Bremen

vorgelegt von

Jannis Kuhlmann

Bremen, Juni 2014

Tag des öffentlichen Kolloquiums / day of public colloquium

10.10.2014

15:30 Uhr, Geo-Hörsaal 1550

Gutachter der Dissertation / thesis reviewer

Prof. Dr. Katrin Huhn

MARUM – Center for Marine Environmental Sciences

Universität Bremen

Bremen, Germany

Dr. Fabio Trincardi

Istituto di Scienze Marine (ISMAR-CNR)

Venezia, Italy

Weitere Mitglieder des Prüfungsausschusses / further committee members

Prof. Dr. Dierk Hebbeln

Prof. Dr. Tobias Mörz

Dr. Alice Lefebvre

Lennart Siemann

Erklärung

Hiermit versichere ich, dass ich

1. die Arbeit ohne unerlaubte fremde Hilfe angefertigt habe

2. keine anderen als die von mir angegebenen Quellen und Hilfsmittel benutzt habe und

3. die den benutzten Werken wörtlich oder inhaltlich entnommenen Stellen als solche kenntlich gemacht habe.

Bremen, den 30.06.2014

_____

(Jannis Kuhlmann)

Preface

This cumulative Ph.D. thesis is the outcome of a research project funded by DFG through the MARUM *Incentive Funds* scheme and compiles studies carried out from July 2011 until June 2014 at MARUM (Center for Marine Environmental Sciences) and the Faculty of Geosciences at the University of Bremen. It summarizes three years of effort in acquiring, analysing and interpreting a wealth of data in order to contribute to our understanding of submarine landslide processes, their pre-conditioning factors and trigger mechanisms. Within this framework, I participated in a variety of national and international conferences (DGG 2012, ISSMMTC 2014, EGU 2014) as well as workshops (ECORD Summer School 2012, Bremen PhD days 2012/2013) and GLOMAR-organised in-house research courses. I was further given the chance to extend my scientific knowledge base during a two-month research stay at the Istituto di Geoscienze e Georisorse (CNR-UOS di Padova), for which I am very grateful.

In the following chapters and sections, nomenclature is kept consistent and the term ‘landslide’ is referred to as a generic expression encompassing all forms of slope failure, irrespective of process. Other terms used imply a particular process as introduced in the respective section. Similarly, the resulting deposits of such processes are termed ‘mass transport deposits’.

Chapter 1 outlines the motivation behind the investigation of submarine landslides in general and this thesis in particular. It introduces the type of processes involved in landsliding, their distribution and connection to specific environments as well as the state-of-the-art with regard to causing factors, and draws the connection to socio-economic impacts. The chapter is completed by a literature review on cyclic deposition and undulated sediment features at Quaternary continental margins and their relevance within the framework of slope instability. **Chapter 2** shortly recaps the existing problems and delineates the many open questions in this research field, which funnel in the definition of main research questions that outline the objectives of this thesis. Subsequently, **chapter 3** provides an overview of the own research that emerged from these objectives and summarizes the methodological approach and major outcomes of each manuscript. **Chapter 4** encompasses the regional context to this thesis and introduces to the geological, seismic and oceanographic setting in the Strait of Sicily in general and the study site at Gela Basin in particular. Equally, it reports on previous topic-related studies and summarizes their findings. **Chapter 5** documents the various applied methods and provides information with regard to the processing and interpretation of acquired datasets. The four manuscripts embracing the core of this thesis are then presented in **chapters 6-9**, before their results are compiled and discussed in **chapter 10**, wich equally serves to outline open problems and prospective future studies.

Content

Abstract

The investigation of processes and mechanisms involved in the destabilisation of submarine slopes is a subject of intense research, mainly owing to the inherent hazardous consequences associated with landslide activities. Favoured by a wide range of extensive studies involving both industry and academia, our knowledge on preconditioning factors and trigger mechanisms has vastly improved over the last decades. Still, key parameters controlling sediment instabilities are largely dependent on a multitude of environmental parameters and have to be assessed individually for each case study. In this context, it is not only important to answer questions about the spatial distribution of submarine landsliding, but as well about their temporal evolution and response to changes in environmental conditions – a task that is indispensable not only for the understanding of sedimentary processes but also for landslide-related risk assessment.

This thesis aims to address this gap by studying frequent failure on a shallow-shelf setting at Gela Basin on the southern continental shelf of Sicily. In summary, it integrates high-resolution acoustic datasets with a wealth of data retrieved from drilled core material in order to address (1) the role of climatic fluctuations in shaping the sedimentary architecture and associated depositional processes, (2) the timing and recurrence of landslide events, especially with regard to the governing environmental conditions, and (3) the mechanisms of failure including the evaluation of predisposing factors and trigger mechanisms.

In a first step, an integrated chronological framework for two shelf- and one slope-borehole was developed that heavily relies on foraminifera-based eco-biostratigraphy, oxygen isotope stratigraphy, tephrochronology, and radiometric datings. It provided quasi-continuous age control on the Last Glacial-Interglacial depositional cycle and was used to calibrate shelf sedimentary units, thus reinforcing sequence-stratigraphic interpretations. Successively, sedimentary records in the study area could be shown to adhere to Milankovitch-type cyclicity and to respond not only to Glacial-Interglacial depositional cycles (100-ka), but as well to higher-frequency and ultra-high-frequency (sub-Milankovitch) climatic fluctuations punctuating this cycle. Unlike many other margins, the bulk of sedimentation was shown to relate to highstand deposits during MIS 5 Interstadials. Rapid sediment accumulation during this overall arid time was likely favoured by two mechanisms: (1) drowning of the Mediterranean shelves and intensified activity of Levantine Intermediate Water (LIW); and (2) hyperpycnal river plumes generated by extreme precipitation events. The latter mechanism was equally considered to explain paleo-undulations in this area, as a detailed assessment precluded a genetic origin from slope deforming processes.

The chronostratigraphic interpretation of the shelf sediments formed the basis for subsequent analysis of the processes and mechanics involved in failure as well as the dating of emplaced mass transport

deposits. A total of eight failure events could be discerned from the acoustic record. Accurate age control of these deposits was either achieved through direct radiocarbon dating (in three cases) or indirect dating relying on isotope stratigraphy and micropaleontological considerations. The oldest landslide, a buried basin-wide failure event called *Father Slide* deposited at 87 ka and is interpreted as a debris avalanche. Successively, other deposits were emplaced in form of disintegrative mudflows, with ages of 59 ka, 40-45 ka, 30 ka, 24 ka and 8.5 ka. Further sliding, though more localized and smaller-scaled is related to a highstand interval at 70-87 ka. However, the majority of the recognised mudflows could be related to the falling limb of the sea level curve or sea level lowstand. The most recent landslides, the coeval *Twin Slides* were shown to relate to 2 distinct failure stages, a debris avalanche and a successive slump/slide. All other events involve the translational movement along discrete glide planes that mainly relate to sequence-stratigraphic boundaries associated to sea level fluctuations. In case of the 8.5 ka mudflow, the glide plane was recovered by a drilled core and microscopic thin section analysis revealed, next to discrete shear bands, the presence of volcanoclastic material.

In terms of predisposing factors and trigger mechanisms, it is hypothesized that the most important factor adding to slope instability in the study area is related to the rapid loading of the continental shelf and successive generation of excess pore water pressure. This is strongly supported by the presence of bottom currents locally emplacing rapidly accumulating contourites and overall high sedimentation rates, especially during the highstand units of the MIS 5. To account for the frequent failure of the slope in the study area, seismic activity is proposed as a recurrent trigger event. Though the historical record shows a low affinity to eartquakes it could be shown from a geotechnical slope stability analysis, that moderate earthquakes with a magnitude of M = 4.0 – 4.8 in the direct vicinity of the study area (<10 km) are sufficient to provoke slope failure at the current state of observation.

Overall, the results imply that frequent failure on the continental slope of Gela Basin is related to a complex interaction of individual predisposing factors, but mainly involves (1) high sedimentation rates and generation of excess pore water pressure, (2) presence of sub-horizontal weak layers related to volcanoclastic material and paleoclimatic fluctuations, (3) recurrent seismic activity.

1 Introduction and objectives

1.1 Motivation

Serving as one of the main agents in the (re-)distribution of sediments along the continental margins of the world (Masson et al., 2006), the phenomena of submarine landslides and their inherent consequences impact a wide range of environments such as open slopes, fjords, active river deltas, volcanic island flanks and canyons (e.g., Hampton et al., 1996; Mulder and Cochonat, 1996). Given their potential to affect seabed structures and coastlines alike, the occurrence of submarine landslides and associated geohazards, e.g. tsunami events (Locat and Mienert, 2003; Cochonat et al., 2007), pose a great challenge to society in terms of possible loss of lives, environmental damage and economic impact (Camerlenghi et al., 2007). A striking example for the potentially disastrous consequences of landslide-generated geohazards is the 1998 tsunami on the northern coast of Papua New Guinea, which destroyed a large number of villages and caused ~2200 casualties (e.g., Tappin et al., 2001, 2008; Synolakis et al., 2002). In the wake of ever increasing population densities along the coastlines and associated offshore industrial and economic activities, a thorough understanding of the processes affecting slope stability (both evolution and triggering) is hence of particular socio-economic importance (e.g., Locat and Lee, 2002; Masson et al., 2006).

In this context, the Mediterranean basin is of great interest to the scientific community, mainly owing to the following aspects: (1) its strong vulnerability to marine geohazards, which is ultimately linked to the density of coastal population as well as its small dimensions and associated close proximity between tsunami sources and impact areas; and (2) its function as a miniature ocean encompassing a broad diversity in tectonic and sedimentary environments (Camerlenghi et al., 2010). Given that mass-transport deposits occupy an estimated 18% of its seafloor (Urgeles and Camerlenghi, 2013), the Mediterranean Sea thus represents a type area for the investigation of failure processes and trigger mechanisms.

During the last decades, the popularization of ultra-high resolution acquisition techniques gave rise to the widespread availability of seafloor and sub-seafloor imagery of unprecedented quality. As a result, an increasing number of case studies and international campaigns have mapped and monitored slope failures in the Mediterranean Sea and elsewhere in order to unravel the processes and conditions at the base of these features (e.g., STRATAFORM – Nittrouer, 1999; COSTA – Canals et al., 2004, and references therein). Intensively investigated study sites include, e.g., the Storegga Slide off the Norwegian coast in the NW-Atlantic, where a mega-size slide of ~3000 km³ volume extends over several hundreds of km (e.g., Haflidason et al., 2003, 2004; Sultan et al., 2003; Bryn et al., 2003, 2005; Solheim et al., 2005a, b), or the 1929 Grand Banks event off the coast of Newfoundland in the

NE-Atlantic, where a turbidity current with velocities of up to 30 m/s progressively broke several submarine cables (Heezen and Ewing, 1952; Piper et al., 1999; Fine et al., 2005). At these specific sites, several types and combinations of both pre-conditioning factors and trigger mechanisms have been suggested to provoke landsliding (see references above). However, in several cases the particular factors leading to the emplacement of mass transport deposits (MTDs) are still poorly understood (e.g., Camerlenghi et al., 2007; Cochonat et al., 2007). Instead, speculations about the role of individual processes in the destabilization of submarine sediments are favoured by a broad spectrum of recognized pre-conditioning factors (e.g., weak layers) and trigger mechanisms (e.g., seismic activity) (Masson et al., 2006; Lee et al., 2007). Hence, great uncertainty persists as to why a given slope fails whereas another adjacent remains stable. In this context, small-scaled landslide events such as those found along the southern Sicilian continental margin are of particular interest, as they allow for a full data coverage of the sediment complexes involved in failure. Complemented by coring of both MTDs and their source deposits, this enables the investigation of physical and kinematic processes during failure as well as testing a wide range of trigger hypotheses such as external tectonic triggers or climatically modulated ones (section 1.2).

At the same time, the evolution of slope instability is closely coupled to pre-conditioning factors resulting from changes in the governing depositional conditions. Cyclic climate fluctuations and related sea-level changes strongly impact the sedimentary architecture of continental margins (section 1.3), as they influence both sediment supply and distribution, e.g. through modification of current strengths and pathways. These fluctuations may manifest in distinct sedimentary features such as contourite drifts or sediment undulations (section 1.4) and can play a significant role in the destabilization of slopes (e.g., Laberg and Camerlenghi, 2008; Cattaneo et al., 2004). Additionally, rapid changes in sea level and concomitant landward and seaward shifts in sediment supply favour the development of weak layers that may act as preferential slip planes (section 1.2). In the framework of slope failure investigations it is hence of vital importance to ascertain the paleo-environmental conditions controlling the depositional architecture of the slope, a task that is often not adequately accounted for.

Owing to the above-mentioned shortcomings and difficulties in submarine landslide research, the overarching aim of this thesis is to contribute to the understanding of how submarine landslides are related to pre-conditioning factors and trigger mechanisms on a shallow-shelf continental margin dominated by frequent, but small-scaled failure (Minisini et al., 2007; Minisini and Trincardi, 2009). A wealth of both acoustic and core data from NE Gela Basin offshore southern Sicily (chapter 4) were analysed in a multi-methodological approach (chapter 5) in order to:

- unravel the shelf sedimental architecture as shaped by fluctuations in paleo-environmental conditions and sea-level changes (chapter 6)
- reconstruct the temporal evolution of landsliding and assess the nature of stratigraphic surfaces acting as weak layers (chapter 7, 8)
- evaluate the role of pre-conditioning factors and trigger mechanisms, their interplay and environmental conditions that favour landslide intiation (chapter 8, 9)

1.2 Submarine landslides

1.2.1 Types and distribution

Along the continental margins of the world, sediments from fluvial and coastal input form thick (temporary) depocenters on the shelf and shallow slopes, thus creating the ocean's largest repository for sediment masses (Kennett, 1982). However, before reaching their final burial sites these sediments undergo several cycles of transport and re-deposition through a variety of powerful agents, as illustrated in the schematic diagram presented in *Figure 1.1* (e.g., Stow and Mayall, 2000; Masson et al., 2006). Originating from rivers or erosional activities of waves, storms as well as oceanic currents, suspended sediment may be transported through surface and bottom currents across the shelf, where particles eventually settle. A more instantaneous factor in the redistribution of sediments to open waters is provided by submarine landslides and associated gravity-driven downslope transport of great volumes of material (*Figure 1.1*). In order to assemble the complex phenomena related to these mass transports into a simplified framework of their geomorphological and geotechnical characteristics, several classification schemes have been proposed by a variety of authors (e.g., Varnes, 1958, 1978; Prior, 1984; Norem et al., 1990; Mulder and Cochonat, 1996). Consequently, and mainly owing to the limited information in the submarine environment, the use of landslide terminology in the literature is rather inconsistent and may range from a few end-members only (e.g., Masson et al., 2006) to a complex set of individual processes (e.g., Mulder and Cochonat, 1996; Mulder and Alexander, 2001).

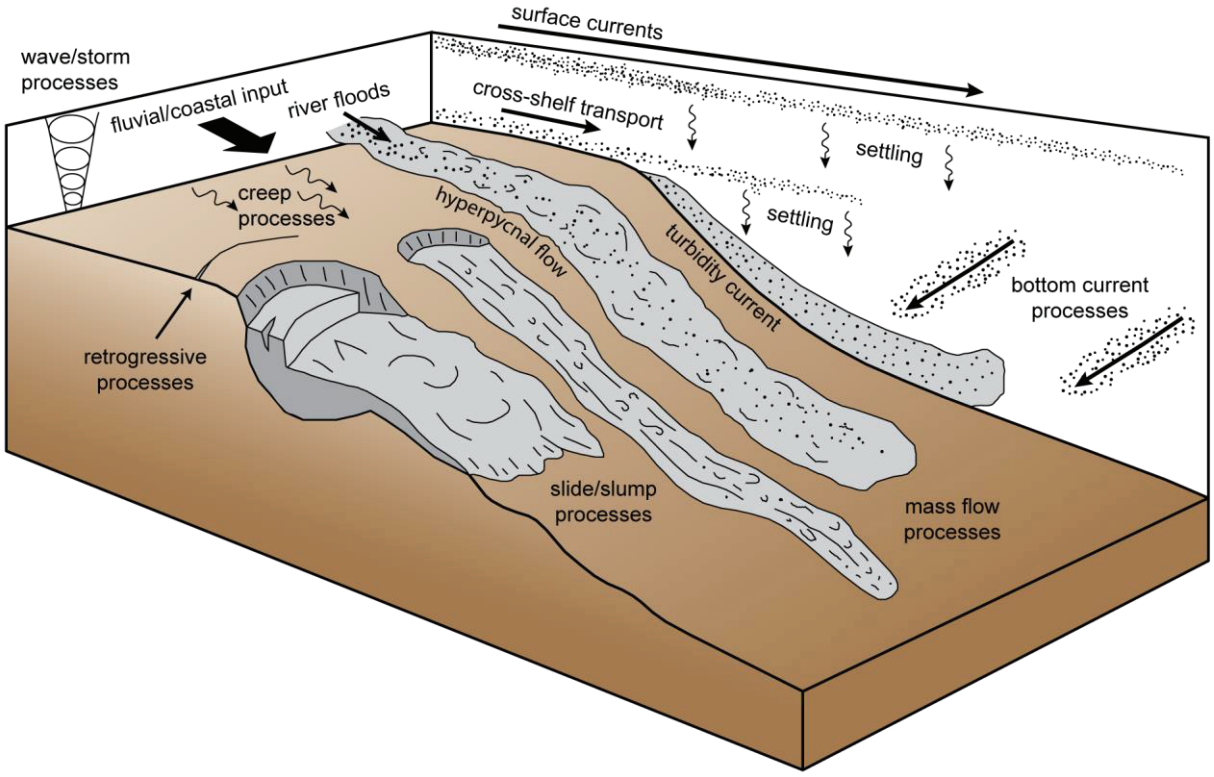

Figure 1.1. Composite diagram of the range of major processes that influence transport and deposition of fine-grained sediments from coastal sources into deep-water environments (modified after Stow and Mayall, 2000).

In this study a modified classification scheme based on Varnes (1958) is used as presented in *Figure 1.2*. Simplified, the landslide may either move as an essentially rigid, internally undeformed mass along discrete slip planes (*slides*) or it may take a form that resembles a viscous fluid comprising considerable internal deformation and innumerable invisible or short-lived internal shear surfaces (*mass flows*; Lee et al., 2007). The list below gives an overview about further subcategories (following Hampton et al., 1996; Mulder and Cochonat, 1996; Shanmugam, 2000; Stow and Mayall, 2000; Mulder and Alexander, 2001; Locat and Lee, 2002; Lee et al., 2007):

- *Translational slides* describe a movement along a planar shear surface that is often characterized by mechanical inhomogeneities. At most, affected sediments may display minor internal deformation structures, a slight rotation into the rupture plane and disintegration into smaller blocks. Upslope progression of adjacent failures is termed 'retrogressive'.
- *Rotational slides* or *slumps*, in contrast, involve motion of failed material along a curved (concave upward) shear surface. Backtilted blocks may show significant internal deformation as a result of the rotational character of movement.
- *Debris flows* resemble a type of *mass flow* that is characterized by laminar, cohesive flows of heterogeneous material that may contain larger clasts supported by a fine-grained matrix. Deposited facies typically develop a basal shear zone and comprise inverse grading of clasts in a moderate to high matrix content.
- *Debris avalanches* are rapid flows of cohesionless rock and sediment fragments, in which energy dissipation relates to grain contact.
- *Mudflows* exhibit high concentration of silts and clays (in excess of 50%) and behave as a highly viscous fluid mass capable of supporting large clastic material.
- In *turbidity currents*, a relatively dilute suspension of sediment grains is supported by the upward component of fluid turbulence (i.e., no inherent fluid strength). Formation is often related to the disintegration of debris flows through an increase of water content, but may originate equally from plunging of hyperpycnal river discharge (Piper and Normark, 2009). Various bedforms with a multitude of scales may be produced by turbidity currents (e.g., Mulder and Alexander, 2001, and references therein).

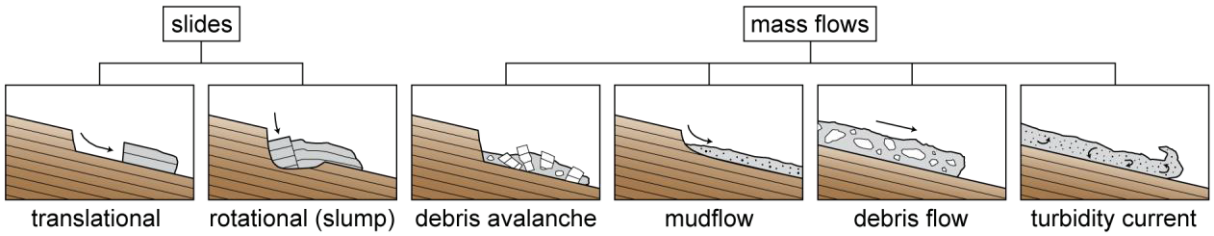

Figure 1.2. General classification of submarine landslides (redrawn after Varnes, 1958). See text for further details about the individual sub-processes.

- An additional mechanism capable of transporting sediments, though at a significantly slower rate, is *creeping* (*Figure 1.1*). It causes long-term elastic deformation resulting from the readjustment of particle contacts after primary consolidation (Muir Wood, 1991) and may indicate potential future sliding.

It is noteworthy that such static classifications as introduced above do not adequately account for changes that may occur to a given landslide during its postfailure evolution, i.e. in the time from motion initiation to final deposition. A generally accepted paradigm states that cohesive landslides may undergo a successive downslope transition from slide to debris flow to turbidity current due to a gradual increase of water entrainment and disintegration (e.g., Norem et al., 1990; Normark and Piper, 1991; Mulder and Cochonat, 1996; Ilstad et al., 2004; Bryn et al., 2005). A famous example for such a disintegrative slide is the 1929 Grand Banks landslide, where a major submarine slide successively transformed into a debris flow that travelled ~80 km before initiating a turbidity current covering a distance of at least another 1000 km (e.g., Piper et al., 1988; Locat et al., 1990). However, the scope of this study lies on landslide events of much smaller scale and shorter runout distances that limit the degree of slide disintegration. For a more holistic slide classification recognizing individual processes of postfailure slide disintegration the reader is hence referred to the corresponding literature (e.g., Mulder and Cochonat, 1996; Mulder and Alexander, 2001).

In terms of distribution of the above introduced landslide types, *slide* processes are predominantly linked to settings dominated by cohesive deposition, while *mass flows* are found more frequently in areas bearing their non-cohesive counterparts (e.g., McAdoo et al., 2000; Shanmugam, 2000; Lee et al., 2007). Similarly, there is widespread evidence over a preference of numerous, but smaller landslide events (i.e., *slides*) along tectonically active margins as opposed to larger *mass flows* of lower recurrence rates along passive margins (e.g., Hampton et al., 1996; Urgeles and Camerlenghi, 2013; *Table 1.1*). Though submarine landslides occur in a variety of environments, their distribution over the world's oceans is not uniform and has been related to a broad range of pre-conditioning factors and trigger mechanisms (section 1.2.2). However, certain geologic environments seem to favour their emplacement, including those featuring rapid deposition of soft sediments, steep slopes and/or high environmental loads. Consequently, five distinct environments are found to be exceptionally vulnerable to frequent landsliding (e.g., Hampton et al., 1996; Masson et al., 2006; Lee et al., 2007):

(1) *Fjords*. Landsliding poses a particular hazard to humans along the steep walls and delta-fronts of these submerged glacially eroded valleys, where thick accumulations of fine-grained sediments resulting from glacier-draining streams seem to favour landslide formation (e.g., Jorstad, 1968; Kulikov et al., 1996; Locat et al., 2003).

(2) At *active river deltas*, landslide initiation is strongly coupled with the rapid accumulation of large quantities of fine-grained sediment on the continental slope (locally exceeding 1 m/yr). Prominent examples include the Mississippi and Amazonas fans (e.g., respectively, Prior and Coleman, 1982; Bea et al., 1983; Piper et al. 1997).

Table 1.1. Compilation of submarine landslides illustrating the range of type, slope angle, age, volume and thickness of deposits on active and passive margins and volcanic island flanks.

Name	Location	Type	Slope angle [°]	Age [ka]	Volume [km³]	Thickness [m]	Reference
			Active margins				
Brunei Slide	NW Borneo Trough	*slide*	2-4	1-7	1200	-	Gee et al. (2007)
CADEB creep	Centr. Adriatic deformation belt	*creep, slide*	0.55	0-5.5	-	up to 20	Canals et al. (2004)
Heceta Slide Coos Basin Slide Blanco Slide	Oregon (W-coast U.S.)	*debris flow*	14-20	110 450 1210	75.6	30-400	Goldfinger et al. (2000); McAdoo et al. (2000)
Insular slope	Puerto Rico	*slide*	8.5		1500	-	Schwab et al. (1993)
Latakia slope	Syrian margin	*slump, slide*	8-12		10	-	Tahchi et al. (2010)
Sur landslide	California (W-coast U.S.)	*slide*	5	0.5-5	30	-	Gutmacher and Normark (1993)
			Passive margins				
Afen Slide	NW Sheltland Islands	*debris flow*	2.5-0.7	5.8	1000	20	Wilson et al. (2004)
Amazon fan	NE Brazil	*slump, debris flow, trubidite*	<1	14-45	2000	50-100	Piper et al. (1997); Maslin et al. (1998)
Bed 5	NW-Africa	*slide, turbidite*	<0.1	60	162	-	Wynn et al. (2010)
Big ‘95	E-coast Spain	*debris flow*	<2	11.5	26	35	Casas et al. (2002); Canals et al. (2004); Lastras et al. (2002)
Cape Fear slide	North Carolina (E-coast U.S.)	*slide, debris flow*	3	16.8	1700	-	Popenoe et al. (1993); Lee (2009)
Hinlopen/ Yermak slide	NW Norway	*debris flow, turbidite*	0.8-3.5	18-30	1350	-	Vanneste et al. (2006); Winkelmann et al. (2008)
Storegga	NW Norway	*debris flow, turbidite*	0.5-2	6-50	2400-3200	up to 430	Haflidason et al. (2004); Bryn et al. (2005)
			Volcanic island flanks				
El Golfo avalanche	Canary Islands (Spain)	*debris avalanche*	-	1-10	150-180	up to 200	Masson (1996)
Nuuanu slide	Hawaii (U.S.)	*debris avalanche*	-	-	5000	up to 2000	Moore et al. (1989)

(3) Particularly voluminous *submarine canyon-fan systems* around the world proof their importance as a major transport agent deep into the ocean and are frequently fed by landslide processes initiating from storms or earthquakes (e.g., Malouta et al., 1981; McAdoo et al., 2000).

(4) At *volcanic island flanks*, initiation of landslides is presumably related to the strong relief (locally up to 15°), loading due to volcanic processes and dyke intrusion (e.g., Moore et al., 1989; Masson et al., 2002). The giant masses involved in individual flank collapses (see *Table 1.1*) pose tsunami threats on trans-oceanic scales (Ward and Day, 2001), which are hypothesized to potentially match the magnitude of the 2004 Indian Ocean tsunami (Lay et al., 2005).

(5) Roughly half of the number of globally detected landslides relates to the various settings of *open continental margins* (e.g., Canals et al., 2004; Lee et al., 2007). This includes glaciated margins, such as the Storegga Slide on the Norwegian margin (e.g., Haflidason et al., 2004; Bryn et al., 2005), non-glaciated ones, such as the Bed 5 event on the NW African margin (e.g., Wynn et al., 2000), passive ones, such as the Cape Fear slide at the eastern U.S. continental margin (Lee, 2009) as well as active ones, such as the North Agean Trough slide on the eastern Mediterranean margin (Lykousis et al., 2002).

While the mechanisms that lead to landsliding are well understood for most of the above mentioned environments and are dictated by their specific setting (e.g. the steep slopes of *fjords* and *volcanic islands*), the situation at *open continental margins* is somehow more intriguing. As Hampton et al. (1996) pointed out, the "controls on most identified slides are obscure", despite the replete literature on this topic. With this in mind, it becomes very important to delineate the importance of individual landslide-generating factors (section 1.2.2) in dependence to specific environmental settings.

1.2.2 Pre-conditioning factors and trigger mechanisms

In general terms, slope failure occurs when the downslope forces that act on seafloor and subsurface material (shear stress) exceed the forces acting to resist its deformation (shear strength; e.g., Hampton et al., 1996; Lee et al., 2007). The shear strength (T_f) of sediment can be expressed by the Mohr-Coulomb relation (Coulomb, 1773) and is a function of its cohesion (c), the amount of internal friction (φ) and the total normal stress applied to the failure plane (σ_n):

$$T_f = c + \sigma_n \tan \varphi \qquad (1)$$

Terzaghi (1943) introduced the principle of the effective stress (σ_{eff}) that accounts for the effect of pore fluid pressure (u) to:

$$\sigma_{eff} = \sigma_n - u \qquad (2)$$

Application to equation (1) results in the modified Mohr-Coulomb failure criterion for saturated sediments:

$$T_f = c + (\sigma_n - u)\tan\varphi = c + \sigma_{eff}\tan\varphi \qquad (3)$$

If loading of the observed slope is restricted to gravitational forces only, the shear stress (T_s) for an infinite surface acting downslope is dependent on the submerged density of the sediment (y), which is defined as the difference of sediment and sea water density, the depth below seafloor (z) and the inclination of the slope (α) to

$$T_s = yz\sin\alpha \qquad (4)$$

According to Morgenstern and Price (1965), the ratio between these forces can be expressed as the factor of safety (FS) to

$$FS = T_f/T_s, \qquad (5)$$

indicating either sediment stability ($FS > 1$) or instability ($FS \leq 1$).

In most cases, slope inclination is below a critical angle and an additional stimulus is required to initiate failure. Within the last decades, a variety of factors have been proposed that may contribute to slope destabilization by either increasing the environmental loads (T_s), decreasing the strength of the sediment (T_f), or a combination of both (*Figure 1.3*; e.g., Hampton et al., 1996; Sultan et al., 2004; Masson et al., 2006; Lee et al., 2007; Leynoud et al., 2009). These factors can operate on timescales of minutes (e.g., *earthquakes* – Piper et al., 1999; Fine et al., 2005) to hundreds of thousands of years (e.g., *climate change* – Weaver and Kuijpers, 1983) and may be subdivided into trigger mechanisms and pre-conditioning factors (following Masson et al., 2006). The former comprises transient external events (e.g., *earthquakes* or *sea level change*), while the latter are related to internal material characteristics (e.g., presence of a *weak layer* – e.g., Haflidason et al., 2003; Huhn et al., 2006; Kock and Huhn, 2007). In the following, the main characteristics of these factors will be summarized in relation to whether the phenomenon of landsliding is approached geologically or geotechnically.

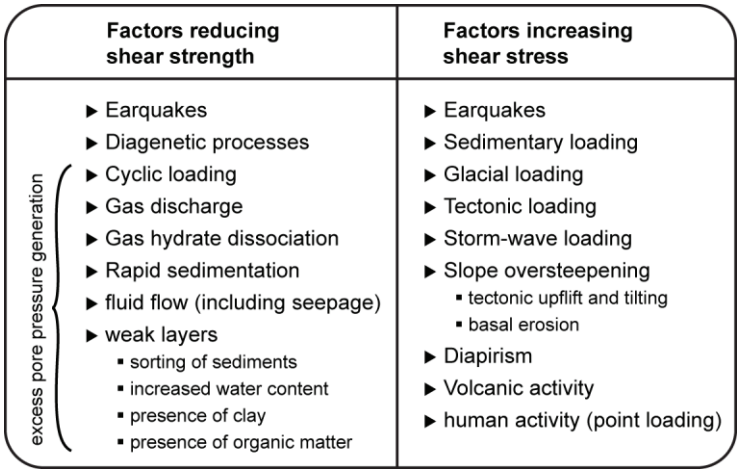

Figure 1.3. Compilation of factors causing submarine landslides (after Hampton et al., 1996; Locat and Lee, 2002; Masson et al., 2006; Lee et al., 2007).

The geological approach recognizes various factors that are capable of decreasing the shear resistance of sediments, such as (1) *excess pore pressure generation* through either *gas charging* (migration or decay of organic matter) and *gas hydrate destabilization* (e.g., Kayen and Lee, 1991; Sultan et al., 2003; Mienert et al., 2005; Behrmann et al., 2006), *rapid sedimentation* (e.g., Prior and Coleman, 1982), *fluid flow* (e.g., Sangrey, 1977; Robb, 1984; Bohannon and Gardner, 2004) or *cyclic loading* (i.e., liquefaction through cyclic earthquake or storm wave activity); (2) *diagenetic processes* such as the alteration of clay (illite to montmorillonit) and opal (opal-A to opa-CT, Laberg and Camerlenghi, 2008); and (3) *under-consolidation* reflecting the rigid behaviour of biogenic particles and/or rapid sedimentation. Geological factors that lead to an increase in applied shear stress include (1) *loading*, including sedimentary, glacial and tectonic overloading as well as seismic and storm-wave loading (e.g., Bea et al., 1983; Van Kessel and Kranenburg, 1998); (2) *slope oversteepening* through tectonic uplift, tilting at accretionary prism fronts or basal erosion on a submarine slope (e.g., Assier-Rzadkiewicz et al., 2000; Greene et al., 2002); (3) *diapirism* (e.g., Martin and Bouma, 1982); and (4) *volcanic activity* (e.g., Moore et al., 1989; Holcomb and Searle, 1991; Normark et al., 1993; Masson et al., 2002).

The geotechnical approach evaluates the failure behaviour of sediments at a given stress state in consideration of their index properties and geotechnical parameters (Laberg and Camerlenghi, 2008). In this context, the shear resistance of sediments is known to inversely correlate with an increase in the (1) *degree of sorting*; (2) *water content*; (3) *clay amount* (in cohesive sediments); (4) *clay type* (the high water content of montmorillonites affects shear strength negatively with respect to illite and kaolinite); and (5) *organic matter* (if comprising >2% of the total sediment volume). However, two of the most important factors influencing the shear strength are the rate of stress application and the stress history of the sediment. Rapid loading can significantly reduce shear resistance by a decrease of effective stresses within the sediment, while over-consolidated sediments (e.g., below an erosional unconformity) show higher shear strength with regard to normally consolidated ones (e.g., Hampton et al., 1996; Lee et al., 2007).

The broad range of both geological and geotechnical factors demonstrate the difficulty in relating slope failure to one single cause (Laberg and Camerlenghi, 2008) and many if not all landslides involve a combination of the above-mentioned pre-conditioning factors and trigger mechanisms (*Table 1.2*). In the case of the Storegga slide off the Norwegian coast for example, weak layers comprise water- and clay-rich sediments, which in turn relate to current-derived contourites. Overlying sediments originate from rapid loading during glacial periods, thus inducing excess pore pressure within the weak clayey layers. However, an additional earthquake was required to trigger a giant landslide with a runout disctance of about 810 km and an assumed volume of 2400 to 3200 km³ (Haflidason et al., 2004; Bryn et al., 2005; Kvalstad et al., 2005).

Aside these naturally generated factors, *human activities* may also contribute to slope destabilization. One of the more prominent examples is the 1979 Nice Airport landslide in France, which caused several casualties and excerted consideral damage to local communities and harbours. Loading of the upper slope during construction works at the airport have been proposed as a potential

causing factor here, along with the presence of sensitive weak clays ('quick clays') and heavy rainfall (Sultan et al., 2004; Dan et al., 2007).

It is clear from the examples above that each particular site of submarine landslide investigation provides a unique combination of environmental processes and conditions, which may additionally show complex interactions between each other. Consequently, the broad range of these factors often leads to speculations about relative importances of pre-conditioning factors and trigger mechanisms and remains a major topic of ongoing research (e.g., Lee at al., 2007; Leynaud et al., 2009). In this context, an accurate examination of the deposits associated to landsliding is equally important in order to reconstruct failure evolution and assess the impact of environmental changes (such as sea level variations; e.g., Maslin et al., 2004) on the stability of sediments in a given area (e.g., Canals et al., 2004).

Table 1.2. List of factors contributing to landslide initiation and prominent examples (after Mulder and Cochonat, 1996; Masson et al., 2006; Lee et al., 2007). Note that multiple factors may contribute to a single landslide event.

documented/suggested	Examples	Type	References
Earthquake	Grand Banks (Canada) Alika (Hawaii) Kidnappers (Australia)	turbidity current slump / rock avalanche successive slumps	Hughes Clarke (1990); Fine et al. (2005) Lipman et al. (1988) Barnes et al. (1991)
Hurricanes/cyclic loading	Mississippi delta (U.S.)	silt and mud flows	Prior and Coleman (1978, 1982)
Loading / slope oversteepening	Nice (France) Canary Islands Huanghe river (China)	slide / turbidity current slide / debris flow HF / turbidity current	Assier-Rzadkiewicz et al. (2000) Masson et al. (1998) Milliman and Meade (1983)
Underconsolidation (overpressure)	Mississippi delta (U.S.) Kitimat (Canada)	silt and mud flows retrogressive sand flow	Prior and Coleman (1982) Murty (1979); Prior et al (1984)
embedded weak layers	Storegga (Norway)	slide / debris flow	Haflidason et al. (2003)
Gas hydrate dissociation	Storegga (Norway)	slide / debris flow	Sultan et al. (2003)
Sea-level change	Madeira Abyssal Plain	turbidity current	Weaver and Kuijpers (1983)
Volcanic activity	Nuuanu (Hawaii) El Golfo (Canaries)	debris avalanche debris avalanche	Moore et al. (1989) Masson et al. (2002)

1.2.3 Societal and economic impact

Apart from the many open questions as to why, when and where submarine landslides occur, an important aspect of their investigation relates to their inherent consequences, which may often have devastating societal and economic impacts (e.g., Locat and Mienert, 2003). During the last decades, ever growing population numbers and infrastructures along the coastlines of the world led to a notable increase of damages in these highly susceptible areas due to submarine landslides themselves or related geohazards such as tsunami events (e.g., Locat and Mienert, 2003; Cochonat et al., 2007; Costanza and Farley, 2007).

The wide range of processes inherent to submarine landslides (section 1.2.1) poses significant risks to a variety of offshore installations, such as communication cables, pipelines, wind farms as well as oil and gas exploitation facilities (e.g., Hampton et al., 1996; Locat and Lee, 2002; Sultan et al., 2004;

Masson et al., 2006). For the hydrocarbon industry alone, the costs related to damages from submarine landsliding were approximated by the society for underwater technology (SUT) to about 400 million US dollars per annum (Mosher et al., 2010). These numbers and the prospect of detecting new hydrocarbon reservoirs raises the interest of the industry to identify submarine landslide processes and understand involved mechanisms (e.g., Stow and Mayall, 2000; Leynaud et al., 2009). Major consequences of these interests are the joint multidisciplinary investigations of academia and industry in studying the Storegga slide complex, which brought about new insights on the occurrence and dynamics of submarine landslides on (formerly) glaciated margins (references are given in previous sections).

In terms of landslide-triggered geohazards, tsunami events pose the greatest risk to society. Disastrous examples causing widespread destruction of coastal villages and claiming a great amount of casualties include the 1998 Sissano event in Papua New Guinea as well as, though less catastrophic, the 1945 Makran event in the Arabian Sea and the 1929 Grand Banks event in Canada (e.g., respectively, Tappin et al., 2001; Heidarzadeh et al., 2008; Piper et al., 1999).

An area especially susceptible to submarine landslides and associated geohazards is the Mediterranean Sea, which encompasses a broad spectrum of tectono-sedimentary systems (i.e., active and passive margins as well as volcanic island flanks; Camerlenghi et al., 2010; Urgeles and Camerlenghi, 2013). About 18% of its seafloor is covered by landslide deposits (*Figure 1.4*) and it claims almost 10% of the tsunami recorded worldwide, making the Mediterranean Sea the most geohazardous in Europe (e.g., Tinti et al., 2001; Urgeles and Camerlenghi, 2013). In combination of a densely-populated coastline and a high density of seabed infrastructure, this demonstrates the need for a proper risk estimation related to the societal and economic impacts of submarine landslides.

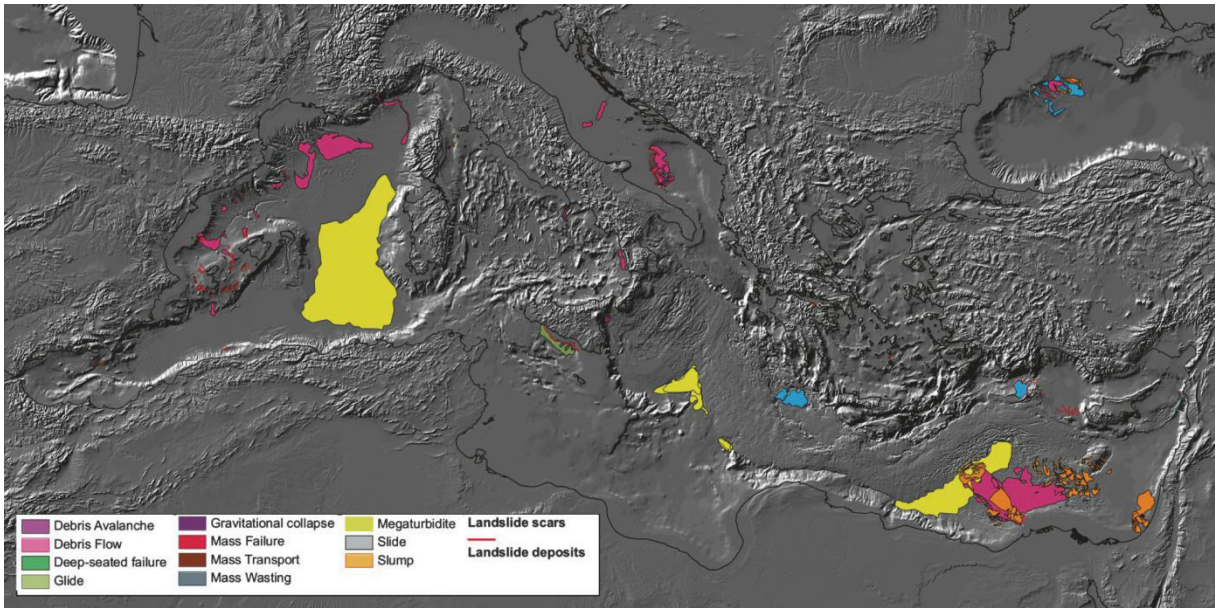

Figure 1.4. Shaded relief map of Mediterranean bathymetric and topographic features showing the locations of submarine mass-movement deposits (MTDs) in the sub-basins of the Mediterranean Sea (modified after Camerlenghi et al., 2010). Note that MTD classification does not follow uniform nomenclature, as it relates to independent manuscripts (see Camerlenghi et al., 2010, and references therein).

According to Locat and Lee (2002), this hazard and risk assessment "is in its infancy" and requires consistent datasets, espially with regard to frequency and extent of events. A first step towards such a database has been taken only recently by Urgeles and Camerlenghi (2013), who compiled a catalogue of submarine landslides and their statistics in the Mediterranean Sea. However, this catalogue is still incomplete, especially with regard to small-scaled slides and robust age dating of landslides.

1.3 High-frequency cyclicity in Quaternary sedimentary records

The sedimentary strata deposited on Quaternary continental margins are impacted by a complex set of processes within the atmosphere, lithosphere and biosphere, which may work over a broad range of time scales. However, the stratigraphic appearance of the strata is predominantly linked to sea-level oscillations of different duration and amplitude that record rapid and abrupt climate changes (*Figure 1.5*; e.g., Shackleton and Opdyke, 1973; Imbrie et al., 1984; Martinson et al., 1987; Raymo, 1997; Lourens, 2004). It is widely accepted that such climatic fluctuations are related to variations in the earth's precession, obliquity and eccentricity (Milankovitch, 1930), as expressed in the modulation of solar radiation with periodicities of ca. 20, 40 and 100 ka, respectively (Schwarzacher, 2000). Since their first detection in the marine geological record (Emiliani, 1955), these Milankovitch cycles have been shown to correspond to sea-level variations as expressed in Marine Isotope Stages and Substages (MIS) of Quaternary $\delta^{18}O$ records (e.g., Hays et al., 1976; Gallup et al., 1994; Lea et al., 2002; Waelbroeck et al., 2002; Lisiecki and Raymo, 2005).

Stratigraphically, Milankovitch cyclicity could be identified in various sedimentary records during the last two decades (Lobo and Ridente, 2014, and reference therein). In particular, the development and preservation of high-frequency depositional sequences appear to be favoured along shallow-shelf settings with high sedimentation rates on subsiding continental margins (Mitchum and Van Wagoner, 1991). Generally, different parts of the Quaternary depositional history are dominated by specific Milankovitch frequencies, though the underlying reasons are still under debate (Lobo and Ridente, 2014). While stratigraphic architecture during the Pliocene and Lower Pleistocene was predominantly paced by 40 ka cyclicity (e.g., Carter et al., 1998; Massari et al., 1999; Kitamura et al., 2000), sea-level and, hence, sediment deposition during the last 800 ka has been strongly controlled by 100 and 20 ka cyclicity (*Figure 1.5*).

Most of the sedimentary sequences on modern continental margins show a dominant influence of 100 ka Glacial-Interglacial cycles, including well-studied Mediterranean areas (e.g., Piper and Aksu, 1992; Chiocci, 2000; Tesson et al., 2000; Rabineau et al., 2005; Ulug et al., 2005; Liquete et al., 2008), the Gulf of Mexico (Sydow and Roberts, 1994) or the Chinese Sea (Hiscott, 2001; Berné et al., 2002). Each sequence comprises an overall progradational and regressive set of internally similar clinoforms and is bounded by shelf-wide unconformities relating to subaerial erosion and transgressive reworking (Lobo and Ridente, 2014). Stratigraphical expression of 20 ka Stadial-Interstadial cycles is more variable and, depending on the environmental setting, may culminate in two major erosional surfaces relating to the sea-level lowstands during MIS 4 and MIS 2 (e.g., Osterberg, 2006) as well as multiple progradational events during MIS 5 (e.g., Somoza et al., 1997; Hernández-Molina et al, 2000;

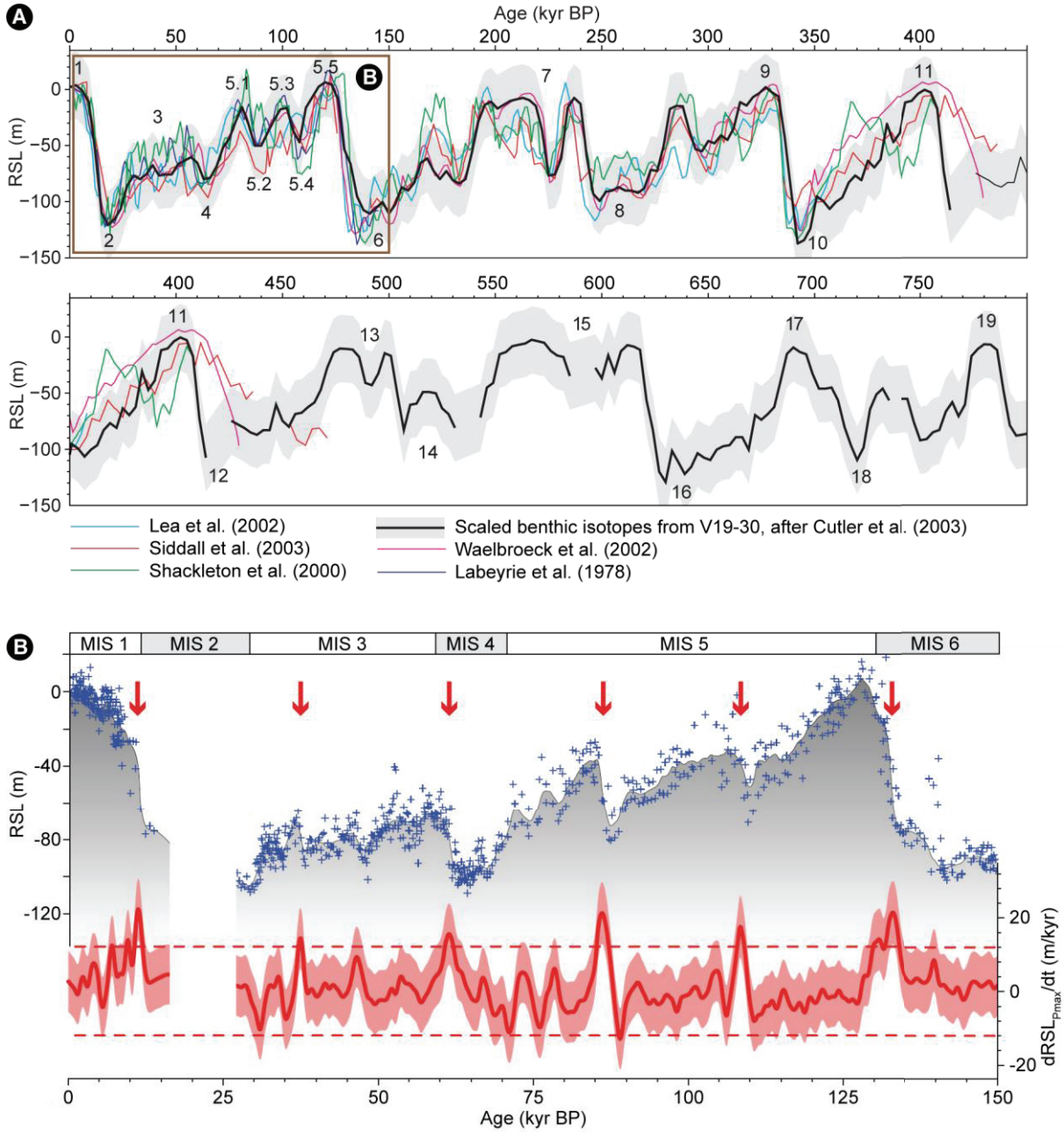

Figure 1.5. Summary of the pattern of sea level change that leads to Milankovitch-type depositional shelf architecture. A: sea level curve of the last 800 ka as obtained from different oxygen isotopic sources. Numbers correlate to Marine Isotope Stages and Substages (modified after Siddall et al., 2007). B: Pattern of sea-level change for the last 150 ka (modified after Grant et al., 2012). Blue crosses mark relative sea-level data, while grey shading indicates the maximum probability of relative sea-level. The red line displays respective rates of sea-level change, while pink shading delimits the corresponding 95% confidence interval. High rates of sea-level change (+/-15 m/ka) associated with rapid changes in sediment supply are identified by a dashed red line and red arrows indicate rapid sea-level rise of more than 15 m/ka. RSL = Relative sea level.

Liu et al., 2010) and/or during MIS 3-2 (e.g. Marsset et al., 1996; Liu et al., 2000). More recently, sub-Milankovitch climate and sea-level fluctuations related to MIS 3 have been documented in the Gulf of Lions (Sierro et al., 2009), where short-lived prograding sequences could be linked to 5-10 ka cycles matching the occurrence of Heinrich events (Bassetti et al., 2008).

The numerous studies reporting on high-frequency (Milankovitch) and ultra-high-frequency (sub-Milankovitch) cyclicity in Quaternary depositional sequences suggest that a general pattern on their preservation in the stratigraphic record cannot be applied. While 100 ka sequences show a certain uniform representation, the expression of 20 ka cyclicity seems to be highly variable and influenced by local variations in the depositional environment (Lobo and Ridente, 2013). However, the identification of bounding surfaces relating to Milankovitch-type sediment units (i.e., surfaces of erosion or condensation) is of great importance in the investigation of submarine landslides, since these indicate sudden changes in both sediment supply and distribution and may act as weak layers (section 1.2.2). This becomes especially important in settings comprising sediment sequences of very homogeneous material, where climatically induced bounding surfaces provide horizons with distinct material properties and thus may indicate preferential planes of sliding.

1.4 Undulated sediment features in shelf-edge settings

Undulated sediment features present a well-known phenomenon along the Holocene mud wedges of the Mediterranean Sea, although they can equally be encountered in both shallow- and deep-water settings worldwide (Urgeles et al., 2011, and references therein). Early studies relying on seismic reflection profiles frequently interpreted these structures as either soft sediment deformation or incipient landsliding, since shear planes appeared to separate individual undulations (e.g., Gallignani, 1982; Aksu and Piper, 1983; Ercilla et al., 1995; Correggiari et al., 2001). However, the subsequent emergence of high resolution acoustic profiling and bathymetric mapping provided increasing evidence against a genesis by sediment deformation processes alone and a variety of sediment transport processes in the bottom boundary layer were proposed instead (e.g., Cattaneo et al., 2004; Urgeles et al., 2007). As summarized by Urgeles et al. (2011), it is now commonly accepted that sediment undulations are invoked by a single one or a mix of the following genetic mechanisms (*Table 1.3*): (1) sediment creep, (2) slope failure, (3) waves and tides, (4) bottom currents, (5) internal waves, and (6) hyperpycnal flows. Though the morphologic and geometric characteristics of observed sediment undulations often appear to rule out a genesis by incipient landsliding alone, their initial formation has been related to sediment deformation processes in some cases. A well-investigated example is represented by the Holocene prodelta clinoforms of the Adriatic Sea, where initial sediment deformation and subsequent growth by differential sediment accumulation patterns were proposed as the main genetic mechanisms (Cattaneo et al., 2004). Additionally, as these features can be associated with localized variations in current strength and/or pathways as well as sediment supply, sediment undulations may indicate areas of potential future landsliding. Hence, an assessment of their genetic mechanism should be taken into account when investigating submarine landslides.

Table 1.3. Characteristics of sediment undulation fields with respect to assigned genetic mechanism (modified after Urgeles et al., 2011).

Genetic mechanism	Shape of sediment wave field	Crest elongation relative to isobaths	Mean L/H	Range of water depth	Other features	Examples
Internal waves	Elongated parallel to shoreline	Parallel	190-230	30-90		Central Adriatic, Llobregat, Ter
Hyperpycnal flows	Elongated perpendicular to shoreline / circular	Parallel	60-170	3-110	Channels	Guadelfeo, Seco, Verde, Gulachos, Albuñol, Adra, Po
Bottom Currents	Elongated parallel to shoreline	Oblique to perpendicular	~450	60-100		Fluvià-Muga
Longshore currents	Circular to parallel to shoreline	Subparallel to perpendicular	~200	3-15		Ebro

2 Scientific objectives and approach

The fact that it is often speculated about the causes of submarine landslide events (e.g., Masson et al., 2006; Lee et al., 2007) manifests that current knowledge on their mechanisms is, despite the vast literature on this topic, still rather incomplete (e.g., Camerlenghi et al., 2007; Cochonat et al., 2007). This is especially true for open continental margin settings, where the diversity of environmental settings allows consideration of a broad range of distinctive pre-conditioning and triggering factors (as opposed to the more limiting environments of, e.g., fjords and volcanic island flanks). Due to a variety of international projects (e.g., STRATAFORM and COSTA) as well as joint investigations of academia and industry (e.g., the Storegga slide) within the last decades, the modes of operation of individual factors have been intensively studied and are well-understood. However, each study site reveals a distinctive depositional setting that relates to complex interactions of environmental processes. Hence, slope destabilization regularly requires the interplay of several destabilizing factors and demands a detailed analysis for each case study in order to shed light on the prevailing mechanisms of failure.

In addition, the destabilizing influence of individual factors may strongly vary both in time and space (e.g., changing location of a river mouth), especially with regard to a full Glacial-Interglacial cycle. However, the influence of climatic fluctuations on the sediment dispersal and associated shelf architecture is often not fully recognized. A thorough analysis of submarine landslides should hence take into consideration the paleo-environmental changes associated to these climatic cycles, which may involve changes in the stacking pattern of submarine strata through variability in sediment flux and dispersal, ultimately generating the conditions for the formation of weak layers (e.g., through changes in lithology, the generation of firm to hard grounds in response to decreased accumulation, generation of permeability barriers etc.). Equally important in this context is not only the question where (in the stratigraphic record) a landslide occurs, but as well when it occurs and whether this occurrence can be related to specific environmental conditions (e.g., sea level variations). The use of long cores is indispensable for this task, as it allows assessing both landslide frequencies as well as accompanying environmental conditions and processes in time. At the same time, full stratigraphic recovery of landslide deposits allows to assess the mechanical interactions at their basal shearing surface.

Finally, acknowledging the close proximity between the densely populated coastlines of the Mediterranean Sea and its landslide-related geohazards, there is a strong need for the development of a robust hazard assessment. This not only requires information on the type of failure and involved mechanisms, but more essentially on the frequency of landslide processes. Case studies may help in

the development of large consistent databases that may be used to estimate – and ultimately eliminate – risks related to the impact of submarine landslides and associated tsunami events on offshore infrastructure and coastal communities alike.

Consequently, this study aims to (1) identify the processes and mechanisms of submarine landsliding at NE Gela Basin during the Last Glacial-Interglacial cycle, (2) assess the frequency of failure and its spatial distribution, and (3) relate landslide occurrence to (paleo-)environmental conditions. The following interrogative framework outlines the main objectives of this thesis:

- What are the driving factors that lead to slope instability?
- Which pre-conditioning factors dominate the depositional setting?
- Can specific stratigraphic surfaces be identified along which landsliding takes place?
- What is the role of seismic activity in triggering landslides?
- What are the mechanisms involved in failure?
- What is the slide frequency in the study area?
- What is the role of climatic fluctuations in shaping slope architecture?
- Can periods of enhanced landslide activity be identified that relate to certain periods of the past Glacial-Interglacial cycle?

In order to adequately address these questions, several continuous to semi-continuous sedimentary records from three boreholes on the continental shelf and slope at Gela Basin in the Strait of Sicily have been analysed. They allow a detailed chronological reconstruction of the depositional architecture in response to paleo-environmental fluctuations. Together with a wealth of high-resolution bathymetric seafloor and parametric subbottom data they constitute the investigative framework to the exploration of submarine landslide processes.

3 Overview of own research

The scientific objectives of this thesis as outlined in chapter 2 were addressed within three individual manuscripts that have either been published in, are currently under review by or in preparation for submission to peer-reviewed international journals and special publications. The results of these studies are presented and discussed in chapters 6-8. Furthermore, chapter 9 presents the findings of a published manuscript by Dr. Fei Ai et al. (2014), to which I contributed the borehole stratigraphy.

The following section briefly summarizes the results of the above mentioned manuscripts and comments on their contribution with respect to the presented objectives. All first-author manuscripts (chapters 6-8) and figures within were prepared by myself, including data generation through core sampling, preparation and core-physical measurements (chapters 5.1 and 5.3) as well as processing and interpretation of acoustic data (chapter 5.2). In general, all co-authors provided fruitful discussions on the results and interpretations, valuable comments for each manuscript and assisted in defining sampling strategies. Introduced age models for the recovered cores benefitted from a strong contribution in micropaleontological determinations by one of the co-authors (Dr. Alessandra Asioli, IGG-CNR, Padova, Italy), who provided section 5.1 (*Foraminifera biostratigraphy*) in chapter 6.

The first manuscript (chapter 6),

Sedimentary response to Milankovitch-type climatic oscillations and formation of sediment undulations: evidence from a shallow-shelf setting at Gela Basin on the Sicilian continental margin

J. Kuhlmann, A. Asioli, F. Trincardi, A. Klügel, and K. Huhn

sets the scene for a detailed investigation of submarine landslide processes at NE Gela Basin by unravelling the depositional shelf architecture, especially with regard to climatic fluctuations and associated sequence-stratigraphic boundaries (which may serve as week layers). The manuscript integrates key datasets (foraminifera-based eco-biostratigraphy, oxygen stable isotopes, radiocarbon datings and tephrochronologic marker) from two boreholes for a chronostratigraphic calibration of shelf sedimentary units. Based on this, it (1) assesses the control of paleoclimatic (Milankovitch-type) cyclicity on depositional sequences and their bounding surfaces, (2) speculates on the mechanisms regulating sediment flux and dispersal, and (3) investigates the type and genesis of undulated sediment features.

The second manuscript (chapter 7),

"Integrated Stratigraphic and Morphological Investigation of the Twin Slide Complex Offshore Southern Sicily"

J. Kuhlmann, A. Asioli, M. Strasser, F. Trincardi, and K. Huhn

aims at disentangling the complex failure architecture in the study area. It introduces first results from high-resolution acoustic datasets and drilled shelf edge boreholes and presents new evidence on the morphological evolution as well as stratigraphic context of the most recent landslide events, the *Twin Slide* complex. Core-seismic correlations are used to identify multiple failure stages associated to these landslides. In detail, a carbon and oxygen isopte stratigraphy integrated with eco-biostratigraphic considerations is used to unravel the stratigraphic units involved in failure. A new conceptual model is proposed that accounts for distinct morphological appearances and revises previous suggestions. Further evidence is presented on the role of sub-horizontal weak layers and sub-vertical faults and scarps with regard to slope destabilisation.

The third manuscript (chapter 8),

"Landslide frequency and failure mechanisms - the cas of NE Gela Basin (Strait of Sicily)"

J. Kuhlmann, A. Asioli, F. Trincardi, A. Klügel, and K. Huhn

reports on the frequency of failure, discusses relevant predisposing factors and trigger mechanisms and provides evidence on the importance of prefailure stratal architecture. It introduces an integrated chronological framework for the borehole on the lower slope (GeoB14401), correlates observed deposits to dated horizons and summarizes the temporal occurrence and distribution of landslide events within the last ~90 ka. The manuscript further identifies the main predisposing factors and highlights the role of sequence-stratigraphic boundaries and volcanoclastic layers as prefential glide planes. Finally, it discusses the role of seismicity as a potential trigger mechanism inducing failure.

The fourth manuscript (chapter 9),

"Submarine Slope Stability Assessment of the Central Mediterranean Continental Margin: The Gela Basin"

F. Ai, J. Kuhlmann, K. Huhn, M. Strasser, and A. Kopf

geotechnically investigates the source sediments of *Northern Twin Slide* in the framework of a slope stability analysis in order to ascertain the current state of the slope and to infer potential mechanisms of failure at Gela Basin. It reports on undrained shear and consolidation tests and testifies strongly under-consolidated sediments that reflect rapid sedimentation. Additionally, results from oedometer experiments are introduced, which indicate very low permeability. It is suggested that the latter may add to overpressure build-up by inhibiting fluid seepage. Finally, a slope stability analysis is carried out to identify the current status of the slope. It is reported that an external seismic shock is necessary in order to induce failure.

4 Regional setting

The study site at the NE portion of Gela Basin lies within a tectonically active region and is oceanographically strongly influenced by the Mediterranean current system. Since the stability of submarine slopes is largely controlled by their stratigraphic nature, depositional character and seismic potential as well as temporal fluctuations within these parameters (chapter 1), the following sections provide an introduction to the general context of the regional setting.

4.1 Geologic setting and seismic activity

Filled with as much as 2500 m of shallowing-upward marine sediments, the Gela Basin represents the most recent (Pliocene-Quaternary) foredeep basin of the Maghrebian fold-and-thrust belt, which reflects the ongoing subduction of the African plate beneath the Eurasian one (*Figure 4.1*; Colantoni, 1975; Argnani, 1990). It is situated north of the NW-SE trending Sicily Strait rift zone that originated from extensional faulting and is characterized by the relatively deep (> 1000 m) basins of Pantelleria, Linosa and Malta (Finetti, 1984). The corresponding rifting phase initiated in the late Miocene to early Pliocene and lasted through the Quaternary (Grasso, 1993). In the North, Gela Basin is overthrusted by the Gela Nappe – a southwest migrating contractional front representing the southernmost thrust wedge of the Maghrebian chain (*Figure 4.1B*; Argnani, 1990; Butler et al., 1992). It consists of an accretionary chaotic assemblage, which is overlain by a relatively undisturbed cover. Plunging in direction of the basin, the surface slope in the frontal area of Gela Nappe contributes to instability of overlaying sediments and manifests in the frequent emplacement of mass-wasting deposits along the shelf edge (Trincardi and Argnani, 1990; Minisini et al., 2007; Minisini and Trincardi, 2009). Subsequent to the emplacement of Gela Nappe, a phase of general uplift associated with widespread volcanic activity characterized the mid-Pliocene to late Quaternary (Gardiner et al., 1993). To the East, Gela Basin is confined by the steep western flank of the Malta Plateau, the seaward counterpart of the Hyblean plateau on mainland Sicily (*Figure 4.1B*). The southwestward dipping Hyblean-Malta platform is composed of Mesozoic carbonate rocks comprising intercalated volcanic deposits from the upper Triassic to the Quaternary (Barberi et al., 1974). A Mesozoic-Cainozoic palaeographic boundary separates this carbonate platform in the East from the Pliocene-Quaternary successions of progradational basin sequences in the West. As a result, depositional sequences in the study area show a SW-dipping character and gradually steepen with time, favouring the occurrence of extensive mass transport complexes at their base.

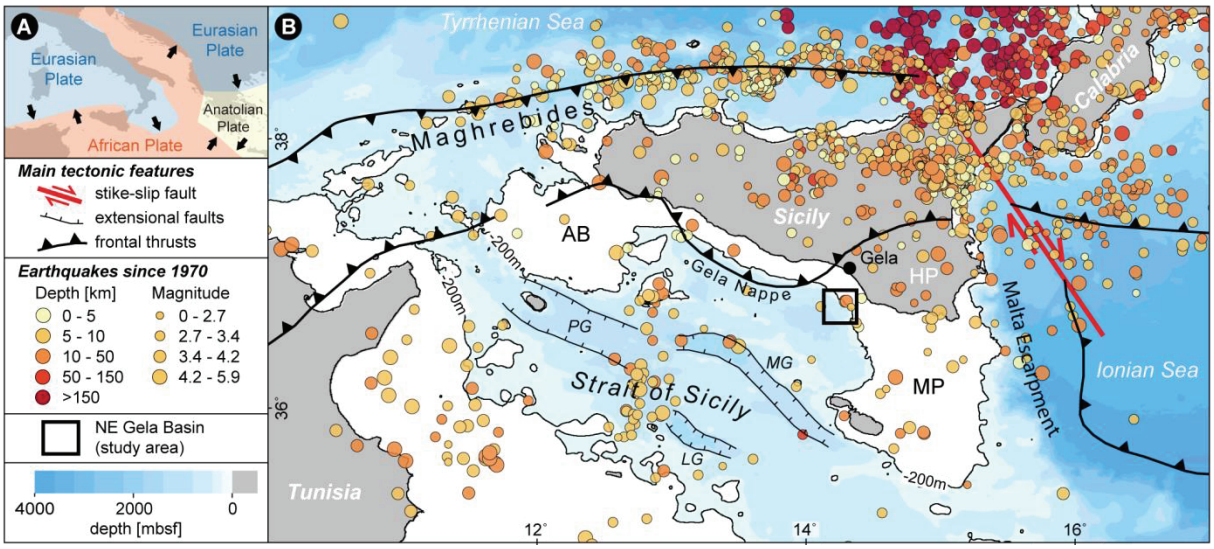

Figure 4.1. A) Simplified sketch of the central Mediterranean plate boundaries with arrows indicating direction of plate motion (after Dilek and Sandvol, 2009; Camerlenghi et al., 2010). B) Bathymetric map of the study area in the Strait of Sicily illustrating main tectonic and geographic elements (after Jenni et al., 2006; Accaino et al., 2010; Civile et al., 2010; bathymetric data taken from GEBCO database). Superposed on this map is the U.S. Geological Survey (USGS) earthquake record since 1970, both size- and colour-coded depending on the magnitude and depth of the event, respectively (see legend on the left hand side). The Pantelleria graben (PG), the Malta graben (MG) and the Linosa graben (LG) are the principal tectonic depressions in the area. AB = Adventure Bank; MP = Malta Plateau.

Seismicity at Gela Basin is relatively low when compared with other Mediterranean areas, as indicated by the instrumental and historical series of the USGS NEIC database (U.S. Geological Survey, National Earthquake Information Center; http://earthquake.usgs.gov/earthquakes/search/), plotted in *Figure 4.1B*. Since 1970, seven epicentres with low to moderate magnitudes ranging from 2.8 to 4.2 were registered in the immediate proximity of NE Gela Basin. However, this arguably low number indicates significant seismic frequency if extrapolated to longer temporal intervals. Minisini et al. (2007) proposed a rough estimate of about 2000 seismic shocks over the period of the last post-LGM interval. They additionally argued that full account of the maximum possible earthquake magnitude and spatial distribution of the epicentres in the historical record may have been hindered by a variety of reasons: (1) the difficulty to infer past offshore epicentres; (2) the bias of onland distribution of historical earthquakes associated with the location of ancient settlements; and (3) the incidental absence of potential extreme events in the short interval of observation. Hence, the regional seismic potential may be underestimated with regard to the limited temporal interval at the base of the USGS database.

4.2 Oceanographic setting

The present day Mediterranean Sea is a semi-enclosed mid-latitude basin encompassed by the African continent in the South, Europe in the North and the Middle East in the East (*Figure 4.2A*). It is connected to the Atlantic Ocean via the narrow Strait of Gibraltar in the West and comprises two main

basins, the Eastern and Western Mediterranean Sea, as well as a number of smaller sub-basins. Evaporation generally exceeds the combined contribution of precipitation and river runoff, making the Mediterranean Sea the most important source of high-salinity water masses in the global oceanic system (e.g., Pinardi and Masetti, 2000; Millot and Taupier-Letage, 2005).

Oceanographically, water circulation is driven by an anti-estuarine thermohaline pattern forced by the negative hydrological balance and the density gradient with regard to the Atlantic Ocean (Robinson and Golnaraghi, 1994). The surface inflow of relatively fresh and light waters from the Atlantic (Modified Atlantic Water, MAW) is accompanied by a concurrent subsurface outflow of relatively more saline Mediterranean waters (mostly Levantine Intermediate Water, LIW) that form in the course of intense evaporation in the Levantine Basin during winter convection events in February-March (POEM group, 1992). Similarly, warm surface and intermediate waters are transformed into colder and denser deep water during winter cooling at two secondary thermohaline cells in the Gulf of Lions and the Adriatic Sea (e.g., Lascaratos et al., 1999; *Figure 4.2A*). During passage through the Strait of Gibraltar, this deeper bottom water is mixed with the LIW and enters the Atlantic as the homogeneous Mediterranean outflow water (MOW), which flows in northward direction along the Iberian slope.

At sub-basin scale, the general large-scale circulation pattern of the Mediterranean Sea is modulated by meso-scale dynamic processes as well as wind forcing and complex topographic constraints and mixing processes (Standsfield et al., 2003; Ismail et al., 2012).

Connecting the eastern and western Mediterranean sub-basins via two sill systems of about 560 m (Ionian Sea to the East) and 430 m depth (Thyrrhenian Sea to the West), the Strait of Sicily forms a key area controlling water exchange between both (e.g., Astraldi et al., 2001). Large scale circulation within the Strait of Sicily and, hence, along the NE Gela Basin is forced by the anti-estuarine thermohaline circulation of the Mediterranean Sea and can be schematized as a two-layer flow regime involving (1) an eastward directed fresher surface layer of MAW occupying the first 100-200 m of water column, and (2) a westward flowing salty bottom layer mainly consisting of LIW (*Figure 4.2B*; Astraldi et al., 1999; Robinson et al., 1999; Sammari et al., 1999). Approximately one third of the MAW enters the Tyrrhenian Sea and follows the northern coast of Sicily (Bethoux, 1980), while the remainder splits into two branches (Herbaut et al., 1998; Robinson et al., 1999; Béranger et al., 2004): (1) the Atlantic Tunisian Current (ATC) following the 200 m isobaths southward over the Tunisian shelf (Sammari et al., 1999; Onken et al., 2003; Béranger et al., 2004), and (2) the Atlantic Ionian Stream (AIS) meandering south-eastward off the southern coast of Sicily (Lermusiaux and Robinson, 2001; Béranger et al., 2004). ATC is thought to be more energetic in winter (Pierini and Rubino, 2001; Sorgente et al., 2003; Béranger et al., 2004), while in summer most of MAW is advected by the AIS meandering around three semi-permanent mesoscale structures, the cyclonic Adventure Bank Vortex (ABV), the anticyclonic Maltese Channel Crest (MCC) and the cyclonic Ionian Shelfbreak Vortex (ISV) (*Figure 4.2B*; Robinson et al., 1999; Lermusiaux and Robinson, 2001). Finally, AIS enters the Ionian Sea, where it feeds the mid-Mediterranean Jet on its way to the central Levantine basin in the Eastern Mediterranean Sea.

In summary, the study area at Gela margin is significantly affected by the presence of surface and intermediate waters relating to the thermohaline Mediterranean current pattern. The presence of the anticyclonic MCC and a LIW-related subsurface eddy reaching velocities greater than 13 cm/s (Lermusiaux and Robinson, 2001) may severely impact sediment transport and dispersal in this area and, hence, contribute to slope instability. This is supported by the presence of muddy contourite deposits along the shelf edge as reported on by Verdicchio and Trincardi (2008).

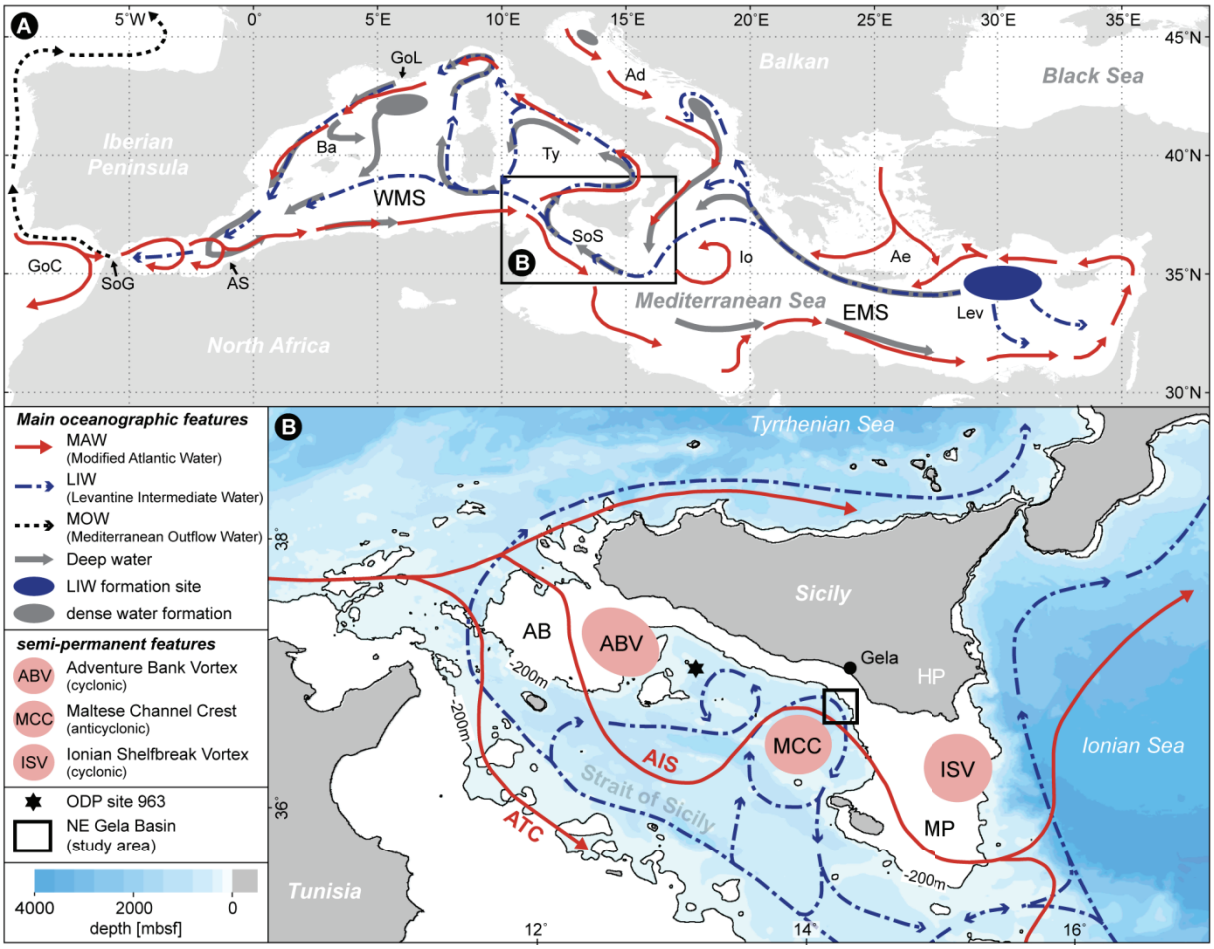

Figure 4.2. A) General thermohaline circulation pattern of the Mediterranean Sea showing main pathways of surface (Modified Atlantic Water, MAW, red arrows) and intermediate (Levantine Intermediate Water, LIW, blue arrows) waters as well as formation area of the latter (after Millot, 1999; Asioli et al., 2001; Hernández-Molina et al., 2006). Ad = Adriatic Sea; Ae = Aegean Sea; AS = Alboran Sea, Ba = Balearic Sea; EMS = Eastern Mediterranean Sea; GoC = Gulf of Cádiz; GoL = gulf of Lions; Io = Ionian Sea; Lev = Levantine Sea; SoG = Strait of Gibraltar; SoS = Strait of Sicily; Ty = Tyrrhenian Sea; WMS = Western Mediterranean Sea. B) Scheme of two-layer exchange exchange circulation in the Strait of Sicily, modified from Lermusiaux and Robinson (2001), Béranger et al. (2004) and Ciappa (2009). Fresh surface waters from the Atlantic Ocean (MAW) meander along the Tunisian and Sicilian shelf (red arrows, between 0 and 200 m), accompanied by a concurrent subsurface outflow of relatively more saline Mediterranean waters (LIW, blue arrows, between 200 and 600 m). See legend for prominent semi-permanent summer features. AB = Adventure Bank; HP = Hyblean Plateau; MP = Malta Plateau.

4.3 Gela Basin

Previous work by Trincardi and Argnani (1990), Minisini et al. (2007) and Minisini and Trincardi (2009) provides a wealth of acoustic evidence for widespread and recurrent mass wasting processes along the continental slopes of Gela Basin. The seafloor morphology in the study area documents both, remnants of old and partially buried landslide scars as well as more recent and typically exposed equivalents (*Figure 4.3*). For the sake of consistency, the terminology (i.e. naming of failure events) established by Minisini et al. (2007) is adopted herein after.

The most prominent seafloor feature is the *Twin Slide* complex, two recent mass failures that are characterized by sub-rounded scarps in a depth of about 200-230 mbsf, reliefs that exceed 100 m, dips of up to 27°, runout lengths of 10-12 km and bathymetric bulges at the base of the slope that represent evacuated material with a volume of < 1 km³ (Minisini et al., 2007). The shelf edge/upper slope area in between these scarps accommodates a depression that dips steeper (~8°) than the surrounding shelf deposits (~3°) and reflects the buried headscarp of an older landslide termed *Father Slide* (*Figure 4.3*). At present, this area is affected by bottom-current related sediment drift and associated erosional moat (see section 4.2; Verdicchio and Trincardi, 2008). Based on evidence from chirp-sonar profiles, Minisini and Trincardi (2009) report on a succession of five stacked mass transport deposits that accumulated between the initial *Father Slide* and the most recent *Twin Slides*. Remnant bathymetric evidence of their presence is discernable in form of paleo-scarps of up to 10 m in relief (*Figure 4.3*). Additionally, the area displays evidence of fluid expulsion interpreted as pockmarks as well as draped gullies along the shelf edge.

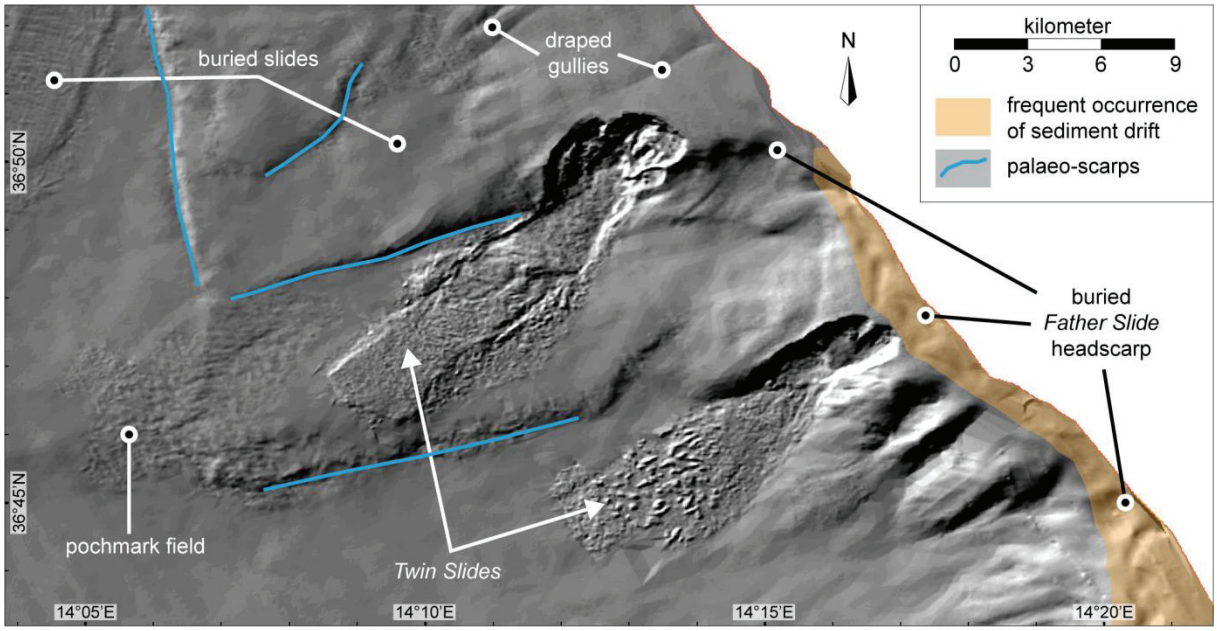

Figure 4.3. Multibeam shaded relief of NE Gela Basin showing morphological seafloor features (after Minisini et al. (2007), Minisini and Trincardi (2009); bathymetric source: ISMAR multibeam surveys; artificial lighting from NW, sun angle 45°). Two prominent and seafloor-exposed landslides form the *Twin Slide* complex, which covers older and buried events (e.g. the *Father Slide*). Other prominent features include pockmarks and draped gullies. The shelf edge is affected by sediment drift and contourite deposits (Verdicchio and Trincardi, 2008).

5 Material and applied methods

5.1 Study material and sediment sampling

This study is based on material collected in 2010 during *R/V Maria S. Merian* cruise MSM15/3 in the central Mediterranean Sea and comprises datasets originating from (1) a parametric sediment echosounder, (2) two bathymetric multibeam echosounder systems and (3) coring devices.

A dense grid of subbottom profiles were collected with the hull-mounted Atlas Parasound system operating with a 4 kHz signal, which is focused within a cone of 4-5 ° opening angle. It provides a dm-scale vertical resolution, while the horizontal resolution encompasses about 7 % of the water depth. The suit of multibeam systems operates at 12 kHz (Kongsberg Simrad EM120) and 95 kHz (Kongsberg Simrad EM1002) and allows bathymetric reproduction at a 10-m-resolution and better. The acoustic record was complemented by multibeam (Kongsberg Simrad EM300 and RESON 8160) and chirp-sonar (2-7 kHz sweep-modulated band width) data from ISMAR, Italy, that were collected during four cruises on board *R/V Odin Finder* (2000) and *R/V Urania* (2003, 2004 and 2005).

Coring is restricted to three strategically located drill sites sampling both undisturbed sediments from the shelf edge that nourished buried and exposed slope failures (sites GeoB14403 and GeoB14414) as well as sequences from the lower slope section that record associated mass transport deposits (GeoB14401). At each drill site, a standard gravity core (GC) with lengths ranging between 4.18 m and 5.32 m was supplemented by one or two deployments of the Bremen seafloor drill rig MeBo (Freudenthal andWefer, 2007; Freudenthal and Wefer, 2013), thus allowing sediment recovery to a maximum depth of about 55 mbsf. At the shelf boreholes, high water content in the upper sediment column led to gravitational sinking of the MeBo drill rig as well as vertical compression of sediments within the GCs. Required adaption of the core depth schemes relied on core-seismic correlation of the prominent erosive unconformity (ES1) related to the LGM as well as adjustment through foraminiferal assemblages and core-physical measurements. An overview of the drill sites and selected metadata is given in *Table 5.1*.

The dominant lithology of the recovered sediments is a silty nannofossil clay accompanied by quartzose silt, volcanic glass and minor amounts of foraminifera and authigenic pyrite. With the exception of reworked sediments at site GeoB14401, no systematic downcore changes are evident and lithologic variability is limited to the scattered presence of silty laminae, bioturbation and black organic matter.

Prior to their opening, gravity cores were subdivided into one metre sections. Subsequently, both gravity and MeBo cores were split into working and archive halves following the standard procedure

of the MARUM core repository. Working halves were subsampled (~30 ml per sample) at ≤ 20 cm intervals for further analyses (see below), yielding a temporal resolution of centennial to millennial scale (depending on the sediment accumulation ratio within the observed sequence). Additional samples were taken from various core depths for purposes of radiometric dating and geochemical glass shard analysis (see section 5.3).

Table 5.1. Overview of metadata at sampling stations associated with this study (GC = gravity corer; MeBo = Bremen seafloor drill rig; mbsl = meters below sea level; mbsf = meters below seafloor).

Station	Gear	Water depth	Geographic position		Top depth	Bottom depth	Length	Recovery rate
GeoB #		[mbsl]	Latitude	Longitude	[mbsf]	[mbsf]	[m]	
14401-2	GC	634.3	36°47.17'N	14°11.91'E	0.00	4.18	4.18	100%
14401-3	MeBo	613.8	36°47.20'N	14°11.90'E	0.00	20.49	20.49	26%
14401-5	MeBo	601.3	36°47.19'N	14°11.89'E	14.45	35.6	21.15	84.8%
14403-1	GC	193.4	36°51.41'N	14°13.92'E	0.07	7.83 (*5.05**)	7.76 (*4.98**)	100%
14403-2	MeBo	191.5	36°51.44'N	14°13.92'E	5.55 (*5.05**)	18.24 (*17.74**)	12.69	83.9%
14403-8	MeBo	182.0	36°51.41'N	14°13.91'E	17.57 (*16.80**)	54.57 (*53.80**)	37.00	85.3%
14414-1	MeBo	146.0	36°48.13'N	14°18.17'E	0.50 (*0.00**)	27.48 (*26.98**)	26.98	81.8%
14414-2	GC	145.2	36°48.14'N	14°18.18'E	0.00	7.71 (*5.32**)	7.71 (*5.32**)	100%

* = original values used in Kuhlmann et al. (2014). The core depth schemes were adapted to account for (1) gravitational sinking of the MeBo drill rig into the muddy seafloor and (2) vertical compression of soft sediments within the gravity cores.

5.2 Processing and interpretation of acoustic data

In order to allow identification as well as lateral tracing of seafloor and sub-seafloor sediment features, this study relies on high-resolution records of both multibeam echosounder and parametric sediment echosounder systems (see section 5.1). These instruments provide, respectively, a continuous mapping of the seafloor as well as an accurate image of sub-surface sedimentary structures within the study area. However, certain measures of data manipulation were applied to optimize the overall quality of these datasets. This section intends to (1) shortly summarize the procedures adopted within the framework of data preparation, processing and application, and (2) report on the general approach to acoustic data interpretation in this study.

The general susceptibility to sea conditions and a negative correlation between data quality and water depth usually requires processing of the bathymetric data acquired by multibeam echosounder systems. Accordingly, identification and removal of artifacts and outliers was achieved through single beam editing within MB-System (Caress and Chayes, 2006), with subsequent gridding at 10 m resolution. ArcGIS, Fledermaus and GMT (Generic Mapping Tool; Wessel and Smith, 1998) were invoked for visualization purposes such as 3D bathymetric rendering or the generation of shaded relief and slope gradient plots, all of which serving the ambition to facilitate interpretation of seafloor architecture or surficial tracking of sub-surface structures and failure scars. Where local bathymetric data was unavailable, it was replaced by the global 30 arc-second grid GEBCO_08 (General Bathymetric Chart of the Ocean), as provided by the British Oceanographic Data Centre (BODC).

Subbottom profiles gathered with the hull-mounted Atlas Parasound system displayed very good pre-processing quality and depth penetration (> 100 m). Data manipulation was thus limited to the removal of dead channels and successive signal interpolation as well as noise reduction through bandpass frequency filtering, and was carried out with Vista (Seismic Image Software Ltd.). Complementary chirp-sonar profiles from ISMAR underwent similar treatment to assure congruency of data sets. Subsequent identification and tracing of sedimentary units in terms of their acoustic character was realized with the commercial seismic interpretation software Kingdom Suite (Seismic Micro-Technology Inc.). Gravitational mass-transport deposits (MTDs) were identified with respect to the characteristic pattern of chaotic to transparent acoustic units that is intrinsic to high sediment deformation (e.g., Lee et al., 2007). Consequently, tracing of their vertical and lateral outline relied heavily on the sharp contact to neighbouring, well-stratified patterns that relate to undeformed sedimentary successions. Likewise, sub-vertical faults relating to syn- and post-depositional tectonic activity were recognized through tracing of vertical off-sets in the lateral distribution of stratified acoustic reflector packages. Sequence-stratigraphic interpretation of sedimentary successions grounded on the identification of onlapping units in proximal clinoform remnants as well as stratigraphic key surfaces of erosion and condensation manifesting in high-amplitude reflectors.

5.3 Core measurements and methods

A wide suite of methods and proxies were applied to the recovered sediment cores in order to unravel climatic fluctuations as well as site specific dynamics and processes that act on various temporal scales (*Table 5.2*). This multi-proxy approach is key not only to a chrono-stratigraphic control of the shelf architecture (chapter 6), but as well to the identification and interpretation of failure-related processes and sedimentary surfaces (chapter 8). In the following, the applied methods and their relevance for this study are briefly summarized.

Table 5.2. Overview of analyses carried out on the core material (AMS – Accelerator Mass Spectrometry).

Station GeoB #	Gear	AMS ^{14}C dating		MSCL	XRF	Stable isotopes	Grain size analysis	Glass shard geochemistry	Thin sections
		mono-specific	mixed						
14401-2	GC		1	1 cm	2 cm	x			
14401-3	MeBo			1 cm	2 cm	x	1		1
14401-5	MeBo	2	1	1 cm	2 cm	x	1		2
14403-1	GC	2	2	1 cm	2 cm	x			
14403-2	MeBo	1	3	1 cm	2 cm	x			
14403-8	MeBo	1	1	1 cm	2 cm	x		1	
14414-1	MeBo			1 cm	2 cm	x	2		2
14414-2	GC	1	1	1 cm	2 cm	x			

5.3.1 Core-physical properties

The method of core scanning is a fast, direct and non-destructive approach to gain a quasi-continuous downcore record of physical properties at cm-scale resolution. Related measurements are frequently used to infer changes in depositional settings and to detect stratigraphic boundaries (e.g., through variations in the magnetic susceptibility record as suggested by Radhakrishnamurty et al., 1968). However, reliable implications on palaeoclimatic variability and stratigraphic evolution require consideration of additional proxy records. Hence, core-physical measurements from this study were rather used to complement other records and support core-seismic correlations (chapter 7) or the recognition of failure-related surfaces (chapter 7,8).

For non-destructive measurements on the undisturbed archive halves of the sediment cores, a GEOTEK Ltd. multi-sensor core logger (MSCL; Blum, 1997) with a resolution of 1 cm housed at MARUM (University of Bremen, Germany) was utilized. Acquired core-physical properties include (1) GRAPE density (Evans, 1965) through attenuation of gamma rays, (2) velocity of compressional waves, and (3) the amount of magnetically susceptible material present in the sediment. GRAPE density values were corrected using moisture and density parameters (MAD) determined according to the IODP shipboard practices (Blum, 1997). Additionally, outliers and bad data associated with reduced signal strengths and/or the top and bottom parts of individual core sections were manually identified and removed.

5.3.2 X-ray fluorescence (XRF)

Similar to core scanning for physical properties (see chapter 5.3.1), X-ray fluorescence (XRF) spectrometry is a non-destructive method that provides quasi-continuous bulk-sediment chemistry records at very high resolutions (up to 1 mm). These records have been proven useful in a variety of marine research fields, as a significant part of palaeoclimatic change is recorded in the chemical composition of sediments (e.g., Zachos, 2005; Richter et al., 2006; Schefuß et al., 2011). It is important to mention, though, that the quality of measurements may be significantly influenced by surface roughness and lithologic inhomogeneities (Richter et al., 2006). However, these inconsistencies are considered to be less pronounced with regard to the fine-grained, homogeneous nature of sediments found in the study area.

Geochemical logging for light elements (Al to Fe) was performed on the undisturbed archive halves of the sediment cores using an Avaatech II core scanner housed at MARUM (University of Bremen, Germany). Data on elemental intensities was collected in a step interval of 2 cm (local features were resolved at 1 cm) with a slit size of 1 cm down-core and 1.2 cm cross-core. The scanner was run with an excitation potential of 10 kV, an X-ray current of 0.2mA and a count time of 20 seconds. Prior to scanning, core sections were allowed 1h of thermal adjustment to room temperature in order to avoid generation of water condensation, which could severely reduce light element XRF intensities (e.g., Tjallingii et al., 2007). Subsequently, the split core surface was covered with a polypropylene foil to prevent contamination of the XRF measurement unit and desiccation of the sediment. Processing of measured raw data spectra was achieved using the WIN AXIL Batch software

(Analysis of X-ray spectra by Iterative Least square, Canberra Eurisys, Benelux, Avera Group), revealing reliable data for the elements Al, Si, S, K, Ca, Ti, Fe and Mn (the latter for high peaks only).

Since measurement principles dictate a data output of relative elemental concentrations, it is strongly advised and widely accepted to use elemental ratios instead of element concentrations for the presentation and interpretation of XRF data (e.g., Richter et al., 2006). However, since XRF ratios have the undesirable property of asymmetry (e.g., conclusions based on evaluation of A/B cannot be directly translated into an equivalent statement about B/A) they are expressed in terms of logarithms (e.g., log[A/B]) in this study, following the suggestions of Weltje and Tjallingii (2008).

5.3.3 Planktic and benthic foraminifera assemblage

The abundance and excellent preservation of foraminiferal fossils in marine sediments as well as their capacity to record palaeoenvironmental changes has made both planktonic and benthic foraminifera a popular proxy for the reconstruction of a wide range of oceanographic parameters, such as surface-water properties, bottom water oxygen content or the extent and/or seasonality of organic flux (Kucera, 2007; Jorissen et al., 2007). In this study, the foraminiferal record from the size fraction > 63 µm was used to develop an eco-biostratigraphy relying on the identification of (temporary) disappearance and (re-)occurrence of individual species, which was carried out by Alessandra Asioli at the Istituto di Geoscienze e Georisorse (CNR-UOS di Padova, Italy). Variations in the relative abundance of different species allowed identification of paleoenvironmental changes already defined in the Central Mediterranean (Jorissen et al., 1993; Asioli et al., 2001; Sbaffi et al., 2001) as well as Sicily Channel (Vergnaud-Grazzini et al., 2002; Asioli et al., 2002; Sprovieri et al., 2003; Sprovieri et al., 2006; Incarbona et al., 2010) and Gela Basin (Minisini et al., 2007). A detailed description of the results is given in chapters 6, 7 and 8.

Prior to analysis, sediment subsamples with a resolution of at least 20 cm (see section 5.1) and a weight of 20-50 g each were prepared at MARUM (University of Bremen, Germarny). The samples were freeze-dried, soaked in distilled water and washed over a 63 µm mesh sieve (Schröder et al., 1987).

5.3.4 ^{14}C AMS radiometric dating

Absolute age determination is an essential tool for the purpose of reconstructing core chronologies. Provided that sediment samples are not contaminated and calibration as well as reservoir correction is thoroughly accounted for, ^{14}C radiometric dating of marine records yields accurate results for the last 50 ka (e.g., Hughen et al., 2007). Consequently, radiocarbon derived datings are used two-fold in this study: (1) as robust tie-points in the age-depth models of undisturbed shelf sediments recovered at sites GeoB14403 and GeoB14414 (chapter 6), and (2) in the framework of temporally confining mass-transport deposits recovered from the lower slope at site GeoB14401 (chapter 8).

For this purpose Accelerator Mass Spectrometry (AMS) analyses were performed on a set of 16 mono-specific and mixed foraminifera samples by the Poznan Radiocarbon Laboratory (PRL, Poznan, Poland) and the National Ocean Sciences Accelerator Mass Spectrometry Facility (NOSAMS, Woods

Hole Oceanographic Institution, USA). To avoid contamination, handpicked specimens from the size fraction > 150 µm were ultrasonically cleaned prior to analysis. Obtained ages were converted to calendar years (cal. ka BP, present is AD 1950) using the Calib 7.0.0 Radiocarbon Calibration Program (Stuiver and Reimer, 1993) and the Marine13 calibration curve (Reimer et al., 2013). To account for reservoir effects, a calculated weighted mean ΔR value of 71 years and a standard derivation of 50 years were selected from the Calib database (Siani et al., 2000). An overview of the results is presented in *Table 5.3*.

Table 5.3. Overview of all AMS ^{14}C datings on monospecific and mixed foraminifera samples. Calibration is based on Calib 7.0.0 Radiocarbon Calibration Program (Stuiver and Reimer, 1993). Calibration data set: Marine13 according to Reimer et al. (2013). Reservoir correction: The calculated weighted mean ΔR value is 71 with a standard derivation of 50 (Siani et al., 2000). Symbology: ^ = ^{14}C age exceeds calibration limit; * = rejected dating (due to contamination/bioturbation).

Lab #	Core	Section # depth [cm]	Material	^{14}C age [yr BP]	2σ cal. intercept [cal. ka BP]
OS-106893	GeoB14401-2 (GC)	IV 80-84	*N. Pachyderma, G. Bulloides*	16400 ± 95	19.22 ± 0.29
OS-106666	GeoB14401-5 (MeBo)	1P-1 40-46	*N. Pachyderma, G. Bulloides, N. Dutertrei*	15800 ± 55	18.59 ± 0.18
OS-106889	GeoB14401-5 (MeBo)	7P-2 0-5	*N. Pachyderma*	25300 ± 290	28.88 ± 0.66
OS-106890	GeoB14401-5 (MeBo)	9P-2 62-67	*N. Pachyderma*	26700 ± 350	30.31 ± 0.71
Poz-53709	GeoB14403-1 (GC)	II 80-83	*G. ruber, G. sacculifer*	5285 ± 35	5.58 ± 0.13
Poz-53710	GeoB14403-1 (GC)	IV 20-22	*G. ruber, G. sacculifer*	7870 ± 35	8.26 ± 0.12
Poz-53711	GeoB14403-1 (GC)	IV 80-83	*U. peregrina*	9110 ± 50	9.75 ± 0.22
Poz-53712	GeoB14403-1 (GC)	V 40-42	*C. laevigata carinata*	11010 ± 60	12.40 ± 0.24
Poz-53713	GeoB14403-2 (MeBo)	3P-2 32-36	*U. peregrina*	25750 ± 160	29.32 ± 0.44
OS-106891	GeoB14403-2 (MeBo)	4P-1 61-67	*E. Crispum, M. Barleeanum, C. lobatulus*	29300 ± 490	32.72 ± 1.13
Poz-53715	GeoB14403-2 (MeBo)	5P-1 86-99	*H. balthica, C. pachyderma*	34000 ± 360	37.69 ± 0.99
OS-106838	GeoB14403-2 (MeBo)	6P-1 57-64	*H. balthica, U. peregrina, M. barleeanum*	41600 ± 890	44.56 ± 1.51
OS-106892	GeoB14403-8 (MeBo)	2P-cc 3-11	*U. Peregrina*	50400 ± 6800	^
Poz-53716	GeoB14403-8 (MeBo)	5P-1 100-119	*U. peregrina, B. marginata*	47000 ± 2000	^
Poz-53717	GeoB14414-2 (GC)	V 60-62	*U. peregrina*	10520 ± 50	11.58 ± 0.31
Poz-53745	GeoB14414-2 (GC)	VI 40-43	*A. beccarii, C. lobatulus, E. crispum*	31240 ± 300	34.69 ± 0.60*

5.3.5 Stable isotope analysis

The stable oxygen and carbon isotopic compositions of foraminiferal calcite reflect the isotopic composition and temperature of the ambient sea water at the time of shell calcification (e.g., McCrea, 1950; Shackleton, 1967; Rohling and Cooke, 2003). Foraminiferal $\delta^{18}O$ and $\delta^{13}C$ records are hence frequenctly used as a paleothermometer capturing Milankovitch-type climate cyclicity (Ravelo and Hillaire-Marcel, 2007, and references therein) and serve in a variety of studies as proxies for, respectively, bottom water temperature (e.g., Waelbroeck et al., 2002; Chiessi et al., 2008; Thornalley et al., 2010) or palaeoproductivity and deep water-mass configuration (e.g. Bickert and Mackensen, 2004; Curry and Oppo, 2005). For this study, stable isotope analysis is ued to identify Marine Isotope Stages and Substages (MIS; Emiliani, 1995; Shackleton and Opdyke, 1973) relating to paleoclimatic fluctuations (chapter 6, 7 and 8) as well as to trace changes in palaeoproductivity (chapter 6, 7).

Analyses were performed with a resolution of at least 20 cm (see section 5.1) on the benthic *Bulimina marginata* and the planktonic *Globigerinoides ex gr. ruber*. Specimens from the size fraction > 150 µm that showed no signs of diagenetic alteration were ultrasonically cleaned to remove contaminants such as detrital infilling, coccoliths and overgrowths. Measurements were acquired at MARUM (University of Bremen, Germany) with a Finnigan MAT 252 mass spectrometer coupled with a carbonate preparation device type "Bremen". Isotopic compositions are expressed as per mil (‰) deviation with respect to the Pee Dee Belemnite (PDB) standard and have not been corrected for the ice-volume effect (e.g., Rohling and Cooke, 2003). The long-term laboratory analytical standard deviation is < 0.07 ‰ for the $\delta^{18}O$ and < 0.05 ‰ for the $\delta^{13}C$ record.

5.3.6 Geochemical analysis of volcanic glass shards

Since volcanic tephras are erupted and deposited effectively instantaneously with respect to geological time-scales, their intercalation in the marine record provides the means to transfer ages via geochemical matching with dated equivalents (e.g., Lowe, 2011). These tephrochronologic principles are exploited in this study as an independent dating method to the recovered sedimentary successions (chapter 6). For a detailed introduction to the methods applied to extract and geochemically analyse glass shards from tephra deposits the reader is referred to section 6.4.3.

5.3.7 Grain size analysis

Grain size distributions of a sedimentological record are classically used to infer information with regard to depositional mechanisms, transport processes and sediment sources at the drill site (e.g., Tucker, 2001; Frenz et al., 2009). Consequently, this method is applied to elucidate sedimentological changes in the vicinity of glide planes within Gela Basin (chapter 8).

Since both terrigenous and biogenic fractions of the sampled sediment are relevant in the framework of slope stability, chemical pre-treatment prior to analysis was neglected. Samples were measured with the Laser Diffraction Particle Size Analyzer (Beckman Coulter) LS-13320 at MARUM grain-size lab (University of Bremen, Germany) and reported in volume percentages of 92 size classes from 0.4 to 2000 µm.

5.3.8 Thin section analysis

For the analysis of microstructures and identification of minerals within depositional horizons acting as failure planes, thin sections were prepared from selected stratigraphic layers by Dettmar dissection Technology in Bochum, Germany (chapter 8). The identification of the material and individual minerals relied on non-destructive polarized-light microscopy.

6 Manuscript I

"Sedimentary response to Milankovitch-type climatic oscillations and formation of sediment undulations: evidence from a shallow-shelf setting at Gela Basin on the Sicilian continental margin"

Authors: Kuhlmann, Jannis (MARUM, University of Bremen, Germany)
Asioli, Alessandra (Istituto di Geoscienze e Georisorse, CNR-UOS di Padova, Italy)
Trincardi, Fabio (Istituto di Scienza Marine, ISMAR-CNR,Venezia, Italy)
Klügel, Andreas (Department of Geosciences, University of Bremen, Germany)
Huhn, Katrin (MARUM, University of Bremen, Germany)

Status: Accepted for publication in *Quaternary Science Reviews* (22 October 2014)
doi: 10.1016/j.quascirev.2014.10.030

Objectives:

- Addressing the role of climatic fluctuations in shaping the depositional slope architecture at Gela Basin
- Identifying paleo-environmental changes in sediment supply and dispersal mechanisms
- Recognizing sequence-stratigraphic boundaries that imply major and abrupt changes in the depositional regime (and thus potential prefential planes of failure)
- Providing age control on shelf depositional units

Sedimentary response to Milankovitch-type climatic oscillations and formation of sediment undulations: evidence from a shallow-shelf setting at Gela Basin on the Sicilian continental margin

Jannis Kuhlmann[1], Alessandra Asioli[2], Fabio Trincardi[3], Andreas Klügel[4], Katrin Huhn[1]

[1]MARUM – Center for Marine Environmental Sciences, University of Bremen, Bremen, Germany
[2]Istituto di Geoscienze e Georisorse, CNR-UOS di Padova, Padova, Italy
[3]Istituto di Scienze Marine, ISMAR-CNR, Venezia, Italy
[4]Department of Geosciences, University of Bremen, Bremen, Germany

A multi-proxy chronological framework along with sequence-stratigraphic interpretations unveils composite Milankovitch cyclicity in the sedimentary records of the Last Glacial-Interglacial cycle at NE Gela Basin on the Sicilian continental margin. Chronostratigraphic data (including foraminifera-based eco-biostratigraphy and $\delta^{18}O$ records, tephrochronological markers and ^{14}C AMS radiometric datings) was derived from the shallow-shelf drill sites GeoB14403 (54.6 m recovery) and GeoB14414 (27.5 m), collected with both gravity and drilled MeBo cores in 193 m and 146 m water depth, respectively. The recovered intervals record Marine Isotope Stages and Substages (MIS) from MIS 5 to MIS 1, thus comprising major stratigraphic parts of the progradational deposits that form the last 100-ka depositional sequence. Calibration of shelf sedimentary units with borehole stratigraphies indicates the impact of higher-frequency (20-ka) sea level cycles punctuating this 100-ka cycle. This becomes most evident in the alternation of thick interstadial highstand (HST) wedges and thinner glacial forced-regression (FSST) units mirroring seaward shifts in coastal progradation. Albeit their relatively short-lived depositional phase, these subordinate HST units form the bulk of the 100-ka depositional sequence. Two mechanisms are proposed that likely account for enhanced sediment accumulation ratios (SAR) of up to 200 cm/ka during these intervals: (1) intensified activity of deep and intermediate Levantine Intermediate Water (LIW) associated to the drowning of Mediterranean shelves, and (2) amplified sediment flux along the flooded shelf in response to hyperpycnal plumes that generate through extreme precipitation events during overall arid conditions. Equally, the latter mechanism is thought to be at the origin of undulated features resolved in the acoustic records of MIS 5 Interstadials, which bear a striking resemblance to modern equivalents forming on late-Holocene prodeltas of other Mediterranean shallow-shelf settings.

Key words: Gela Basin; Strait of Sicily; Milankovitch cyclicity; Late Quaternary; Sediment undulations; Planktic foraminifera; Benthic foraminifera; Biofacies; Oxygen isotope records

6.1 Introduction

It is widely accepted that the high-frequency patterns of climate change and sea level fluctuations are controlled by modulations in solar radiation, which in turn are ultimately linked to orbital cyclicity (Milankovitch, 1930). First detected in marine records through variations in the ocean's isotopic composition (Emiliani, 1955; Shackleton and Opdyke, 1973; Hays et al., 1976), these patterns were subsequently used to reconstruct the astronomically paced SPECMAP curve (e.g., Imbrie et al., 1984; Martinson et al., 1987; Raymo, 1997; Petit et al., 1999; Lourens, 2004). Recognition of orbital cyclicity within shelf depositional units, however, has long been impeded by the difficult task of correlating $\delta^{18}O$-derived deep-sea stratigraphy with the sea level shaped depositional architecture on continental shelves (Ridente et al., 2008). Only the successive popularization of very high resolution subbottom imagery during the past two decades enabled researchers to unravel the control of composite Milankovitch cyclicity upon the internal organisation of depositional (seismic) units. While 40 ka cyclicity predominantly controlled stratigraphic shelf architecture during the Pliocene and Lower Pleistocene (e.g., Carter et al., 1998; Massari et al.,

1999; Kitamura et al., 2000), post-800 ka sequence generation is led by 100-ka/20-ka eustatic sea level fluctuations (e.g., Clark et al., 2006; further references provided below). As development and preservation of such high-frequency sequences is favoured by high sedimentation and comparable subsidence rates (Mitchum and Van Wagoner, 1991), they are typically recognised at shallow-shelf (mainly prodeltaic) settings on Quaternary continental margins both within and outside the Mediterranean (e.g., Piper and Aksu, 1992; Sydow and Roberts, 1994; Marsset et al., 1996; Berné et al., 1998; Rodero et al., 1999; Trincardi and Correggiari, 2000; Hiscott, 2001; Ridente and Trincardi, 2002; Osterberg, 2006; Ridente et al., 2008, 2009; Liu et al., 2010). Internal architecture of their stratigraphic record is predominantly ascribed to 100-ka glacio-eustatic cycles comprising progradational clinoforms that record deposition during distinct systems tracts (TST: transgressive systems tract; HST: highstand systems tract; FSST: falling-stage systems tract; LST: lowstand systems tract). Lack of clear seismic evidence of inter-unit stratigraphic boundaries, however, often led authors to interpret these successions as a single regressive (FSST) sequence (e.g., Ercilla et al., 1994; Chiocci, 2000; Hübscher and Spieß, 2005; Liquete et al., 2008). Less frequently, a dominance of 20-ka paced sequences has been reported, manifesting in the presence of a subordinate sequence boundary during Marine Isotope Stage (MIS) 4 (e.g., Osterberg, 2006) and multiple progradational events during MIS 5 (e.g., Hiscott, 2001; Liu et al., 2010) as well as MIS 3 (e.g., Marsset et al., 1996). Only few continental shelf settings (such as the Adriatic Sea and the Gulf of Cádiz) display both orders of Milankovitch cyclicity, the Glacial-Interglacial 100-ka periodicity and the higher-frequency 20-ka periodicity (respectively, Ridente et al., 2008; Somoza et al., 1997).

In this paper we present evidence of full composite Milankovitch cyclicity recorded in thick sedimentary successions from a shallow-shelf muddy setting at Gela Basin on the southern Sicilian continental margin (*Figure 6.1*). Two drill sites, the 54.6-m-long GeoB14403 and the 27.5-m-long GeoB14414 from respective water depths of ~193 m and ~146 m, are strategically located to recover key segments of the progradational units related to the Last Glacial-Interglacial cycle and cover MIS 1 – MIS 5 sedimentary units. Accompanied by high-resolution acoustic subbottom imagery, they provide the chronostratigraphic framework for a physical correlation to shelf deposits in order to decipher the internal stratigraphic signature of composite 20-ka/100-ka cyclicity. Coevally, the erosive unconformity related to the Last Glacial Maximum (LGM) exposes undulation features within MIS 5 units that can be compared to those found in late-Holocene HST prodeltas on other Mediterranean margins (e.g., Cattaneo et al., 2004; Urgeles et al., 2007; Rebesco et al., 2009).

In essence, we exploit a rich dataset comprising drilled sedimentary records and high-resolution acoustic profiles in order to (1) develop a multi-proxy based chronostratigraphic framework for boreholes GeoB14403 and GeoB14414 integrating foraminifera-based eco-biostratigraphy and oxygen isotope stratigraphy with bioevents, tephrochronological markers and ^{14}C AMS radiometric datings; (2) establish a precise correlation between the borehole stratigraphy and the shelf depositional sequences to reveal their internal architecture; (3) identify depositional units that can be related to composite Milankovitch cyclicity and associated 100-ka/20-ka glacio-eustatic sea level fluctuations (as defined in GeoB14403 and GeoB14414); and (4) report on evidence of undulated sediment features related to depositional units of the MIS 5 interval (as apparent in acoustic profiles).

6.2 Geologic setting

The Gela Basin represents the most recent (Pliocene-Quaternary) foredeep basin of the Maghrebian fold-and-thrust belt and is filled with as much as 2500m of shallowing-upward marine sediments (*Figure 6.1B*; Colantoni, 1975; Argnani, 1990). It is situated north of the NW-SE-trending

Sicily Strait rift zone that is characterized by relatively deep basins originating from extensional faulting (Finetti, 1984). The corresponding rifting phase initiated in the late Miocene to early Pliocene and lasted through the Quaternary (Grasso, 1993). In the north, Gela Basin is overthrusted by the Gela Nappe – a southwest migrating contractional front representing the southernmost thrust wedge of the Maghrebian chain (*Figure 6.1B*; Argnani, 1990; Butler et al., 1992). Plunging in direction of the basin, the surface slope in the frontal area of Gela Nappe contributes to instability of overlaying sediments and manifests in frequent failure along the shelf edge in the study area (*Figure 6.2*; Trincardi and Argnani, 1990; Minisini et al., 2007; Minisini and Trincardi, 2009; Kuhlmann et al., 2014). To the East, Gela Basin is confined by the Malta Plateau (MP), the seaward counterpart of the Hyblean plateau (HP) on mainland Sicily (*Figure 6.1B*). Separated by the Messinian unconformity, this south-westward dipping carbonatic ramp is overlain by a Pliocene-Quaternary succession of progradational sequences (Barberi et al., 1974; Patacca et al., 1979), resulting in a peculiar setting of SW-dipping sediment bodies in the study area.

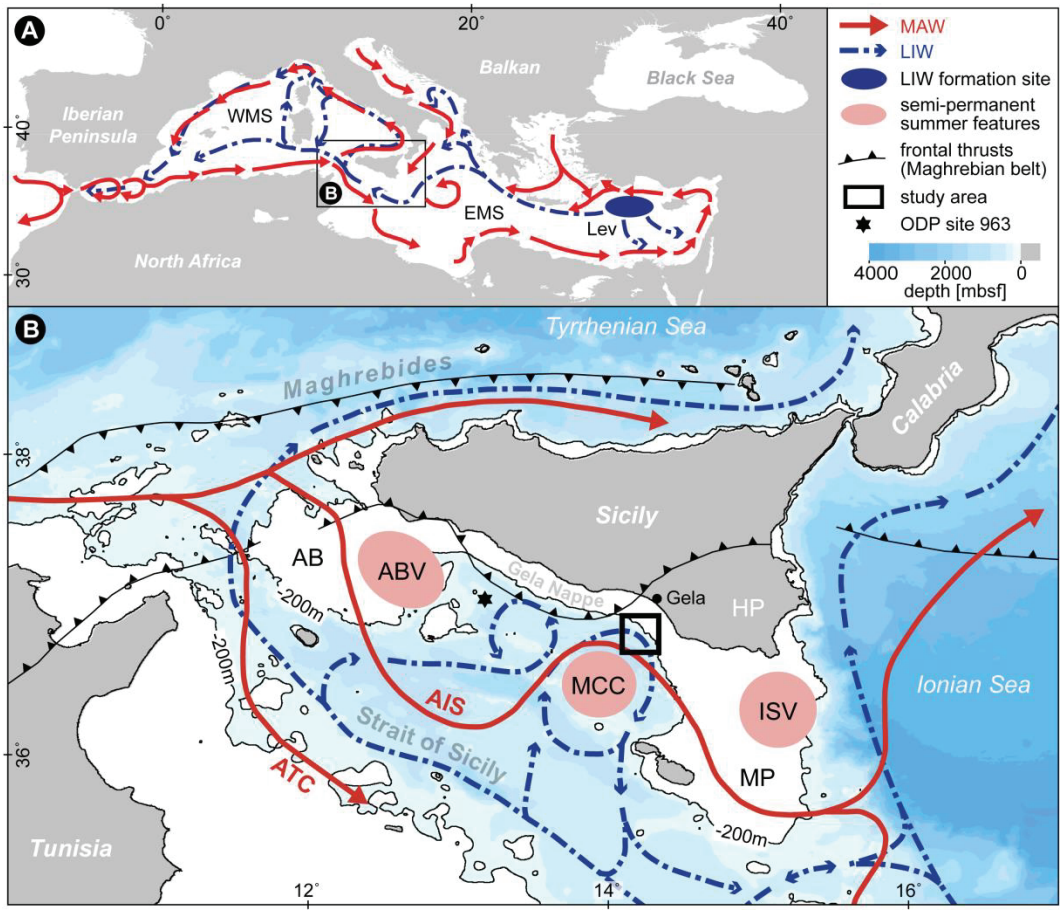

Figure 6.1. A) Main pathways of surface (Modified Atlantic Water, MAW) and intermediate (Levantine Intermediate Water, LIW) waters in the Mediterranean Sea showing formation area of the LIW (after Millot, 1999; Hernández-Molina et al., 2006). WMS = Western Mediterranean Sea; EMS = Eastern Mediterranean Sea; Lev = Levantine Sea. B) Scheme of two-layer exchange circulation in the Strait of Sicily (SoS), modified from Lermusiaux & Robinson (2001), Béranger et al. (2004) and Ciappa (2009). Fresh surface waters from the Atlantic Ocean meander along the Tunisian and Sicilian shelf (red arrows, between 0 and 200 m), accompanied by a concurrent subsurface outflow of relatively more saline Mediterranean waters (blue arrows, between 200 and 600 m). Main water masses: MAW = Modified Atlantic Water, LIW = Levantine Intermediate Water; surface water branches: AIS = Atlantic Ionian Stream, ATC = Atlantic Tunisian Current; mesoscale summer features: ABV = Adventure Bank Vortex (cyclonic); MCC = Maltese Channel Crest (anticyclonic); ISV = Ionian Shelfbreak Vortex (cyclonic); AB = Adventure Bank; HP = Hyblean Plateau; MP = Malta Plateau. Main tectonic elements are redrawn according to Jenny et al. (2006).

6.3 Oceanographic setting

The Strait of Sicily (SoS) connects the eastern and western subbasins of the semi-enclosed Mediterranean Sea and controls water exchange between both (*Figure 6.1A*). At depth it is delimited by two sill systems: to the east, connection with the Ionian Sea is established through a ~560 m deep passage south of Malta Plateau (MP; *Figure 6.1B*); on the western side, connection to the Tyrrhenian Sea is composed of two passages of about 365 and 430 m depth, respectively (Astraldi et al., 2001). Large scale circulation in SoS is driven mainly by anti-estuarine thermohaline circulation of the Mediterranean Sea, ultimately forced by a negative hydrological balance and the density gradient with regard to the Atlantic Ocean (Robinson and Golnaraghi, 1994). It can be schematized as a two-layer flow regime involving an eastward directed fresher surface layer occupying the first 100-200 m of water column (Modified Atlantic Water, MAW) and a westward flowing salty bottom layer, mainly consisting of Levantine Intermediate Water (LIW) (*Figure 6.1B*; Astraldi et al., 1999; Robinson et al., 1999; Sammari et al., 1999). The latter forms in the Rhodes area through cooling of surface water and associated salt enrichment during winter convection events in February-March (*Figure 6.1A*; POEM group, 1992). At the entrance of SoS, approximately one third of MAW enters the Tyrrhenian Sea and follows the northern coast of Sicily (Bethoux, 1980), with the remainder splitting into two branches (Herbaut et al., 1998; Robinson et al., 1999; Béranger et al., 2004): (1) the Atlantic Tunisian Current (ATC) following the 200 m isobaths southward over the Tunisian shelf (Sammari et al., 1999; Onken et al., 2003; Béranger et al., 2004), and (2) the Atlantic Ionian Stream (AIS) meandering south-eastward off the southern coast of Sicily (Lermusiaux and Robinson, 2001; Béranger et al., 2004). ATC is thought to be more energetic in winter (Pierini and Rubino, 2001; Sorgente et al., 2003; Béranger et al., 2004), while in summer most of MAW is advected by the AIS meandering around three semipermanent mesoscale structures, the cyclonic Adventure Bank Vortex (ABV), the anticyclonic Maltese Channel Crest (MCC) and the cyclonic Ionian Shelfbreak Vortex (ISV) (*Figure 6.1B*; Robinson et al., 1999; Lermusiaux and Robinson, 2001). Finally, AIS enters the Ionian Sea, where it feeds the Mid-Mediterranean Jet on its way to the central Levantine basin in the eastern Mediterranean Sea.

The study area at Gela Basin is situated along the northern tip of MCC (*Figure 6.1B*), where the long-term impact of deep contour-parallel bottom currents associated to LIW has been related to both erosional and depositional features (Verdicchio & Trincardi, 2008). Anticyclonic subsurface eddies in this region are reported to reach velocities in excess of 13 cm/s (Lermusiaux and Robinson, 2001) and may severely impact the regional sediment transport and dispersal patterns.

6.4 Materials and methods

This work is based on a dense grid of acoustic subbottom profiles and sediment cores acquired by MARUM aboard RV Maria S. Merian during cruise MSM15/3 in 2010. Main acoustic devices used include a parametric sediment echosounder with dm-scale vertical resolution operating at 4 kHz (Atlas Parasound) and two bathymetric multibeam echosounder systems (Kongsberg Simrad EM120 and EM1002) operating at 12 kHz and 95 kHz, respectively. Sequence stratigraphic analysis and line tracing of prominent seismic reflectors was facilitated by complementing Chirp sonar profiles acquired by ISMAR (CNR) using a 2-7 kHz sweep-modulated band width (Minisini et al., 2007; Minisini & Trincardi, 2009).

6.4.1 Coring

Drill sites GeoB14403 and GeoB14414 sample the undisturbed shelf deposits nourishing recent slope failures at average recovery rates of 87 % and 86 %, respectively (*Figure 6.2*). Each site is composed of a single gravity core (GC), accompanied by one or two deep-drilled sequences collected with the Bremen

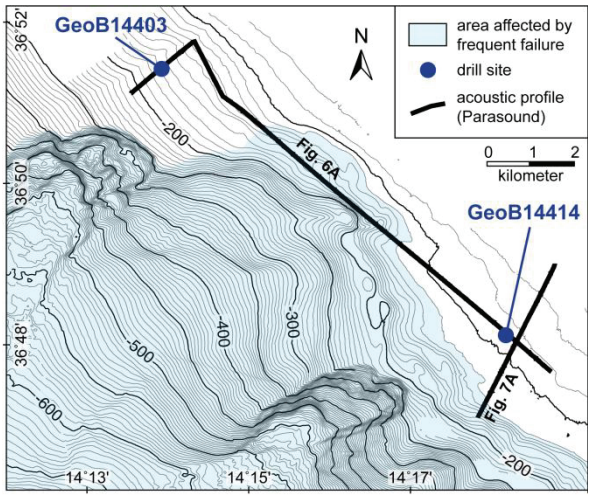

Figure 6.2. Bathymetric isobaths along the shelf edge of NE Gela Basin and location of drill sites GeoB14403 and GeoB14414 (see *Figure 6.1* for geographic context). Distal parts of the study area are affected by both exposed and buried slope failures. Track lines refer to acoustic subbottom profiles reported in *Figures 6.6A* and *6.7A*.

seafloor drill rig MeBo (Freudenthal and Wefer, 2007; Freudenthal and Wefer, 2013). Required adaption of the core depth schemes were carried out based on core-seismic correlation of the prominent erosive unconformity ES1 related to the LGM as well as adjustment through foraminiferal assemblages and core-physical measurements (Kuhlmann et al., 2014). An overview of core meta data is provided in *Table 6.1*. The dominant lithology of the homogeneous sedimentary record is silty nannofossil clay with quartzose silt, accompanied by minor amounts of foraminifera and authigenic pyrite (Kuhlmann et al., 2014).

6.4.2 *Micropaleontology*

For foraminiferal analysis, subsamples of 1 cm (GC) and 2 cm (MeBo) thickness were obtained with a vertical resolution of at least 20 cm throughout the core (a total of 247 samples at site 14403 and 142 at site 14414). Temporal resolution of the foraminiferal records, however, varies with the sediment accumulation rates (SAR) from about 105 to 650 yrs. The subsamples were freeze-dried, soaked in distilled water and washed over a 63 µm mesh sieve (Schröder et al., 1987). The foraminiferal content was examined with an optical microscope and a semiquantitative analysis was performed on the fraction >63 µm mesh sieve. Note that *Globigerinoides ruber* comprises *Globigerinoides ruber* (pink and white varieties) and *Globigerinoides elongatus*, while *Globigerinoides sacculifer* includes *Globigerinoides trilobus*, *Globigerinoides quadrilobatus* and *Globigerinoides sacculifer* according to Hemleben et al. (1989).

6.4.3 *Tephra extraction and chemical analysis*

In this study, the analysis of tephra layers serves as a complementary tool towards a robust core age model rather than forming the basis of a comprehensive tephrostratigraphic study. Tephra detection was hence limited to layers visible to the naked eye and containing analysable glass shards in the size fraction > 40 µm, thus excluding potential cryptotephra and tephra layers featuring smaller sized particles. Given these limitations, a single tephra-rich layer of dm-scale exhibiting normal grading and a relatively sharp base could be identified, intercalated at site GeoB14403 in a depth of ~28.4 mbsf. Sample material was washed over a 40 µm sieve and glass shards were hand-picked, mounted on epoxy resin beads and suitably polished to avoid compositional variations related to surface alteration processes. Major element analysis was obtained using wavelength-dispersive spectrometry electron probe

Table 6.1. Overview of core meta data at boreholes GeoB14403 and GeoB14414.

Name	Type	Water depth	Position		Top depth	Bottom depth	Length	Recovery rate
		[mbsl]	Latitude	Longitude	[mbsf]	[mbsf]	[m]	
GeoB14403-1	gravity core (GC)	193.4	36°51.41'N	14°13.92'E	0.07	7.83	7.76	100%
GeoB14403-2	MeBo	191.5	36°51.44'N	14°13.92'E	5.55	18.24	12.69	83.9%
GeoB14403-8	MeBo	182.0	36°51.41'N	14°13.91'E	17.57	54.57	37.00	85.3%
GeoB14414-1	MeBo	146.0	36°48.13'N	14°18.17'E	0.50	27.48	26.98	81.8%
GeoB14414-2	gravity core (GC)	145.2	36°48.14'N	14°18.18'E	0.00	7.71	7.71	100%

microanalysis (WDS-EPMA) in order to ensure compatibility with lacustrine and marine key datasets (e.g. Wulf et al., 2004; Bourne et al., 2010). A JEOL JXA 8200 housed at the GEOMAR Helmholtz Centre for Ocean Research Kiel (Kiel, Germany) was utilised, operating with a 15 kV accelerating voltage, a 6nA current and a 5µm beam diameter. For calibration and monitoring, a combination of glass and mineral standards from the Smithsonian collection of natural reference materials (Jarosewich et al., 1980) was used. For data comparison, all analytical results were normalized to 100% water- and volatile-free. The complete analyses are provided in the supplementary data.

Trace element contents were determined by laser ablation inductively coupled plasma mass spectrometry (LA-ICP-MS) using a Thermo Element2 coupled to a NewWave UP193ss (wavelength 193 nm) at the Department of Geosciences at Bremen University. Helium (0.8 l/min) was used as carrier gas and argon (0.8-0.9 l/min) was added as make-up gas, while plasma power was 1200 W. Formation of oxides in the plasma was low (ThO/Th ca. 0.15%) so that no interference corrections were applied. Samples and standards were ablated with an irradiance of ~1 GW/cm^2 and a pulse rate of 5 Hz. Beam diameter varied between 25 and 35 µm, and the sample was moved at 5 µm/s. Prior to ablation, the blank intensities were acquired during 25 s. All isotopes were analyzed at low resolution with five samples in a 20% mass window and a total dwell time of 25 ms per isotope. For data quantification the Cetac GeoPro™ software was used with ^{43}Ca as internal standard and ATHO-G rhyolite glass (Jochum et al., 2000) as external calibration standard. Analytical quality was controlled by repeated analyses of andesite glass StHs6/80-G (Jochum et al., 2000) and yielded precision <5% and accuracy <10% for most elements (see supplementary data).

6.4.4 Radiometric dating

Samples for radiometric dating were taken from selected core horizons in order to corroborate stratigraphic interpretations inferred from micropaleontological considerations. Analyses were performed by the Poznan Radiocarbon Laboratory (PRL, Poznan, Poland) and the National Ocean Sciences Accelerator Mass Spectrometry Facility (NOSAMS, Woods Hole Oceanographic Institution, USA) on mono-specific and mixed foraminifera in the size fraction >63 µm (*Table 6.2*). Obtained AMS ^{14}C ages were converted into 2σ calibrated ages using Calib 7.0.0 Radiocarbon Calibration Program (Stuiver and Reimer, 1993) and the Marine13 calibration data set (Reimer et al., 2013). The reservoir correction was selected from the Calib database for the Strait of Sicily, with a calculated weighted mean ΔR value of 71 years and a standard derivation of 50 years (Siani et al., 2000). All dates reported are given in calibrated

Table 6.2. AMS ^{14}C and calibrated ages based on monospecific and mixed foraminifera.

Lab #	Core	Section # and depth [cm]	Material	^{14}C age [yrs BP]	2σ cal. intercept [cal. ka BP]
Poz-53709	GeoB14403-1 (GC)	II 80-83	*G. ruber, G. sacculifer*	5285 ± 35	5.58 ± 0.13
Poz-53710	GeoB14403-1 (GC)	IV 20-22	*G. ruber, G. sacculifer*	7870 ± 35	8.26 ± 0.12
Poz-53711	GeoB14403-1 (GC)	IV 80-83	*U. peregrina*	9110 ± 50	9.75 ± 0.22
Poz-53712	GeoB14403-1 (GC)	V 40-42	*C. laevigata carinata*	11010 ± 60	12.40 ± 0.24
Poz-53713	GeoB14403-2 (MeBo)	3P-2 32-36	*U. peregrina*	25750 ± 160	29.32 ± 0.44
OS-106891	GeoB14403-2 (MeBo)	4P-1 61-67	*E. crispum, M.barleeanum, C. lobatulus*	29300 ± 490	32.72 ± 1.13
Poz-53715	GeoB14403-2 (MeBo)	5P-1 86-99	*H. balthica, C. pachyderma*	34000 ± 360	37.69 ± 0.99
OS-106838	GeoB14403-2 (MeBo)	6P-1 57-64	*H. balthica, U. peregrina, M. barleeanum*	41600 ± 890	44.56 ± 1.51
OS-106892	GeoB14403-8 (MeBo)	2P-cc 3-11	*U. peregrina*	50400 ± 6800	^
Poz-53716	GeoB14403-8 (MeBo)	5P-1 100-119	*U. peregrina, B. marginata*	47000 ± 2000	^
Poz-53717	GeoB14414-2 (GC)	V 60-62	*U. peregrina*	10520 ± 50	11.58 ± 0.31
Poz-53745	GeoB14414-2 (GC)	VI 40-43	*A. beccarii, C. lobatulus, E. crispum*	31240 ± 300	34.69 ± 0.60*

Calibration is based on Calib 7.0.0 Radiocarbon Calibration Program (Stuiver & Reimer, 1993). Calibration data set: Marine13 according to Reimer et al. (2013). Reservoir correction: The calculated weighted mean ΔR value is 71 with a standard derivation of 50 (Siani et al., 2000). Symbology: ^ = ^{14}C age exceeds calibration limit; * = rejected dating (see text for reasons).

thousands of years before present (cal. ka BP).

6.4.5 Stable isotope analysis

Subsamples obtained for micropaleontology (20 cm resolution) were equally used to determine oxygen and carbon isotopic compositions of the benthic *Bulimina marginata* (234 measurements at site GeoB14403 and 102 at site GeoB14414) and the planktonic *Globigerinoides ex gr. ruber* (142 at site GeoB14403 and 113 at site GeoB14414). Hand-picked specimens showing no signs of diagenetic alteration were ultrasonically cleaned to remove contaminants such as overgrowths, coccoliths and detrital infilling. Analyses were performed at the Zentrum für Marine Umweltwissenschaften (MARUM, Bremen, Germany) using a Finnigan MAT 252 mass spectrometer coupled with a carbonate preparation device type "Bremen". Isotopic composition is expressed as per mil (‰) deviation with respect to the Pee Dee Belemnite (PDB) standard, with a long-term laboratory analytical standard deviation of < 0.07 ‰ for the stable oxygen and < 0.05 ‰ for the stable carbon isotope data. Note that none of the isotopic data presented here has been corrected for the ice-volume effect.

6.5 Chronostratigraphic framework

The chronological framework for the recovered cores follows a multi-proxy approach and is based on (1) an eco-biostratigraphy relying on main microfaunistic bioevents, (2) a tephrochronological analysis on the basis of single glass shards, (3) foraminifera-based radiometric datings, and (4) an oxygen isotope stratigraphy identifying both Marine Isotope Stages and Substages (MIS) as well as Dansgaard-Oeschger Interstadials (D/O). Results from these stratigraphic proxies including obtained age control points (*Table 6.4*) funnelled in a detailed age model that provides the chronostratigraphic basis for a successive calibration of the shelf deposits at Gela Basin.

6.5.1 Foraminifera biostratigraphy

The foraminifera-based eco-biostratigraphy relies on the identification of (temporary) disappearance and (re)occurrence of foraminifera species already recorded in this area (e.g., Sprovieri et al., 2003; Minisini et al., 2007; Rouis-Zaragouni et al., 2010; Incarbona et al., 2010) and in nearby Central Mediterranean basins (see also Capotondi et al.,1999; Negri et al., 1999; Ducassou et al., 2007; Melki et al., 2009; Incarbona et al., 2008; Piva et al., 2008; Siani et al., 2010; Lirer et al., 2013). The following bioevents were recognized in the two boreholes:

- Peak of *Globorotalia truncatulinoides* right coiling clearly recorded during the late Holocene in the Channel of Sicily by Sprovieri et al. (2003), Minisini et al. (2007) and Rouis-Zaragouni et al. (2010). A similar bioevent has been also reported by Capotondi et al. (1999) for the Tyrrhenian Sea
- LCO *Neogloboquadrina pachyderma* at top of Sapropel 1 equivalent and predating the maximum flooding surface
- Temporary disappearance of *G. truncatulinoides* along with a *Globorotalia inflata* frequency minimum detecting the base of Sapropel 1 equivalent (Sprovieri et al., 2003, Minisini et al., 2007)
- Temporary absence of *Globorotalia inflata* in MIS3. *Globorotalia inflata* is absent after 33-39 ka BP in the Gulf of Lyon (core BC15 by Rohling et al., 1998 and core MD99-2346 by Melki et al., 2009), it shows very scarce but continuous presence after 33 ka BP in the South Tyrrhenian (core LC07 by Incarbona et al., 2008), it is absent after 39 ka BP in the Adriatic basin (borehole PRAD1-2 after Piva et al., 2008 and Bourne et al., 2010) and after ca. 35 ka BP in the Eastern Mediterranean (core 84MD637 by Ducassou et al. 2007) and shows continuous but scattered presence in the Alboran Sea (cores MD95-2043 and ODP 977 by Pérez-Folgado et

al., 2003). On the basis of the $\delta^{18}O$ stratigraphy developed in this study and supported by radiocarbon datings, this interesting widespread bioevent, present in the Central and Eastern Mediteranean, shows an age of ca. 38 ka BP in correspondence of the base of the D/O 8.

In addition to the above described bioevents, changes in composition of the planktonic and benthonic foraminifera assemblages and their paleoenvironmental interpretation play an important role in biostratigraphy (cenozones): the detecting and interpretation of paleoenvironmental variations represent a good tool to obtain an event stratigraphy. In *Table 6.3* we report a list of planktonic (P) and benthonic (B) foraminifera biofacies, each described by a characteristic assemblage along with the environment they reflect, the appropriated references, to which the reader is referred for more information, and the time interval during which they occur in the two investigated boreholes. For each assemblage the key species (if abundant or very important for paleoenvironmental reconstruction) are marked in bold, while common and rare taxa are highlighted in underlined italics and in italics, respectively.

In general, the sequence of the biofacies in the two boreholes describes climate cyclicity (for instance, cold/warm intervals), paleoceanographic changes (related to important paleoceanographic/ paleoclimatic events at regional scale, such as Sapropel deposition in the Eastern Mediterranean) and sea-level fluctuations.

In both boreholes the warmest water planktonic assemblage (PIa), quite similar to the modern one, corresponds to the Holocene interval (Interglacial), while in borehole GeoB14403 the temperate assemblages PIIa and PIIb identify mainly D/O warm oscillations. The cold water biofacies PIII and PIV, characterized also by not abundant assemblage, are mainly related to cold intervals (for instance MIS 4 in GeoB14403) as defined by the $\delta^{18}O$ stratigraphy. In borehole GeoB14414 the interval below 12m is largely dominated by biofaces PIb, indicating Interglacial conditions different by the Holocene, with persistent presence of warm species along with neogloboquadrinids (*N. pachyderma* and *N. dutertrei*) and absence of *G. inflata* and *G. truncatulinoides*. This biofacies is compatible with the assemblage reported by Incarbona et al. (2010) for the MIS 5e in the Channel of Sicily.

The benthic foraminifera biofacies reflect changes in the bottom conditions, from BI (typical of outer shelf/upper slope) to BIV (inner shelf) through mid-shelf biofacies (BII and BIII) with assemblages somehow relatable to the modern clay belt environment (see Van der Zwaan and Jorissen, 1991 for the interpretation model). Biofacies BIV represents the shallowest environment and includes inner shelf (*Ammonia* + *Elphidium*) and epiphytic species. It is, nevertheless, always recorded within other deeper biofacies. Hence, these species are always interpreted as displaced. Biofacies V is composed by terrigenous, also oxidized, including broken and/or filled foraminifera tests, suggesting reworking. It is further related to the presence of erosional surfaces in the seismic profiles.

At last, it is worthy to highlight three intervals characterized by planktonic and benthonic assemblages (biofacies PSa, PSb, PSc, BSa, BSb) composed by species/ecophenotypes indicating peculiar paleoceanographic conditions: positioned within the Holocene, biofacies PSa records, among the other taxa, *G. ruber rosea*, absence of *G. truncatulinoides* and a frequency drop of *G. inflata*. It is coeval with the deposition of the Sapropel 1 in the Eastern Mediterranean, as already reported by Sprovieri et al. (2003) and Minisini et al. (2007) in the Channel of Sicily.

The temperate biofacies PSb is here related to the Sapropel 3 deposition because of the presence of neogloboquadrinids (*N. pachyderma* and *N. dutertrei*), presence of *G. inflata*, absence of *G. truncatulinoides*, and small *G. scitula* (Doucassou et al., 2007; Incarbona et al., 2010; Piva et al., 2008). Moreover, the concurrent presence of the benthic biofacies BSa, indicating low oxygen condition at the bottom,

Table 6.3: planktonic and benthonic foraminifera biofacies defined for the boreholes GeoB14403 and GeoB14414.

Biofacies	Assemblage	Environment	References	Time interval
PIa	***Globigerinoides ruber***, ***Globorotalia inflata***, ***Globorotalia truncatulinoides* l.c.** , *Orbulina*, *Globigerinoides sacculifer*, *Globigerinella aequilateralis*, *Globigerina bulloides*, *Globigerina quinqueloba*, *Globigerina praecalida*, *Zeaglobigerina rubescens*	Warm water assemblage with deep dwellers (winter mixing)	Thunell (1978), Hemleben et al. (1989), Pujol and Vergnaud-Grazzini (1995)	Interglacial (Holocene)
PIb	***G. ruber***, *Orbulina*, *G. sacculifer*, *G. aequilateralis*, *G. bulloides*, *G. quinqueloba*, *G. praecalida*, *Z. rubescens*, *Neogloboquadrina pachyderma* r.c., *Neogloboquadrina dutertrei*	Warm water assemblage without deep dwellers (no winter mixing), Deep Chlorophyll Maximum developed	Thunell (1978), Hemleben et al. (1989), Pujol and Vergnaud-Grazzini (1995)	Interglacial (lower interval in GeoB 14414)
PIIa	***G. ruber***, *G. bulloides*, *G. inflata*, ***N. pachyderma* r.c.**, *Globigerinita glutinata*, *Orbulina*, *G. quinqueloba*, *G. praecalida*	Temperate water assemblage, DCM developed, winter mixing	Thunell (1978), Hemleben et al.(1989), Pujol and Vergnaud-Grazzini (1995)	Interstadials (DOIS 20 and 16 in GeoB 14403)
PIIb	***G. ruber***, *G. bulloides*, ***N. pachyderma* r.c.**, *G. glutinata*, *Orbulina*, *G. quinqueloba*, *Z. rubescens*	Temperate water assemblage, DCM developed, no winter mixing	Thunell (1978), Hemleben et al. (1989), Pujol and Vergnaud-Grazzini (1995)	Interstadials (DOIS 8,7 and 6 in GeoB 14403) and Interglacial (lower interval in GeoB 14414)
PIII	planktonic assemblage scarce (*G. quinqueloba*, *G. inflata*, *G. bulloides*, *N. pachyderma* r.c., *G. ruber*)	Cold and productive water assemblage	Thunell (1978), Hemleben et al. (1989), Pujol and Vergnaud-Grazzini (1995)	Stadials
PIV	***G. quinqueloba***, ***N. pachyderma* r.c.**, ***G. bulloides***, *G. ruber*, *G. glutinata*	Cold and productive water assemblage	Thunell (1978), Hemleben et al. (1989), Pujol and Vergnaud-Grazzini (1995)	Stadials
PSa	***G. ruber***, *G. inflata* R, *G. ruber rosea*, *Orbulina*, *G. sacculifer*, *G.aequilateralis*, *G. bulloides*, *G. quinqueloba*, *G. praecalida*, *Z. rubescens*	Warm water assemblage with strong decrease of deep dwellers (weak winter mixing)	Negri et al. (1999), Sprovieri et al. (2003), Minisini et al.(2007)	Interval related to the Sapropel 1 deposition
PSb	***G. ruber***, ***G. inflata***, *G. bulloides*, ***N. pachyderma* r.c.**, ***N. dutertrei***, *G. glutinata*, *Globorotalia scitula*, *Orbulina*, *G. quinqueloba*, *Globigerina praedigitata*	Temperate water assemblage, DCM developed, winter mixing, possible surface water freshening	Rohling and Gieskes (1989), Negri et al. (1999)	Interval related to the Sapropel 3 deposition
PSc	***G. ruber* FF (var. *rosea* with thin and inflated chambers)**, *G. bulloides*, ***N. pachyderma* r.c.**, ***N. dutertrei***, ***Z. rubescens, G.sacculifer***, *G. glutinata*, *Orbulina*, *G. quinqueloba*, *G. aequilateralis* **(no *Globorotalia*)**	warm water assemblage, DCM developed, no winter mixing, surface water freshening	Rohling and Gieskes (1989), Negri et al. (1999), Cane et al. (2002), Incarbona et al. (2010)	Interval related to the Sapropel 5 deposition
BI	***Brizalina catanensis* F**, *Cassidulina laevigata carinata*, *Uvigerina peregrina*, *Uvigerina mediterranea*, *Bulimina marginata*, *Hyalinea balthica*, *Globocassidulina subglobosa*, *Cibicidoides pachyderma*, *Gyroidinoides umbonatus*, *Bulimina inflata*, *Bigenerina nodosaria*	outer-shelf/upper slope (mesotrophic environment)	Jorissen (1987), De Stigter et al. (1998), De Rijk et al. (1999), Schmiedl et al. (2000)	Interglacial (Holocene) and Interstadial DOIS 20 (GeoB 14403)
BIIa	***C. laevigata carinata* F or FF**, *Elphidium decipiens*, *U. mediterranea*, *U. peregrina* , *B. aenariensis M.barleeanum*, *H. balthica*, *G. subglobosa*, *V. complanata*	mid-outer shelf	Jorissen (1987), Van der Zwaan and Jorissen (1991), De Stigter et al. (1998), Schmiedl et al. (2000)	Interstadials (GeoB 14403)
BIIb	***C. laevigata carinata* F or FF**, *Elphidium decipiens*, *M. barleeanum*, *H. balthica*, *G. subglobosa*, *Valvulineria complanata*, *U. peregrina* , *B. alata*	mid shelf, external to the modern clay belt, far from riverine influence	Jorissen (1987), Van der Zwaan and Jorissen (1991), De Stigter et al. (1998), Schmiedl et al. (2000)	Stadials and pars of lower Interglacial in GeoB14414
BIII	***C. laevigata carinata* + *V. complanata*** + *E. decipiens* + ***Nonionella turgida***	mid shelf (close to the outer modern clay belt)	Van der Zwaan and Jorissen (1991)	Stadials
BIV	*Ammonia beccarii*, *Elphidium crispum*, *Rosalina globularis*, *Asterigerinata mamilla*, *Reussella spinulosa*	Inner shelf species (including epiphytic species)	Jorissen (1987), Langer (1993)	Species frequently present between 7 and 38 m in GeoB 14403
BV	oxidized and fine terrigenous; foraminifera broken and fill C, shell remains	Reworked sediment and microfauna		Close to erosional surfaces
BSa	***U. peregrina***, *B. marginata*, *B. catanensis*, *Brizalina alata, Brizalina dilatata*, *Globobulimina affinis*, *Chilostomella mediterranensis*, *Fursenkoina* spp, *H. balthica*, *C. pachyderma*,,*C. laevigata carinata*, *G. subglobosa*, *Bulimina inflata/costata*, *M. barleeanum*	outer-shelf/upper slope (mesotrophic environment, with more organic matter accumulation and lower bottom ventilation as B I)	Jorissen (1987,1999), De Stigter et al. (1998), De Rijk et al. (1999), Schmiedl et al. (2000)	Sapropel 1 and 3 deposition
BSb	***B. catanensis FF,*** *B. marginata, G. affinis, C. mediterranensis, C. laevigata carinata, M. barleeanum, Florilus boueanum, F. complanata, Brizalina aenariensis, B. alata, Cassidulinoides bradyi, Uvigerina bononiensis, B. costata, A beccarii* and *E. decipiens* R; **abundant vegetal remains**	outer-shelf/upper slope (mesotrophic environment, with high organic matter accumulation and lower bottom ventilation, fluvial runoff)	Jorissen (1987,1999), De Stigter et al. (1998), De Rijk et al. (1999), Schmiedl et al. (2000)	Sapropel 5 deposition

supports the correlation with the interval of the Sapropel 3 deposition.

The biofacies PSc contains *G. ruber rosea* very frequent with thin tests and inflated chambers along with abundant *N. pachyderma* r.c. and *N. dutertrei*, *Z. rubescens* and *G. sacculifer* as well as absence of globorotaliids, suggesting very warm waters, strong oligotrophy in the mixed layer, and development of a Deep Chlorophyll Maximum, surface water freshening and water column stratification. The concurrent light $\delta^{18}O$ *G. ruber* values along with the benthic biofacies BSb dominated by infaunal and deep infaunal species (low oxygen and high accumulation of organic matter tolerant) strongly support the correlation with Sapropel 5 deposition (Rohling and Gieskes, 1989; Negri et al., 1999; Cane et al., 2002; Doucassou et al., 2007). The abundance of vegetal remains may point out riverine influence, in turn possibly linked to rainy conditions.

The recognition of biostratigraphic and paleoceanographic conditions on shelf environments correlatable with the Sapropel deposition in Eastern Mediterranean in sequences not displaying clear lithologic evidences (dark sediment) is very important, as these Sapropel-equivalent intervals can be used as additional tool for the chronology (see Piva et al., 2008).

6.5.2 Tephra analysis

In order to determine proximal counterparts and origin of the GeoB14403 tephra layer the geochemical compositions of extracted glass shards and selected key tephra layers from other Mediterranean sites are presented in *Figure 6.3*. Glass shards from tephra GeoB14403 has a trachytic to phonolitic composition (*Figure 6.3A,B*) and correlates well with lacustrine ash layers TM-19 and TM-20 from Lago Grande di Monticchio (Wulf et al., 2004; Tomlinson et al., in review), the marine equivalents PRAD 1870 (central Adriatic Sea; Bourne et al., 2010) and Y-7 (core RC9-191, Ionian Sea; Keller et al., 1978) as well as the terrestrial pumice fall from the Monte Epomeo Green Tuff (MEGT) eruption of Ischia (Brown et al., 2008). Glasse show a consistent dominance of sodium over potassium ($K_2O/Na_2O < 1$) and mainly fall within the typical range of Ischia volcanic eruptions, as defined by Paterne et al. (1988) and the selected reference data sets (*Figure 6.3C*). Identified affinity between samples is reflected by strong similarity of trace elemental patterns (*Figure 6.3D*). However, the data reveal a twofold compositional nature of tephra GeoB14403, bearing a strong resemblance to TM-19 and TM-20 datasets (Tomlinson et al., in review), respectively. Wulf et al. (2004) ascribed TM-19, which has been directly dated by $^{40}Ar/^{39}Ar$ to 55 ± 2 ka (Watts et al., 1996), to the MEGT *Tufo verde Epomeo sensu strictu* (TVEss) eruption of Ischia. TM-20 was correlated with the marine Y-7 tehpra, dated on sanidine by $^{40}Ar/^{39}Ar$ to 56 ± 4 ka (Kraml, 1997; Allen et al., 1999). Its terrestrial equivalent is thought to relate to the Unita di Monte San Angelo (UMSA), an early phase of the Ischia MEGT eruption (Wulf et al., 2004). As suggested by the trace elemental data, the stratigraphic record at site GeoB14403 seems to comprise the distal fallout facies of both eruption phases (TVEss and UMSA) and hence suggests a significant dispersal from their source area Ischia towards the south. Following considerations of Bourne et al. (2010) made for the PRAD1870 tephra the age of 56 ± 4 ka was preferred in the age-depth model (*Table 6.4*), linking tephra GeoB14403 with the marine marker tephra Y-7.

6.5.3 Isotope stratigraphy

At both drill sites, oxygen stable isotope compositions of the planktic foraminifer *G. ruber* and the benthic *B. marginata* show consistent, subparallel trends along the full length of recovered sequences (*Figure 6.4*). The benthic records are systematically shifted towards heavier isotopic composition, with sporadic gaps at certain intervals relating to poor core recovery in these depths. Isotopic compositions show clear and significant oscillations within a range of about 3‰, allowing not only the reconstruction of

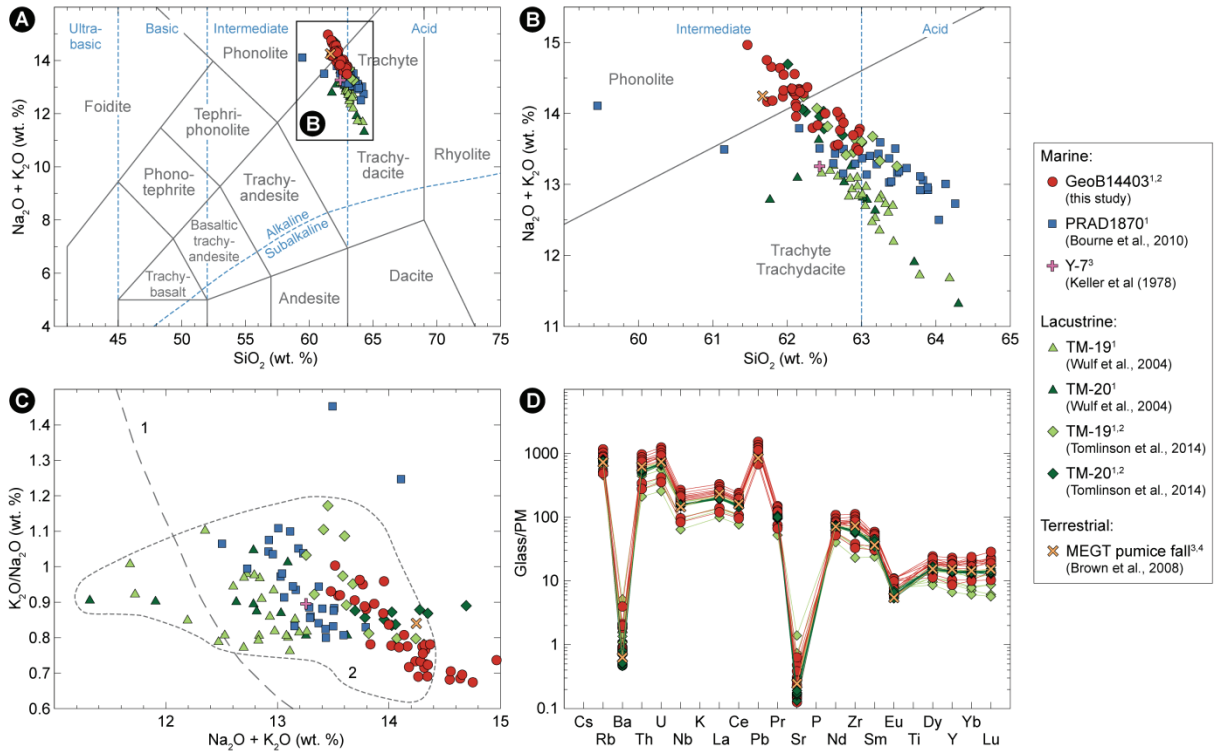

Figure 6.3. Chemical correlation of GeoB14403 tephra layer with marine, lacustrine and terrestrial equivalents. Major and trace elemental data are based on single glass shard (marine and lacustrine sources) and whole rock analyses (terrestrial source), major element compositions are normalized to 100% water- and volatile-free. Methods of data acquisition: [1] = WDS-EPMA, [2] = LA-ICP-MS, [3] = XRF, [4] = ICP-MS. (A) and (B): Total alkali vs. silica plot (Le Bas et al., 1986) illustrating the trachytic to phonolitic composition of the GeoB14403 tephra. (C): Alkali ratio biplot reveals distinctive groupings of ash layers. Compositional range of tephra from the Campanian Volcanic Zone (1) and Ischia (2) are shown for comparison, based on Paterne et al. (1988), Wulf et al. (2004) and Bourne et al. (2010). (D): Primitive mantle-normalized (Sun and McDonough, 1989) incompatible element-diagram reveals twofold compositional nature of GeoB14403 glass shards, suggesting equivalency to lacustrine tephra TM-19 and TM-20, respectively.

main stratigraphic events relating to the Last Glacial-Interglacial cycle (Marine Isotope Stages, MIS), but as well the identification of superimposing subordinate climatic oscillations (Dansgaard-Oeschger events, D/O).

Major gaps in the planktic records are apparent between 30 and 34 mbsf at site GeoB14403 and between 9 and 12 mbsf at site GeoB14414. These intervals represent periods of colder climate and lowered eustatic sea level (e.g. Glacials and Stadials), limiting the growth of planktic foraminifera (mainly the deep-dwellers) and causing dilution-related scarcity in the terrigenous-rich sediment samples.

At around 10 mbsf (site GeoB14403) and 7 mbsf (site GeoB14414), the erosive unconformity ES1 related to the sea level lowstand during the Last Glacial Maximum (LGM) provides a depositional hiatus and subdivides the isotopic records, further related to as upper and lower core sections. The most abrupt isotopic shifts in the upper core sections are apparent at approximately 7 mbsf at site GeoB14403 and 5.5 mbsf at site GeoB14414, where isotope valuesof *B. marginata* fall from a maximum of approximately 3.5‰ to values around 1.5‰. Paralleled by similar shifts in the *G. ruber* record ranging from 1.5‰ to -0.5‰, these patterns can be ascribed to isotopic Termination I at the end of MIS 2.

The lower core sections beneath ES1 show very distinctive isotopic patterns for each drill site, which relate to the peculiar stratigraphic setting of SW dipping sediments and associated differences in the recovered units. The lowest part of site GeoB14414 (below 12 mbsf) samples a stratigraphic unit of isotopic uniformity with only minor variations especially for the benthic record, pointing towards a

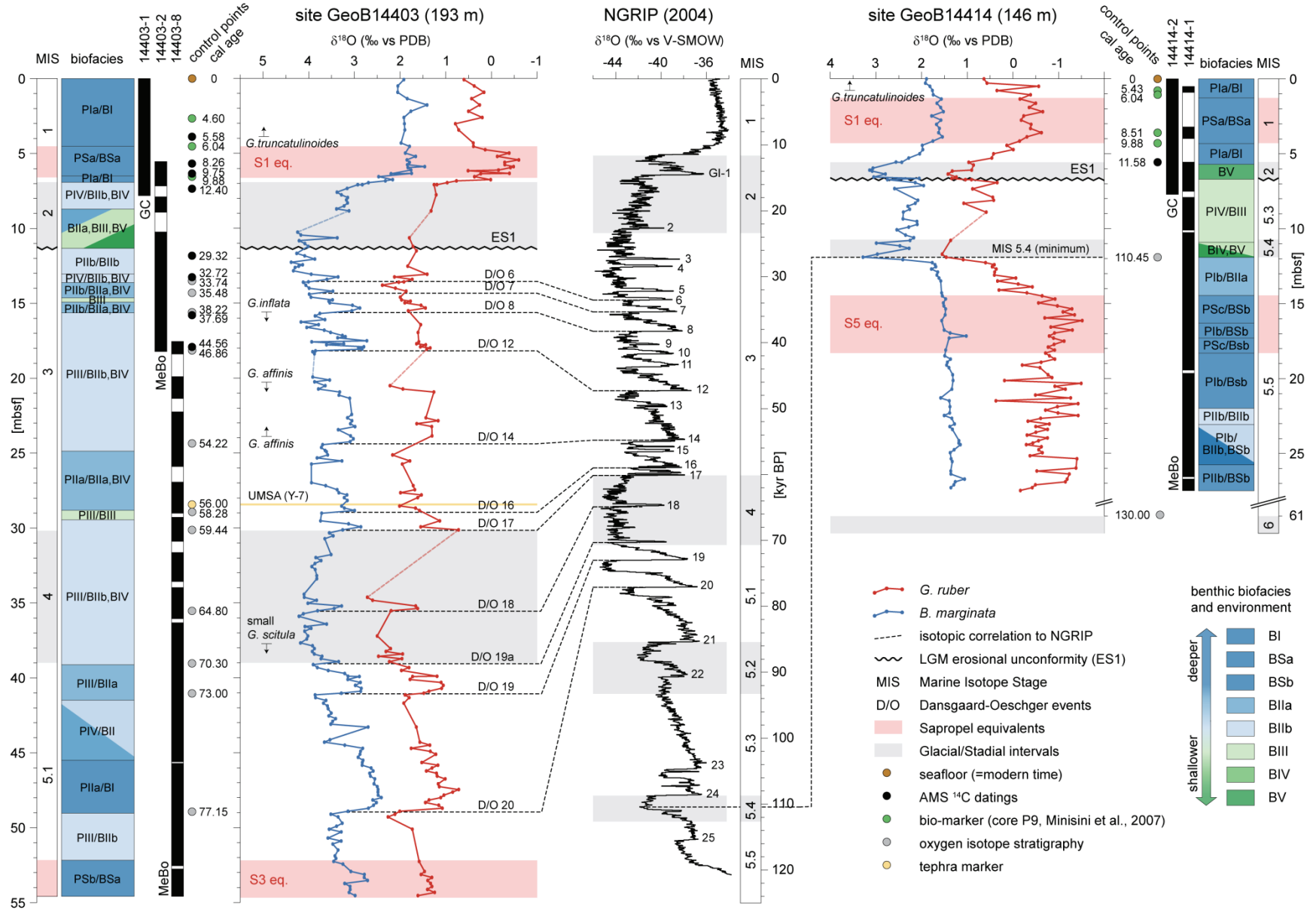

Figure 6.4. Overview of the stratigraphic framework for drill sites GeoB14403 and GeoB14414 illustrating the distribution of biofacies (colour-coded with regard to the appropriate environmental conditions as indicated by benthic foraminifera), drill schemes, position and calibrated ages of chronostratigraphic control points, position and nature of major biostratigraphic events as well as isotopic fine-tuning of benthic and planktic $\delta^{18}O$ compositions with the NGRIP record (NGRIP members, 2004), revealing subordinate D/O oscillations. Legend as indicated in the figure.

constant climatic regime. Extremely light $\delta^{18}O$ values of *G. ruber* (up to -1.5‰) are compatible to the warm MIS 5.1, 5.3 and 5.5 substage records from the Ionian Basin (core KC01B; Lourens, 2004) and the Strait of Sicily (ODP site 963; Sprovieri et al., 2006). The existence of a Sapropel equivalent as well as the distinctive foraminiferal assemblage of this unit (see section 6.4.1) suggest the presence of a quite expanded MIS 5.5 interval. The top of this interval is marked by an abrupt positive shift (~1.5‰) in both isotopic records, indicating a lowered eustatic sea level and an associated erosional surface. As absolute values are too light to infer the presence of MIS 4 (in comparison with core KC01B; Lourens, 2004), this surface is tentatively ascribed to the relative sea level lowstand during MIS 5.4 Stadial. Consequently, a return to lighter values in the overlying section capped by ES1 is associated with the MIS 5.3 Interstadial.

Being based on a Sapropel equivalent deposition (S3 eq, see section 6.4.1), the lower core section of site GeoB14403 provides a continuous record of MIS 5.1 Interstadial, MIS 4 Glacial and MIS 3 Interglacial units. The high resolution of isotope records in this succession allows for the recognition of short-lived D/O events – mild Interstadials with abrupt shifts toward lighter $\delta^{18}O$ values overprinting the general isotopic trend (Johnsen et al., 1972; Dansgaard et al., 1982, 1993) at an average periodicity of 1470 years (Bond et al., 1997). Under the assumption of synchronicity, a fine-tuned correlation of site GeoB14403 $\delta^{18}O$ records to the NGRIP record (NGRIP members, 2004) has been carried out. Oscillations in the higher resolved benthic record typically show abrupt subtle shifts of 0.5 to more than 1‰, which are significantly higher than the analytical error (< 0.07‰). Wiggle matching with the NGRIP record enabled to recognize most of the D/O events from D/O 20 to D/O 6 at site GeoB14403. Tie-points between the individual records were set at the mid-points of DOIS onsets and were used as control points in the chronological framework of the core (*Table 6.4*). Corresponding NGRIP ages and uncertainties were adapted from Anderson et al. (2006) for D/O 6 to 8 and Svensson et al. (2008) for D/O 12 to 17. Ages for the remaining events were extracted from the NGIRP dataset, assuming an uncertainty of 1.5 ka.

6.5.4 Radiometric datings

Calibrated ^{14}C ages reported in *Table 6.2* further constrain the chronological framework at the drill sites for the last ~50 ka, corroborating inferences from bio- and isotope-stratigraphic considerations. Radiometric datings used in the age-depth model are given in *Table 6.4*, including their corresponding depths within the recovered sediments. At site GeoB14403, the position of the mean flooding surface (mfs) as inferred from the biostratigraphy is supported by the sample at 3.88 mbsf (Poz-53709), reporting a calibrated age of 5.58 ka. Similarly, the proposed hiatus at the MIS 2/Holocene-boundary (isotopic Termination I) could be confirmed by the samples at 6.34 mbsf (Poz-53711) and 7.35 mbsf (Poz-53712), reporting ages of 9.75 and 12.40 ka, respectively. The age of 29.32 ka for sample Poz-53713 at a depth of 11.82 mbsf just below the ES1 unconformity suggests major erosive activity related to the eustatic sea level lowstand during the LGM chronozone, defined between 19 and 23 cal. ka BP (Mix et al., 2001). The Last Common Occurrence (LCO) of *G. inflata* during MIS 3, a major biomarker in the Mediterranean Sea, was sampled at 15.79 mbsf and dates 37.69 ka. The remaining datings at site GeoB14403 validate the positioning of D/O events through fine-tuning of the oxygen isotope record (see section 6.4.3). The last two samples taken from the lower core section (OS-106892 and Poz-53716) were omitted as their ^{14}C ages exceeded the calibration limit of the Marine13 data set (Reimer et al., 2013). At site GeoB14414, the base of the Holocene unit could be confirmed in a depth of 5.56 mbsf (Poz-53717, 11.58 ka). Dating Poz-53745, sampled just below the ES1 unconformity, was neglected as the stratigraphic setting implies much older sedimentary units (early MIS 5). Due to the proximity to the erosive surface, mixing with younger sediment through bioturbation cannot be ruled out.

6.5.5 *Age model*

The integrated stratigraphy as discussed above and summarized in *Figure 6.4* was adopted to develop an age-depth model for both drill sites. Selected control points are presented in *Table 6.4* and comprise: (1) the core top, which in the absence of further evidence is assumed to be of modern age, (2) nine ^{14}C AMS radiometric datings based on mono-specific and mixed foraminifera, (3) seven major foraminifera-based biostratigraphic events, calibrated with ^{14}C AMS radiometric datings from adjacent core P9 (Minisini et al., 2007), (4) one ^{40}Ar/^{39}Ar dating of a volcanic eruption chemically assigned to the prominent tephra layer at site GeoB14403, (5) eleven D/O-type events, calibrated through fine-tuning of planktic and benthic oxygen isotope records to the NGRIP record (NGRIP members, 2004), (6) the age of the isotopic minimum during MIS 5.4 with reference to the NGRIP records, and (7) the age of isotopic Termination II at the MIS 6/5 boundary as reported by Lisiecki and Raymo (2005) [the stratigraphic position for this control point was derived from sequence-stratigraphic considerations, see *Figure 6.6*].

In order to provide a continuous age-depth model, the Bayesian accumulation model "Bacon" (Blaauw and Christen, 2011) was employed. The distribution of the individual control points as well as the models 95% confidence interval is presented in *Figure 6.5*. It is accompanied by the corresponding linear SAR, which results from linear interpolation between the intercepts of the calibrated ages. Where available, radiometric datings were preferred over other control points for this interpolation in order to exclude uncertainties related to potential asynchronism between datasets (e.g., isotopic fine-tuning to NGRIP dataset, Blaauw, 2012). In general, sedimentation rates in the recovered units range between around 30 to 110 cm/ka within the last ~70 ka (including marine isotope stages and substages from MIS 4 to MIS 1), with figures rising to approximately 200 cm/ka within MIS 5 units. This is an order of magnitude higher than numbers deriving from the Quaternary sediments recovered from ODP Site 963 at NW Gela Basin in 470 m water depth (Di Stefano, 1998). During post-LGM times (including MIS 2 and Holocene units), sedimentation rates at both drill sites display comparable ranges from around 40 to 100 cm/ka. However, units related to MIS 2 as well as the most

Table 6.4. Overview of the control points used for the age-depth models of sites GeoB14403 and GeoB14414.

Site GeoB14403			
Depth [mbsf]	Event	Age [cal. yrs BP]	Reference
0	Modern time	-60	this work
2.66	Peak in *G. truncatulinoides r.c.*	4600 ± 182	(1)
3.88	^{14}C AMS	5577 ± 132	this work
4.52	Top of Sapropel 1 eq.	6037 ± 145	(1)
5.67	^{14}C AMS	8264 ± 122	this work
6.34	^{14}C AMS	9745 ± 220	this work
6.55	Base of Sapropel 1 eq.	9882 ± 332	(1)
7.35	^{14}C AMS	12405 ± 240	this work
11.82	^{14}C AMS	29322 ± 443	this work
13.25	^{14}C AMS	32717 ± 566	this work
13.5	D/O 6	33740 ± 606	(2)
14.3	D/O 7	35480 ± 661	(2)
15.6	D/O 8	38220 ± 724	(2)
15.79	^{14}C AMS	37689 ± 992	this work
17.91	^{14}C AMS	44561 ± 1506	this work
18.15	D/O 12	46860 ± 956	(3)
24.35	D/O 14	54220 ± 1150	(3)
28.42	Tephra (MEGT/UMSA, Y-7)	56000 ± 4000	(4,5)
28.93	D/O 16	58280 ± 1256	(3)
30.13	D/O 17	59440 ± 1287	(3)
35.53	D/O 18	64800 ± 1439	(6)
39.03	D/O 19a	70300 ± 1589	(6)
41.03	D/O 19	73000 ± 1662	(6)
48.93	D/O 20	77150 ± 1774	(6)
Site GeoB14414			
Depth [mbsf]	Event	Age [cal. yrs BP]	Reference
0	Modern time	-60	this work
0.777	Reoccurrence *G. truncatulinoides*	5434 ± 135	(1)
1.059	Top of Sapropel 1 eq.	6037 ± 145	(1)
3.586	Base of Sapropel 1 eq. break	8507 ± 145	(1)
4.292	Base of Sapropel 1 eq.	9882 ± 332	(1)
5.56	^{14}C AMS	11583 ± 313	this work
11.9	δ^{18}O minimum in MIS5.4	110450 ± 2677	(6)
61*	MIS 5/6 boundary (Termination II)	130000 ± 4000	(7)

References: (1) Minisini et al. (2007); (2) Anderson et al. (2006); (3) Svensson et al. (2008); (4) Kraml (1997); (5) Allen et al. (1999); (6) ages taken from the NGRIP dataset (NGRIP members, 2004), errors estimated from trend in (3); (7) Lisiecki and Raymo (2005). * = estimated from acoustic profile in *Figure 6.6*.

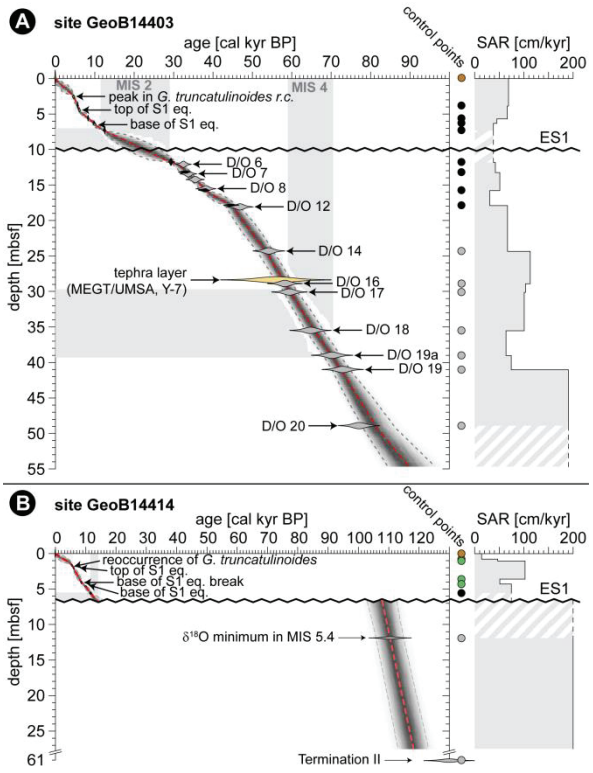

Figure 6.5. Integrated Bayesian age-depth model of recovered sediments at site GeoB14403 (A) and GeoB14414 (B), overlying the distribution of individual dates (colour coded according to the nature of their associated event, as in *Figure 6.4*). Grey dotted lines refer to the model's 95% probability interval; the red dotted line represents the calculated mean; grey areas correspond to Glacial intervals. Corresponding linear sedimentation rates (LSR) are displayed on the right-hand side of the main panel, based on selected control points as indicated by adjoining dots (colour coded as in *Figure 6.4*).

recent deposits close to the core top are significantly less developed at site GeoB14414, cumulating in an overall reduced thickness of the sedimentary succession with regard to site GeoB14403 (by about 3.5 m) and suggesting local variability in the sediment flux and/or current pattern (e.g. drift-related starvation as reported on by Verdicchio and Trincardi (2008).

6.6 Results

6.6.1 *Calibration of shelf sedimentary units with GeoB14403/GeoB14414 stratigraphy*

The integrated chronological framework developed for sites GeoB14403 and GeoB14414 documents major sea level and paleoceanographic changes within shelf sedimentary units at Gela Basin (*Figure 6.4*). Marine Isotope Stages/Substages (MIS) and subordinate climate oscillations (D/O events) could be precisely defined and allow to calibrate the shelf architecture based on core-seismic correlation of key stratigraphic surfaces (*Figure 6.6*). The high-resolution acoustic profile in *Figure 6.6A* reveals the peculiar setting of W- to SW-dipping sedimentary units between sites GeoB14403 in the NW and GeoB14414 in the SE. The buried proximal part of a paleo-failure intersects these units midway through the profile. Clearly distinguishable erosional unconformities reflecting subaerial exposure during sea level fall and lowstand (ES2 and ES1) bracket the overall progradational depositional sequence of the last 100-ka glacio-eustatic cycle. They unveil two alternating types of internal seismic units: (1) uniform and subparallel seismic reflector packages, and (2) onlapping units of converging seismic reflector packages pinching out towards shallower depths (*Figure 6.6A* and *6.6B*). Core-seismic stratigraphic correlation links the former to progradational units deposited during the warmer substages MIS 5.1, MIS 5.3 and MIS 5.5 (*Figure 6.6C* and *6.6D*), which display thicknesses ranging between 35 and 45 m each. Bounded by high-amplitude reflectors, onlapping units with markedly thinner extents represent the upper/proximal clinoform remnants that correspond to the Glacial interval of MIS 4 (*Figure 6.6B* and *6.6D*) as well as the colder substage MIS 5.4 (*Figure 6.6C* and *6.6D*). The sedimentary record of their basal contacts provides evidence of stratigraphic condensation (variations in core-physical parameters, Kuhlmann et al., 2014). Hence they are interpreted, respectively, as a subordinate sequence boundary (SB, *Figure 6.6B* and *6.6D*) and a basal surface of forced regression (in the sense of Hunt and Tucker, 1992), recording the seaward shift of coastal progradation driven by sea level fall (*Figure 6.6C* and *6.6D*). Upper contacts along even more pronounced reflectors coincide with isotopic shifts at the end of MIS 4 and

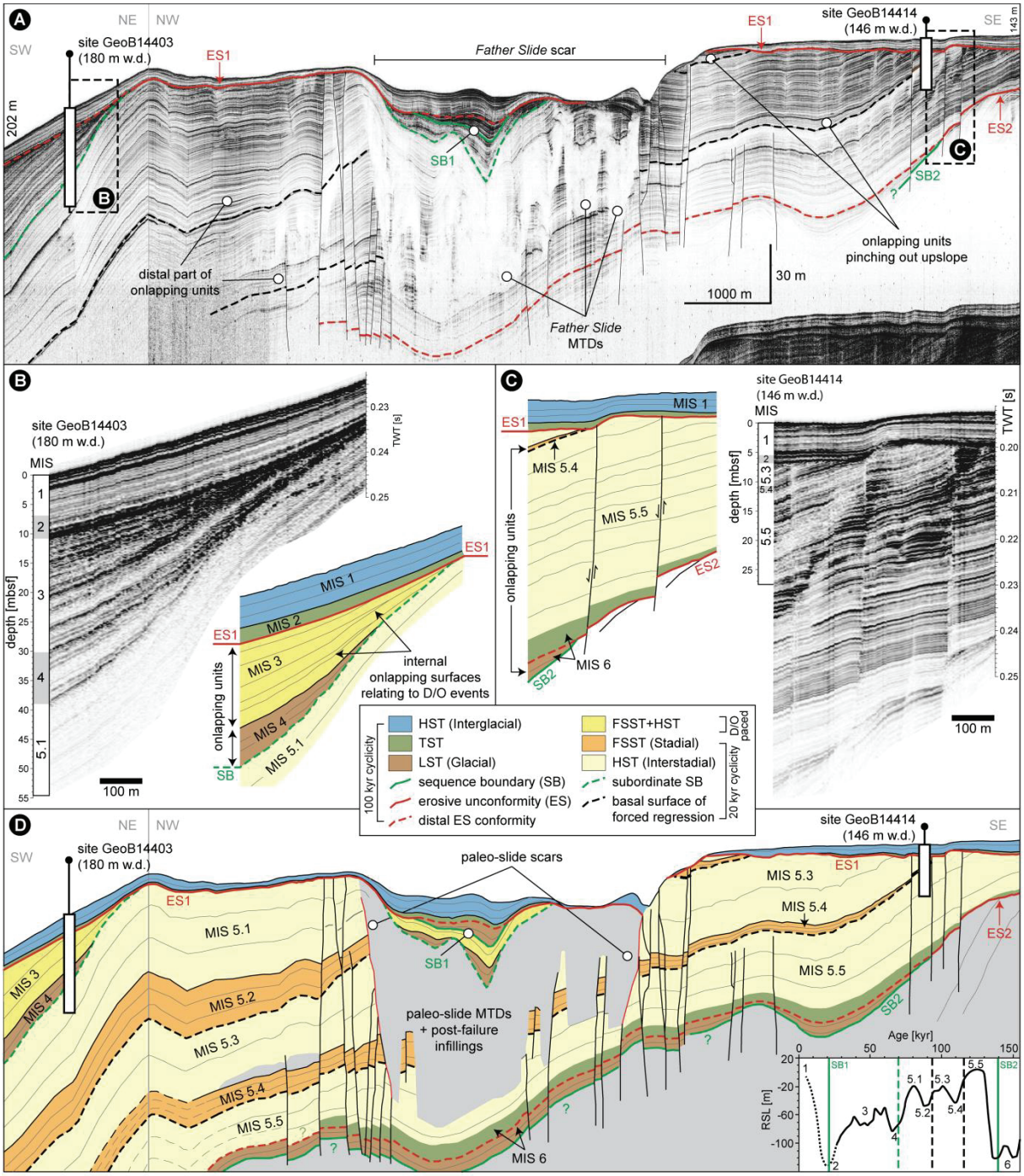

Figure 6.6. A: Acoustic subbottom profile correlating drill sites GeoB14403 and GeoB14414 over remnants of a prominent paleo-scar, revealing the stratigraphic architecture at the shelf edge. B and C: Stratigraphic calibration of seismic units based on chronostratigraphic framework proposed for the drill sites. Note the frequent strong seismic reflectors within units relating to MIS 3. D: Sequence-stratigraphic interpretation indicating composite Milankovitch cyclicity relating to 100-ka/20-ka sea level fluctuations. The inset in the lower right hand side indicates the position of Marine Isotope Stages and Substages as well as sequence stratigraphic boundaries with regard to the sea level curve of the Last Glacial-Interglacial cycle (from Waelbroeck et al., 2002). Legend: HST – Highstand Systems Tract; TST – Transgressive Systems Tract; LST – Lowstand Systems Tract; FSST – Falling Stage Systems Tract; D/O – Dansgaard-Oeschger events.

MIS 5.4 (*Figure 6.4*), indicating the landward shift of facies associated to a rapid sea level rise and associated condensation. An exception to this pattern is represented by the onlapping units of MIS 3, where multiple inter-sequential onlapping surfaces are accompanied by alternating proximal and distal shifts in coastal progradation, each separated by prominent acoustic reflectors (*Figure 6.6B*). These variations are, though on a smaller scale, comparable to the depositional pattern within MIS 5 units and likely reflect major high-frequency sea level oscillations superimposing the long-term sea level fall during MIS 3 (D/O events, *Figure 6.4*).

Stratigraphic tracing of the above introduced surfaces and recognition of the landward onlapping unit associated to MIS 5.2 Stadial (not recovered by the cores) reveals the full sequence stratigraphic setting on the southern Sicilian shelf at Gela Basin during the course of the Last Glacial-Interglacial cycle (*Figure 6.6D*). Sedimentation is dominated by intervals of relative highstand (HST) as recorded by the thick units formed during the warmer isotope substages MIS 5.1, MIS 5.3 and MIS 5.5. Gradually thinning in down-dip direction, these are intercalated by relatively thin forced-regression units (FSST) that pinch out up-dip and reflect intervals of relative sea level fall during the colder isotopic substages (MIS 5.2 and MIS 5.4). Towards the shelf edge, MIS 5 units are overlain by up-dip converging and onlapping sedimentary units comprising (1) the wedge complex formed during the maximum lowstand/early rise of sea level related to MIS 4 (LST), and (2) the alternating HST and FSST units of MIS 3, likely being paced by the subordinate high-frequency oscillations relating to D/O events. The latter units are truncated by the erosive unconformity of the LGM, separating it from late Pleistocene to Holocene transgressive deposits (TST) and the Holocene highstand units (HST).

6.6.2 Sediment undulations in MIS 5 HST deposits

Along the SE part of the shelf at Gela Basin, the interplay between SW-dipping sediments and the erosive character of the ES 1 unconformity exposes sedimentary units of MIS 5 at shallow depths and reveals undulated features affecting highstand deposits related to MIS 5.3 and MIS 5.5 units (*Figure 6.7*). As these features share some morphologic and stratigraphic characteristics with those found in deeper-water sediment waves, the respective terminology for their description is adapted here (e.g., Nakajima and Satoh, 2001). However, since direct information on the possible direction of current flow is lacking, terms such as ‘stoss side’ and ‘lee side’ are referred to as upslope and downslope limbs (with respect to the seaward slope), following the suggestion of Cattaneo et al. (2004).

The undulations generally occupy a laterally continuous belt within MIS 5 highstand units and are distally confined by the shelf edge and associated frequent slope failure (Minisini et al., 2007; Minisini & Trincardi; 2009; Kuhlmann et al., 2014). Though limited seismic coverage impedes the exact recognition of their extent, undulations can be traced for at least 3 – 3.5 km perpendicular to the modern isobaths along a slope inclining at approximately 0.3 – 0.5°. A representative section of the undulated features at the study site is presented in *Figure 6.7*, displaying an acoustic profile acquired sub-perpendicular to the modern shelf isobaths. It reveals clearly distinguishable individual undulations that are separated by convex planes, albeit showing continuity of seismic reflectors. At depth, the features appear to be rooted on specific stratigraphic surfaces (basal surface of undulations, *Figure 6.7A*) that occasionally merge upsection. They form a staircase morphology with sub-horizontal to gently landward-dipping upslope limbs, delimited seaward by steeper downslope limbs (*Figure 6.7A*). Some of the largest undulations formed by this upward merger may reach wavelengths of about 200 m and maximal amplitudes (heights) of 1.5 – 2 m, whereas distal features root at younger reflectors and typically are smaller in size(*Figure 6.7A*). However, the reported values reflect apparent dimensions only, since the acoustic profile is expected to be at angle to the undulation crests, and may thus be misleading. Hence, comparisons to well-known cases of similar

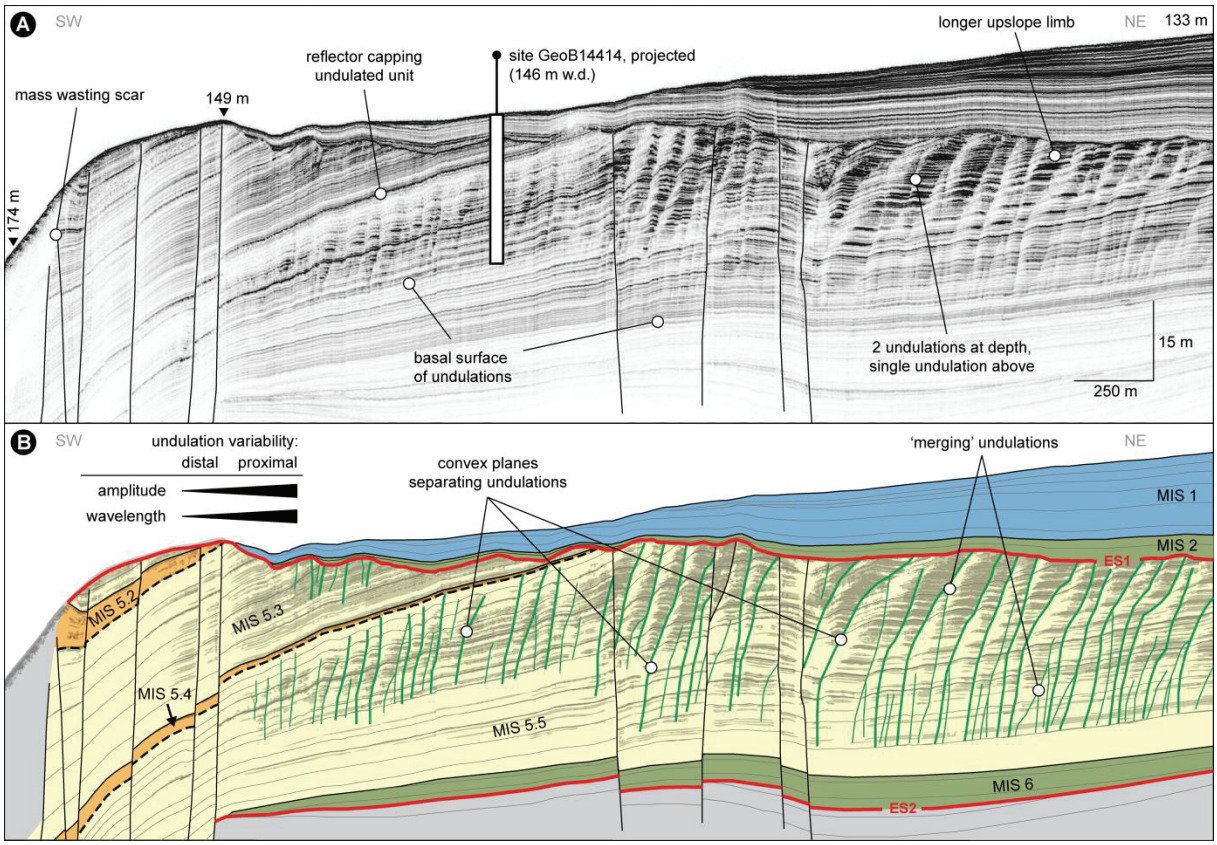

Figure 6.7. A: Acoustic subbottom profile showing along-slope section at site GeoB14414, revealing an extended field of undulated features. B: Sequence stratigraphic interpretation of A showing highlighting main characteristics of the undulations. Legend: see *Figure 6.6*.

undulation features found on late-Holocene Mediterranean prodeltas (Urgeles et al., 2011, and references therein) should be treated with care. Nonetheless, both wavelength and amplitude show a decrease in downslope direction as well as with depth. Interestingly, the undulations appear in deeper stratigraphic levels proximally and progressively in younger units proceeding seaward, possibly suggesting that, in a regressive setting, a certain sediment accumulation rate should be attained before these features form. At their top, sediment undulations are frequently truncated by the erosive unconformity ES1 relating to subaerial exposure during the LGM. Where preserved more seaward, the staircase morphology is capped by the basal surface of forced regression (FSST), which records the seaward shift of coastal progradation and separates the individual highstand units related to MIS 5.5 and MIS 5.3 (*Figure 6.7B*).

Site GeoB14414, penetrating the stratigraphic units affected by undulation features, reveals a consistent and homogenous lithology with very high SAR of about 200 cm/ka (*Figure 6.5B*). No signs of sediment deformation and failure are evident that could potentially relate to the manifestation of undulated features within the HST units of MIS 5. With the exception of an extended section ascribed to the Sapropel 5 eq., lithologic variability is limited to the scattered presence of silty laminae, bioturbation and black organic matter.

6.7 Discussion

6.7.1 Depositional variability at Gela Basin

The proposed high-resolution stratigraphy for drill sites GeoB14403 and GeoB14414 (*Figure 6.4*, *Figure 6.5*) provides a detailed overview of the depositional variability at the NE portion of Gela Basin during the

Last Glacial-Interglacial cycle. A striking outcome is the observation of exceptionally high sedimentation rates, especially with regard to MIS 5 Interstadial conditions. Mean SAR for this interval amount to ~200 cm/ka, which is about an order of magnitude higher than figures retrieved from nearby ODP Site 963 (Di Stefano, 1998; Sprovieri et al., 2006). Situated just 100 km NW of the study area within the same basin, though on a plateau detached from the mainland slope, this raises questions about potential mechanisms at the origin of such strong local variations in sediment flux, at both orbital and suborbital time scales.

Generally, continental shelf settings with high sedimentation rates often occur in areas off river outlets, e.g. the Tiber River prodelta off Rome (Tincardi and Normark, 1988; Chiocci et al., 1996) or the Llobregat River prodelta off Barcelona (Sánchez-Cabeza et al., 1999). However, Sicilian river basins hold one of the most arid conditions in the Mediterranean and river discharge is extremely low (e.g., Q=0.02 km³/yr at Gela river, Milliman and Farnsworth [2011]) when compared to these settings (0.47 km³/yr at Llobregat river, 7.38 km³/yr at Tiber river, UNEP [2003]). Hence, we relate the enhanced sediment flux and depositional variability at the study site to the current regime controlled by Quaternary climatic oscillations. As schematized in *Figure 6.1*, bottom currents within Strait of Sicily are mainly of thermohaline origin, strictly reflecting the anti-estuarine circulation pattern of the Mediterranean. At Gela Basin, the present LIW forms an anticyclonic subsurface eddy reaching velocities of about 13 cm/s (Lermusiaux and Robinson, 2001), which is capable of transporting sediment in suspension along the contour lines of the outer shelf. The strong impact of these bottom currents on sediment dispersal and deposition is evidenced by the local variability of post-LGM sedimentary thicknesses as recorded by the boreholes (*Figure 6.4*). While there is no recognizable imprint of bottom currents at site GeoB14403 (*Figure 6.6A*), sediment deposition is significantly disturbed at site GeoB14414, where the recent deposition of thick sedimentary successions is limited to the upslope region of the borehole (*Figure 6.7A*). Further evidence of the current system is seen in the presence of extensive muddy shelf-edge contourites in this area, as reported on by Minisini et al. (2007) and Verdicchio and Trincardi (2008) based on seismic stratigraphy. Their simple geometry suggests a relatively constant path of the bottom currents and thus argues against major contributions from other current generating processes such as wind forcing (e.g. Flemming, 1981), internal waves and tides (e.g. Cacchione et al., 1988), which are commonly associated with substantial variability in both velocity and direction.

Variations in the formation, strength and pathways of thermohaline-driven currents are ultimately linked to major palaeogeographic modifications associated with Quaternary climatic oscillations that relate predominantly to the drowning and successive emersion of continental shelves. During colder Glacial intervals, subaerial exposure of the southern Sicilian shelf likely reduced sediment dispersal at the study site by hampering circulation and changing pathways of bottom currents (*Figure 6.8*). Conversely, flooding during the warmer Interglacials culminated in a strengthening of bottom-current circulation and, provided availability of sediment, a peak in SAR – as documented by the occurrence of contourite deposits (Minisini et al., 2007; Verdicchio and Trincardi, 2008). This pattern of sediment dispersal is similar to that proposed by Ridente et al. (2008, 2009) for the Adriatic margin, albeit lacking the dominant influence of a major river. Although being most relevant during the eccentricity-paced (100-ka) Glacial-Interglacial cycles, the scheme may equally be applied to precession-related (20-ka) Stadial-Interstadial cycles. In addition to the fluctuations in thermohaline-driven bottom currents, we suggest another mechanism that might contribute to the high SAR associated with MIS 5 Interglacials, albeit acting on a much shorter timescale: extreme precipitation events. Given that Sicilian watersheds predominantly comprise erodible and less vegetated land, sudden and excessive rainfalls (flash floods) during overall arid conditions may transport significant amounts of fine-grained sediment towards

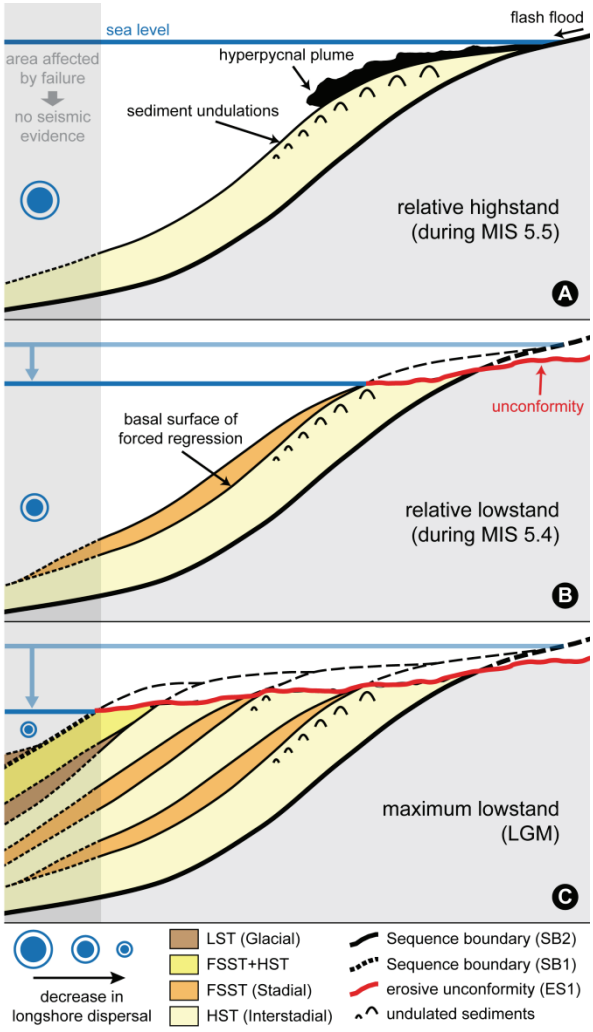

Figure 6.8. Simplified scheme illustrating the combined influence of sea level change, sediment supply and dispersal on depositional geometry of the Last Glacial-Interglacial depositional cycle. A: Enhanced supply from river flood discharge and strong alongshore dispersal of sediments associated to shelf drowning lead to the development of thick highstand clinoforms during MIS 5 Interstadials. Hyperpycnal plumes from flash floods induce the formation of sediment undulations on the shelf. B: intervening sea level fall reduces alongshore sediment dispersal, increases erosion along proximal surfaces (unconformity) and leads to the emplacement of progradational clinoforms. C: Alternation of these patterns relating to 20-ka cyclicity continues with further sea level fall, while alongshore sediment dispersal further decreases until the sea level reaches maximum lowstand during the LGM. Legend: LST – Lowstand Systems Tract; FSST – Falling Stage Systems Tract; HST – Highstand Systems Tract.

the shelf area via hyperpycnal plumes (*Figure 6.8A*; e.g., Milliman and Syvitski, 1992; Mulder et al., 2003; Dadson et al., 2005; Warrick at al., 2008). Owing to small, mountainous drainage basins the river-ocean system in the study area is strongly coupled and storms simultaneously affect coastal waters and the hinterland (Wheatcroft et al., 1997). As a result, sediment discharge associated to these episodic events occurs during highly energetic conditions and favours the emplacement of widely dispersed, relatively thin and stratigraphically simple deposits (e.g. Wheatcroft and Borgeld, 2000; Talling, 2014). A typical example for this type of sediment dispersal is the 5-yr return flash flood at the Têt River basin in the Gulf of Lions, where fine sediments – separated from coarser ones at the river mouth – are transported along the shelf via hyperpycnal plumes (Bourrin et al., 2008).

6.7.2 Composite Milankovitch cyclicity as reflected by depositional sequences

Quaternary depositional sequences on modern shallow-shelf settings largely reflect climatic and eustatic variability related to Milankovitch cyclicity. However, most records are dominated either by the 100-ka Glacial-Interglacial cycle (e.g., Piper and Aksu, 1992; Ercilla et al., 1994; Chiocci, 2000; Hübscher and Spieß, 2005; Liquete et al., 2008) or the higher-frequency 20-ka periodicity (e.g., Marsset et al., 1996; Hiscott, 2001; Osterberg, 2006; Liu et al., 2010). At Gela Basin, borehole-supported calibration of depositional sequences reveals a stratigraphic pattern displaying both orders of cycles as distinct stratigraphic motifs that can be interpreted in terms of composite (100-ka and 20-ka) cyclicity. Analogue to other margins, eccentricity-related 100-ka glacio-eustatic fluctuation represents the primary factor controlling the deposition of sequences. Bounded by unconformities relating to subaerial exposure during the sea level lowstands of MIS 2 and MIS 6 (*Figure 6.6A*, *6.8C*), the youngest of these Quaternary Glacial-Interglacial sequences manifests in a succession of predominantly fine-grained (Kuhlmann et al., 2014) and overall progradational units recording the classical systems tracts (TST, HST, FSST and LST).

The most evident signature of higher-frequency 20-ka cyclicity punctuating this depositional cycle is reflected by alternating HST and FSST units relating

to the MIS 5 interval (*Figure 6.8*). A similar stratigraphic pattern is found, e.g., on the SW Spanish margin (Somoza. et al., 1997; Hernández-Molina et al., 2000), the South China Sea (Hiscott, 2001) and the Adriatic margin (Ridente et al., 2008, 2009). Within this interval, two significant sea level falls in the order of several tens of metres (Lea et al., 2002) coinciding with MIS 5.4 and MIS 5.2 provoked a seaward shift of facies that is recorded in a sharp basal surface interpreted as the basal surface of forced regression (in the sense of Hunt and Tucker, 1992; *Figures 6.6* and *6.7*). A concomitant drop of bottom current strengths in response to thermohaline adaption (see section 6.7.1; *Figure 6.8B*) likely reduced sediment dispersal during these times. The onset of successive high-frequency HSTs is accompanied by an abrupt rise in sea level and marks a surface of stratigraphic condensation. No evidence of TST deposits usually related to this interval can be found within the study area along this surface, suggesting a strong proximal shift of clinoforms and potential erosion during the LGM. The lack of a well-preserved high-frequency TST is concordant with other settings, where TST deposits are either absent (e.g., Hiscott, 2001; Banfield and Anderson, 2004; Gámez et al., 2009) or difficult to identify, owing to their limited lateral extent and relative thinness (e.g., Hernández-Molina et al., 2000; Lobo et al., 2002). Equally, no evidence of lowstand units (LST) is detectable in the acoustic record within these intra-MIS 5 20-ka cycles. This likely relates to the limited down-dip preservation state of clinoforms in this area, which are truncated along the shelf edge by slope failure surfaces (*Figures 6.2* and *6.7*; Minisini et al., 2007; Minisini and Trincardi, 2009; Kuhlmann et al., 2014). However, the onlapping LST deposit associated with the relative sea level lowstand during MIS 4 is well preserved and caps, separated by a subordinate sequence boundary, the distal section of the MIS 5 interval. Osterberg (2006) and Çağatay et al. (2009) report on a similar stratigraphic scheme displaying two major erosional surfaces related to the two sea level lowstands during MIS 4 and 2. In the case of Gela Basin though, the proximal erosional component of the subordinate sequence boundary is not preserved.

Separated by prominent flooding surfaces (*Figure 6.6B*), the shelf margin wedges related to MIS 3 appear to respond to shorter-lived and lower magnitude sea level fluctuations punctuating the long-term sea level fall from MIS 3 to LGM. Analogue to findings from the Gulf of Lions (Sierro et al., 2009; Frigola et al., 2012), this suggests the interruption of coastal progradation at the onset of the warmest D/O events. Sea level reconstructions (e.g., Siddall et al., 2003, 2008) provide evidence that the four main rises in sea level during MIS 3 involved amplitudes of 20-30 m and took place in only 300-700 years. Associated coastal retreat likely overcame the rate of sediment supply during this time, leading to a starvation of slope sediments and the emplacement of stratigraphic condensations recorded by sharp seismic reflectors. Hence, this stratigraphic unit is interpreted to reflect alternating HST/FSST intervals.

Summarizing these results, the following points are key:

- The shelf at Gela Basin records three orders of cyclicity associated to changes in relative sea level: (1) an eccentricity-related 100-ka cyclicity comprising progradational deposits as suggested by the classical systems tract concept (HST, FSST, LST, TST); (2) a higher-frequency 20-ka cyclicity pacing alternating HST/FSST deposits within the MIS 5 interval; (3) an ultra-high-frequency (sub-Milankovitch) cyclicity likely reflecting abrupt sea level rises corresponding to major D/O events during MIS 3-2.
- The subordinate 20-ka HST deposits of MIS 5 represent the bulk of the volume of the Last Glacial-Interglacial cycle, albeit representing a short interval in the overall, longer term falling sea level trend.

6.7.3 *Potential mechanisms at the origin of MIS 5 undulated sediment features*

In the last centuries, application of high-resolution seismic and bathymetric data to Mediterranean shallow-shelf settings has provided profuse evidence of undulated sediment features on late-Holocene prodeltas (Urgeles et al., 2011, and referenced therein). Successively, five principal mechanisms for their genesis have been postulated, partly relying on comparisons to self-similar, albeit larger-scale deep-sea equivalents: (1) gravitational downslope sediment deformation/creep (e.g., Diaz and Ercilla, 1993; Ercilla et al., 1995; Chiocci et al., 1996; Correggiari et al., 2001); (2) longshore currents associated to waves and tides in shallow settings (Urgeles et al., 2011); (3) bottom currents (e.g., Trincardi and Normark, 1988; Mosher and Thomson, 2002); (4) hyperpycnal flows (e.g., Bornhold and Prior, 1990); and (5) internal waves (e.g., Puig et al., 2007). This is the first time that comparable undulation fields could be recognized and mapped within the HST units of the MIS 5 Interglacial intervals, representing a past equivalent to the modern features. In the following, we will discuss their main characteristics based on evidence presented elsewhere in order to provide insight into their potential genesis.

Given the buried nature of undulation features in the study area it is noteworthy to remark the lack of control over their morphologic expressions, such as crest alignment and lateral continuity. However, from the acoustic record undulation crests appear to be aligned parallel to the modern isobaths (*Figure 6.7*), thereby indicating no major changes of slope orientation with regard to the modern margin. Their setting at intermediate depths along the shelf edge additionally precludes a participation of waves or tides in the generation of undulations, as in the Mediterranean only major storms are capable of causing sediment resuspension and transport in water depths of 35 m and below (Puig et al., 2001; Palanques et al., 2002). Similarly, a variety of characteristics intrinsic to the undulations in the study area argue against a formation involving downslope sediment deformation/creep: (1) the continuity of seismic reflectors and the absence of diffraction that could indicate rupture of reflectors; (2) the seaward reduction in wavelength, which implies a greater amount of deformation in upslope direction and thus downslope progression of sliding, as opposed to the retrogressive behaviour of most slides (e.g., Canals et al., 2004; Masson et al., 2006); (3) the presence of intricate patterns of upsection merging undulations, which is largely absent in known subaerial and submarine failures (Urgeles et al., 2011); (4) the constant dipping of strata within each undulation, implying that there is no synchronous deformation during deposition as apparent in creep; and (5) the general lack of gassy sediments as opposed to most prodelta settings (e.g. Llobregrat delta [Urgeles et al., 2007]; Adriatic margin [Cattaneo et al., 2004]), which is known to affect slope stability (Vanoudheusden et al., 2004). The evidence summarized above suggests that undulations at Gela Basin most probably are not related to sediment deformation processes/creep. Analogies drawn from deep-sea settings further argue against a genesis through bottom currents, as these typically display no consistent change in wave dimension up- or downslope (e.g., Cunnungham and Barker, 1996) and usually feature wave crests that are aligned at certain angle to the regional contours. Both characteristics are not met by the undulations at Gela Basin. However, more consistency is apparent with undulation fields generated by turbidity currents in deep-sea settings, which can be considered as an analogue to hyperpycnal flows at shallow-shelf settings. These typically reflect the undulation characteristics of the study area, including: (1) distally decreasing wavelengths and heights (e.g., Wynn and Stow, 2002), which might relate to reduced velocities of the turbidity current as it progresses towards flatter areas (Normark et al., 1980); (2) slope-parallel undulation crests; and (3) an upslope sourced undulation pattern expressing in a progressive downslope decrease in thickness of the affected stratigraphic interval (e.g., Ercilla et al., 2002). Finally, Puig et al. (2007) proposed a relation of sediment undulations in the Adriatic Sea (30-90 m

depth range) to wind-generated internal waves, suggesting that these features play a major role in resuspending and transporting sediment in prodeltaic settings.

The arguments brought forward indicate that the most probable mechanism forming the undulations at Gela Basin may relate to hyperpycnal flows from rivers. This is in agreement with the proposed mechanisms likely adding to the high sedimentation rates during MIS 5 (see section 6.7.1). Similarly, internal waves might be related to the generation of undulated features, though length to height ratios of individual undulations in the study area (L/H ~ 100) suggest a relation to hyperpycnal flows (*Figure 6.8A*; Urgeles et al., 2011).

6.8 Conclusions

In this study, we propose a high-resolution stratigraphy for the drill sites GeoB14403 and GeoB14414, situated at the shallow-water shelf at NE Gela Basin on the Sicilian continental margin. The investigation of integrated and independent proxies allow to ascribe the drilled records to a time-interval spanning from late MIS 5 to the Holocene, thus providing a shallow marine record sampling major parts of the last glacio-eustatic cycle. Correlation of borehole stratigraphy with high-resolution acoustic records as well as sequence-stratigraphic reconstruction allows unravelling the stratigraphic architecture at the study area and proposing possible mechanisms that likely control depositional variability. In particular, the following findings are key:

1. The internal architecture of shelf deposits is strongly affected by composite Milankovitch cyclicity. 100-ka (eccentricity-related) Glacial-Interglacial cyclicity is recorded by progradational sequences that are proximally bounded by regional erosional surfaces. 20-ka (precession-related) Stadial-Interstadial cyclicity predominantly manifests in alternating HST and FSST deposits during the MIS 5 interval. Concomitant to warmer substages (MIS 5.5, MIS 5.3, MIS 5.1), HST units form thick wedges that constitute the bulk of progradational sedimentation, while thinner FSST units with sharp basal surfaces record a seaward shift of coastal progradation during colder substages (MIS 5.4, MIS 5.2). Transgressive deposits (TST) are present at the 100-ka scale only and lack evidence at the 20-ka scale. Similarly, suborbital lowstand deposits (LST) are mainly absent, with the exception of the onlapping units of MIS 4, which pinch-out landward. Finally, the shelf margin wedge related to MIS 3 shows alternating HST/FSST successions that appear to express some of the shorter-lived and lower magnitude sea level fluctuations associated to Dansgaard-Oeschger events (i.e., the warmest of these events), which are superimposed on the general falling trend.
2. High sedimentation rates and the predominantly muddy facies within the subordinate HST units of MIS 5 likely reflect two principal mechanisms: (1) The drowning of Mediterranean continental shelves during relatively short-lived sea level highstands, which favours the current activity of deep and intermediate LIW and leads to enhanced sediment dispersal within the study area; (2) The repeated occurrence of extreme precipitation events during arid conditions, which culminates in fine-grained sediment dispersal along the shelf via hyperpycnal plumes.
3. Acoustic subbottom profiles provide evidence of sediment undulations within the subordinate HST units of MIS 5. These undulations are comparable to equivalents forming on late-Holocene prodeltas of other Mediterranean shallow-shelf settings. Their main characteristics indicate hyperpycnal flows and/or internal waves as the principal mechanisms of genesis.

Acknowledgements

This work has been funded by the DFG through MARUM – Universität Bremen. We gratefully acknowledge the constructive reviews by L. Podszun and G. Bartzke and wish to thank the members of cruise MSM15/3 for their work on board. We also thank M. Thöner for assisting in the major element analysis of glass shards. $\delta^{13}C/\delta^{18}O$ analyses were carried out at the lab facilities of MARUM.

References

Andersen, K.K., Svensson, A., Johnsen, S.J., Rasmussen, S.O., Bigler, M., Röthlisberger, R., Ruth, U., Siggaard-Andersen, M.L., Steffensen, J.P., Dahl-Jensen, D., Vinther, B.M., Clausen, H.B., 2006. The Greenland Ice Core Chronology 2005, 15-42 ka. Part 1: constructing the time scale. Quaternary Science Reviews 25, 3246-3257.

Allen, J.R.M., Brandt, U., Brauer, A., Hubberten, H.-W., Huntley, B., Keller, J., Kraml, M., Mackensen, A., Mingram, J., Negendank, J.F.W., Nowaczyk, N.R., Oberhänsli, H., Watts, W.A., Wulf, S., Zolitschka, B., 1999. Rapid environmental changes in southern Europe during the last glacial period. Nature 400, 740-743.

Astraldi, M., Balopulos, S., Candela, J., Font, J., Gacic, M., Gasparini, G.P., Manca, B., Theocharis, A., Tintoré, J., 1999. The role of straits and channels in understanding the characteristics of Mediterranean circulation. Progress in Oceanography 44, 65-108.

Astraldi , M., Gasparini, G.P., Gervasio, L., 2001. Dense water dynamics along the Strait of Sicily (Mediterranean Sea). Journal of Physical Oceanography 31, 3457-3475.

Argnani, A., 1990. The Strait of Sicily rift zone: Foreland deformations related to the evolution of a back-arc basin. Journal of Geodynamics 12(2-4), 311-331. doi: 10.1016/0264-3707(90)90028-S.

Banfield, L.A., Anderson, J.B., 2004. Late Quaternary evolution of the Rio Grande delta: complex response to eustasy and climate change. In: Anderson, J.B., Fillon, R.H. (eds.) Late Quaternary Stratigraphic Evolution of the Northern Gulf of Mexico Margin, SEPM Special Publication, 79, pp 289-306.

Barberi, F., Civetta, L., Gasparini, P., Innocenti, F., Scandone, R., Villari, L., 1974. Evolution of a section of the Africa-Europe plate boundary; paleomagnetic and volcanological evidence from Sicily. Earth and Planetary Science Letters 22(2), 123-132.

Bethoux, J.P., 1980. Mean water fluxes across sections in the Mediterranean Sea, evaluated on the basis of water and salt budgets and of observed salinities. Oceanologica Acta 3(1), 79-88.

Béranger, K., Mortier, L., Gasparini, G.-P., Gervasio, L., Astraldi, M., Crépon, M., 2004. The dynamics of the Sicily Strait: a comprehensive study from observations and models. Deep-Sea Research II 51, 411-440.

Berné, S., Vagner, P., Guichard, F., Lericolais, G., Liu, Z., Yin, P., Trentesaux, A., Yi, H.I., 2002. Pleistocene forced-regressions and tidal sand ridges in the East China Sea. Marine Geology 188(3-4), 293-315.

Blaauw, M., Christen, J.A., 2011. Flexible paleoclimate age-depth models using an autoregressive gamma process. Bayesian Analysis 6(3), 457-474. doi: 10.1214/11-BA618.

Blaauw, M., 2012. Out of tune: the dangers of aligning proxy archives. Quaternary Science Reviews 36, 38-49. doi: 10.1016/j.quascirev.2010.11.012.

Bond, G., Showers, W., Cheseby, M., Lotti, R., Almasi, P., deMenocal, P., Priore, P., Cullen, H., Hajdas, I., Bonani, G., 1997. A pervasive millennial-scale cycle in North Atlantic Holocene and glacial climates. Science 278, 1257-1266. doi: 10.1126/science.278.5341.1257.

Bornhold, B.D., Prior, D.B., 1990. Morphology and sedimentary processes on the subacqueous Noeick river delta, British Columbia, Canada. In: Colella, A., Prior, D.B. (eds.) Coarse-grained Deltas, Spec Publ 10 Int Assoc of Sedimentol, UK, pp 169-184.

Bourrin, F., Friend, P.L., Amos, C.L., Manca, E., Ulses, C., Palanques, A., Durrieu de Madron, X., Thompson, C.E.L., 2008. Sediment dispersal from a typical Mediterranean flood: The Têt River, Gulf of Lions. Continental Shelf Research 28, 1895-1910.

Bourne, A.J., Lowe, J.J., Trincardi, F., Asioli, A., Blockley, S.P.E., Wulf, S., Matthews, I.P., Piva, A., Vigliotti, L., 2010. Distal tephra record for the last ca 105,000 years from core PRAD 1-2 in the central Adriatic Sea: implications for marine tephrostratigraphy. Quaternary Science Reviews 29, 3079-3094.

Brown, R.J., Orsi, G., de Vita, S., 2008. New insights into Late Pleistocene explosive volcanic activity and caldera formation on Ischia (southern Italy). Bulletin of Volcanology 70, 583-603. doi: 10.1007/s00445-007-0155-0.

Butler, R.W.H., Grasso, M., LaManna, F., 1992. Origign and deformation of the Neogene-Recent Maghrebian foredeep at the Gela Nappe, SE Sicily. Journal of the Geological Society (London) 149: 547-556.

Çağatay, M.N., Eris, K., Ryan, W.B.F., Sancar, Ü., Polonia, A., Akcer, S., Biltekin, D., Gasperini, L., Görür, N., Lericolais, G., Bard, E., 2009. Late Pleistocene-Holocene evolution of the northern shelf of the Sea of Marmara. Marine Geology 265(3-4), 87-100.

Cacchione, D.A., Schwab, W.C., Noble, M.A., Tate, G.B., 1988. Internal tides and sediment movement on Horizon Guyot, Mid-Pacific Mountains. Geo-Marine Letters 9(1), 11-17.

Canals, M., Lastras, G., Urgeles, R., Casamor, J.L., Mienert, J., Cattaneo, A., De Batist, M., Haflidason, H., Imbo, Y., Laberg, J.S., Locat, J., Long, D., Longva, O., Masson, D.G., Sultan, N., Trincardi, F., Bryn, P., 2004. Slope failure

dynamics and impacts from seafloor and shallow sub-seafloor geophysical data: case studies from the COSTA project. Marine Geology 213: 9-72.

Cane, T., Rohling, E.J., Kemp, A.E.S., Cooke, S., Pearce, R.B., 2002. High-resolution stratigraphic framework for Mediterranean sapropel S5: defining temporal relationships between records of Eemian climate variability. Palaeogeography, Palaeoclimatology, Palaeoecology 183, 87– 101.

Carter, R.M., Fulthorpe, C.S., Naish, T.R., 1998. Sequence concepts at seismic and outcrop scale: the distinction of physical and conceptual stratigraphic surfaces. Sedimentary Geology 122(1-4), 165-179. doi: 10.1016/S0037-0738(98)00104-3.

Capotondi, L., Borsetti, A.M.,Morigi, C., 1999. Foraminiferal ecozones, a high resolution proxy for the late Quaternary biochronology in the central Mediterranean Sea. Marine Geology 153(1–4), 253–274.

Cattaneo, A., Correggiari, A., Marsset, T., Thomas, Y., Marsset, B., Trincardi, F., 2004. Seafloor undulation pattern on the Adriatic shelf and comparison to deep-water sediment waves. Marine Geology 213: 121-148.

Chiocci, F.L., Esu, F., Tommasi, P., Chiappa, V., 1996. Stability of the submarine slope of the Tiber River delta. In: Senneset, K., (ed.). Landslides. Balkema, The Netherlands, pp 521-526.

Chiocci, F.L., 2000. Depositional response to Quaternary fourth-order sea-level fluctuations on the Latium margin (Tyrrhenian Sea, Italy). In: Hunt, D., Gawthorpe, R.L. (eds.) Sedimentary Responses to Forced Regressions. Geological Society Special Publication, 172, pp 271-289.

Ciappa, A. C., 2009. Surface circulation patterns in the Sicily Channel and Ionian Sea as revealed by MODIS chlorophyll images from 2003 to 2007. Continental Shelf Research 29, 2099-2109.

Clark, P.U., Archer, D., Pollard, D., Blum, J.D., Rial, J.A., Brovkin, V., Mix, A.C., Pisias, N.G., Roy, M., 2006. The middle Pleistocene transition: characteristics, mechanisms, and implications for long-term changes in atmospheric pCO_2. Quaternary Science Reviews 25, 3150-3184.

Colantoni, P., 1975. Note di geologia marina sul Canale di Sicilia. Giornale Geol 40(1), 181-207.

Correggiari, A., Trincardi, F., Langone, L., Roveri, M., 2001. Styles of failure in late Holocene highstand prodelta wedges on the Adriatic shelf. Journal of Sedimentary Research 71: 218-236.

Cunningham, A.P., Barker, P.F., 1996. Evidence for westward-flowing Weddell Sea Deep Water in the Falkland Trough, western South Atlantic. Deep Sea Research Part I: Oceanographic Research Papers 43(5): 643-654.

Dadson, S., Hovius, N., Pegg, S., Dade, B., Horng, M.J., Chen, H., 2005. Hyperpycnal river flows from an active mountain beld. Jornal of Geophysical Research 110, F04016. doi: 10.1029/2004JF000244.

Dansgaard, W., Clausen, H.B., Gundestrup, N., Hammer, C.U., Johnsen, S.J., Kristindottir, P.M., Reeh, N., 1982. A new Greenland deep ice core. Science 218, 1273-1277.

Dansgaard, W., Johnsen, S.J., Clausen, H.B., Dahl-Jensen, D., Gundestrup, N.S., Hammer, C.U., Hvidberg, C.S., Steffensen, J.P., Sveinbjörnsdottir, A.E., Jouzel, J., Bond, G., 1993. Evidence for general instability of past climate from a 250-kyr ice-core record. Nature 364, 218-220.

De Rijk, S., Troelstra, S.R., Rohling, E.J., 1999. Benthic foraminiferal distribution in the Mediterranean Sea. Journal of Foraminiferal Research 29(2), 93–103.

De Stigter, H. C., Jorissen, F. J., Van der Zwaan, G.J., 1998. Bathymetric distribution and microhabitat partitioning of live (Rose Bengal stained) benthic foraminifera along a shelf to deep sea transect in the southern Adriatic Sea. Journal of Foraminiferal Research 28(1), 40–65.

Di Stefano, E., 1998. Calcareous nannofossil quantitative biostratigraphy of Holes 963E and 963B (Eastern Mediterranean). In: Emeis, K.-C., Robertson, A.H.F., Richter, C., Camerlenghi, A. (eds.) Proceedings of the Ocean Drilling Program, Scientific Results 160, 99-112.

Díaz, J.I., Ercilla, G., 1993. Holocene depositional history of the Fluviá-Muga prodelta, northwestern Mediterranean Sea. Marine Geology 111: 83-92.

Ducassou, E., Capotondi, L., Murat, A., Bernasconi, S.M., Mulder, T., Gonthier, E., Migeon, S., Duprat, J., Giraudeau, J., Mascle, J., 2007. Multiproxy Late Quaternary stratigraphy of the Nile deep-sea turbidite system — Towards a chronology of deep-sea terrigenous systems. Sedimentary Geology 200(2007), 1–13.

Emiliani, C., 1955. Pleistocene temperatures. Journal of Geology 63, 538-578.

Ercilla, G., Farrán, M., Alonso, B., Diáz, J.I., 1994. Pleistocene progradational growth pattern of the northern Catalonia continental shelf (northwestern Mediterranean). Geo-Marine Letters 14(4), 264-271.

Ercilla, G., Díaz, J.I., Alonso, B., Farrán, M.,1995. Late Pleistocene-Holocene sedimentary evolution of the northern Catalonia continental shelf (northwestern Mediterranean Sea). Coninental Shelf Research 15: 1435-1451.

Ercilla, G., Wynn, R.B., Alonso, B., Baraza, J., 2002. Initiation and evolution of turbidity current sediment waves in the Magdalena turbidite system. Marine Geology 192(1-3): 153-169.

Finetti, I., 1984. Geophysical studies of the Sicily Channel rift zone. Bolletino di Geofisica Teorica ed Applicata 26, 3-28.

Flemming, B.W., 1981. Factors controlling shelf sediment dispersal along the Southeast African continental margin. Marine Geology 42(1-4), 259-277.

Freudenthal, T., Wefer, G., 2007. Scientific drilling with the sea floor drill rig MeBo. Scientific Drilling 5, 63-66.

Freudenthal, T., Wefer, G., 2013. Drilling cores on the sea floor with the remote-controlled sea floor drilling rig MeBo. Geoscientific Intrumentation, Methods and Data Systems 2, 329-337, doi: 10.5194/gi-2-329-2013.

Frigola, J., Canals, M,. Cacho, I., Moreno, A., Sierro, F.J., Flores, J.A., Berné, S., Jouet, G., Dennielou, B., Herrera, G., Pasqual, C., Grimalt, J.O., Galavazi, M., Schneider, R., 2012. A 500 kyr record of global sea-level oscillations in the Gulf of Lion, Mediterranean Sea: new insights into MIS 3 sea-level variability. Climate of the Past 8, 1067-1077.

Gámez, D., Simó, J.A., Lobo, F.J., Barnolas, A., Carrera, J., Vázquez-Suné, E., 2009. Onshore-offshore correlation of the Llobregat deltaic system, Spain: Development of deltaic geometries under different relative sea-level and growth fault influences. Sedimentary Geology 217(1-4), 65-84.

Grasso, M., 1993. Pleistocene structures along the Ionian side of the Hyblean Plateau (SE Sicily): Implications for the tectonic evolution of the Malta Escarpment. In: Max, M.D., Colantoni, P. (eds.) Geological Development of the Sicilan-Tunusian Platform. UNESCO Technical Report in Marine Sciences 58, 49-55.

Hays, J.D., Imbrie, J., Shackleton, N.J., 1976. Variations in the Earth's orbit: Pacemaker of the ice ages. Science 194, 1121-1132. doi: 10.1126/science.194.4270.1121.

Hemleben, C., Spindler, M., Anderson, O.R., 1989. Modern Planktonic foraminifera. Springer-Verlag, New York. p. 1–363.

Herbaut, C., Codron, F., Crépon, M., 1998. Separation of a coastal current at a strait level: case of the Strait of Sicily. Journal of Physical Oceanography 28, 1346-1362.

Hernández-Molina, F.J., Somoza, L., Lobo, F., 2000. Seismic stratigraphy of the Gulf of Cádiz continental shelf: a model for Late Quaternary very high-resolution sequence stratigraphy and response to sea-level fall. In: Hunt, D., Gawthorpe, R.L. (eds.) Sedimentary Responses to Forced Regressions. Geological Society Special Publication, 172, pp 329-362.

Hernández-Molina, F.J., Llave, E., Stow, D.A.V., García, M., Somoza, L., Vázquez, J.T., Lobo, F.J., Maestro, A., Díaz del Rio, V., León, R., Medialdea, T., Gardner, J., 2006. The contourite depositional system of the Gulf of Cádiz: A sedimentary model related to the bottom current activity of the Mediterranean outflow water and its interaction with the continental margin. Deep-Sea Research II 53, 1420-1463.

Hiscott, R.N., 2001. Depositional sequences controlled by high rates of sediment supply, sea-level variations, and growth faulting: the Quaternary Baram Delta of north-western Borneo. Marine Geology 175(1-4), 67-102.

Hübscher, C, Spieß, V., 2005. Forced regression systems tracts on the Bengal Shelf. Marine Geology 219(4), 207-218.

Hunt, D., Tucker, M.E., 1992. Stranded parasequences and the forced regressive wedge systems tract: deposition during base-level fall. Sedimentary Geology 81, 1-9.

Imbrie, J., Hays, J.D., Martinson, D., McIntyre, A. Mix, A., Morley, J., Pisias, N., Prell, W., Shackleton, N.J., 1984. The orbital theory of Pleistocene climate: Support from a revised chronology of the marine $\delta^{18}O$ record. In: Berger, A., et al. (eds.) Milankovitch and climate, Part 1. Hingham, Massachusetts, D. Reidel, p. 269-305.

Incarbona, A., Di Stefano, E., Sprovieri, R., Bonomo, S., Censi, C., Dinarès-Turell, J., Spoto, S., 2008. Variability in the vertical structure of the water column and paleoproductivity reconstruction in the central-western Mediterranean during the Late Pleistocene. Marine Micropaleontology 69, 26–41.

Incarbona, A., Di Stefano, E., Sprovieri, R., Bonomo, S., Pelosi, N., Sprovieri, M., 2010. Millennial-scale paleoenvironmental changes in the central Mediterranean during the last interglacial: Comparison with European and North Atlantic records. Geobios 43, 111–122.

Jarosewich, E., Nelen, J.A., Norberg, A., 1980. Reference Samples for Electron Microprobe Analysis. Geostandards Newsletter 4(1), 43-47.

Jenny, S., Goes, S., Giardini, D., Kahle, H.-G., 2006. Seismic potential of Southern Italy. Tectonophysics 415, 81-101.

Jochum, K.P., Dingwell, D.B., Rocholl, A., Stoll, B., Hofmann, A.W., Becker, S., Besmehn, A., Bessette, D., Dieze, H.-J., Dulski, P., Erzinger, J., Hellebrand, E., Hoppe, P., Horn, I., Janssens, K., Jenner, G.A., Klein, M., McDonough, W.F., Maetz, M., Mezger, K., Müker, C., Nikogosian, I.K., Pickhardt, C., Raczek, I., Rhede, D., Seufert, H.M., Simakin, S.G., Sobolev, A.V., Spettel, B., Straub, S., Vincze, L., Wallianos, A., Weckwerth, G., Weyer, S., Wolf, D., Zimmer, M., 2000. The preparation and preliminary characterisation of eight geological MPI-DING reference glasses for in-situ microanalysis. Geostandards and Geoanalytical Research 24(1), 87-133.

Johnsen, S.J., Dansgaard, W., Clausen, H.B., Langway Jr., C.C., 1972. Oxygen isotope profiles through the Antarctic and Greenland ice sheets. Nature 359, 311-313.

Jorissen, F.J., 1987. The distribution of benthic foraminifera in the Adriatic Sea. Marine Micropaleontology 12, 21-48.

Jorissen, F.J., 1999. Benthic foraminiferal successions across Late Quaternary Mediterraenan sapropels. Marine Geology 153, 91-101.

Keller, J., Ryan, W.B.F., Ninkovich, D., Altherr, R., 1978. Explosive volcanic activity in the Mediterranean over the past 200,000 yr as recorded in deep-sea sediments. Geological Society of America Bulletin 89(4), 591-604.

Kitamura, A., Matsui, H., Oda, M., 2000. Constraints on the timing of systems tract development with respect to sixth-order (41 ka) sea level changes: an example from the Pleistocene Omma Formation, Sea of Japan. Sedimentary Geology 131 (1-2), 67-76. doi: 10.1016/S0037-0738(99)00126-8.

Kraml, M., 1997. Laser-40Ar/39Ar-Datierungen an distalen marinen Tephren des jung-quartären mediterranen Vulkanismus (Ionisches Meer, METEOR-Fahrt 25/4). PhD Thesis, University of Freiburg, 216 pp.

Kuhlmann, J., Asioli, A., Strasser, M., Trincardi, F., Huhn, K., 2014. Integrated stratigraphic and morphological investigation of the Twin Slide complex offshore southern Sicily. In: Krastel, S., Behrmann, J.-H., Völker, D., Stipp, M., Berndt, C., Urgeles, R., Chaytor, J., Huhn, K., Strasser, M.,

Harbitz, C.B. (eds.) Submarine mass movements and their consequences. Springer, Heidelberg, pp. 583-594.

Langer, M. R., 1993. Epiphytic foraminifera: Marine Micropaleontology 20, 235–265.

Le Bas, M.J., Le Maitre, R.W., Streckeisen, A., Zanettini, B., 1986. A chemical classification of volcanic rocks based on the Total Alkali-Silica diagram. Journal of Petrology 27, 745-750. doi: 10.1093/petrology/27.3.745.

Lea, D.W., Martin, P.A., Pak, D.K., Spero, H.J., 2002. Reconstructing a 350 ky history of sea level using planktonic Mg/Ca and oxygen isotope records from a Cocos Ridge core. Quaternary Science Reviews 21(1-3), 283-293.

Lermusiaux, P.F.J., Robinson, A.R., 2001. Features of dominant mesoscale variability, circulation patterns and dynamics in the Strait of Sicily. Deep-Sea Research I 48, 1953-1997.

Lisiecki, L.E., Raymo, M.E., 2005. A Pliocene-Pleistocene stack of 57 globally distributed benthic d18O records. Paleoceanography 20, PA1003. doi: 10.1029/2004PA001071.

Liu, J., Saito, Y., Kong, X., Wang, H., Wen, C., Yang, Z., Nakashima, R., 2010. Delta development and channel incision during marine isotope stages 3 and 2 in the western South Yellow Sea. Marine Geology 278(1-4), 54-76.

Liquete, C., Canals, M., De Mol, B., De Batist, N., Trincardi, F., 2008. Quaternary stratal architecture of the Barcelona prodeltaic continental shelf (NW Mediterranean). Marine Geology 250(3-4), 234-250.

Lirer, F., Sprovieri, M., Ferraro, L., Vallefuoco, M., Capotondi, L., Cascella, A., Petrosino, P., Insinga, D.D., Pelosi, N., Tamburrino, S., Lubritto, C., 2013. Integrated stratigraphy for the Late Quaternary in the eastern Tyrrhenian Sea. Quaternary International 292, 71-85.

Lobo, F.J., Hernández-Molina, F.J., Somoza, L., Díaz del Río, V., Dias, J.M.A., 2002. Stratigraphic evidence of an upper Pleistocene TST to HST complex on the Gulf of Cádiz continental shelf (south-west Iberian Peninsula). Geo-Marine Letters 22(2), 95-107.

Lourens, L.J., 2004. Revised tuning of Ocean Drilling Program Site 964 and KC01B (Mediterranean) and implications for the $\delta^{18}O$, tephra, calcareous nannofossil, and geomagnetic reversal chronologies of the past 1.1. Myr. Paleoceanography 19, PA3010. doi: 10.1029/2003PA000997.

Marsset, T., Xia, D., Berné, S., Liu, Z., Bourillet, J.-F., Wang, K., 1996. Stratigraphy and sedimentary environments during the Late Quaternary, in the Eastern Bohai Sea (North China Platform). Marine Geology 135(1-4), 97-114.

Martinson, D.G., Pisias, N.G., Hays, J.D., Imbrie, J., Moore, T.C., Shackleton, N.J., 1987. Age dating and the orbital theory of the ice ages: Development of a high-resolution 0 to 300,000-year chronostratigraphy. Quaternary Research 27, 1-29. doi: 10.1016/0033-5894(87)90046-9.

Massari, F., Sgavetti, M., Rio, D., D'Alessandro, A., Prosser, G., 1999. Composite sedimentary record of falling stages of Pleistocene glacio-eustatic cycles in a shelf setting (Crotone basin, south Italy). Sedimentary Geology 127 (1-2), 85-110. doi: 10.1016/S0012-8252(01)00069-1.

Masson, D.G., Harbitz, C.B., Wynn, R.B., Pedersen, G., Lvholt, F., 2006. Submarine landslides: processes, triggers and hazard prediction. Philosophical Transactions of the Royal Society A 364, 2009-2039. doi: 10.1098/rsta.2006.1810.

Melki, T., Kallel, N., Jorrissen, F.J., Guichard, F., Dennielou, B., Berné, S., Labeyrie, L., Fontugne, M. 2009. Abrupt climate change, sea surface salinity and paleoproductivity in theWestern Mediterranean (Gulf of Lion) during the last 28 kyr. Palaeogeography, Palaeoclimatology, Palaeocology 279, 96–113.

Milankovitch, M., 1930. Mathematische Klimalehre und astronomische Theorie der Klimaschwankungen. In: Köppen, W., Geiger, R. (eds.), Handbuch der Klimatologie, 1(A). Berlin, Gebrüder Borntraeger, 1-176.

Milliman, J.D., Syvitski, J.P.M., 1992. Geomorphic/tectonic control of sediment discharge tot he ocean: the importance of mountainous rivers. Journal of Geology 100, 525-544.

Milliman, J.D., Farnsworth, K.L., 2011. River discharge tot he coastal ocean: a global synthesis. Cambridge University Press.

Millot, C., 1999. Circulation in the Western Mediterranean Sea. Journal of Marine Systems 20, 423-442.

Minisini, D., Trincardi, F., Asioli, A., Canu, M., Foglini, F., 2007. Morphologic variability of exposed mass-transport deposits on the eastern slope of Gela Basin (Sicily channel). Basin Research 19, 217-240. doi: 10.1111/j.1365-2117.2007.00324.x.

Minisini, D., Trincardi, F., 2009. Frequent failure of the continental slope: The Gela Basin (Sicily Channel). Journal of Geophysical Research 114, F03014, doi: 10.1029/2008JF001037.

Mitchum, R.M.J., Van Wagoner, J.C., 1991. High-frequency sequences and their stacking patterns: sequence-stratigraphic evidence of high-frequency eustatic cycles. Sedimentary Geology 70(2-4), 131-160. doi: 10.1016/0037-0738(91)90139-5.

Mix, A.C., Bard, E., Schneider, R., 2001. Environmental processes of the ice age: land, oceans, glaciers (EPILOG). Quaternary Science Reviews 20, 627-657.

Mosher, D.C., Thomson, R.E., 2002. The forseslope hills: large-scale, fine-grained sediment waves in the Strait of Georgia, British Columbia. Marine Geology 192: 275-295.

Mulder, T., Syvitski, J.P.M., Migneon, S., Faugere, J.C., Savoye, B., 2003. Marine hyperpycnal flows: initiation, behavior, and related deposits. A review. Marine and Petroleum Geology 20, 861-882.

Nakajima, T., Satoh, M., 2001. The formation of large mudwaves by turbidity currents on the levees of the Toyama deep-sea channel, Japan Sea. Sedimentology 48, 435-463.

Negri, A., Capotondi, L., Keller, J., 1999. Calcareous nannofossils, planktonic foraminifera and oxygen isotopes in the late Quaternary sapropels of the Ionian Sea. Marine Geology 157, 89–103.

Normark, W.R., Hess, G.R., Stow, D.A.V., Bow, A.J., 1980. Sediment waves on the Monterrey fan levee: a preliminary physical interpretation. Marine Geology 42: 201-232.

North Greenland Ice Core Project Members, 2004. High-resolution record of Northern Hemisphere climate extending into the last interglacial period. Nature 431, 147-151.

Onken, R., Robinson, A.R., Lermusiaux, PF.J., Haley Jr., P.J., Anderson, L.A., 2003. Data-driven simulations of synoptic circulation and transports in the Tunisia-Sardinia-Sicily region. Journal of Geophysical Research 108, 8123-8136.

Osterberg, E.C., 2006. Late Quaternary (marine isotope stages 6-1) seismic sequence stratigraphic evolution of the Otago continental shelf, New Zealand. Marine Geology, 229(3-4), 159-178.

Palanques, A., Puig, P., Guillén, J., Jiménez, J., Gracia, V., Sánchez-Arcilla, A., Madsen, O., 2002. Near-bottom suspended sediment fluxes on the microtidal low-energy Ebro continental shelf (NW Mediterranean). Continental Shelf Research 22: 285-303.

Patacca, E. scandone, P., Giunta, G., Liguori, V., 1979. Mesozoic paleotectonic evolution of the Ragusa zone (Southeastern Sicily). Geol Romana 18: 331-369.

Paterne, M., Guichard, F., Labeyrie, J., 1988. Explosive activity of the south Italian volcanoes during the past 80,000 years as determined by marine tephrochronology. Journal of Volcanology and Geothermal Research 34, 153-172.

Pérez-Folgado, M., Sierro, F.J., Flores, J.A., Cacho, I., Grimalt, J.O., Zahn, R., Shackleton, N., 2003. Western Mediterranean planktonic foraminifera events and millennial climatic variability during the last 70 kyr. Marine Micropaleontology 48, 49-70.

Petit, J.R., Jouzel, J., Raynaud, D., Barkov, N.I., Barnola, J.-M., Basile, I., Bender, M., Chappellaz, J., Davis, M., Delaygue, G., Delmotte, M., Kotlyakov, V.M., Legrand, M., Lipenkov, V.Y., Lorius, C., Pépin, L., Ritz, C., Saltzman, E., Stievenard, M., 1999. Climate and atmospheric history of the past 420,000 years from the Vostok ice core, Antarctica. Nature 399(6735), 429-436. doi: 10.1038/20859.

Pierini. S., Rubino, A., 2001. Modeling the oceanic circulation in the area of the Strait of Sicily: the remotely forced dynamics. Journal of Physical Oceanography 31, 1397-1412.

Piper, D.J.W., Aksu, A.E., 1992. Architecture of stacked Quaternary deltas correlated with global oxygen isotopic curve, Geology 20(5), 415-418.

Piva, A., Asioli, A., Schneider, R.R., Trincardi, F., Andersen, N., Colmenero-Hidalgo, E., Dennielou, B., Flores, J.-A., Vigliotti, L., 2008. Climatic cycles as expressed in sediments of the PROMESS1 borehole PRAD1-2, Central Adriatic, for the last 370 ka, 1: integrated stratigraphy. Geochemistry, Geophysics, Geosystems 9(1), Q01R01. doi: 10.1029/2007GC001713.

POEM group, 1992. General circulation of the Eastern Mediterranean. Earth-Science Reviews 32, 285-309.

Puig, P., Palanques, A., Gullién, J., 2001. Near-bottom suspended sediment variability caused by storms and near-inertial internal waves on the Ebro mid continental shelf (NW Mediterranean). Marine Geology 178(1-4): 81-93.

Puig, P., Ogston, A.S., Guillén, J., Fain, A.M.V., Palanques, A., 2007. Sediment transport processes from the topset to the foreset of a crenulated clinoform (Adriatic Sea). Continental Shelf Research 27: 452-474.

Pujol, C., Vergnaud Grazzini, C., 1995. Distribution patterns of live planktic foraminifera as related to regional hydrography and productive systems of the Mediterranean Sea. Marine Micropaleontology 25, 187–217.

Raymo, M.E., 1997. The timing of major climate terminations. Paleoceanography 12(4), 577-585. doi: 10.1029/97PA01169.

Rebesco, M., Neagu, R.C., Cuppari, A., Muto, A., Accettella, D., Dominici, R., Cova, A., Romano, C., Caburlotto, A., 2009. Morphobathymetric analysis and evidence of submarine mass movements in the western Gulf of Taranto (Calabria margin, Ionian Sea). International Journal of Earth Sciences 98(4), 791-805.

Reimer, P.J., Bard, E., Bayliss, A., Beck, J.W., Blackwell, P.G., Bronk Ramsey, C., Buck, C.E., Cheng, H., Edwards, R.L., Friedrich, M., Grootes, P.M., Guilderson, T.P., Haflidason, H., Hajdas, I., Hatté, C., Heaton, T.J., Hoffman, D.L., Hogg, A.G., Hughen, K.A., Kaiser, K.F., Kromer, B., Manning, S.W., Niu, M., Reimer, R.W., Richards, D.A., Scott, E.M., Southon, J.R., Staff, R.A., Turney, C.S.M., van der Plicht, J., 2013. IntCal13 and Marine13 radiocarbon age calibration curves 0-50,000 years cal BP. Radiocarbon 55(4), 1869-1887.

Ridente, D., Trincardi, F., 2002. Eustatic and tectonic control on deposition and lateral variability of Quaternary regressive sequences in the Adriatic basin. Marine Geology 184(3-4), 273-293.

Ridente, D., Trincardi, F., Pica, A., Asioli, A., Cattaneo, A., 2008. Sedimentary response to climate and sea level changes during the past ~ 400 ka from borehole PRAD1-2 (Adriatic margin). Geochemistry Geophysics Geosystems 9(Q09R04).

Ridente, D., Trincardi, F., Piva, A., Asioli, A., 2009. The combined effect of sea level and supply during Milankovitch cyclicity: evidence from shallow-marine $\delta^{18}O$ records and sequence architecture (Adriatic margin). Geology 37(11), 1003-1006.

Ridente, D., Trincardi, F., Piva, A., Asioli, A., 2013. The combined effect of sea level and supply during Milankovitch cyclicity: Evidence from shallow-marine d18O records and sequence architecture (Adriatic margin). Geology 37, 1003-1006. doi: 10.1130/G25730A.1.

Robinson, A.R., Golnaraghi, M., 1994. The physical and dynamical oceanography of the Mediterranean. In: Malanotte-Rizzoli, P., Robinson, A.R. (Eds.), Ocean Processes in Climate Dynamics: Global and Mediterranean Examples. Kluwer Academic Publishers, the Netherlands, pp. 255-306.

Robinson, A.R., Sellschopp, J., Warn-Varnas, A., Leslie, W.G., Lozano, C.J., Haley Jr., P.J., Anderson, L.A., Lermusiaux, P.F.J., 1999. The Atlantic Ionian Stream. Journal of Marine Systems 20, 129-156.

Rodero, J., Pallares, L., Maldonado, A., 1999. Late Quaternary seismic facies of the Gulf of Cadiz Spanish margin: depositional processes influenced by sea-level change and tectonic controls. Marine Geology 155(1-2), 131-156.

Rohling E.-J., Gieskes, W.W.C., 1989. Late Quaternary changes in Mediterranean lntermediate Water density and formation rate. Paleoceanography 4, 531-545.

Rohling, E.-J., Hayes, A., De Rijk, S., Kroon, D., Zachariasse, W.-J., Eisma, D., 1998. Abrupt cold spells in the Northwest Mediterranean. Paleoceanography 13, 316–322.

Rouis-Zaragouni, I., Turon, J.-L., Londeix, L., Essallami, L., Kallel, N., Sicre, M.-A., 2010. Environmental and climatic changes in the central Mediterranean Sea (Siculo–Tunisian Strait) during the last 30 ka based on dinoflagellate cyst and planktonic foraminifera assemblages. Palaeogeography, Palaeoclimatology, Palaeoecology 285, 17–29.

Sammari, C., Millot, C., Taupier Letage, I., Stefani, A., Brahim, M., 1999. Hydrological characteristics in the Tunisia-Sardinia-Sicily area during spring 1995. Deep-Sea Research I 46, 1671-1703.

Sánchez-Cabeza, J.A., Masqué, P., Ani-Ragolta, I., Merino, J., Alvisi, F., Palnques, A., Puig, P., 1999. Sediment accumulation rates in the southern Barcelona continental margin (NW Mediterranean Sea) derived from 210Pb and 137Cs chronology. Progress in Oceanography 44, 313-332.

Schmiedl, G., de Bovée, F., Buscail, R., Charrière, B., Hemleben, C., Medernach, L., Picon, P., 2000. Trophic control of benthic foraminiferal abundance and microhabitat in the bathyal Gulf of Lions, western Mediterranean Sea. Marine Micropaleontology 40(3), 167– 188.

Schröder, C.J., Scott, D.B., Medioli, F.S., 1987. Can smaller benthic foraminifera be ignored in paleoenvironmental analyses? Journal of Foraminiferal Research 17(2), 101-105

Shackleton, N.J., Opdyke, N.D., 1973. Oxygen isotope and palaeomagnetic stratigraphy of equatorial Pacific core V28-238: Oxygen isotope temperature and ice volumes on a 10^5 and 10^6 year scale. Quaternary Research 3, 39-59. doi: 10.1016/0033-5894(73)90052-5.

Siani, G., Paterne, M., Arnold, M., Bard, E., Métivier, B., Tisnerat, N., Bassinot, F., 2000. Radiocarbon reservoir ages in the Mediterranean Sea and Black Sea. Radiocarbon 42, 271-280.

Siani, G., Paterne, M., Colin, C. 2010. Late glacial to Holocene planktic foraminifera bioevents and climatic record in the South Adriatic Sea. Journal of Quaternary Science 25(5): 808-821.

Sierro, F.J., Andersen, N., Bassetti, M.A., Berné, S., Canals, M., Curtis, J.H., Dennielou, B., Abel Flores, J., Frigola, J., Gonzalez-Mora, B., Grimalt, J.O., Hodell, D.A., Jouet, G., Pérez-Folgado, Schneider, R., 2009. Phase relationship between sea level and abrupt climate change. Quaternary Science Reviews 28, 2867-2881.

Siddall, M., Rohling, E.J., Almogi-Labin, A., Hemleben, Ch, Meischner, D., Schmelzer, I., Smeed, D.A., 2003. Sea-level fluctuations during the last glacial cycle. Nature 423, 853-858.

Siddall, M., Rohling, E.J., Thompson, W.G., Waelbroeck, C., 2008. Marine Isotope Stage 3 sea level fluctuations: data synthesis and new outlook. Reviews of Geophysics 46, RG4003. doi: 10.1029/2007RG000226.

Somoza, L., Hernández-Molina, F.J., De Andrés, J.R., Rey, J., 1997. Continental shelf architecture and sea-level cycles: Late Quaternary high-resolution stratigraphy of the Gulf of Cádiz, Spain. Geo-Marine Letters 17(2), 133-139.

Sorgente, R., Drago, A.F., Ribotti, A., 2003. Seasonal variability in the Central Mediterranean Sea circulation. Annales Geophysicae 21, 299-322.

Sprovieri, R., Di Stefano, E., Incarbona, A., Gargano, M.E., 2003. A high-resolution record of the last deglaciation in the Sicily Channel based on foraminifera and calcareous nannofossil quantitative distribution. Palaeogeography, Palaeoclimatology, Palaeoecology 202, 119–142.

Sprovieri, R., Di Stefano, E., Incarbona, A., Oppo, D.W., 2006. Suborbital climate variability during Marine Isotopic Stage 5 in the central Mediterranean basin: evidence from calcareous plankton record. Quaternary Science Reviews 25, 2332-2342. doi: 10.1016/j.quascirev.2006.01.035.

Sun, S.-S., McDonough, W.F., 1989. Chemical and isotopic systematics of oceanic basalts: implications for mantle composition and processes. Geological Society, London, Special Publications 42, 313-345. doi: 10.1144/GSL.SP.1989.042.01.19.

Stuiver, M., Reimer, P.J., 1993. Extended 14C database and revised CALIB radiocarbon calibration program. Radiocarbon 35, 215-230.

Svensson, A., Andersen, K.K., Bigler, M., Clausen, H.B., Dahl-Jensen, D., Davies, S.M., Johnsen, S.J., Muscheler, R., Parrenin, F., Rasmussen, S.O., Röthlisberger, R., Seierstad, I., Steffensen, J.P., Vinther, B.M., 2008. A 60000 year Greenland stratigraphic ice core chronology. Climate of the Past 4, 47-57.

Sydow, J., Roberts, H.H., 1994. Stratigraphic framework of a late Pleistocene shelf-edge delta, Northeast Gulf of Mexico. American Association of Petroleum Geologists Bulletin 78(8), 1276-1312.

Talling, P.J., 2014. On the triggers, resulting flow types and frequencies of subaqueous sediment density flows in different settings. Marine Geology 352, 155-182. doi: 10.1016/j.margeo.2014.02.006.

Thunell, R.C., 1978. Distribution of recent planktonic foraminifera in surface sediments of the Mediterranean Sea. Marine Micropaleontology 3, 147–173.

Tomlinson, E.L., Albert, P.G., Wulf, S., Brown, R.J., Smith, V.C., Keller, J., Orsi, G., Bourne, A.J., Menzies, M.A., 2014. Age and geochemistry of tephra layers from Ischia, Italy: constraints from proximal-distal correlations with Lago Grande di Monticchio. Journal of Volcanology and Geothermal Research 287: 22-39.

Trincardi, F., Argnani, A., 1990. Gela submarine slide: a major basin-wide event in the Plio-Quaternary foredeep of Sicily. Geo-Marine Letters 10, 13-21.

Trincardi, F., Normark, W.R., 1988. Sediment waves on the Tiber prodelta slope. Geo-Marine Letters 8, 149-157.

Trincardi, F., Correggiari, A., 2000. Quaternary forced regression deposits in the Adriatic basin and the record of composite sea-level cycles. In: Hund, D., Gawthorpe, R.L.G. (eds.) Sedimentary responses to forced regressions. Geological Society, London, Special Publications, p. 245-269.

Urgeles, R., De Mol, B., Liquete, C., Canals, M., De Batist, N., Hughes-Clarke, J.E., Amblás, D., Arnau, P.A., Calafat, A.M., Casamor, J.L., Centella, V., De Rycker, K., Fabrés, J., Frigola, J., Lafuerza, S., Lastras, G., Sànchez, A., Zuniga, D., Versteeg, W., Willmott, V., 2007. Sediment undulations on the Llobregat prodelta: Signs of early slope instability or bottom current activity? Journal of Geophysical Research 112, Art. No. B05102.

Urgeles, R., Cattaneo, A., Puig, P., Liquete, C., De Mol, B., Amblàs, D., Sultan, N., Trincardi, F., 2011. A review of undulated sediment features on prodeltas: distinguishing sediment transport from sediment deformation. Marine Geophysical Research 32: 49-69.

UNEP (United Nations Environment Programme), 2003. Riverine transport of water, sediments and pollutants to the Mediterranean Sea. MAP Technical Reports Series 141, Athens, 111 pp

Van der Zwaan, G.J., Jorissen, F.J., 1991. Biofacial patterns in river-induced shelf anoxia. In: Tyson, R.V., Pearson, T.H. (eds.) Modern and Ancient Continental Shelf Anoxia. Geological Society Special Publication 58. p. 65-82.

Vanoudheusden, E., Sultan, N., Cochonat, P., 2004. Mechanical behaviour of unsaturated marine sediments: experimental and theoretical approaches. Marine Geology 213, 323-342.

Verdicchio, G., Trincardi, F., 2008. Mediterranean shelf-edge muddy contourites: examples from the Gela and South Adriatic basins. Geo-Marine Letters 28, 137-151. doi: 10.1007/s00367-007-0096-9.

Waelbroeck, C., Labeyrie, L., Michel, E., Duplessy, J.C., McManus, J.F., Lambeck, K., Balbon, E., Mabracherie, M., 2002. Sea-level and deep water temperature changes derived from benthic foraminifera isotopic records. Quaternary Science Reviews 21(1-3), 295-305.

Warrick, J.A., Xu, J., Noble, M.A., Lee, H.J., 2008. Rapid formation of hyperpycnal sediment gravity currents offshore of a semi-arid California river. Continental Shelf Research 28, 991-1009.

Watts, W.A., Allen, J.R.M., Huntley, B., 1996. Vegetation history and palaeoclimate of the last glacial period at Lago Grande di Monticchio, southern Italy. Quaternary Science Reviews 15, 133-153.

Wheatcroft, R.A., Sommerfield, C.K., Drake, D.E., Borgeld, J.C., Nittrouer, C.A., 1997. Rapid and widespread dispersal of flood sediment on the northern California margin. Geology 25, 163-166. doi: 10.1130/0091-7613(1997)025<0163:RAWDOF>2.3.CO;2.

Wheatcroft, R.A., Borgeld, J.C., 2000. Oceanic flood deposits on the northern California shelf: large-scale distribution and small-scale physical properties. Continental Shelf Research 20, 2163-2190.

Wulf, S., Kraml, M., Brauer, A., Keller, J., Negendank, J.F.W., 2004. Tephrochronology of the 100 ka lacustrine sediment record of Lago Grande di Monticchio (southern Italy). Quaternary International 122, 7-30. Doi: 10.1016/j.quaint.2004.01.028.

Wynn, R.B., Stow, D.A.V., 2002. Classification and characterization of deep-water sediment waves. Marine Geology 192, 7-22.

Table 6.A.1. Raw data of main elemental analysis (WDS-EPMA) on individual glass shards from tephra-rich layer GeoB14403.

		Main elemental composition (WDS-EPMA)														
Sample Name	#	SiO2	TiO2	Al2O3	FeO	MnO	MgO	CaO	Na2O	K2O	P2O5	SO3	Cl	F	TOTAL (volatile-free)	TOTAL
14403-8_5P-2_I_P1	9	59.29	0.55	18.02	2.43	0.17	0.37	1.24	6.80	6.52	0.06	0.12	0.52	0.22	95.45	96.30
14403-8_5P-2_I_P2	10	61.24	0.54	17.82	2.56	0.20	0.35	1.24	7.29	6.33	0.08	0.18	0.52	0.25	97.65	98.60
14403-8_5P-2_I_P3	11	60.13	0.54	18.09	2.51	0.33	0.28	1.02	8.44	5.78	0.02	0.05	0.76	0.30	97.14	98.24
14403-8_5P-2_I_P5	13	60.32	0.53	17.90	2.35	0.17	0.34	1.24	6.79	6.45	0.10	0.13	0.54	0.18	96.19	97.04
14403-8_5P-2_I_P7	15	58.20	0.50	17.90	2.43	0.23	0.25	0.98	8.16	6.01	0.03	0.07	0.73	0.30	94.69	95.79
14403-8_5P-2_I_P8	16	59.82	0.58	18.00	2.52	0.32	0.28	1.04	8.37	5.82	0.06	0.10	0.74	0.33	96.82	97.99
14403-8_5P-2_I_P9	17	59.83	0.54	18.05	2.45	0.22	0.39	1.21	7.04	6.20	0.04	0.15	0.51	0.07	95.97	96.70
14403-8_5P-2_I_P10	18	59.57	0.58	18.02	2.86	0.34	0.29	1.13	7.70	5.97	0.04	0.13	0.68	0.29	96.50	97.60
14403-8_5P-2_I_P11	19	60.30	0.56	17.98	2.45	0.19	0.25	0.96	7.59	5.90	0.04	0.03	0.67	0.19	96.21	97.10
14403-8_5P-2_I_P12	20	60.38	0.57	18.20	2.61	0.31	0.28	0.97	8.62	5.81	0.06	0.10	0.80	0.34	97.82	99.06
14403-8_5P-2_I_P13	21	59.41	0.54	18.24	2.49	0.21	0.26	0.98	7.48	6.04	0.00	0.09	0.77	0.31	95.65	96.81
14403-8_5P-2_I_P14	22	60.99	0.57	17.90	2.47	0.22	0.31	1.30	6.54	6.56	0.06	0.11	0.51	0.13	96.92	97.66
14403-8_5P-2_I_P15	23	58.77	0.54	17.84	2.54	0.27	0.24	1.04	7.52	5.81	0.04	0.04	0.78	0.33	94.60	95.75
14403-8_5P-2_I_P17	25	60.17	0.55	18.36	2.54	0.33	0.26	1.07	7.98	5.85	0.03	0.09	0.75	0.30	97.14	98.27
14403-8_5P-2_I_P18	26	60.74	0.57	18.19	2.63	0.29	0.28	1.03	8.48	5.78	0.05	0.07	0.72	0.27	98.04	99.10
14403-8_5P-2_I_P19	27	61.10	0.54	18.20	2.72	0.26	0.26	0.97	8.40	5.92	0.01	0.05	0.78	0.30	98.39	99.51
14403-8_5P-2_I_P20	28	61.53	0.57	18.32	2.78	0.28	0.24	1.00	8.40	5.80	0.07	0.06	0.77	0.39	98.99	100.21
14403-8_5P-2_I_P21	49	61.50	0.54	18.03	2.49	0.20	0.41	1.20	7.17	6.42	0.03	0.16	0.53	0.14	98.00	98.82
14403-8_5P-2_I_P22	50	61.78	0.49	18.16	2.37	0.16	0.37	1.24	7.16	6.36	0.02	0.19	0.48	0.15	98.10	98.93
14403-8_5P-2_I_P23	51	60.54	0.56	18.68	2.73	0.25	0.30	1.00	8.09	5.80	0.00	0.10	0.76	0.35	97.96	99.17
14403-8_5P-2_I_P24	52	60.69	0.54	18.27	2.54	0.27	0.30	0.98	8.11	5.88	0.03	0.09	0.74	0.29	97.62	98.73
14403-8_5P-2_I_P25	53	59.92	0.53	18.01	2.57	0.18	0.25	1.02	8.04	5.75	0.05	0.08	0.77	0.33	96.32	97.50
14403-8_5P-2_I_P26	54	60.27	0.49	17.34	2.53	0.12	0.41	1.31	6.70	6.45	0.10	0.18	0.42	0.08	95.73	96.41
14403-8_5P-2_I_P27	55	60.09	0.52	18.15	2.56	0.32	0.26	0.98	7.80	6.04	0.06	0.05	0.74	0.30	96.79	97.88
14403-8_5P-2_I_P28	56	60.49	0.57	18.37	2.49	0.29	0.25	1.02	8.22	5.67	0.02	0.04	0.74	0.33	97.39	98.50
14403-8_5P-2_I_P29	57	61.38	0.56	18.39	2.64	0.25	0.28	1.02	8.13	5.96	0.04	0.06	0.78	0.20	98.65	99.70
14403-8_5P-2_I_P30	58	60.76	0.57	18.35	2.70	0.16	0.32	1.12	7.96	6.09	0.05	0.07	0.74	0.22	98.08	99.10
14403-8_5P-2_II_P1	29	59.89	0.57	17.77	2.63	0.17	0.32	1.22	6.75	6.20	0.09	0.15	0.51	0.17	95.61	96.43
14403-8_5P-2_II_P2	30	59.63	0.51	17.60	2.80	0.10	0.35	1.18	6.72	6.18	0.04	0.12	0.53	0.13	95.13	95.91
14403-8_5P-2_II_P3	31	59.01	0.58	17.67	2.49	0.30	0.28	1.06	7.65	5.96	0.05	0.07	0.73	0.29	95.05	96.14
14403-8_5P-2_III_P1	32	61.18	0.55	18.12	2.57	0.26	0.31	1.14	7.46	6.24	0.04	0.10	0.61	0.21	97.87	98.79
14403-8_5P-2_III_P2	33	61.28	0.58	18.20	2.45	0.18	0.36	1.17	7.94	6.20	0.05	0.10	0.63	0.19	98.41	99.33
14403-8_5P-2_III_P3	34	60.12	0.53	17.73	2.39	0.19	0.33	1.20	6.87	6.22	0.03	0.11	0.54	0.19	95.60	96.44
14403-8_5P-2_III_P5	36	60.60	0.55	18.18	2.72	0.35	0.25	0.97	8.13	5.88	0.02	0.09	0.80	0.36	97.64	98.88
14403-8_5P-2_III_P6	37	58.34	0.59	17.19	2.22	0.26	0.32	1.23	6.47	6.02	0.02	0.12	0.56	0.22	92.66	93.57
14403-8_5P-2_III_P8	39	59.46	0.59	17.84	2.52	0.24	0.30	1.12	7.40	5.78	0.02	0.10	0.68	0.25	95.27	96.30
14403-8_5P-2_III_P11	42	60.72	0.56	18.39	2.41	0.22	0.29	1.05	7.96	6.01	0.05	0.05	0.76	0.37	97.66	98.84
Average		60.26	0.55	18.04	2.54	0.24	0.30	1.10	7.63	6.04	0.04	0.10	0.66	0.25	96.75	97.76
std-deviation	n=37	0.87	0.03	0.30	0.14	0.06	0.05	0.11	0.63	0.25	0.02	0.04	0.11	0.08	1.39	1.45

Table 6.A.2. Raw data of trace and rare earth elemental analysis (LA-ICP-MS) on individual glass shards from tephra-rich layer GeoB14403.

		trace and rare earth elements (LA-ICP-MS)																								
Sample Name	#	Rb	Sr	Y	Zr	Nb	Ba	La	Ce	Pr	Nd	Sm	Eu	Gd	Tb	Dy	Ho	Er	Tm	Yb	Lu	Hf	Ta	Pb	Th	U
14403-8_5P-2_I_P3	11	551.92	2.65	81.74	961.91	149.34	3.44	176.01	342.08	33.47	111.09	19.96	0.94	16.30	2.39	13.08	2.96	8.44	1.53	8.26	1.40	20.24	6.92	79.54	62.82	19.37
14403-8_5P-2_I_P8	16	495.82	4.92	71.94	817.61	126.51	6.40	157.86	300.41	30.19	103.20	19.28	1.30	15.53	2.45	13.50	2.85	8.57	1.56	7.64	1.57	18.29	6.26	73.24	54.96	18.61
14403-8_5P-2_I_P10	18	475.83	6.49	79.49	780.39	125.74	6.12	153.07	312.93	32.69	113.26	26.12	1.83	16.52	2.67	14.19	2.59	8.06	1.25	9.66	1.48	17.68	6.82	72.74	52.93	16.33
14403-8_5P-2_I_P11	19	523.56	5.77	77.39	886.75	132.85	6.16	167.06	326.19	32.05	110.24	18.91	1.56	15.98	2.36	12.91	3.09	9.55	1.56	9.38	1.39	19.10	6.65	75.04	57.63	18.04
14403-8_5P-2_I_P12	20	567.38	5.91	85.35	959.06	146.89	12.85	179.16	342.38	33.30	117.58	20.96	1.11	17.08	2.51	14.80	3.15	10.23	1.50	10.04	1.62	21.29	6.86	87.33	65.31	19.34
14403-8_5P-2_I_P13	21	733.79	3.12	104.91	1248.09	189.73	3.30	224.75	425.02	41.00	146.09	24.27	1.82	20.65	2.67	17.90	3.68	11.89	1.79	11.57	2.12	25.93	8.03	107.85	81.69	25.93
14403-8_5P-2_I_P14	22	323.76	10.15	47.13	425.76	68.55	14.74	95.39	190.51	20.62	77.84	15.06	1.76	10.84	1.82	9.30	1.76	4.90	0.81	5.08	1.02	10.88	3.60	53.98	28.89	8.73
14403-8_5P-2_I_P15	23	649.74	3.55	95.21	1131.82	169.99	5.81	204.38	395.04	39.30	127.95	22.43	1.80	17.95	2.67	16.19	3.42	9.57	1.54	9.60	1.69	24.23	7.78	95.45	73.34	23.67
14403-8_5P-2_I_P17	25	539.88	13.35	78.82	924.87	143.38	27.74	169.79	330.21	32.17	109.12	20.06	1.17	16.79	2.40	15.06	2.65	8.00	1.55	9.21	1.62	20.37	6.18	87.74	63.13	19.55
14403-8_5P-2_I_P19	27	527.49	3.38	78.74	918.74	137.62	3.35	164.15	318.98	31.42	103.30	18.36	1.29	14.35	2.62	13.88	2.94	7.54	1.26	11.04	1.38	20.10	6.07	78.04	59.63	18.50
14403-8_5P-2_I_P22	50	305.74	8.09	39.34	367.07	59.41	13.86	81.67	169.27	18.28	69.94	13.59	1.65	9.68	1.58	8.34	1.60	4.41	0.63	4.94	0.76	8.20	3.23	47.75	23.46	7.39
14403-8_5P-2_I_P28	56	574.76	5.71	83.69	1022.07	157.44	5.47	185.59	358.11	34.77	116.78	23.09	1.24	16.81	2.64	16.50	3.45	8.77	1.51	11.68	2.11	22.03	7.22	86.74	67.21	21.13
Average		522.47	6.09	76.98	870.35	133.95	9.10	163.24	317.59	31.61	108.87	20.17	1.46	15.71	2.40	13.80	2.85	8.33	1.37	9.01	1.51	19.03	6.30	78.79	57.58	18.05
std-deviation	n=12	119.14	3.15	18.08	255.44	37.45	7.16	40.27	73.30	6.51	20.12	3.59	0.32	2.96	0.35	2.76	0.63	2.08	0.34	2.22	0.38	5.04	1.47	16.51	16.68	5.33

7 Manuscript II

"Integrated stratigraphic and morphological investigation of the Twin Slide complex offshore southern Sicily"

Authors: Kuhlmann, Jannis (MARUM, University of Bremen, Germany)
Asioli, Alessandra (Istituto di Geoscienze e Georisorse, CNR-UOS di Padova, Italy)
Michael Strasser (Geological Institue, ETH Zurich, Switzerland)
Trincardi, Fabio (Istituto di Scienza Marine, ISMAR-CNR,Venezia, Italy)
Huhn, Katrin (MARUM, University of Bremen, Germany)

Status: Published in: Krastel, S., Behrmann, J.-H., Völker, D., Stipp, M., Berndt, C., Urgeles, R., Chaytor, J., Huhn, K., Strasser, M., Harbitz, C.B. (eds.) *Submarine mass movements and their consequences. Advances in Natural and Technological Hazards Research Vol. 37*. Springer, Heidelberg, pp. 581-594.
doi: 10.1007/978-3-319-00972-8_52

Objectives:

- Unravelling the complex failure architecture related to frequent landsliding during the late Quaternary
- Disentangling individual failure stages of the coeval *Twin Slide* complex and providing a conceptual model for their temporal evolution
- Identifying the origin of distinct morphological seafloor appearances with regard to *Twin Slide* mass transport deposits
- Assessing potential failure mechanisms

Integrated stratigraphic and morphological investigation of the Twin Slide complex offshore southern Sicily

Jannis Kuhlmann[1], Alessandra Asioli[2], Michael Strasser[3], Fabio Trincardi[4], Katrin Huhn[1]

[1]MARUM – Center for Marine Environmental Sciences, University of Bremen, Bremen, Germany
[2]Istituto di Geoscienze e Georisorse, CNR-UOS di Padova, Padova, Italy
[3]Geological Institute, ETH Zurich
[4]Istituto di Scienze Marine, ISMAR-CNR, Venezia, Italy

The Holocene Twin Slides form the most recent of recurrent mass wasting events along the NE portion of Gela Basin within the Sicily Channel, central Mediterranean Sea. Here, we present new evidence on the morphological evolution and stratigraphic context of this coeval slide complex based on deep-drilled sediment sequences providing a >100 ka paleo-oceanographic record. Both Northern (NTS) and Southern Twin Slide (STS) involve two failure stages, a debris avalanche and a translational slide, but are strongly affected by distinct preconditioning factors linked to the older and buried *Father Slide*. Core-acoustic correlations suggest that sliding occurred along sub-horizontal weak layers reflecting abrupt physical changes in lithology or mechanical properties. Our results show further that headwall failure predominantly took place along sub-vertical normal faults, partly through reactivation of buried *Father Slide* headscarps.

Key words: Twin Slide complex, Gela Basin, stratigraphy, morphology, isotope records

7.1 Introduction

Submarine landslides occur at all margins worldwide (e.g., Masson et al. 2006). To enhance knowledge on slope failure processes and trigger mechanisms, small-scaled slide complexes are uniquely positioned, as full data coverage often allows for a detailed definition of the internal structure (e.g., Canals et al., 2004; Lee, 2005). One prominent example is the Twin Slide complex at the NE portion of Gela Basin within Sicily Channel, Central Mediterranean Sea. These coeval multistage failures occur only 6 km apart from each other and feature similar runout lengths and fall heights – yet their failure areas and mass-transport deposits (MTDs) show markedly different morphologies (Minisini et al., 2007; Minisini and Trincardi, 2009).

To unravel the architecture of the Twin Slide complex and elaborate on available stratigraphic models, this study presents two deep-drilled sediment sequences recovered with gravity cores and Bremen seafloor drill rig MeBo (Freudenthal and Wefer, 2007). We introduce a detailed age model relying on foraminifera-based eco-biostratigraphy as well as $\delta^{13}C$ and $\delta^{18}O$ records, and propose revised stratigraphic models based on the correlation of core data to acoustic sub-bottom profiles.

7.1.1 Geological setting

The Twin Slide complex is located along the NE part of Gela Basin within the Strait of Sicily, Central Mediterranean Sea (*Figure 7.1*). The basin represents a Pliocene-Quaternary foredeep of the Maghrebian fold-and-thrust belt and is filled with 2.5 km of shallowing-upward marine sediments (Colantoni, 1975; Argnani, 1990). In the north, Gela Basin is overthrusted by the Gela nappe, the southwest migrating outermost thrust wedge of the Maghrebian chain (Butler et al., 1992). Its tip parallels the present-day shelfbreak and plunges in direction of the basin, thus favouring a steeply sloped morphology (Trincardi and Argnani, 1990).

7.1.2 Material and methods

The data set for this study was acquired aboard RV Maria S. Merian during cruise MSM15/3 in 2010. Main devices used include a parametric sediment

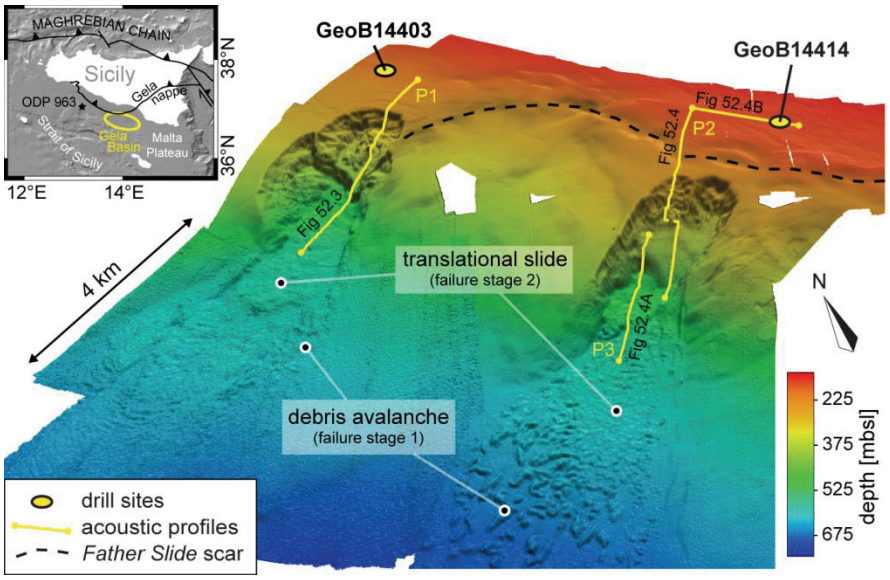

Figure 7.1. 3D multibeam shaded relief of the Twin Slides in the Gela Basin (lighting from NE, sun angle 35°, vertical exaggeration 5, grid spacing 10 m); yellow circles indicate core locations, yellow lines sub-bottom echosounder profiles P1 and P2/P3 shown in *Figure 7.3* and *7.4*, respectively; dashed black line marks the outline of the *Father Slide* headscar (Minisini et al. 2007); variability in data resolution derives from the two distinct multibeam systems used. Inset: location of the Gela Basin in the Strait of Sicily, central Mediterranean (from GEBCO database).

echosounder with dm-scale vertical resolution operating at 4 kHz (Atlas Parasound), two bathymetric multibeam echosounder operating at 12 kHz (Kongsberg Simrad EM120) and 95 kHz (EM1002), and coring devices (gravity corer up to 6 mbsf, MeBo up to 51.9 mbsf).

A GEOTEK Ltd. multi-sensor core logger (MSCL) was used for non-destructive measurements of core-physical properties including bulk density, compressional wave velocity, and magnetic susceptibility.

Geochemical logging for light elements (Al to Fe) was performed on an Avaatech II core scanner using a generator setting of 10 kV, 0.2 mA and a sampling time of 20 s. Ca/Fe ratios served as an indicator for major lithological changes within the cored sequences.

For micropaleontology, sediment subsamples (20-50 g each) were taken with a vertical resolution of at least 20 cm. The sediment was freeze-dried, soaked in distilled water and washed through a 63 µm mesh sieve. A foraminifera-based eco-biostratigraphy relying on the identification of (temporary) disappearance and (re)occurrence of planktic species was developed to identify paleo-environmental changes already defined in Central Mediterranean (e.g., Minisini et al., 2007; Incarbona et al., 2010). Similarly, an isotope stratigraphy was established based on $\delta^{13}C$ and $\delta^{18}O$ records of benthic *Bulimina marginata* and planktonic *Globigerinoides ex gr. ruber*. Measurements were performed at MARUM using a Finnigan MAT 252 mass spectrometer coupled with a carbonate preparation device type "Bremen" (standard deviation <0.05‰ for $\delta^{13}C$ and <0.07‰ for $\delta^{18}O$).

7.2 Morphology and stratigraphy

High resolution bathymetric data shows the Twin Slide complex as a prominent feature on the NE continental slope of the Gela Basin (*Figure 7.1*). The upper slope exhibits the crescent-shaped, irregular morphological expression of an extensive buried slide termed *Father Slide* (Minisini et al., 2007). Southern Twin Slide (STS) affected the downslope area of this structure, while Northern Twin Slide (NTS) emanated from undisturbed sediment units along the edge of the *Father Slide* scar. Both failure areas expose two

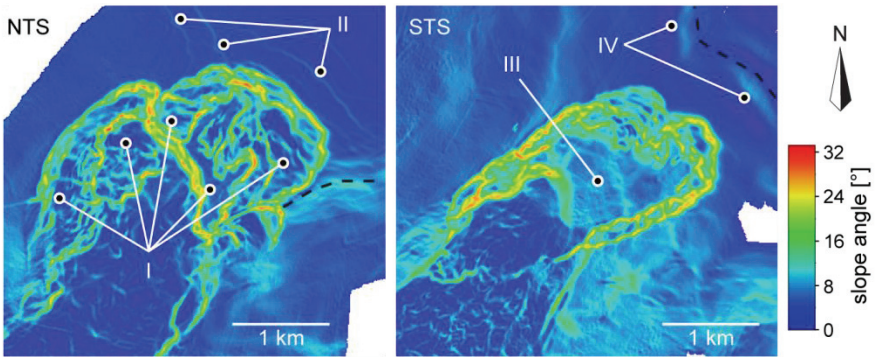

Figure 7.2. Gradient maps of the upper failure zones of NTS and STS (grid spacing 10 m); I: individual slide terraces reflecting source sediments of NTS; II: scarps indicating retrogressive failure; III: constant slope gradient reflecting post *Father Slide* morphology; IV: moat structures indicating sediment drift.

distinct MTDs of varying extend indicating individual failure stages: a debris avalanche deposit with blocks appearing elongated dominantly in the direction of motion (stage 1), and an overriding translational slide deposit likely affecting less consolidated units of the upper slope (stage 2).

Pre-failure depositional variation induced by the *Father Slide* manifests in the morphological appearance of upper failure areas as presented in *Figure 7.2*. NTS shows a terrace-like structure with several individual slide scarps dipping by as much as 32° (I), reflecting multiple failure phases that affected planar, well-layered source units (see section 7.2.1). Pronounced morphological steps of 1-2.5 m upslope of the headwall indicate incipient scarping through retrogressive failure (II). In contrast, the upper failure area of STS exhibits a constant slope gradient of 8-10° (III) reflecting the underlying post *Father Slide* morphology (see section 7.2.2) and is confined by steep lateral headwalls dipping 15-20°. Upslope, contour-parallel crests with asymmetric slopes indicate erosional moat and related drift deposits (*Figure 7.2*, IV), likely adding to the slopes instability through rapid sedimentation and successive generation of excess pore pressure (Verdicchio and Trincardi, 2008).

7.2.1 Site GeoB14403 (NTS)

Parasound profile P1 (*Figure 7.3*) across the upper failure zone of NTS reveals the stratigraphic context of site GeoB14403. The drilled sequence penetrates three sequence stratigraphic units (after Minisini et al. 2007, *Figure 7.3A*): (I) deposits resting on top of erosive unconformity ES1, (II) a progradational wedge pinching out towards NE and (III) deposits beneath sequence boundary SB1. Truncated acoustic reflections within units II and III mark two individual slide scarps, presumably deriving from failure stage 2 (solid red lines, *Figure 7.3B*). Upslope, prominent faults with clear reflection offsets show normal sense of shear and thus a downslope mass movement component, indicating locations of incipient scarping and retrogressive failure (solid black lines, *Figure 7.3*). Two horizons acting as glide planes can be identified beneath the base of acoustically transparent units within this upper failure zone (dashed blue lines), one of which being intersected by the drilled cores. Downslope, older and potentially more consolidated sedimentary units were dissected and transported basinward in the debris avalanche of failure stage 1. Associated scars are filled with a thick, acoustically transparent layer. As suggested by the bathymetric data (*Figure 7.1*) and estimations on the amount of involved material (*Figure 7.3*), this layer represents the slide deposit of failure stage 2, possibly covering stage 1 avalanche deposits.

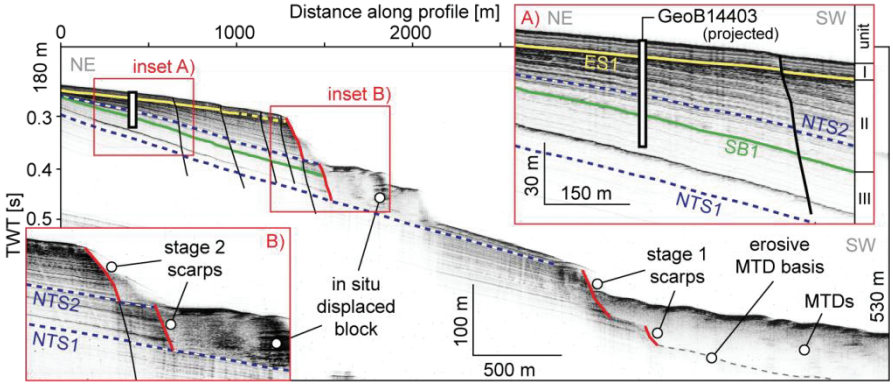

Figure 7.3. Parasound profile P1 illustrating the stratigraphic framework of NTS. Solid/dashed yellow line: erosive unconformity/conformity ES1; solid green line: sequence boundary SB1; dashed blue lines: glide planes of stage 2 failure; solid black lines: faults indicating locations of potential retrogressive failure; solid red lines: slide scarps. Inset A: magnification of drill site area indicating sequence stratigraphic units. Inset B: magnification of stage 2 slide scarps showing glide planes beneath acoustically transparent units.

7.2.2 Site GeoB14414 (STS)

Parasound profiles P2 and P3 correlate drilled sediment units with the downslope failure area of STS and reveal a complex pre-failure setting dominated by buried *Father Slide* (*Figure 7.4*). MTDs of this event can be traced as acoustically transparent facies into two prominent scarps (dashed red lines), which sharply truncate reflector packages of upslope sediment units. Post-failure deposits infilling the *Father Slide* scar appear to have failed by reactivation of the downslope scarp, which correlates with the position of sub-vertical normal faults, as indicated by offsets of neighbouring reflections. Similarly, the more recent and seafloor-exposed slide deposit of failure stage 2 dissected sedimentary sequences of units I, II and III along with interstratified, highly sensitive drift deposits (Verdicchio and Trincardi 2008). Downslope, a marked morphological step of ~50 m indicates headwall failure of post *Father Slide* units associated with stage 1 debris avalanche (*Figure 7.4A*).

The location of the drill site upslope of *Father Slide* scar does not allow for an investigation of sediment units affected by STS. However, the bases of MTDs originating from the *Father Slide* event rest on top of three strong, bedding parallel acoustic reflectors (FS1-FS3). The upper two of these sub-horizontal layers can be traced back into the sediment sequence recovered at station GeoB14414 (*Figure 7.4B*). Besides the shallow ES1, a second discontinuity truncates underlying seismic reflectors in greater depth (ES2, solid green line), interpreted as a shelf-wide erosional unconformity of the penultimate sea level lowstand during Marine Isotope Stage 6 (MIS6; Sprovieri et al., 2006, and references therein).

7.3 Morphology and stratigraphy

At average recovery rates of 91 % (site GeoB14403) and 88 % (site GeoB14414) gravity and MeBo cores provide a sediment sequence reaching down to 51.9 mbsf and 27.0 mbsf, respectively. The dominant lithology is a silty nannofossil clay with quartzose silt, volcanic glass, and minor amounts of foraminifers and authigenic pyrite. A thin ash layer of dm-scale exhibiting normal grading and a relatively sharp base is intercalated at a depth of ~25.7 mbsf (GeoB14403). A more detailed analysis of geotechnical properties of the sequence recovered at site GeoB14403 is presented by Ai et al. (2014).

7.3.1 Site GeoB14403 (NTS)

The composite plot depicted in *Figure 7.5* integrates physical/chemical log data with stable

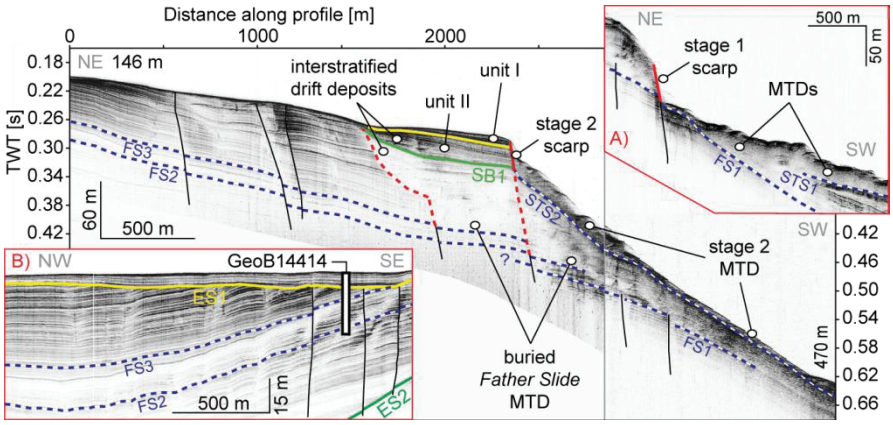

Figure 7.4. Parasound profile P2 illustrating the stratigraphic framework of STS. Annotations analogue to Fig 3. Dashed blue lines: glide planes of stage 2 failure (STS) and buried Father Slide (FS); solid black lines: faults; dashed red lines: Father Slide scarps. Inset A: lower slope showing headscarp of failure stage 1 and resulting MTDs (profile P3 in *Figure 7.1*). Inset B: magnification of drill site area (for location see *Figure 7.1*).

isotope measurements and related Marine Isotope Stages (MIS) and Dansgaard-Oeschger Interstadials (DOIS; Sprovieri et al., 2006, and references therein). A vertical acoustic profile of the drill site is added for reference, converted into depth scheme using core velocity logs. Magnetic susceptibility values are cut at 40 SI x 10^{-5} to reveal their general pattern. The combined data suggests a division of the drilled sediment sequence into the following intervals:

1. 0 – 4.5 mbsf. Holocene interval without systematic changes in lithology. Heavier values in the $\delta^{13}C$ *B. marginata* record indicate sapropel 1 equivalent (S1 eq), accompanied by high Ca/Fe ratios. Foraminifera assemblages suggest the presence of Pre-Boreal at the base of this interval as do correlations to the $\delta^{18}O$ records of core A236P09 from Gela Basin (Asioli and Trincardi, unpublished data).

2. 4.5 – 10.4 mbsf. Interval with scarce and cold planktic assemblage along with middle shelf benthic assemblage dominated by *Cassidulina laevigata carinata*, similar to an interval in core P08 (Minisini et al., 2007) referred to as MIS2. The erosive base correlates to the strong acoustic reflection of ES1.

3. 10.4 – 29.1 mbsf. Interval with scarce and cold planktic and middle shelf benthic assemblages interpreted as MIS3. In accordance with borehole PRAD1-2 (Piva et al., 2008) the bioevent Last Common Occurrence of *Globorotalia inflata* (LCO *G.i.*) is positioned in DOIS12. Accordingly, DOIS17 at the base of this interval marks MIS4/3 boundary, which correlates with the upper glide plane NTS2.

4. 29.1 – 36.8 mbsf. $\delta^{18}O$ records of *G. ruber* (up to 2.72‰) are comparable with MIS4 values of core KC01B (Lourens, 2004) from the Ionian Basin. Sequence boundary SB1, accompanied by an offset in Ca/Fe ratio, marks the end of DOIS19 and defines MIS5/4 boundary according to Sprovieri et al. (2006).

5. 36.8 – 51.9 mbsf. Two relatively warm subintervals (42.0 – 46.5 and 49.6 down-core) alternate with colder ones marked by scarce planktic and middle shelf benthic assemblages. The presence of *G. ruber*, *Neogloboquadrina dutertrei* and vegetal remains along with a benthic assemblage dominated by intermediate and deep infaunal taxa may indicate a sapropel equivalent deposition (S3 eq) at the lower warm interval.

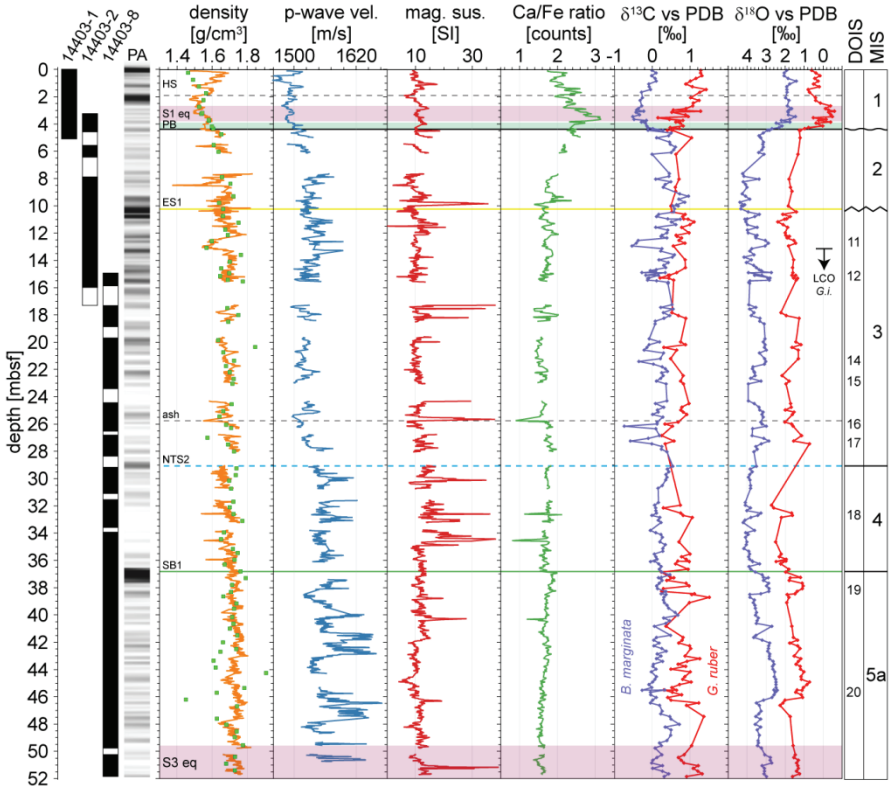

Figure 7.5. Composite plot integrating acoustic, physical and chemical logs with stable isotope measurements of site GeoB14403. Chronological interpretations according to Marine Isotope Stages (MIS) and Dansgaard-Oeschger Interstadials (DOIS). Green squares: MAD density parameters determined according to IODP shipboard practices (Blum 1997); light red area: sapropel equivalents; PB: Pre-Boreal; HS: high-stand system tract; LCO *G.i.*: bioevent Last Common Occurrence of *G. inflata*; PA: vertical acoustic profile at drill site; PDB: Pee Dee Belemnite standard.

7.3.2 Site GeoB14414 (STS)

Analogue to station GeoB14403, the combined data of the composite plot presented in *Figure 7.6* suggests a division of the sediment sequence into three intervals as follows:

1. 0 – 4.3 mbsf. Holocene interval coherent to that of site GeoB14403, but with a sharp erosive base that correlates to a pronounced acoustic reflection and is represented in all core logs (e.g., sudden decrease of Ca/Fe values from 2.8 to 2.0).

2. 4.3 – 6.2 mbsf. Short interval with augmented content of organic matter reflected by greater variability in magnetic susceptibility. Down-core, the interval is limited by an erosive base correlating to the strong acoustic reflection of ES1. At the interval top, lighter values in the $\delta^{18}O$ record of *B. marginata* suggest the presence of Bolling-Allerod. Though this interpretation cannot be validated by foraminifera assemblages (planktic taxa too scarce) the interval is ascribed to MIS2.

3. 6.2 – 27.0 mbsf. An extended interval that has been ascribed to MIS5 and may be further divided into three subintervals (from bottom to top):

   (III) 12.0 – 27.0 mbsf. A Sapropel equivalent deposit records very warm conditions (light red area). $\delta^{18}O$ records of *G. ruber* (up to -1.5‰) are compatible to MIS5a, c and e records from the Ionian Basin (core KC01B, Lourens, 2004; ODP site 963, Sprovieri et al., 2006). However, the presence of *Globigerinoides sacculifer* and the absence of *Globorotalia inflata* suggest a quite expanded MIS5e interval (Incarbona et al., 2010).

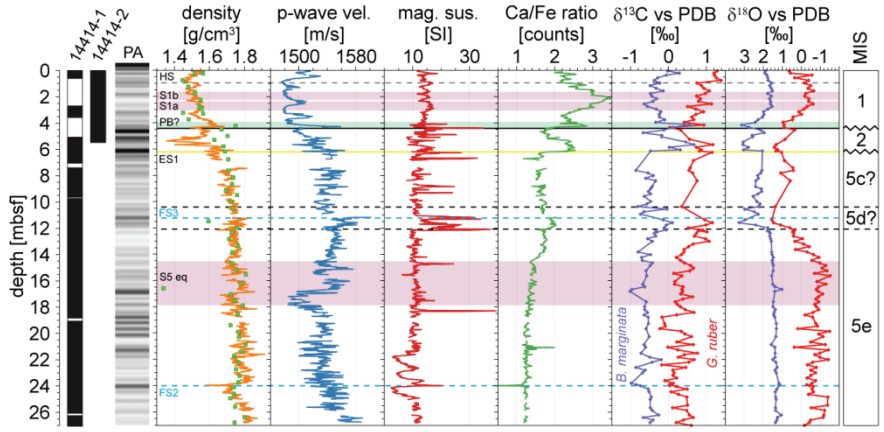

Figure 7.6. Composite plot integrating acoustic, physical and chemical logs with stable isotope measurements of site GeoB14414. Annotations analogue to *Figure 7.5*.

(II) 10.5 – 12.0 mbsf. Short interval with elevated values of p-wave velocity, magnetic susceptibility and Ca/Fe ratio. Both $\delta^{18}O$ records show values heavier than the underlying interval, which are too light to infer the presence of MIS4 (in comparison with core KC01B, Lourens, 2004). Hence, this interval has been tentatively ascribed to MIS5d.

(III) 6.2 – 10.5 mbsf. This interval shows values lighter than those of the underlying interval for both $\delta^{18}O$ records, indicating the relatively warmer phase related to MIS5c.

7.4 Discussion and conclusions

Based on deep drilled cores and acoustic datasets, this study introduces an integrated chronological framework to the architecture of the Twin Slide complex, both revising and extending stratigraphic records presented earlier (Minisini et al., 2007; Minisini and Trincardi, 2009). A conceptual model of the Twin Slides combining acoustic evidence (section 7.2) with the developed age model (section 7.3) is shown in *Figure 7.7*. Both events appear to involve two failure stages, but are strongly controlled by their distinctive pre-failure architecture. NTS affected undisturbed units at the edge of buried *Father Slide* and cut down MIS5 deposits during failure stage 1, resulting in a debris avalanche preserved along the sides of the slide (*Figure 7.1*). Most of this blocky outrun, however, is covered by a translational slide deposit of failure stage 2 deriving from retrogressive failure of younger units (predominantly MIS4/3) in the upslope region.

In contrast, STS rests on the infillings of buried *Father Slide*, which affected early MIS5(e-c) sedimentary units overlying the erosional unconformity of the penultimate sea level lowstand during MIS6. The stage 1 failure (debris avalanche) reworked *Father Slide* MTD as well as stratified post-failure deposits, while the stage 2 failure dissected progradational units of MIS4/3 – interstratified by drift deposits – along the reactivated shear zone of *Father Slide*. Unlike NTS, the resulting slide deposit only partly covers stage 1 debris avalanche (*Figure 7.1*).

Summarizing these findings, failure stages of both Twin Slides appear to involve sedimentary units of similar stratigraphic age. This contrasts previous assumptions by Minisini et al. (2007), who related observed dissimilarities in geomorphology to distinct stratigraphic units affected by failure. Instead, these dissimilarities may simply reflect differences in the amount of material involved in the two failure stages. Similarly, core-acoustic correlations suggest that headwall failure of the Twin Slides predominantly occurs along sub-vertical normal faults (*Figure 7.3, 7.4*) and translational sliding along sub-horizontal weak layers reflecting abrupt physical changes in

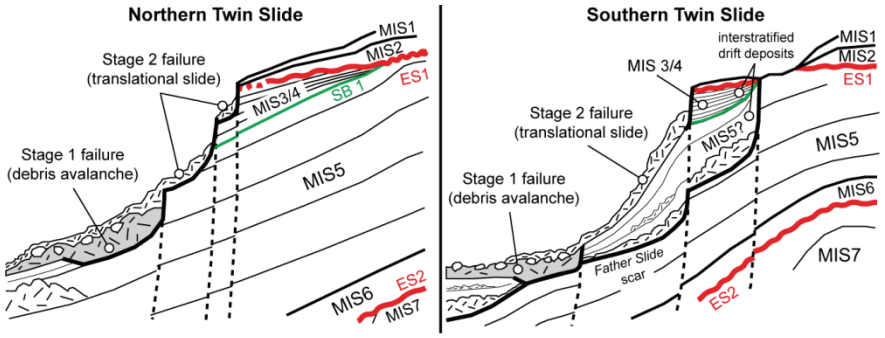

Figure 7.7. Schematic sketch of NTS (left) and STS (right) illustrating implications of the presented stratigraphic record. MIS: Marine Isotope Stage; ES: unconformities associated with 100 ka Glacial cycles: SB: sequence boundary.

lithology or mechanical properties (*Figure 7.5, 7.6*). The shallowest part of NTS failed along the MIS4/3 boundary and correlates to a section identified by Ai et al. (2014) as a preferential slip plane due to its reduced internal friction angle. They further propose a moderate earthquake (M = 4.0-4.8) to be sufficient to trigger failure of this layer. Acoustic data suggests that similar mechanisms may have been responsible for the stage 2 failure of STS (*Figure 7.7*). Stage 1 failure of STS, instead, partly reactivated the shear plane previously followed by *Father Slide* (*Figures 7.4* and *7.7*). To further assess the role of these layers in sediment failure, however, additional data on their geotechnical properties is required.

Acknowledgements

We gratefully acknowledge the constructive reviews by Yasuhiro Yamada and Frank Strozyk. $\delta^{13}C/\delta^{18}O$ analyses, MSCL and XRF core scanning were carried out at the lab facilities of MARUM. This study is funded through DFG-Research Center/Cluster of Excellence "The Ocean in the Earth System".

References

Ai, F., Kuhlmann, J., Huhn, K., Strasser, M., Kopf, A., 2014. Submarine slope stability assessment of the central Mediterranean continental margin: the Gela Basin. In: Krastel, S., Behrmann, J.-H., Völker, D., Stipp, M., Berndt, C., Urgeles, R., Chaytor, J., Huhn, K., Strasser, M., Harbitz, C.B. (eds.) Submarine mass movements and their consequences. Springer, Heidelberg, pp. 225-236.

Argnani, A., 1990. The strait of Sicily Rift Zone: foreland deformation related to the evolution of a back-arc basin. Journal of Geodynamics 12, 311-331.

Blum, P., 1997. Physical properties handbook: a guide to the ship board measurement of physical properties of deep-sea cores. ODP Tech Note 26, College Station, Tex.

Butler, R.W.H., Grasso, M., LaManna, F., 1992. Origin and deformation of the Neogene-Recent Maghrebian foredeep at the Gela Nappe, SE Sicily. Journal of the Geological Society (London) 149, 547-556.

Canals, M., Lastras, G., Urgeles, R., Casamor, J.L., Mienert, J., Cattaneo, A., De Batist, M., Haflidason, H., Imbo, Y., Laberg, J.S., Locat, J., Long, D., Longva, O., Masson, D.G., Sultan, N., Trincardi, F., Bryn, P., 2004. Slope failure dynamics and impacts from seafloor and shallow sub-seafloor geophysical data: case studies from the COSTA project. Marine Geology 213(1-4), 9-72.

Colantoni, P., 1975. Note di geologia marina sul Canale di Sicilia. Giornale di Geologica 40(1), 181-207.

Freudenthal, T., Wefer, G., 2007. Scientific drilling with the sea floor drill rig MeBo. Scientific Drilling 5, 63-66.

Incarbona, A., Di Stefano, E., Sprovieri, R., Bonomo, S., Pelosi, N., Sprovieri, M., 2010. Millenial-scale paleoenvironmental changes in the central Mediterranean during the last interglacial: Comparison with European and North Atlantic records. Geobios 43(1), 111-122.

Lee, H.J., 2005. Undersea landslides: extent and significance in the Pacific Ocean, an update. Natural Hazards and Earth System Sciences 5, 877-892.

Lourens, L.J., 2004. Revised tuning of Ocean Drilling Program Site 964 and KC01B (Mediterranean) and implications for the $\delta^{18}O$, tephra, calcareous nannofossil, and geomagnetic reversal chronologies of the past 1.1 Myr. Paleoceanography 19(3), PA3010. doi: 10.1029/2003PA000997.

Masson, D.G., Harbitz, C.B., Wynn, R.B., Pedersen, G., Løvholt, F., 2006. Submarine landslides: processes, triggers and hazard prediction. Philosophilcal Transactions of the Royal Society A 364, 2009-2039. doi: 10.1098/rsta.2006.1810.

Minisini, D., Trincardi, F., 2009. Frequent failure of the continental slope: The Gela Basin (Sicily Channel). Journal of

Geophysical Research 114, F03014. doi: 10.1029/2008JF001037.

Minisini, D., Trincardi, F., Asioli, A., Canu. M., Foglini, F., 2007. Morphologic variability of exposed mass-transport deposits on the eastern slope of Gela Basin (Sicily channel). Basin Research 19, 217-240. doi: 10.1111/j.1365-2117.2007.00324.x.

Piva, A., Asioli, A., Schneider, R.R., Trincardi, F., Andersen, N., Colmenero-Hidalgo, E., Dennielou, B., Flores, J.-A., Vigliotti, L., 2008. Climatic cycles as expressed in sediments of the PROMESS1 borehole PRAD1-2, central Adriatic, for the last 370 ka: 1. Integrated stratigraphy. Geochemistry Geophysics Geosystems 9(1), Q01R01. doi:10.1029/2007GC001713.

Sprovieri, R., Di Stefano, E., Incarbona, A., Oppo, D.W., 2006. Suborbital climate variability during Marine Isotopic Stage 5 in the Central Mediterranean basin: evidence from calcareous plankton record. Quaternary Science Reviews 25, 2332-2342. doi: 10.1016/j.quascirev.2006.01.035.

Trincardi, F., Argnani, A., 1990. Gela Submarine Slide: A Major Basin-Wide Event in the Plio-Quaternary Foredeep of Sicily. Geo-Marine Letters 10, 13-21.

Verdicchio, G., Trincardi, F., 2008. Mediterranean shelf-edge muddy contourites: examples from the Gela and South Adriatic basins. Geo-Marine Letters 28, 137-151. doi: 10.1007/s00367-007-0096-9.

8 Manuscript III

"Landslide frequency and failure mechanism - the case of NE Gela Basin (Strait of Sicily)"

Authors: Kuhlmann, Jannis (MARUM, University of Bremen, Germany)
Asioli, Alessandra (Istituto di Geoscienze e Georisorse, CNR-UOS di Padova, Italy)
Trincardi, Fabio (Istituto di Scienza Marine, ISMAR-CNR,Venezia, Italy)
Klügel, Andreas (Department of Geosciences, University of Bremen, Germany)
Huhn, Katrin (MARUM, University of Bremen, Germany)

Status: In preparation for *Marine Geology*

Objectives:

- Providing an extensive database on the frequency and timing of landsliding at Gela Basin
- Identifying and evaluating regional pre-conditioning factors and trigger mechanisms
- Analyzing glide planes and investigating their microstructure and origin
- Assessing the role of prefailure stratal architecture, especially with regard to sequence-stratigraphic boundaries

Landslide frequency and failure mechanisms - the case of NE Gela Basin (Strait of Sicily)

Jannis Kuhlmann[1], Alessandra Asioli[2], Fabio Trincardi[3], Andreas Klügel[4], Katrin Huhn[1]

[1]MARUM – Center for Marine Environmental Sciences, University of Bremen, Bremen, Germany
[2]Istituto di Geoscienze e Georisorse, CNR-UOS di Padova, Padova, Italy
[3]Istituto di Scienze Marine, ISMAR-CNR, Venezia, Italy
[4]Department of Geosciences, University of Bremen, Bremen, Germany

This study uses an integrated chronological framework from two boreholes and complementary ultra-high-resolution acoustic profiling in order to assess the frequency of submarine landsliding at the continental margin of NE Gela Basin. A total of eight mass transport deposits have been recognized that occurred within the last 87 ka. Accurate age control was achieved through direct radiocarbon dating (in three cases) or indirect dating relying on isotope stratigraphy and micropaleontological considerations. The majority of recognized events occurred during conditions of sea level fall and lowstand and comprises translational movement of mudflows along sub-horizontal weak layers that relate to (1) sequence-stratigraphic boundaries reflecting paleoenvironmental fluctuations, and (2) volcanoclastic material. The major predisposing factor in this area resembles rapid loading of fine-grained homogenous strata and successive generation of excess pore pressure, as expressed by several fluid escape structures. Recurrent failure, however, requires repeated generation of favourable conditions and seismic activity, though comparably low in this area, is shown to represent a legitimate trigger mechanism.

Key words: Gela Basin, Strait of Sicily, slope failure, failure frequency, predisposing factors, trigger mechanisms

8.1 Introduction

Frequent slope failure is a common phenomenon along active continental margins (e.g., Hampton et al., 1996; Masson et al., 2006). In the last decades considerable effort has been undertaken, partly in joint efforts of academia and industry, in order to elucidate the mechanisms and processes at the origin of these events (e.g., Vanneste et al., 2014, and references therein). In order to understand the key parameters that control sediment instabilities in a given setting, however, it is essential to study not only their spatial distribution but as well the frequency of submarine landslides (e.g., McAdoo et al., 2000; Canals et al., 2004). Evaluation of the recurrence of landslide processes is key not only to the assessment of potential hazards (e.g., Locat and Lee, 2002), but as well to unravel the influence of paleoenvironmental fluctuations on the role of predisposing factors and trigger mechanisms. This task requires great care in order to discern individual failure events and is facilitated through unprecedented quality of modern acoustic devices and the availability of long cores that provide age control on retrieved sediment successions.

In this study, we present a detailed investigation of the historical landslide record intercalated in the late-Quaternary sedimentary sequences at the continental margin of NE Gela Basin. Ultra-high-resolution parametric subbottom profiles are correlated with two drilled boreholes on the shelf edge (GeoB14403, ~m) and the lower slope (GeoB14401, ~m) and allow full stratigraphic control on observed landslide deposits by either (1) direct dating through 14C radiometric analyses, (2) indirect dating through centennial- to millennial-scale oxygen isotope stratigraphies and micropaleontologic interpretations of foraminifera assemblages, and (3) tracing of acoustic reflectors. On the basis of this wealth of data, we present an estimate on the recurrence of failure and evaluate their temporal distribution as well as causing factors and involved mechanisms. Recovery and microscopic analysis of a glide plane allow to draw

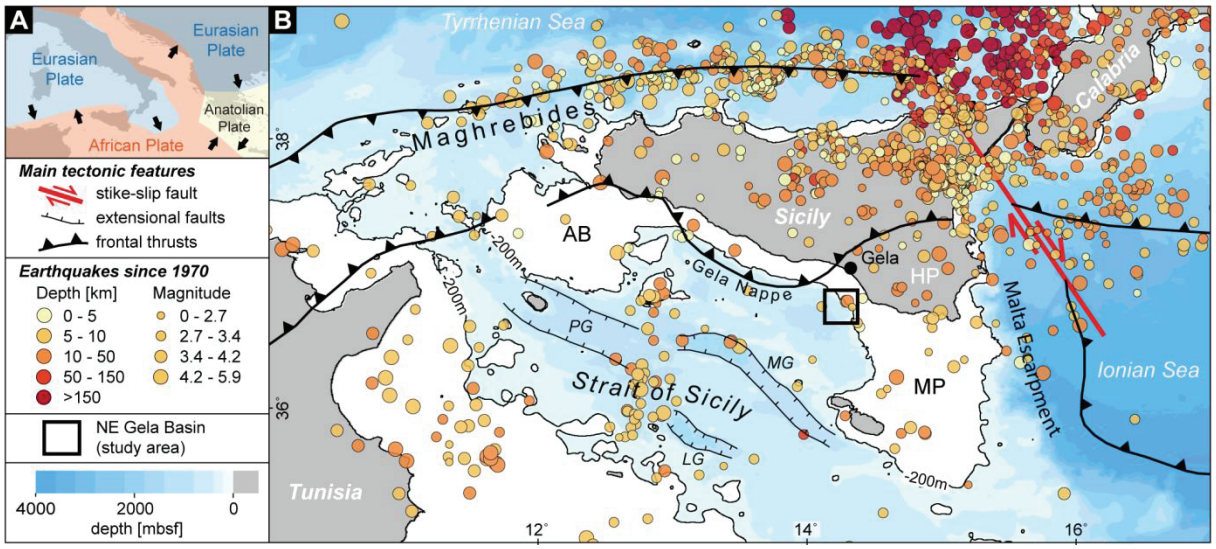

Figure 8.1. A) Simplified sketch of the central Mediterranean plate boundaries with arrows indicating direction of plate motion (after Dilek and Sandvol, 2009; Camerlenghi et al., 2010). B) Bathymetric map of the study area in the Strait of Sicily illustrating main tectonic and geographic elements (after Jenni et al., 2006; Accaino et al., 2010; Civile et al., 2010; bathymetric data taken from GEBCO database). Superposed on this map is the U.S. Geological Survey (USGS) earthquake record since 1970, both size- and colour-coded depending on the magnitude and depth of the event, respectively (see legend on the left hand side). The Pantelleria graben (PG), the Malta graben (MG) and the Linosa graben (LG) are the principal tectonic depressions in the area. AB = Adventure Bank; MP = Malta Plateau.

further conclusions on the role of prefailure stratal architecture.

8.2 Regional setting

8.2.1 Geological setting and seismic activity

Filled with as much as 2500 m of shallowing-upward marine sediments, the Gela Basin represents the most recent (Pliocene-Quaternary) foredeep basin of the Maghrebian fold-and-thrust belt, which reflects the ongoing subduction of the African plate beneath the Eurasian one (Figure 8.1A; Colantoni, 1975; Argnani, 1990). In the North, it is overthrusted by the Gela Nappe – a southwest migrating contractional front representing the southernmost thrust wedge of the Maghrebian chain (Figure 8.1B; Argnani, 1990; Butler et al., 1992). Plunging in direction of the basin, the surface slope in the frontal area of Gela Nappe contributes to instability of overlaying sediments and manifests in frequent failure along the shelf edge in the study area (Figure 8.2). An extensive basin-wide landslide deposit, the 600 ka BP *Gela Slide*, occurred immediately above the tip of this tectonic element and covers an estimated 1500 km² (Tincardi and Argnani, 1990; Di Stefano et al., 1993). Evidence of more recent and significantly smaller landslide events was presented by Minisini et al. (2007), Minisini and Trincardi (2009) and Kuhlmann et al. (2014a). Subsequent to emplacement of Gela Nappe, a phase of general uplift associated with widespread volcanic activity characterized the mid-Pliocene to late Quaternary, favouring the deposition of eruptive material in the study area (Gardiner et al., 1993). To the East, Gela Basin is confined by the Malta Plateau, the seaward counterpart of the Hyblean plateau on mainland Sicily (Figure 8.1B). The south-westward dipping depositional ramp of the Hyblean-Malta platform is overlain by a Pliocene-Quaternary succession of progradational sequences, resulting in a peculiar setting of SW-dipping sediment bodies in the study area (Figure 8.3). The southern margin of the Gela Basin corresponds to the extensional area of the NW-SE-trending Sicily Channel rift zone including the basins of Pantelleria, Malta and Linosa. The corresponding rifting phase initiated in the late Miocene to early Pliocene and lasted through the Quaternary (Grasso, 1993).

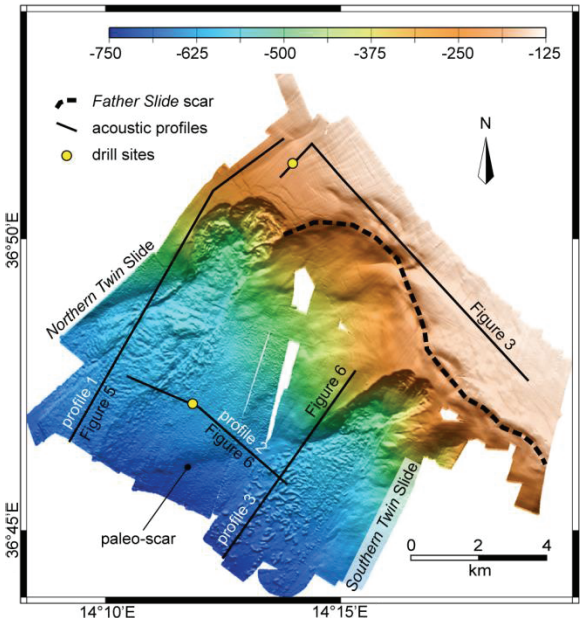

Figure 8.2. A) Overview of the study area in the context of the Mediterranean Sea. B) Location of the study area within the Strait of Sicily and main tectonic features of the region (source: GEBCO dataset). C) Multibeam shaded relief of the NE Gela Basin illustrating the position of prominent features, drill sites and acoustic profiles used in this study.

As indicated by the instrumental and historical series of the USGS NEIC database (U.S. Geological Survey, National Earthquake Information Center; http://earthquake.usgs.gov/earthquakes/search/), seismicity at Gela Basin is relatively low if compared to other Mediterranean areas (Figure 8.1B). Within nearly half a decade (since 1970), only seven epicentres were registered in the immediate proximity of NE Gela Basin that showed low to moderate magnitudes ranging from 2.8 to 4.2 M.

8.2.2 Oceanographic setting

Oceanographic currents in the Strait of Sicily are driven by the anti-estuarine thermohaline circulation system of the Mediterranean Sea and involve an eastward directed fresher surface layer of Modified Atlantic Water (MAW; first 200 m of water column) and a concurrent westward flow of relatively more saline Mediterranean waters (mostly Levantine Intermediate Waters, LIW; Robinson et al., 1999; Sammari et al., 1999). Along the continental slope of the study site, a regional branch of LIW reaches velocities of 13 cm/s (Lermusiaux and Robinson, 2001) and has been linked to the emplacement of muddy shelf-edge contourites capable of generating excess pore pressures and, hence, reducing slope stability (Figure 8.2; Verdicchio and Trincardi, 2008).

8.2.3 Local stratigraphy

Within the study area, high sediment accumulation ratios (up to 2m/ka) and strong bottom currents favour the formation of thick progradational shelf clinoforms on the continental shelf (Figure 8.3). Kuhlmann et al. (2014b) related these depositional sequences to cyclic fluctuations in sea level, which in turn are paced at Milankovitch-type (100-ka and 20-ka) and sub-ordinate (Dansgaard-Oeschger events, D/O) frequencies (Figure 8.3B). The late-Quaternary depositional sequence of the last glacial-interglacial cycle at NE Gela Basin involves an overall progradational pattern comprising, from bottom to top (Figure 8.3): (1) alternating highstand (HST – Highstand Systems Tract) and forced regression units (FSST – Falling Stage Systems Tract) correlating to the Marine Isotope Stages and Substages (MIS) of MIS 5; (2) a lowstand unit (LST – Lowstand Systems Tract) that is basally confined by a subordinate sequence boundary and correlates to MIS 4; (3) a shelf margin wedge comprising alternating HST/FSST units that formed during the falling sea level limb associated to MIS 3-2 until glacial lowstand; (4) a faintly stratified transgressive drape (TST – Transgressive Systems Tract) that accumulated during the phases of drowning of the continental shelf driven by the post-glacial sea level rise; and (5) a progradational shelf wedge forming since the onset of the modern sea level at about 5.5 ka BP (HST).

8.3 Materials and methods

The basis of this work is formed by a dense grid of acoustic subbottom profiles, high-resolution bathymetric data and several complementing sediment cores acquired during one MARUM cruise on board

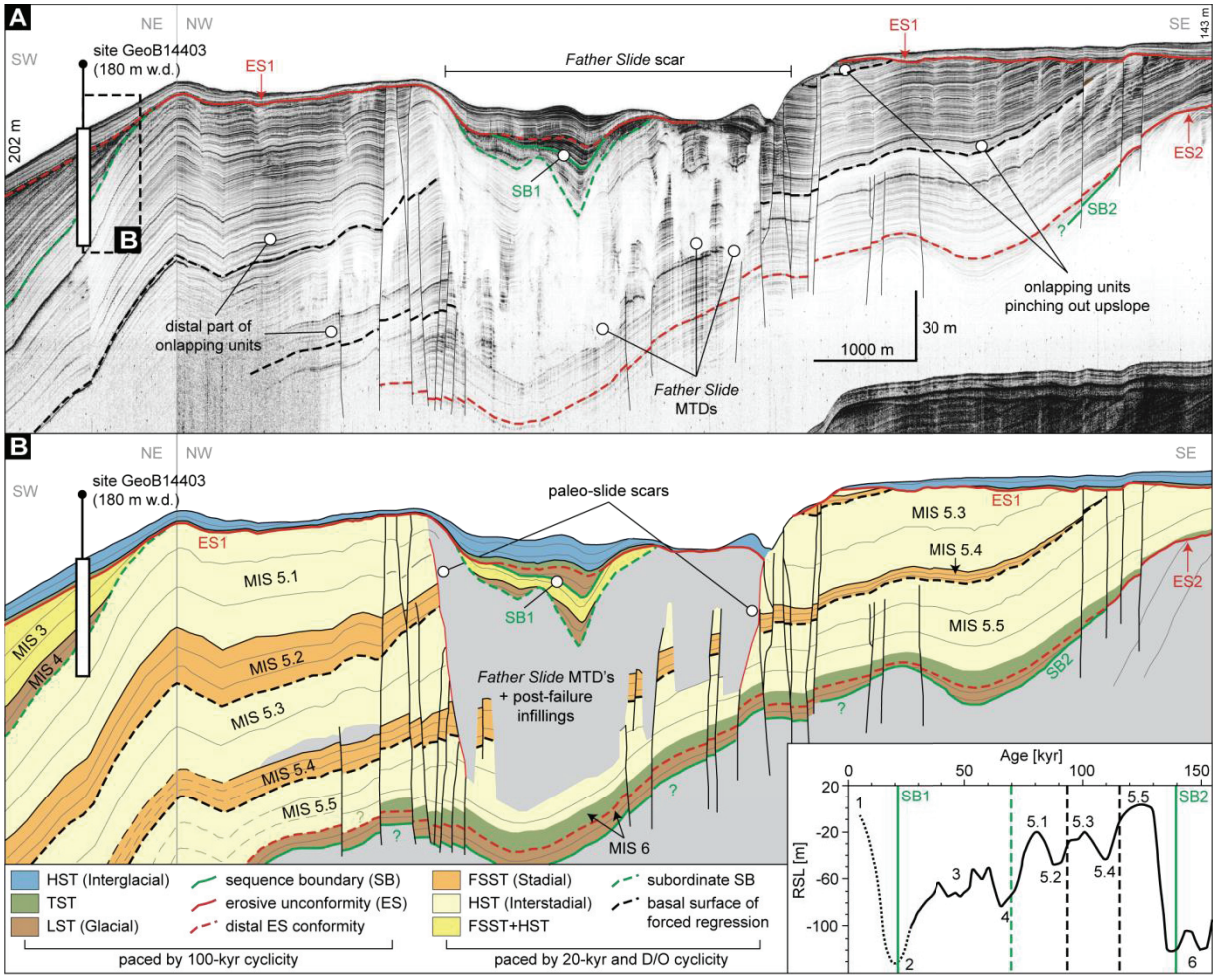

Figure 8.3. A) Along-shelf acoustic profile at the study site indicating the thick sedimentary successions deposited on the continental margin and the signature of the basin-wide *Father Slide* event. B) Core-supported sequence-stratigraphic interpretation of the acoustic profile in A revealing Milankovitch-type forcing of depositional architecture and major bounding surfaces (modified after Kuhlmann et al., 2014b). Inset: position of Marine Isotope Stages and Substages (MIS) as well as of internal sequence boundaries relative to the sea level curve of the Last Glacial-Interglacial cycle (from Waelbroeck et al., 2002). Legend: HST – Highstand Systems Tract; TST – Transgressive Systems Tract; LST – Lowstand Systems Tract; FSST – Falling Stage Systems Tract.

R/V Maria S. Merian (2010) and four ISMAR cruises on board R/V Odin Finder (2000) and R/V Urania (2003, 2004 and 2005). High-resolution bathymetric data derive from a RESON 8160 multibeam and the multibeam echosounder systems Kongsberg Simrad EM-120, EM-300 and EM-1002 operating at 12, 50 and 95 kHz, respectively. Subsurface imagery was conducted with an Atlas Parasound system operating at 4 kHz and a Chirp-sonar system using a 2-7 kHz sweep-modulated band width. Acquired profiles including those presented in this study are overlain on the bathymetric map presented in Figure 8.2.

The acoustic record is complemented by two drill sites that are strategically positioned in order to sample (1) the undisturbed shelf deposits that nourish both recent and exposed slope failures (GeoB14403), and (2) the stacked mass transport deposits from the accumulation zone on the lower slope (GeoB14401; Figure 8.2). Each site comprises a single gravity core (GC), which is accompanied by at least one drilled sequence recovered with the Bremen seafloor drill rig MeBo (Freudenthal and Wefer, 2007; Freudenthal and Wefer, 2013). The dominant lithology of the sedimentary record at both sites is a silty nannofossil clay with quartzose silt, which is accompanied by minor amounts of foraminifera and authigenic pyrite (Kuhlmann et al., 2014a). An overview of main core meta data is provided in Table 8.1.

Table 8.1. Overview of core meta data at boreholes GeoB14401 and GeoB14403.

Name	Type	Water depth	Postion		Top depth	Bottom depth	Length	Recovery rate
		[mbsl]	Latitude	Longitude	[mbsf]	[mbsf]	[m]	
GeoB14401-2	gravity core (GC)	634.3	36°47.17‘N	14°11.91’E	0.00	4.18	4.18	100%
GeoB14401-3	MeBo	613.8	36°47.20‘N	14°11.90’E	0.00	20.49	20.49	26%
GeoB14401-5	MeBo	601.3	36°47.19’N	14°11.89‘E	14.45	35.6	21.15	84.8%
GeoB14403-1	gravity core (GC)	193.4	36°51.41’N	14°13.92’E	0.07	7.83	7.76	100%
GeoB14403-2	MeBo	191.5	36°51.44’N	14°13.92’E	5.55 (*5.05**)	18.24	12.69	83.9%
GeoB14403-8	MeBo	182.0	36°51.41’N	14°13.91’E	17.57 (*16.80**)	54.57	37.00	85.3%

* = original values used in Kuhlmann et al. (2014). The core depth schemes were adapted to account for (1) gravitational sinking of the MeBo drill rig into the muddy seafloor and (2) vertical compression of soft sediments within the gravity cores.

In order to adequately account for compositional variability within specific sediment intervals that were identified to correspond to failure planes, both geophysical and geochemical as well as grain size data was acquired. Additionally, thin sections were prepared from selected horizons for microscopic analysis of landslide-related shear planes.

A GEOTEK Ltd. multi-sensor core logger (MSCL) housed at MARUM (University of Bremen, Germany) was used for non-destructive measurements of core-physical properties including gamma-ray-attenuated density, compressional wave velocity, and magnetic susceptibility. Measured density values were corrected using moisture and density parameters (MAD) determined according to the IODP shipboard practices (Blum, 1997).

Geochemical logging for light elements (Al to Fe) was performed on an Avaatech II core scanner housed at MARUM using a generator setting of 10 kV, 0.2 mA and a sampling time of 20 s. Elemental intensities were measured in a step interval of 2 cm with a slit size of 1cm down-core and 1.2 cm cross-core. Following suggestions by Richter et al. (2006) and Weltje and Tjallingii (2008), results are presented in logarithmic elemental ratios (i.e., log[A/B]) due to the inherent measurement principles.

Grain sizes were measured with the Laser Diffraction Particle Analyzer (Beckman Coulter) LS-13320 at MARUM grain-size lab and are reported in volume percentages of 92 size classes from 0.4 to 2000 µm.

Age control of the boreholes relied on a multi-proxy approach integrating foraminifera-based bio-stratigraphic considerations and radiocarbon datings with a stable oxygen (and carbon) isotope stratigraphy. For foraminiferal analysis, subsamples of 1 cm (GC) and 2 cm (MeBo) thickness were obtained with a vertical resolution of at least 20 cm throughout the cores. The subsamples were freeze-dried, soaked in distilled water and washed over a 63 µm mesh sieve (Schröder et al., 1987).

Similarly, subsamples were used to determine oxygen and carbon isotopic compositions of the benthic *Bulimina marginata* and the planktonic *Globigerinoides ex gr. ruber*. Hand-picked specimens showing no signs of diagenetic alteration were ultrasonically cleaned to remove contaminants such as overgrowths, coccoliths and detrital infilling. Analyses were performed at the Zentrum für Marine Umweltwissenschaften (MARUM, Bremen, Germany) using a Finnigan MAT 252 mass spectrometer coupled with a carbonate preparation device type “Bremen“. Isotopic composition is expressed as per mil (‰) deviation with respect to the Pee Dee Belemnite (PDB) standard, with a long-term laboratory analytical standard deviation of < 0.07 ‰ for the stable oxygen and < 0.05 ‰ for the stable carbon isotope data. Note that none of the isotopic data presented here has been corrected for the ice-volume effect.

For radiometric dating, samples were taken from selected core horizons in order to (1) corroborate stratigraphic interpretations inferred from micropaleontological considerations and (2) provide age control on submarine landslide deposits. Radiocarbon analyses were performed by the Poznan Radiocarbon Laboratory (PRL, Poznan, Poland) and the National Ocean Sciences Accelerator Mass Spectrometry Facility (NOSAMS, Woods Hole

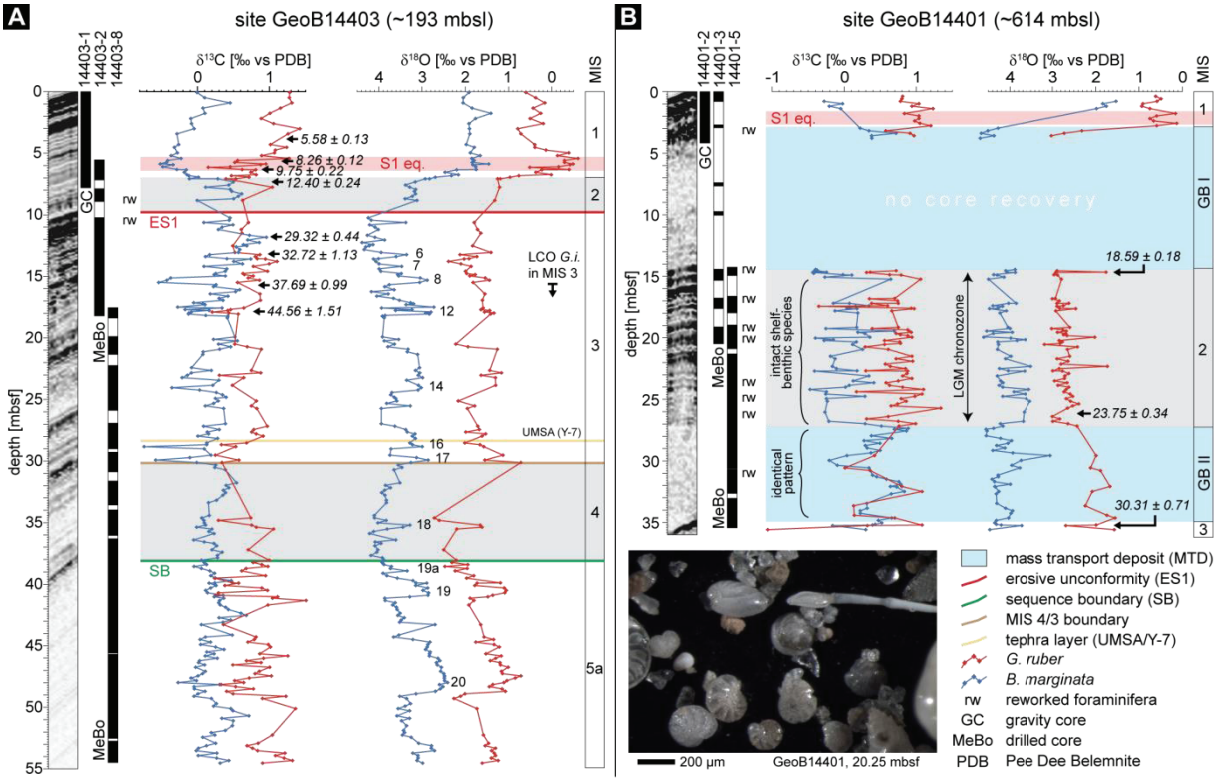

Figure 8.4. Overview of the chrono-stratigraphic framework at boreholes GeoB14403 (A) and GeoB14401 (B) illustrating drill schemes, $\delta^{13}C$ and $\delta^{18}O$ records from benthic *B. marginata* and planktonic *G. ruber*, position and calibrated ages from radiocarbon datings as well as interpreted Marine Isotope Stages and Substages (MIS), Dansgaard-Oeschger oscillations and main biostratigraphic findings. The microscope image in (B) shows shelf-benthic foraminifera specimens in the deep-water core, suggesting reworking.

Oceanographic Institution, USA) on mono-specific and mixed foraminifera in the size fraction > 63 µm (Table 8.2). Obtained AMS ^{14}C ages were converted into 2σ calibrated ages using Calib 7.0.0 Radiocarbon Calibration Program (Stuiver and Reimer, 1993) and the Marine13 calibration data set (Reimer et al., 2013). The reservoir correction was selected from the Calib database for the Sicily Channel, with a calculated weighted mean ΔR value of 71 years and a standard derivation of 50 years (Siani et al., 2000). All dates reported are given in calibrated thousands of years before present (cal. ka BP).

8.4 Results

8.4.1 Borehole stratigraphy and age control

In order to allow a correlation of upslope and downslope sedimentary units and to provide an accurate temporal control on the emplacement of mass transport deposits in the area, this study relies on a core chronological framework integrating evidence from (1) stable isotope data, (2) microfaunistic bioevents as reflected in the foraminiferal assemblage, and (2) foraminifera-based radiometric datings (Figure 8.4).

Borehole GeoB14403, recovered from the undisturbed shelf-edge in ~193 m water depth, provides a quasi-continuous stratigraphic record of late Pleistocene-Holocene sediment successions to a depth of 54.6 mbsf (Figure 8.4A). Changes in the assemblages of benthic and planktonic foraminifera as well as stable oxygen ($\delta^{18}O$) and carbon ($\delta^{13}C$) isotopic compositions from the benthic *Bulimina marginata* and the planktonic *Globigerinoides ex gr. ruber* document sea level fluctuations and paleoceanographic changes, thus allowing for a precise definition of Marine Isotope Stages and Substages (MIS). Supported by a total of eight radiocarbon datings, Kuhlmann et al. (2014b)

Table 8.2. AMS ^{14}C and calibrated ages based on monospecific and mixed foraminifera.

Lab #	Core	Section # and depth [cm]	Material	^{14}C age [yrs BP]	2σ cal. intercept [cal. ka BP]
Poz-53709	GeoB14403-1 (GC)	II 80-83	*G. ruber, G. sacculifer*	5285 ± 35	5.58 ± 0.13
Poz-53710	GeoB14403-1 (GC)	IV 20-22	*G. ruber, G. sacculifer*	7870 ± 35	8.26 ± 0.12
Poz-53711	GeoB14403-1 (GC)	IV 80-83	*U. peregrina*	9110 ± 50	9.75 ± 0.22
Poz-53712	GeoB14403-1 (GC)	V 40-42	*C. laevigata carinata*	11010 ± 60	12.40 ± 0.24
Poz-53713	GeoB14403-2 (MeBo)	3P-2 32-36	*U. peregrina*	25750 ± 160	29.32 ± 0.44
OS-106891	GeoB14403-2 (MeBo)	4P-1 61-67	*E. crispum, M.barleeanum, C. lobatulus*	29300 ± 490	32.72 ± 1.13
Poz-53715	GeoB14403-2 (MeBo)	5P-1 86-99	*H. balthica, C. pachyderma*	34000 ± 360	37.69 ± 0.99
OS-106838	GeoB14403-2 (MeBo)	6P-1 57-64	*H. balthica, U. peregrina, M. barleeanum*	41600 ± 890	44.56 ± 1.51
OS-106893	GeoB14401-2 (GC)	IV 80-84	*N. pachyderma, G. bulloides*	16400 ± 95	19.22 ± 0.29
OS-106666	GeoB14401-5 (MeBo)	1P-1 40-46	*N. pachyderma, G. bulloides, N. dutertrei*	15800 ± 55	18.56 ± 0.18
OS-106889	GeoB14401-5 (MeBo)	7P-2 0-5	*C. pachyderma*	25300 ± 290	28.88 ± 0.66
OS-106890	GeoB14401-5 (MeBo)	9P-2 62-67	*N. pachyderma*	26700 ± 350	30.31 ± 0.71

Calibration is based on Calib 7.0.0 Radiocarbon Calibration Program (Stuiver & Reimer, 1993). Calibration data set: Marine13 according to Reimer et al. (2013). Reservoir correction: The calculated weighted mean ΔR value is 71 with a standard derivation of 50 (Siani et al., 2000).

identified stages and sub-stages ranging from MIS 1 to MIS 5.1 and estimated the entire borehole to cover an interval spanning the last ~80 ka. Fine-tuning with the NGRIP record (NGRIP members, 2004) further allowed to relate higher-frequency oscillations in the isotopic composition to abrupt sea level changes associated to the onset of short-lived D/O Interstadials (Figure 8.4A), thus providing full stratigraphic control on the shelf deposits (Figure 8.3). The warmest (i.e., strongest positive isotopic shifts) of these sub-ordinate D/O events, namely D/O 16, 14, 12, and 8 appear to correlate with sharp basal reflectors in the acoustic record (Figure 8.4A) interpreted as condensed marine flooding surfaces (see Sierro et al., 2009, for a similar condensation patterns in the Gulf of Lions). Together with sequence-stratigraphic boundaries identified by Kuhlmann et al. (2014b), such as the subordinate sequence boundary at the MIS 5 to MIS 4 transition (SB, Figure 8.4a) and deeper stratigraphic units not recovered in the core (e.g., MIS 5a to MIS 5b transition, Figure 8.3A), these surfaces can be traced downslope and form the basis for passive dating of strata through core-acoustic correlations (see Figures 8.5 and 8.6).

Borehole GeoB14401 instead, recovered from the landslide accumulation zone in ~614 m water depth, penetrates two 7-8 m thick acoustically transparent units interpreted as mass transport deposits (GB I and GB II) and hence allows direct age control on these deposits (Figure 8.4B). However, except from an abrupt shift of isotopic composition (> 2‰ for δ^{18}O values) in the upper core section, the isotopic curves show no meaningful variations that could be related to well-known events, especially in the section between GB I and GB II. This suggests an extended interval of similar environmental conditions, which is supported by radiocarbon datings inferring a sedimentation rate of 2m/ka for this interval. Similar evidence comes from micropaleontological investigations, which reveal an abundance of oxidized clasts and fine terrigeneous material (suggesting proximity to the coastline) as well as low oxygen content in the sediment (benthic assemblage composed of *B. aenariensis*, *B. dilatata* common, *M. barleeanum*, *B. marginata*, *C. laevigata carinata*) and cold and productive waters (planktic assemblage dominated by *G. quinqueloga* common, *N. pachyderma* r.c., *N. dutertrei*, *G. bulloides*, *G. glutinata*, *G. scitula* rare, *G. ruber* very rare). Based on this evidence, the interval from about 15-27 m can confidently be ascribed to the Last Glacial Maximum chronozone (LGM), which is defined between 19 and 23 ka BP (Max et al., 2001) and is coeval with the lowest stand of sea level (e.g., Yokoyama et al., 2000). On the upper shelf borehole GeoB14403, the equivalent to this interval is condensed in the prominent erosive unconformity ES1 (Figure 8.4A).

For the upper sedimentary succession topping mass transport deposit GB I (i.e., the first 2.6 m of borehole GeoB14401), foraminifera assemblages

indicate a Holocene age (Figure 8.4B). The base of the highstand (HST) can be positioned at ca. 1.5 m (above which *G. sacculifer* shows common presence and re-occurrence of *G. truncatulinoides* is reported), while the sediment coeval with the deposition of Sapropel 1 in the Eastern Mediterranean (S1 eq.) reaches 2.6 m. The benthic assemblage of HST unit (*U. mediterranea*, *U. peregrina* common, *C. pachyderma*, *C. laevigata carinata* common, *H. balthica*, *M. barleeanum*, *G. altiformis*, *A. tubulosa*) indicates a mesotrophic environment, while the underlying S1 eq. interval suggests reduction of the water columns winter mixing (absence of *G. truncatulinoides*) and higher accumulation of organic matter in the seafloor (*U. peregrina* common). The older pre-Boreal is not present because *G. truncatulinoides*, along with the warm planktic assemblage in which it peaks (Sprovieri et al., 2003), is absent. In fact, it cannot be ruled out the lacking of the older phase of S1 eq., as a literature core collected nearby (core P09 in Minisini et al., 2007; see Figure 8.2) reports a frequency peak of deep infaunal benthic species, while at borehole GeoB14401 these species are present but not common as expected. For the lowermost core section at the base of GB II, radiometric dating suggests an age of about 30 ka (Figure 8.4B). The stable carbon isotopic record reveals an identical pattern for both *G. ruber* and *B. marginata* for the interval related to GB II, possibly indicating the in-situ transport of sediment from the shallower areas.

8.4.2 Evidence of landsliding from the benthic record

Benthic foraminifera species are specialized bottom dwellers that are characteristically linked to certain environments (e.g., outer shelf and inner shelf facies) and are hence excellent indicators of sea level and paleoenvironmental conditions (e.g., Jorissen et al., 1987). The occurrence of individual specimens in an untypical environment can hence be linked to transport processes and may be used to infer landsliding or erosional activities. At borehole GeoB14403 for example, reworked benthic specimens (often broken) are frequently found around the erosive unconformity ES1 relating to the last LGM. However, inner shelf (*Ammonia* and *Elphidium*) and epiphytic species representing the shallowest environment have been identified throughout most of the core, especially within intervals encompassing MIS 3 and MIS 4 that relate to mid- and mid-outer-shelf environments (Kuhlmann et al., 2014b). Though the position of this borehole on the outer shelf does not favour the emplacement of mass transport deposits (unlike borehole GeoB14401 on the lower slope), this indicates downslope sediment displacement.

At borehole GeoB14401, recovered from the accumulation zone on the lower slope section, reworked shelf-benthic specimens (mainly *Elphidium*) can equally be observed (see inset of mircroscopic image in Figure 8.4B). Interestingly, these appear predominantly in the zone associated to the LGM chronozone, which does not show evidence of landsliding in the acoustic record, suggesting syn-depositional, small-scaled transport processes of lower momentum at the origin of displacement. This is supported by the fact that the reworked shelf-benthic specimens show no signs of damage (microscope image in Figure 8.4B). Finally, no sorting events seem to have clearly affected the foraminifera assemblages, which show specimens with different size (both adult as well as young specimens).

8.4.3 Seafloor morphology

The high-resolution bathymetric record shows evidence of recurrent landslide processes along the continental slopes of Gela Basin, as previously reported on by Trincardi and Argnani (1990), Minisini et al. (2007), Trincardi (2009) and Kuhlmann et al. (2014a). In order to keep terminology consistent, the nomenclature introduced by Minisini et al. (2007) is adopted herein after.

The continental slope, dipping generally at about 3°, documents both recent and typically seafloor-exposed landslides as well as remnants of old and partially buried slide scars (Figure 8.2). The most prominent feature is the coeval *Twin Slide* complex,

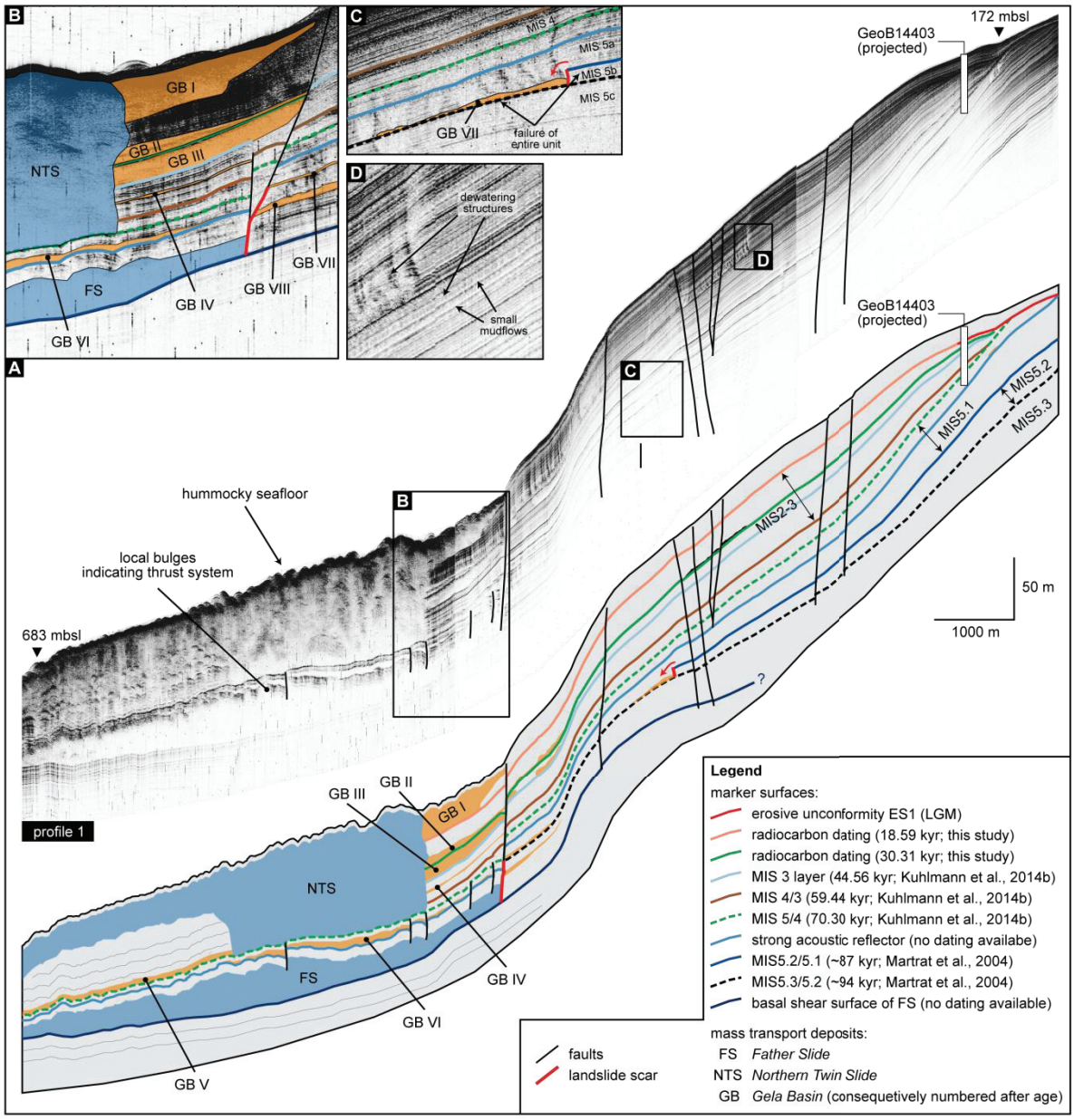

Figure 8.5. A) Along-slope acoustic profile at the *Northern Twin Slide* correlating main marker surfaces from the shelf area (see Legend) with the accumulation zone on the lower slope, thus providing age control over the emplacement of deposits and/or glide planes. Between the buried *Father Slide* and the recent *Northern Twin Slide*, six major events can be distinguished (termed GB I – GB VI). B) Magnification of the failure zone of *Father Slide* showing two additional events that are stratigraphically older (GB VII and GB VIII). C) Evidence of mid-slope failure during relative lowstand of sea level in MIS 5.2. D) Example of clearly visible dewatering structures and evidence for high-frequency, but very-low-magnitude landslides processes.

two recent landslide events on the upper slope (200-230 mbsf) that display sub-rounded scarps and feature reliefs exceeding 100 m. Head scarps incline by a maximum of 32° (Kuhlmann et al., 2014a) and the complex is characterized by runout lengths of 10-12 km, involving material with an estimated volume of < 1 km³ (Minisini et al., 2007). Both landslides have been shown to relate to a multi-stage failure involving a debris avalanche and a successive retrogressive slide/slump (Minisini et al., 2009; Kuhlmann e al., 2014b) that partly covers the debris avalanche deposits. The shelf edge/upper slope area in between these scarps accommodates a depression that dips steeper (~8°) than the surrounding shelf deposits and

reflects the buried headscarp of an older event termed *Father Slide* (Figure 8.2). Remnant bathymetric evidence for the emplacement of additional mass transport deposits within the timespan between the occurrence of *Father Slide* and *Twin Slides* is discernable in form of paleo-scarps of up to 10 m in relief (Minisini et al., 2007; Figure 8.2).

8.4.4 Subbottom imagery

Exhibiting thick acoustically transparent facies (locally up to 50 m), the deposits of the *Father Slide* event (FS) are ubiquitous in deep sedimentary units and form the stratigraphically oldest mass transport deposits (MTDs) that are continuously traceable throughout the area of investigation (Figure 8.5 and 8.6). The upper surface of this unit is rather irregular and shows local bulges indicating the presence of a thrust system (Figure 8.5A). Further upslope, the MTDs are confined by a pronounced head scarp, which sharply cross-cuts the surrounding deposits well into Eemian times (MIS 5.5; see Figure 8.3).

The deposits associated to this basin-wide event are covered by a stack of multiple thinner MTDs with flat tops, showing laterally varying thicknesses that appear to preferentially infill local depressions and smooth out seafloor irregularities (thus regulating the disturbances relating to the *Father Slide* event, Figure 8.5 and 8.6). A total of six major deposits of this kind can be traced in the Gela Basin (GB I – GB VI), all of which are bounded basally by sub-horizontal bedding surfaces interpreted as glide planes, along which translational movement occurred. Typically, they lack signs of scarping and induce subvertical acoustic wipeouts in above stratified layers, suggesting fluid escape structures associated to the emplacement of mudflow deposits (in accordance with Minisini et al., 2007, who presented evidence from core P04 penetrating unit GB I). Two additional events

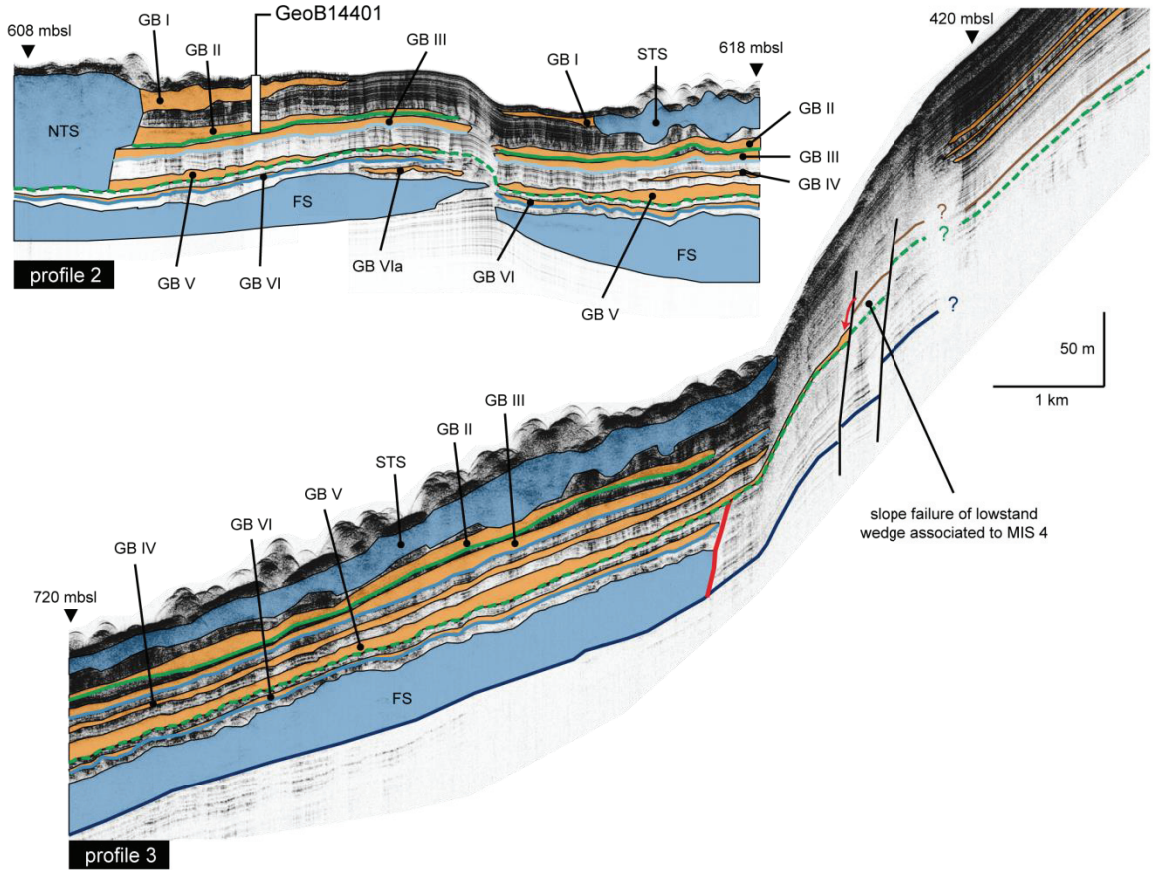

Figure 8.6. Lower slope interpreted acoustic profiles revealing identical stacking pattern of small-scaled landslide deposits as recognized in profile 1 (Figure 8.5). For legend see Figure 8.5.

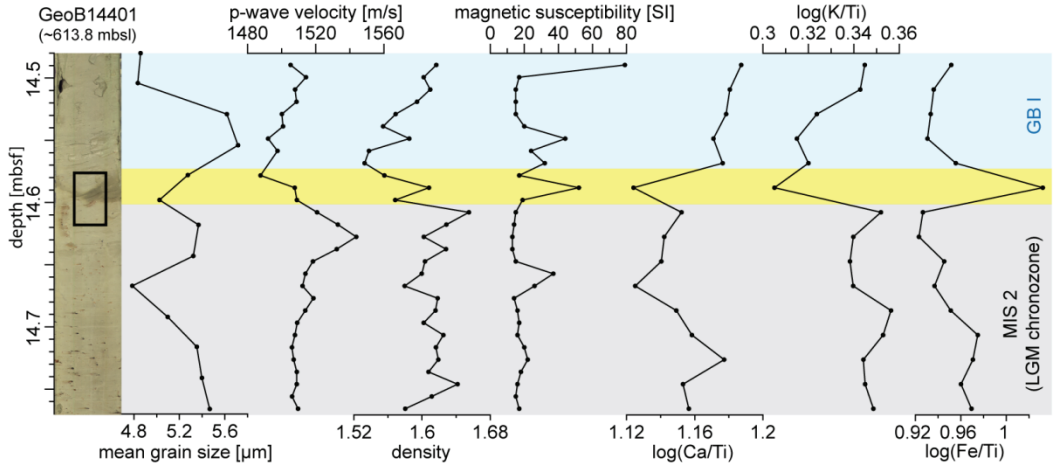

Figure 8.7. Variations in selected material properties at the glide plane corresponding to event GB I, as recorded in the borehole 14401. The yellow band indicates the position of the shear zone and displays higher terrigenous fraction than the surrounding material (elevated magnetic susceptibility; low calcium and high iron concentrations with regard to titanium).

associated to this group could be traced in the stratigraphic section reworked by *Father Slide* (GB VII and GB VIII; Figure 8.5B). These are, however, excluded from the estimation of landslide frequency due to difficulties of their tracing in the deeper stratigraphic units.

Some of the stacked MTDs were reworked by the recent multi-stage failures of *Northern Twin Slide* (NTS) and *Southern Twin Slide* (STS) (section 4.3.1; Minisini et al., 2007; Minisini and Trincardi, 2009; Kuhlmann et al., 2014a). However, given the lack of control on other potential multi-stage failures (e.g. *Father Slide*), these events are not regarded as separate landslide events and are grouped to a single one instead.

For each of the identified landslide events age control was either provided by borehole stratigraphy (Figure 8.4) or through tracing of the respective marker horizons into directly (through 14C) or indirectly (through oxygen isotope stratigraphy and biostratigraphic considerations) dated surfaces (Figure 8.5). The resulting age constraints are discussed in section 8.5.1.

8.4.5 Material properties and microfabrics of glide planes

In order to understand the mechanisms involved in the emplacement of GB I mass transport deposit, the material properties along the respective core section were analysed (Figure 8.7). The interval displays a homogeneous lower unit exhibiting frequent oxidised clasts and relatively constant physical and chemical composition related to the LGM chronozone. The overlying mass transport deposit of GB I is separated by a clearly visible shearing layer with reduced concentrations of Ca and Ka with respect to Ti. Together with enriched Fe concentrations and elevated magnetic susceptibility, this indicates a higher fraction of terrigenous input within this thin layer. The base of the mass transport deposit is characterized by higher mean grain sizes and lower density, which may resemble sorting affects related to the transport process.

To further constrain the failure mechanism, a thin section of the proposed basal gliding surface was analysed for microfabrics and mineralogical composition under a polarizing microscope (Figure 8.8). The surface clearly shows a distinction with regard to the homogenous background material, both in terms of colour as well as mineral content and size (Figure 8.8A, B). Small mud clasts show preferential elongation along the position of counter-directed deformation bands, thus indicating rotational movement within the surface associated to shearing (Figure 8.8B). Contradicting to the grain size results, particle sizes within the glide plane are significantly higher than those of the surrounding material, suggesting unrepresentative sampling of background

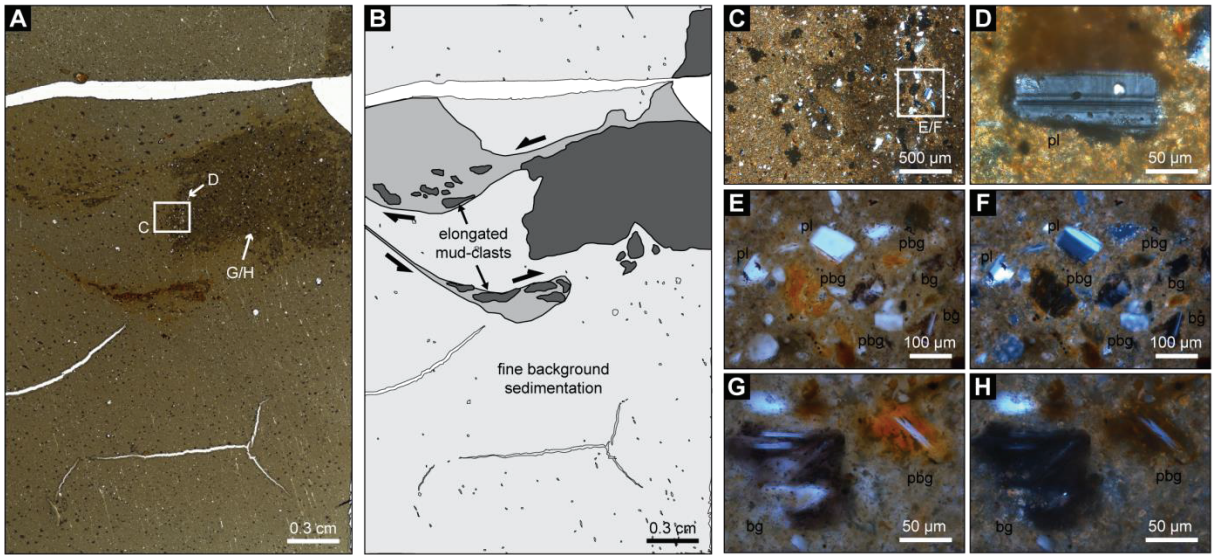

Figure 8.8: Thin section analysis of glide plane GB I under the polarizing microscope showing elongated mud clasts interpreted as preferential direction of shear. Additionally, mineral fragments show evidence of basaltic volcanoclastic origin. A) Full thin section in plane-polarized light. B) schematized overview of A showing the main directions of shear. C) Evidence of significantly higher grain size within the organic-rich brown glide plane. D) Plagioclase (pl) showing characteristic twinning under cross-polarized light. E) Assemblage of volcanoclastic minerals, including glassy basalt (bg) and palogonitic altered (orange) glassy basalt (pbg). F) As in E, but under crossed polarization. G) Detail of irregular shaped fragments of (palagonitic) glassy basalt displaying small laths of plagioclase (with swallowtails) and transparent tiny microliths. H) As in G, but under crossed polarization.

sediment in between the deformation bands (Figure 8.8C). The mineralogical composition of the glide plane is clearly of volcanoclastic origin. It shows widespread occurrence of typical fragments of plagioclase (Figure 8.8D, E and F), showing polysynthetic twinning under crossed polarizers (Figure 8.8D and F). Equally, the presence of irregular shaped fragments of glassy basalts can be observed (Figure 8.8E-H). These display small laths of plagioclase (some showing swallowtails, Figure 8.8G) and transparent tiny microliths and their isotropic matrix appears black under crossed polarizers, independent of orientation. Some of these glassy basalts show orange colours under plane-polarized light, indicating palagonitic alteration through the contact with water.

8.5 Discussion

8.5.1 Timing and frequency of landsliding

A total of eight stacked mass transport deposits with the *Father Slide* event at their base could be observed at Gela Basin. It is noteworthy that we referred to more proximal acoustic profiles for their recognition in order to cover landslides featuring small runout lengths and to exclude an overlap with landslide deposits from other areas of the basin that extend into the deeper parts of the study area. In the following, the main characteristics of the individual landslide events introduced earlier are summarized, including their relation to dated marker surfaces (Figure 8.5). A graphic representation of their timing and distribution outlining the evolution at the continental slope at Gela Basin is depicted in Figure 8.9:

- **NTS/STS**. These form the youngest events of the investigated succession. There is no age control on the exact timing available. However, lack of smoothing of bathymetric features attest that the complex is of very recent age. Although both events involve multiple failures they are counted as one single event.
- **GB I**. This deposit has been sampled by core and analysed in a previous study and was interpreted as a 8.5 ka BP mudlow overlain by thin turbidites (Minisini et al., 2007). This timing is consistent with the foraminifera assemblage at borehole GeoB14401 indicating lacking of the lower

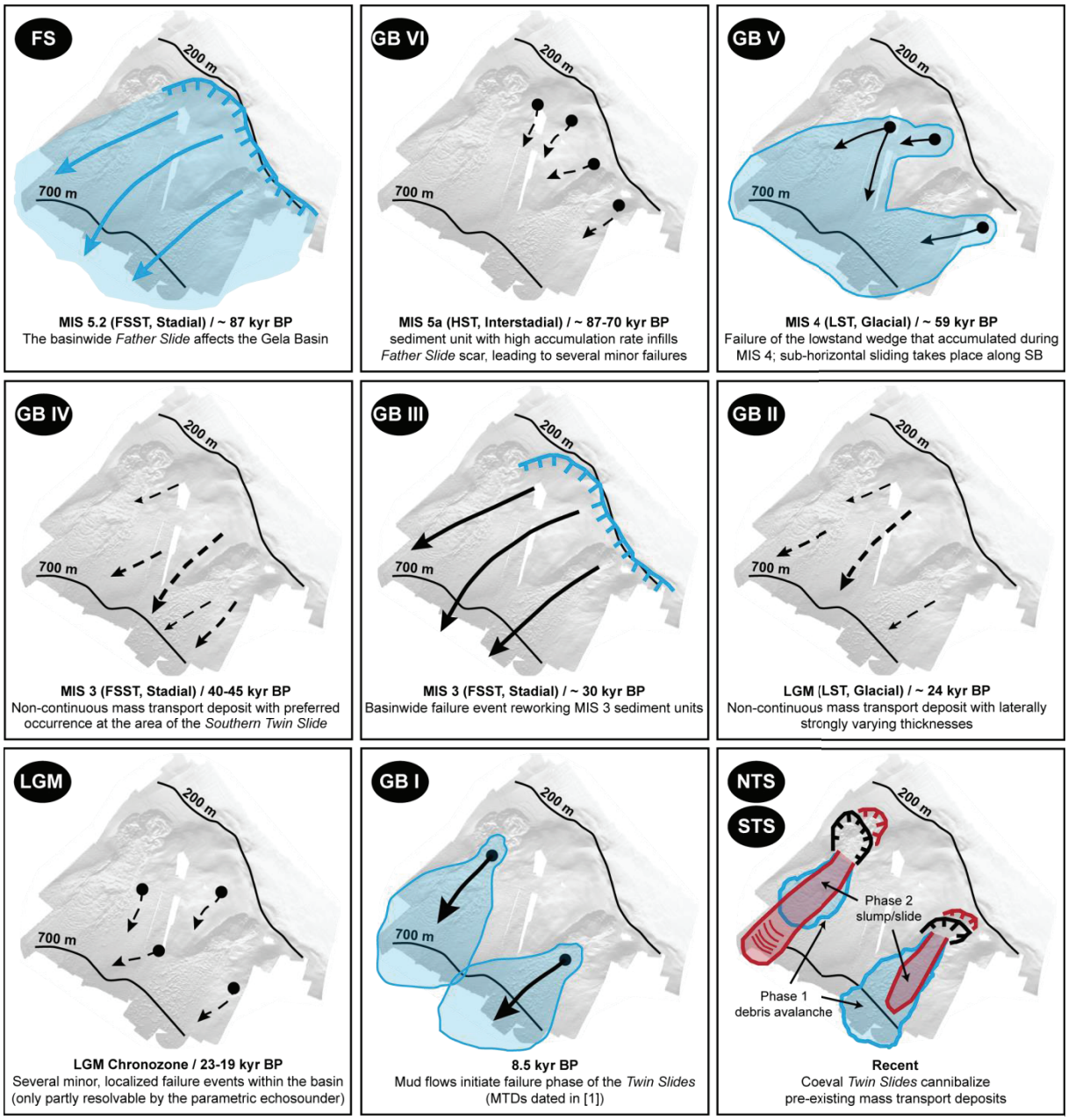

Figure 8.9: Schematic overview of major slide events since the emplacement of *Father Slide* deposits at about 87 ka BP.

Sapropel S1 equivalent and hence is adopted herein. The glide plane as recovered in borehole GeoB14401 is only marginally younger than the 18.59-ka radiometric dating from a sample just below. However, in contrast to most other observed landslides in this group, GB I appears to 'jump' reflectors (profile 2 in Figure 8.6) and is locally confined.

- **GB II**. This deposit shows strong local variations in thickness and continuity. Age control is provided by two radiocarbon datings just below its base and above its top and suggests a deposition at ~24 ka BP and sub-horizontal movement along a surface indicating an age of 30 ka BP.
- **GB III**. A basin-wide failure event reworking sedimentary units of MIS 3. This deposit is

confined upsection by a 30-ka BP radiocarbon dating and basal movement occurred along a surface deposited at around 45 ka (according to upslope tracing into borehole GeoB14401).

- **GB IV**. This deposit occurs preferentially in the area of the *Southern Twin Slide* and shows, if present at all, only thin extent in the area allocated to *Northern Twin Slide*. Moreover, its basal surface cannot be clearly traced into a dated borehole sequence, hence we estimate its age to 40-45 ka based on the two surrounding marker surfaces (a radiocarbon dating and the isotopic MIS 4/3 boundary).

- **GB V**. This event involves the locally confined failure of the lowstand wedge associated with MIS 4 and may be ascertained to 59 ka based on isotopic correlations. Movement takes place along the subordinate sequence boundary related to the MIS 5/4 transition at ~70 ka.

- **GB VI**. This unit in fact involves several smaller and localised landslides that followed the emplacement of FS and subsequent rapid infilling of associated scars. It is assigned the time window in between FS and GB V (i.e., 87-70 ka BP).

- **FS**. The thick deposits of *Father Slide* are basally bounded by a surface that cannot be traced upslope due to limited penetration of the acoustic devices. However, the associated head scarp on the upper slope suggests a penetration at least into Eemian sediments (MIS 5.5). The timing of failure is more intriguing, since associated shear planes hamper the tracing of acoustic reflectors. However, from the acoustic evidence presented in Figure 8.5 we assign the time of failure within the Stadial-Interstadial boundary (MIS 5.2/5.1).

- **LGM**. This group encompasses syndepositional emplacement of very small-scaled landslide events that are not fully resolveable in the acoustic record and can only be fully recognizeded by the micropaleontological analysis. Though this group cannot be counted to major landslide groups as listed above, it is equally important in terms of the assessment of slope stability.

In order to report on the frequency of landsliding, the time span of observance (i.e., the emplacement of FS until modern time) is simply divided by the amount of recognised events. Disregarding any paleoenvironmental constraints on the timing of failure (e.g., with regard to the position of sea level), these eight groups of major slide events provide an estimated frequency of about one event every 11 ka at the continental slope of Gela Basin. This is about three times lower than originally estimated by Minisini and Trincardi (2009), who lacked full stratigraphic control on the emplaced MTDs and proposed a frequency rate of one failure every 3-4 ka. Still, this frequency is too high to imply a correlation to cyclic sea level variations, as proposed in a variety of cases (e.g., Piper et al., 2003; Lebreiro et al., 1997). However, these figures are put into perspective when observing the dated failure times with regard to the respective relative sea level (Figure 8.10). It appears that most of the recognised landslide events (6) are related to a relative sea level lowstand or the falling limb of sea level curve preceding these lowstands, including the initial deposit relating to the basin-wide *Father Slide*. The only exceptions to this comprise the small and localised landslide associated to GB VI as well as the

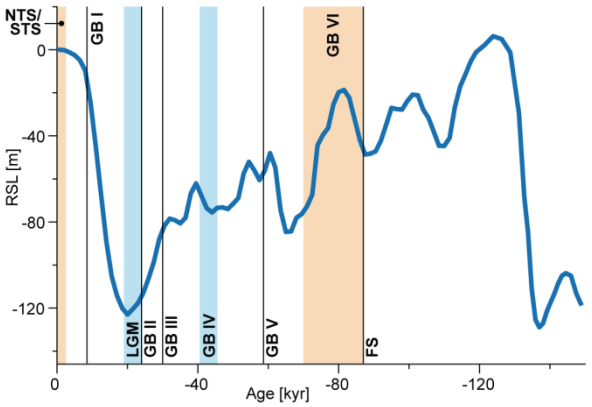

Figure 8.10: Occurrence of mass transport deposits with regard to the relative sea level curve of the Last Glacial-Interglacial cycle (Waelbroeck et al., 2002).

more recent 8.5 ka mudflow (GB I) and the *Twin Slides* (NTS/STS). This rate of 6:3 is consistent with many continental margins that report on higher frequencies of landsliding during falling or lowered sea level than during rising or high sea level (Lee, 2009, and references therein). Similarly, a concentration of events between 45 ka and 19 ka (Figure 8.10) fits well to the observations of Maslin et al. (2004) on non-glaciated margins. Interestingly though, there is no evidence of major landslide deposits within the time of the LGM Chronozone (19-23 ka, Max et al., 2001). Instead, the micropaleontological record reveals frequent sliding on a scale below the resolution of the seismic records during this time. The frequent (i.e., syndepositional) displacement and downslope transport of limited sediment volumes may have counteracted the development of major events during this time by reducing slope angles as well as hampering generation of pore pressure on the upper slope.

8.5.2 Sedimentation rates and excess pore pressure

Sedimentation rates at the study site are reported to reach maximum figures of 2 m/ka during the last glacial-interglacial cycle (Kuhlmann et al., 2014b). This is an order of magnitude higher than at the neighbouring ODP Site 963 at NW Gela Basin (Emeis et al., 1996; Sprovieri et al., 2003) and relates to the presence of strong along-slope bottom currents and increased sediment discharge during hyperpycnal river floods. Both mechanisms favour the rapid deposition of fine-grained and under-compacted sediment (e.g., Warrick et al., 2003) and thus the generation of excess pore pressure in underlying sediments. Steady bottom currents induce additional deposition of contourites with good sorting and thus high water contents (Verdicchio and Trincardi, 2003; Laberg and Camerlengthi, 2008), contributing to a state of weakness of the slope. Another mechanism increasing the overpressure within the sediments is the deposition of landslide events themselves, which exert a rapid loading on the buried material, thus inducing the upward migration of pore fluids and successive generation of overpressure (Minisini and Trincardi, 2009). Evidence for this mechanism is seen in the frequent wipeout structures related to well-stratified units topping landslide deposits (Figure 8.5B,C).

8.5.3 Stratigraphy and glide planes

The acoustic tracing of basal shear surfaces of MTDs to the upper slope section reveals the importance of pre-failure stratal architecture in the study area, as seen on many other settings (e.g., Trincardi et al., 2003). Glide planes of the translational mudflows appear to correlate predominantly with sequence-stratigraphic boundaries that relate to paleoenvironmental changes in the depositional setting, such as (cyclic) variability in sediment flux and sea level (Kuhlmann et al., 2014b). Such surfaces typically coincide with distinctive physical attributes with regard to the surrounding material and hence favour preferential sliding in shallow burial. These attributes can be ascribed to lithological changes as well as alteration processes such as cementation, compaction or biogenetic processes (e.g., Masson et al., 2006; Lee et al., 2007; Laberg and Camerlenghi, 2008).

A good example of a predisposed surface, though resulting from a mechanism other than paleoclimatic variability, is given by the glide plane associated to deposit GB I, which is recovered in borehole GeoB14401. This layer has significantly different lithologic characteristics that are clearly distinguishable in the sediment-physical and –chemical record. The microscopic analysis of a thin section from this layer demonstrates the volcanoclastic origin of the material (Figure 8.8). Its composition of plagioclase and glassy basalt fragments with small laths of plagioclase and transparent microliths suggests a basaltic origin of the volcanic source. Given the geographical position of the Gela Basin and the preferential distribution of eruptive ashes from Mediterranean source volcanoes (e.g., Narcisi and Vezzoli, 1999), we propose Etna as the most probable source. However, further geochemical analysis will be

required to clearly allocate a source. This finding strongly supports the paradigm that volcanoclastic material may form weak layers that eventually act as preferential planes of failure. However, the proposed mechanism of glass shard rearrangement during seismicity-induced ground shaking and associated water expulsion (Harders et al., 2010) may not be applicable in this case, as required glass shards are too few in number with regard to the background material. Nonetheless, the significant differences in grain size and potential sorting may equally lead to a destabilisation when subjected to seismic shaking.

8.5.4 Seismic activity

Considering the high frequency of submarine landsliding within Gela Basin (section 5.1), a trigger mechanism of repetitive character is required in order to recurrently provide conditions capable of destabilising the sedimentary successions on the continental slope. As frequently suggested, seismic activity is the most plausible mechanism considering the land-slide prone conditions of the investigated sediments. Ai et al. (2014) showed in a geotechnical study of borehole GeoB14403 that, at current state, a relatively small horizontal acceleration of 0.03-0.08 g may be sufficient to cause failure on the upper slope. Such an external stimulus could be provided by either moderate earthquakes (M = 4.0 – 4.8) in the direct vicinity of the study area (<10 km) or stronger (M = 7) events in an epicentral distance <20-80 km. As introduced earlier, the instrumental and historical series of the USGS NEIC database document comparably low seismicity at Gela Basin (Figure 8.1B), with only seven epicentres in the immediate proximity showing low to moderate magnitudes of M = 2.8 – 4 (since 1970). Though these numbers may not suggest seismicity as a strong and recurrent local trigger mechanism for submarine landsliding, they indicate significant seismic frequency if extrapolated to longer temporal intervals. Minisini et al. (2007) proposed a rough estimate of about 2000 seismic shocks over the period of the post-LGM interval. They additionally argued that full account of the maximum possible earthquake magnitude and spatial distribution of the epicentres in the historical record may have been hindered by a variety of reasons: (1) the difficulty to infer past offshore epicentres; (2) the bias of onland distribution of historical earthquakes associated with the location of ancient settlements; and (3) the incidental absence of potential extreme events in the short interval of observation. Hence, the regional seismic potential may be underestimated with regard to the limited temporal interval at the base of the USGS database and seismic activity is considered as a main agent controlling the emergence of sediment landslides at Gela Basin.

8.6 Conclusions

This study presents a detailed analysis of landslide activity and failure mechanisms at the continental margin of Gela Basin. A total of eight mass transport deposits could be identified along the lower slope section, representing predominantly disintegrative mudflows that display preferential movement along sub-horizontal, bedding-parallel glide planes. Accurate timing of the individual events is achieved through acoustic correlation with two drilled boreholes that provide centennial to millennial scale age control by integrating biostratigraphic considerations, carbon and oxygen isotope stratigraphies as well as radiocarbon datings. Results reveal a basic failure return interval of ~11 ka, but temporal distribution shows a clear dominance of failure during conditions of sea level fall and lowstand.

A major factor in predisposing slope failure is the depositional continental margin architecture as shaped by Milankovitch-type climiatic oscillations and the intercalation of volcanoclastic material into the rapidly accumulating sediment. Both provide mechanically weak surfaces that may act as preferential planes of failure, as evidenced in a microscope analysis of a thin section. Further predisposing factors capable of reducing slope stability in this area are the exceptionally high sedimentation rates, fluid expulsion

and generation of excess pore pressures in response to rapid loading.

Another noteworthy finding is the occurrence of very small-scaled landslide processes during the Last Glacial Maximum Chronozone (~19-23 ka BP), which are not discernable in the acoustic record but provide direct evidence of downslope transport in the benthic foraminifera assemblage. These may significantly add to the high sedimentation rate during this interval (~2m/ka) and may have counteracted the emplacement of larger landslides.

Acknowledgements

This work has been funded by the DFG through MARUM – Universität Bremen. The research used data acquired at the XRF Core Scanner Lab at the MARUM. All additional analyses, including $\delta^{13}C/\delta^{18}O$, grain size and MSCL logging were carried out at the lab facilities of MARUM.

References

Accaino, F., Catalano, R., Di Marzo, L., Giustiniani, M., Tinivella, U., Nicolich, R., Sulli, A., Valenti, V., Manetti, P., 2011. A crustal seismic profile across Sicily. Tectonophysics 508(1-4), 52-61.

Ai, F., Kuhlmann, J., Huhn, K., Strasser, M., Kopf, A., 2014. Submarine slope stability assessment of the central Mediterranean continental margin: the Gela Basin. In: Krastel, S., Behrmann, J.-H., Völker, D., Stipp, M., Berndt, C., Urgeles, R., Chaytor, J., Huhn, K., Strasser, M., Harbitz, C.B. (eds.) Submarine mass movements and their consequences. Springer, Heidelberg, pp. 225-236.

Argnani, A., 1990. The Strait of Sicily rift zone: Foreland deformations related to the evolution of a back-arc basin. J Geodyn 12, 311-331. doi: 10.1016/0264-3707(90)90028-S.

Blum, P., 1997. Physical properties handbook: A guide to the ship board measurement of physical properties of deep-sea cores. Tech Note 26, Ocean Drill Programm, College Station, Tex.

Butler, R.W.H., Grasso, M., LaManna, F., 1992. Origign and deformation of the Neogene-Recent Maghrebian foredeep at the Gela Nappe, SE Sicily. J Geol Soc (Lond) 149: 547-556.

Camerlenghi, A., Urgeles, R., Fantoni, L., 2010. A database on submarine landslides of the Mediterranean Sea. In: Mosher, D.C., Shipp, C., Moscardelli, L., Chaytor, J., Baxter, C., Lee, H., Urgeles, R. (eds) Submarine Mass Movements and Their Consequences, Springer Netherlands, pp 503-513. doi: 10.1007/978-90-481-3071-9_41.

Canals, M., Lastras, G., Urgeles, R., Casamor, J.L., Mienert, J., Cattaneo, A., De Batist, M., Haflidason, H., Imbo, Y., Laberg, J.S., Locat, J., Long, D., Longva, O., Masson, D., Sultan, N., Trincardi, F., Bryn, P., 2004. Slope failure dynamics and impacts from seafloor and shallow sub-seafloor geophysical data: Case studies from the COSTA project. Marine Geology COSTA Special Issue 213, 9-72.

Civile, D., Lodolo, E., Accettella, D., Geletti, R., Ben-Avraham, Z., Deponte, M., Faccin, L., Ramella, R., Romeo, R., 2010. The Pantelleria graben (Sicily Channel, Central Mediterranean): An example of intraplate 'passive' rift. Tectonophysics 490, 173-183.

Colantoni, P., 1975. Note di geologia marina sul Canale di Sicilia. Giornale Geol 40(1), 181-207.

Di Stefano, E., Infuso, S., Scarantino, S., 1993. Plio-Pleistocene sequence stratigraphy of southwestern offshore Sicily from well logs and seismic sections in a high-resolution calcareous plankton biostratigraphic framework. In: Max, M.D., Colantoni, P. (eds.) UNESCO Technical Report in Marine Sciences 58, 105-110.

Dilek, Y., Sandvol, E., 2009. Seismic structure, crustal architecture and tectonic evolution of the Anatolian-African plate boundary and the Cenozoic orogenic belts in the eastern Mediterranean region. In: Murphy, J.B., Keppie, J.D., Hynes, A.J. (eds) Ancient Orogens and Modern Analogues. Geological Society, London, Special Publications 327, 127-160. doi: 10.1144/SP327.8.

Emeis, K.C., Robertson, A.H.F., Richter, C., et al., 1996. 4. Site 963. Proceedings of the ODP, Initial Reports 160, 55-84.

Finetti, I., 1984. Geophysical studies of the Sicily Channel rift zone. Bol Geofis Teor Appl 26, 3-28.

Freudenthal, T., Wefer, G., 2007. Scientific drilling with the sea floor drill rig MeBo. Sci. Drill. 5, 63-66.

Freudenthal, T., Wefer, G., 2013. Drilling cores on the sea floor with the remote-controlled sea floor drilling rig MeBo. Geosci. Intrum. Method. Data Syst. 2, 329-337, doi: 10.5194/gi-2-329-2013.

Gardiner, W., Grasso, M., Sedgeley, D., 1993. Plio-Pleistocene stratigraphy and fault movement of the Malta Platform. In: Max, M.D., Colantoni, P. (eds.) Geological Development of the Sicilan-Tunusian Platform. UNESCO Tech Rep Mar Sci 58, 111-116.

Grasso, M., 1993. Pleistocene structures along the Ionian side of the Hyblean Plateau (SE Sicily): Implications for the tectonic evolution of the Malta Escarpment. In: Max, M.D., Colantoni, P. (eds.) Geological Development of the Sicilan-Tunusian Platform. UNESCO Tech Rep Mar Sci 58, 49-55.

Hampton, M.A., Lee, H.J., Locat, J., 1996. Submarine landslides. Reviews of Geophysics 34(1), 33-59.

Harders, R., Kutterolf, S., Hensen, C., Moerz, T., Brueckmann, W., 2010. Tephra layers: A controlling factor on submarine translational sliding? Geochemistry, Geophysics, Geosystems 11(5), Q05S23. doi: 10.1029/2009GC002844.

Jenny, S., Goes, S., Giardini, D., Kahle, H.-G., 2006. Seismic potential of Southern Italy. Tectonophysics 415, 81-101.

Kuhlmann, J., Asioli, A., Strasser, M., Trincardi, F., Huhn, K., 2014a. Integrated stratigraphic and morphological investigation of the Twin Slide complex offshore southern Sicily. In: Krastel, S., Behrmann, J.-H., Völker, D., Stipp, M., Berndt, C., Urgeles, R., Chaytor, J., Huhn, K., Strasser, M., Harbitz, C.B. (eds.) Submarine mass movements and their consequences. Springer, Heidelberg.

Kuhlmann, J., Asioli, A., Trincardi, F., Klügel, A., Huhn, K., 2014b. Sedimentary response to Milankovitch-type climatic oscillations and formation of sediment undulations: evidence from a shallow-shelf setting at Gela Basin on the Sicilian continental margin. In review with Quaternary Science Reviews.

Laberg, J.S., Camerlenghi, A., 2008. The significance of contourites for submarine slope stability. Developments in Sedimentology 60, 537-556. doi: 10.1016/S0070-4571(08)10025-5.

Lebreiro, S.M., McCave, N.I., Weaver, P.P.E., 1997. Late Quaternary turbidite emplacement on the Horseshoe abyssal plain (Iberian Margin). Journal of Sedimentary Research 67, 856-870.

Lee, H.J., Locat, J., Desgagnés, P., Parsons, J.D., McAdoo, B.G.. Orange, D.L., Puig, P., Wong, F.L., Dartnell, P., Boulanger, E., 2007. Submarine mass movements on continental margins. In: Nittrouer, C.A., Austin, J.A., Field, M.E., Kravitz, J.H., Syvitski, J.P.M., Wiberg, P.L. (eds.). Continental Margin Sedimentation: From Sediment Transport to Sequence Stratigraphy, Wiley-Blackwell, UK, 213-274.

Lee, H.J., 2009. Timing of occurrence of large submarine landslides on the Atlantic Ocean margin. Marine Geology 264, 53-64.

Lermusiaux, P.F.J., Robinson, A.R., 2001. Features of dominant mesoscale variability, circulation patterns and dynamics in the Strait of Sicily. Deep-Sea Res. I 48, 1953-1997.

Locat, J., Lee, H.J., 2002. Submarine landslides: advances and challenges. Canadian Geotechnical Journal 39(1), 193-212. doi: 10.1139/T01-089.

Martrat, B., Grimalt, J.O., Lopez-Martinez, C., Cacho, I., Sierro, F.J., Abel Flores, J., Zahn, R., Canals, M., Curtis, J.H., Hodell, D.A., 2004. Abrupt temperature changes in the western Mediterranean over the past 250,000 years. Science 306, 1762-1765.

Masson, D.G., Harbitz, C.B., Wynn, R.B., Pedersen, G., Løvholt, F., 2006. Submarine landslides: processes, triggers and hazard prediction. Philosophical Transactions of the Royal Society A 364, 2009-2039. doi: 10-1098/rsta.2006.1810.

Max, M.D., Kristensen, A., Michelozzi, E., 1993. Small-scale Plio-Quaternary sequence stratigraphy and shallow geology of the west-central Malta Plateau. In: Max, M.D., Colantoni, P. (eds.) Geological development of the Sicilian-Tunusian Platform. UNESCO Technical Report in Marine Sciences 58, 117-122.

McAdoo, B.G.L., Pratson, L.F., Orange, D.L., 2000. Submarine landslide geomorphology, US continental slope. Marine Geology 169, 103-136.

Minisini, D., Trincardi, F., Asioli, A., Canu, M., Foglini, F., 2007. Morphologic variability of exposed mass-transport deposits on the eastern slope of Gela Basin (Sicily channel). Basin Research 19, 217-240. doi: 10.1111/j.1365-2117.2007.00324.x.

Minisini, D., Trincardi, F., 2009. Frequent failure of the continental slope: The Gela Basin (Sicily Channel). Journal of Geophysical Research 114, F03014, doi: 10.1029/2008JF001037.

Mix, A.C., Bard, E., Schneider, R., 2001. Environmental processes of the ice age: land, oceans, glaciers (EPILOG). Quaternary Science Reviews 20, 627-657.

Narcisi, B., Vezzoli, L., 1999. Quaternary stratigraphy of distal tephra layers in the Mediterranean – an overview. Global and Planetary Change 21, 31-50.

North Greenland Ice Core Project Members, 2004. High-resolution record of Northern Hemisphere climate extending into the last interglacial period. Nature 431, 147-151.

Piper, D.J.W., Mosher, D.C., Gauley, B.-J., Jenner, K., Campbell, D.C., 2003. The chronology and recurrence of submarine mass movments on the continental slope off southeastern Canada. In: Locat, J., Mienert, J. (eds.) Submarine mass movements and their consequences. Kluwer Academic Publishers, the Netherlands, p. 299-306.

Reimer, P.J., Bard, E., Bayliss, A., Beck, J.W., Blackwell, P.G., Bronk Ramsey, C., Buck, C.E., Cheng, H., Edwards, R.L., Friedrich, M., Grootes, P.M., Guilderson, T.P., Haflidason, H., Hajdas, I., Hatté, C., Heaton, T.J., Hoffman, D.L., Hogg, A.G., Hughen, K.A., Kaiser, K.F., Kromer, B., Manning, S.W., Niu, M., Reimer, R.W., Richards, D.A., Scott, E.M., Southon, J.R., Staff, R.A., Turney, C.S.M., van der Plicht, J., 2013. IntCal13 and Marine13 radiocarbon age calibration curves 0-50,000 years cal BP. Radiocarbon 55(4), 1869-1887.

Richter, T.O., van der Gaast, S., Koster, R., Vaars, A., Gieles, R., de Stigter, H.C., de Haas, H., van Weering, T.C.E., 2006. The AVAATECH XRF Core Scanner: Technical description and applications to NE Atlantic sediments. In: Rothwell, R.G. (ed.) New Techniques in sediment core analysis. Special Publications of the Geological Society 267, p. 39-50.

Robinson, A.R., Sellschopp, J., Warn-Varnas, A., Leslie, W.G., Lozano, C.J., Haley Jr., P.J., Anderson, L.A., Lermusiaux, P.F.J., 1999. The Atlantic Ionian Stream. J. Mar. Syst. 20, 129-156.

Sammari, C., Millot, C., Taupier Letage, I., Stefani, A., Brahim, M., 1999. Hydrological characteristics in the Tunisia-Sardinia-Sicily area during spring 1995. Deep-Sea Res. I 46, 1671-1703.

Schröder, C.J., Scott, D.B., Medioli, F.S., 1987. Can smaller benthic foraminifera be ignored in paleoenvironmental analyses? Journal of Foraminiferal Research 17(2), 101-105.

Siani, G., Paterne, M., Arnold, M., Bard, E., Métivier, B., Tisnerat, N., Bassinot, F., 2000. Radiocarbon reservoir ages in the Mediterranean Sea and Black Sea. Radiocarbon 42, 271-280.

Sprovieri, R., Di Stefano, E., Incarbona, A., Gargano, M.E., 2003. A high-resolution record of the last deglaciation in the Sicily

Channel based on foraminifera and calcareous nannofossil quantitative distribution. Palaeogeography, Palaeoclimatology, Palaeoecology 202, 119-142.

Stuiver, M., Reimer, P.J., 1993. Extended 14C database and revised CALIB radiocarbon calibration program. Radiocarbon 35, 215-230.

Trincardi, F., Cattaneo, A., Correggiari, A., Mongardi, S., Breda, A., Asioli, A., 2003. Submarine slides during sea level rise: Two examples from the eastern Tyrrhenian margin. In: Locat, J., Mienert, J. (eds.) Submarine mass movements and their consequences. Kluwer Academics, Dordrecht, the Netherlands. p. 469-478.

Vanneste, M., Sultan, N., Garziglia, S., Forsberg, C.F., L'Heureux, J.-S., 2014. Seafloor instabilities and sediment deformation processes: The need for integrated, multi-disciplinary investigations. Marine Geology 352, 183-214.

Verdicchio, G., Trincardi, F., 2008. Mediterranean shelf-edge muddy contourites: examples from the Gela and South Adriatic basins. Geo-Marine Letters 28, 137-151. doi: 10.1007/s00367-007-0096-9.

Waelbroeck, C., Labeyrie, L., Michel, E., Duplessy, J.C., McManus, J.F., Lambeck, K., Balbon, E., Mabracherie, M., 2002. Sea-level and deep water temperature changes derived from benthic foraminifera isotopic records. Quaternary Science Reviews 21(1-3), 295-305.

Warrick, J.A., Xu, J., Noble, M.A., Lee, H.J., 2008. Rapid formation of hyperpycnal sediment gravity currents offshore of a semi-arid California river. Continental Shelf Research 28, 991-1009.

Weltje, G.J., Tjallingii, R., 2008. Calibration of XRF core scanners for quantitative geochemical logging of sediment cores: Theory and application. Earth and Planetary Science Letters 274, 423-438.

Yokoyama, Y., Lambeck, K., De Deckker, P., Johnson, P., Fifield, K., 2000. Timing for the maximum of the Last Glacial constrained by lowest sea-level observations. Nature 406, 713-716.

9 Manuscript IV

"Submarine slope stability assessment of the central Mediterranean continental margin: the Gela Basin"

Authors: Ai, Fei (MARUM, University of Bremen, Germany)
Kuhlmann, Jannis (MARUM, University of Bremen, Germany)
Huhn, Katrin (MARUM, University of Bremen, Germany)
Michael Strasser (Geological Institue, ETH Zurich, Switzerland)
Achim Kopf (MARUM, University of Bremen, Germany)

Status: Published in: Krastel, S., Behrmann, J.-H., Völker, D., Stipp, M., Berndt, C., Urgeles, R., Chaytor, J., Huhn, K., Strasser, M., Harbitz, C.B. (eds.) *Submarine mass movements and their consequences. Advances in Natural and Technological Hazards Research Vol. 37*. Springer, Heidelberg, pp. 225-236.
doi: 10.1007/978-3-319-00972-8_20

Objectives:

- Assess the current state of slope stability by means of geotechnical parameters
- Evaluate the requirements for seismic triggering of failure

Submarine slope stability assessment of the central Mediterranean continental margin: the Gela Basin

Fei Ai[1], **Jannis Kuhlmann**[1], Katrin Huhn[1], Michael Strasser[2], Achim Kopf[1]

[1]MARUM – Center for Marine Environmental Sciences, University of Bremen, Bremen, Germany
[2]IGeological Institute, ETH Zurich

This study investigates slope stability for a relatively small scale (5.7 km², 0.6 km³), 8 ka old landslide named Northern Twin Slide (NTS) at the slope of the Gela Basin in the Sicily Channel (central Mediterranean). The NTS is characterized by two prominent failure scars, forming two morphological steps of 110 and 70 m height. Geotechnical data from a drill core upslope the failure scar (GeoB14403) recovered sediments down to ~52 m below seafloor (mbsf). The deposits show low over consolidation ratio (OCR = 0.24–0.4) and low internal friction angle (20–22°) around 28–45 mbsf, which suggests this mechanically weak interval may act as potential location of instability in a future failure event. Oedometer tests attest the sediments are highly under consolidated and the average overpressure ratio (λ*) is ~0.7. Slope stability analyses carried out for different scenarios indicate that the slope is stable both under static undrained and drained conditions. A relatively small horizontal acceleration of 0.03–0.08 g induced by an earthquake may be sufficient to cause failure. We propose that moderate seismic triggers may have been responsible for the twin slide formation and could also cause mass wasting in the future.

Key words: Slope stability, submarine landslide, geotechnical characteristics, central Mediterranean

9.1 Introduction

Submarine landslides are ubiquitous on continental margins. Overpressure near the seafloor plays a significant role in the occurrence of submarine landslides (Flemings et al., 2008). Seismic activity is considered as an important triggering mechanism of submarine landslides (Masson et al., 2006). It is therefore important to evaluate the effects of overpressure as a preconditioning factor and seismic shaking as triggering mechanism for submarine slope instability in earthquake-prone regions. The study area is located between 200 and 800 m water depth along the eastern margin of the Gela Basin of the Sicily Channel, central Mediterranean. The continental slope has a general gradient (approx. 3°) and steep slide head scarps (up to 32° in places) (*Figure 9.1a*). Two recent slides (termed Northern Twin Slide and Southern Twin Slide) show subrounded scars on the upper slope and are characterized by bathymetric bulges at the base of the slope (Minisini et al., 2007). These landslides are described as multiple failures likely controlled by specific stratigraphic surfaces acting as glide planes (Minisini and Trincardi, 2009; Trincardi and Argnani, 1990). In order to provide a possibility to assess future slope instabilities due to overpressure and seismic shaking, undrained and drained infinite slope stability models are introduced to model slope stability under both static and pseudostatic conditions.

9.2 Geological setting

The Gela Basin is the most recent (Plio-Quaternary) foredeep of the Maghrebian fold-and-thrust belt (Argnani et al., 1986). The extensional basin originated in the late Miocene to early Pliocene with the emplacement of the Gela nappe, which lasted until the early Pleistocene (Grasso, 1993). Sequence stratigraphic interpretation on the shelf and upper slope area on the Gela Basin (Minisini and Trincardi, 2009; Kuhlmann et al., 2014) identify, from top to bottom (*Figure 9.1b*): (I) deposits resting on top of erosive unconformity ES1, (II) a progradational wedge pinching out towards NE and (III) deposits beneath sequence boundary SB1. In general, the studied

northern slope of the Gela Basin shows high sedimentation rates of 85–250 mm/ka area result of abundant supply of fine-grained material and tectonic subsidence (Emeis et al., 1996). The NTS is characterized by two prominent failure scars forming two morphological steps of 110 and 70 m height (*Figure 9.1b*). The slope angle of the slide headwall is around 16°, while the surfaces of the displaced masses dip at 1.5–4.5° (Minisini et al., 2007). The accumulation area of the NTS is characterized by a morphologic bulge at the seafloor which extends 7 km downslope and 1.5 km in width. The source area of the NTS is 5.7 km² and the average height of the failure section is approx. 100 m. The runout of the NTS is 11.7 km (Minisini et al., 2007).

9.3 Material and methods

9.3.1 Shipboard and laboratory analysis

The principal data set for this study is based on a MeBo (MARUM seafloor drillrig) core and a co-

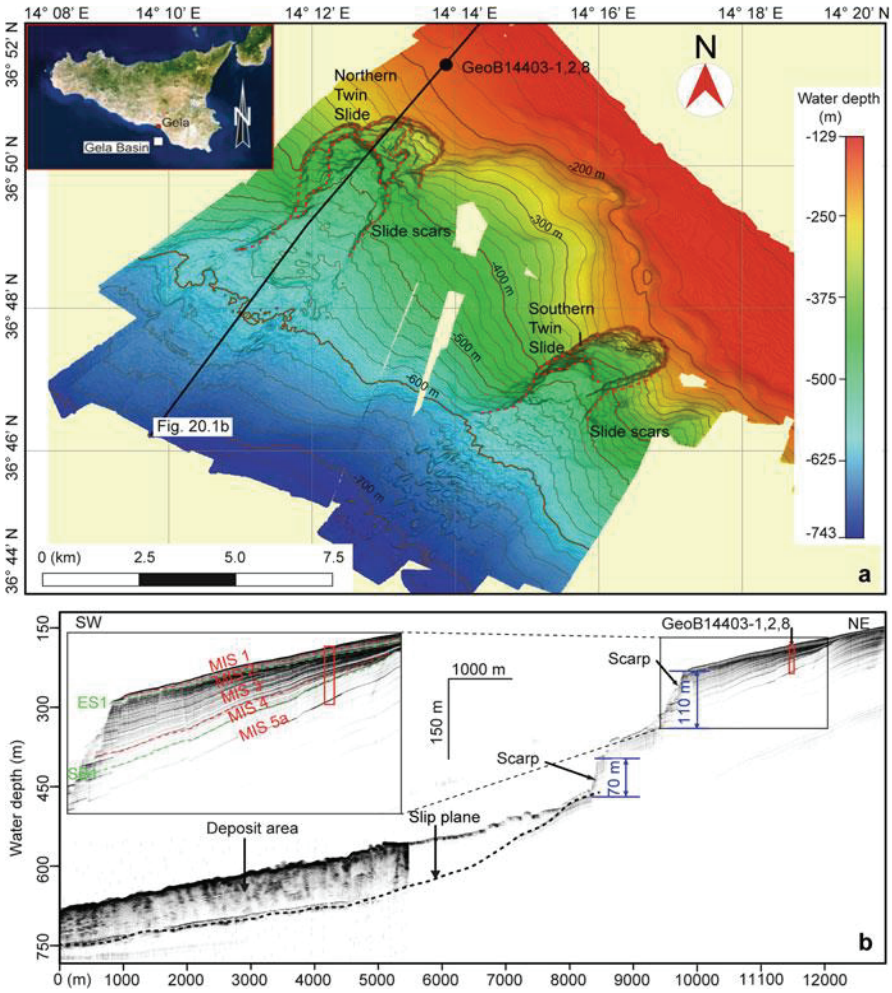

Figure 9.1. A: Overview map showing the morphology of the Twin Slides in the Gela Basin offshore Sicily (Italy). *Black dot* indicates the location of core GeoB14403. *Red dashed lines*indicate the scarps of the Twin Slides. *Black lines* indicate the locations of parasound profiles presented in B. B: Parasound sub-bottom profile crossing the NTS. *Red rectangle* shows the location of the core GeoB14403. *Green dashed lines* indicate the Erosion surface 1 (ES1) and the sequence boundary1 (SB1). *Red dashed lines* indicate the boundaries of different Marine Oxygen Isotope Stages (MIS) (Minisini et al., 2007; Kuhlmann et al., 2014). *Black dashed line* indicates the slip surface of the upper retrogressive landslide.

located gravity short core, both acquired during CruiseMSM15/3 in 2010. A 51.9 m-long succession from the undisturbed slope apron upslope the NTS scar was recovered. Visual core description was carried out on board shortly after core recovery on the split core. Discrete samples were taken on board to measure water content and bulk density using oven drying method and pycnometer (Blum, 1997). Undrained shear strength (s_u) was estimated using a Mennerich Geotechnik (Germany) vane shear apparatus (Blum, 1997) and Wykeham Farrance cone penetrometer (Wood, 1985). Laboratory experiments consisted of grain size distribution analysis using a Beckman Coulter LS 13320 particle size analyzer and Atterberg limits using the Casagrande apparatus and rolling thread method (Casagrande, 1932). Consolidation tests were performed using uniaxial incremental loading oedometer system (ASTM, 2004a), with permeability being estimated from the consolidation test results (Lamb and Whitman, 1969). The drained sediment strength parameters, cohesion (c') and internal friction angle ($\emptyset'$) were determined using drained direct shear tests (ASTM, 2004b).

9.3.2 Shipboard and laboratory analysis

Effective stress is an important parameter for slope stability analysis. Overpressure impacts the effective stress as seen in Terzaghi et al. (1996). Overpressure (Δu) is defined as fluid pressure (u) in excess of hydrostatic equilibrium (u_0) (Dugan and Sheahan, 2012). The Terzaghi's effective stress relationship is:

$$\begin{aligned}\sigma_v' &= \sigma_v - u = \sigma_v - (u_0 + \Delta u)\\ &= (\rho_b - \rho_w)gz - \Delta u\\ &= (\gamma - \gamma_w)z - \Delta u = \gamma' z - \Delta u \end{aligned} \quad (9.1)$$

Where σ_v' is vertical effective stress, σ_v is total overburden stress, ρ_b is bulk density (assuming constant), ρ_w is density of water (assuming constant), γ is unit weight, γ_w is unit weight of water, γ' is buoyant weight, z is overburden depth, and g is the acceleration due to gravity.

Preconsolidation stress (σ_{pc}') interpreted from consolidation test is an approach to evaluate overpressure (Casagrande 1936):

$$\Delta u = \sigma_{vh}' - \sigma_{pc}' \quad (9.2)$$

Where σ_{vh}' is vertical effective stress for hydrostatic conditions ($\sigma_{vh}' = \gamma' z$). The overpressure was used to perform back analysis of slope stability under drained conditions.

9.3.3 Slope stability analysis

The infinite slope stability analysis is used to calculate the factor of safety (FS). In the infinite slope approximation $FS \geq 1$ represents stability and $FS < 1$ represents instability. For static conditions the FS calculation after Morgenstern (1967) and Løseth (1999) follows:

$$FS = \frac{s_u}{\gamma' z \sin\theta \cos\theta} \text{ (Undrained)} \quad (9.3)$$

$$FS = \frac{c' + \gamma' z(\cos^2\theta - \lambda^*)\tan\phi'}{\gamma' z \sin\theta \cos\theta} \text{ (Drained)} \quad (9.4)$$

Where θ is slope angle (also assumed angle for slip surface) and λ^* is overpressure ratio ($\lambda^* = \Delta u/\sigma_{vh}'$). The evaluation of slope stability under earthquake loading is commonly based on pseudostatic analysis (ten Brink et al., 2009; Morgenstern, 1967). The overpressure that may be generated during an earthquake is not taken into account for the slope stability analysis. The seismic response included in the FS calculation is the integrated horizontal ground acceleration kg (where k is horizontal acceleration coefficient and g is the acceleration due to gravity), which is assumed to be applied over a time period long enough for the induced shear stress can to be considered constant.

$$FS = \frac{s_u}{\gamma' z[\sin\theta \cos\theta + k(\gamma/\gamma')\cos^2\theta]} \text{ (Undr.)} \quad (9.5)$$

$$FS = \frac{c' + \gamma' z(\cos^2\theta - \lambda^*)\tan\phi'}{\gamma' z[\sin\theta \cos\theta + k(\gamma/\gamma')\cos^2\theta]} \text{ (Dr.)} \quad (9.6)$$

The aim of the stability analysis is to estimate the static FS of the slope and the minimum seismic

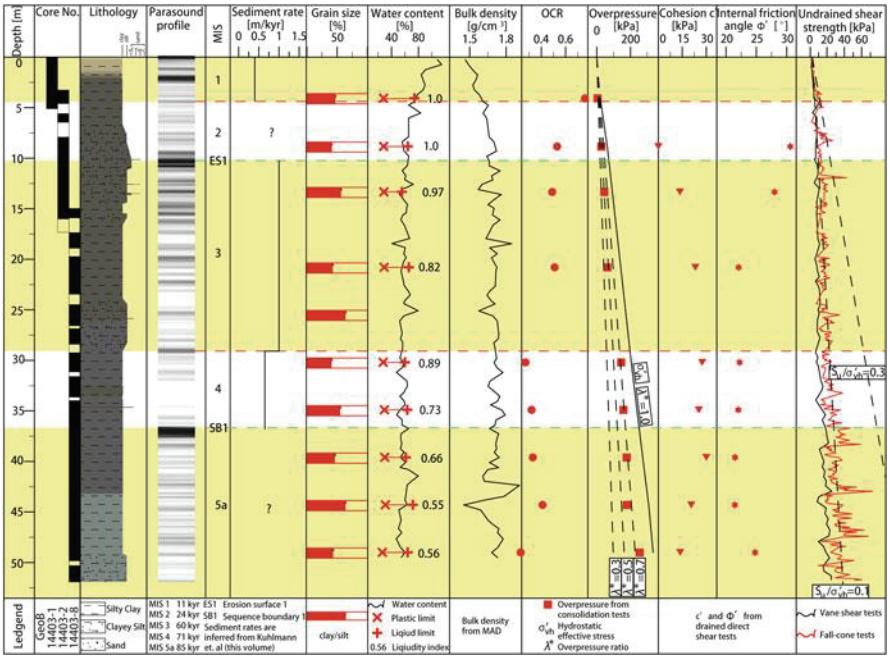

Figure 9.2. Lithological, physical properties and geotechnical properties profile of core GeoB14403 for slope stability assessment.

acceleration required to trigger a slope failure under undrained and drained conditions, respectively.

9.4 Results

9.4.1 Physical and geotechnical properties

The physical properties and geotechnical results are presented in *Figure 9.2*. The dominant lithology is homogeneous silty clay to clayey silt with a narrow range of particle sizes. The sediment's plastic limit is ~28 %, while the liquid limit ranges from 55 to 74%. Natural water content is close to the liquid limit and gradually decreases with depth, while bulk density gradually increases with depth. Undrained shear strength values range from a few kPa near the seafloor to ~50 kPa at depth, where the pocket penetrometer generally shows slightly higher values than vane shear. The undrained shear strength-depth relation obtained from pocket penetrometer tests is: $S_u = 0.6z + 37$ (kPa, $R^2 = 0.64$). The sediment appears to be under consolidated as inferred from low ratios between the undrained shear strength and vertical effective stress at static condition ($S_u/\sigma'_{vh} \approx 0.1$) (Locat and Lee, 2002).

Consolidation tests indicate sediments are slightly under consolidated ($OCR = \sigma'_{pc}/\sigma'_{vh} = 0.76$ at 4.08 mbsf) at shallow subsurface depth and become strongly under consolidated deeper downhole($OCR = 0.23$ at 49 mbsf). Overpressures estimated from consolidation test results using Eq. 9.2 indicate that

Table 9.1. Parameters used for slope stability calculations (data derived from *Figure 9.2*)

	Static or variable/value (in different scenarios)			
Input parameters	Undrained static	Drained static	Undrained seismic	Drained seismic
Undrained shear strength, S_u (kPa)	Static/0.6z+3.7		Static/33.7	
Depth of the failure surface, z (m)	Variable/10-100		Static/50	
Slope angle, θ(°)		Variable/1-5		
Cohesion, c' (kPa)	-	Static/23.5	-	Static/23.5
Internal friction angle ϕ' (°)	-	Static/21	-	Static/21
Overpressure ratio, λ^*	-	Variable/0.4-1.0	-	Static/0.7
Unit weight, γ (kN/m²)	-	-	Static/16.4	
Horizontal acceleration coefficient, k	-	-	Variable/0-0.09	
Buoyant weight, γ' (kN/m²)		6.6		
Gravitational acceleration, g (m/s²)		9.81		
FS/k	1.9/0	3.6/0	1/0.02	1/0.053

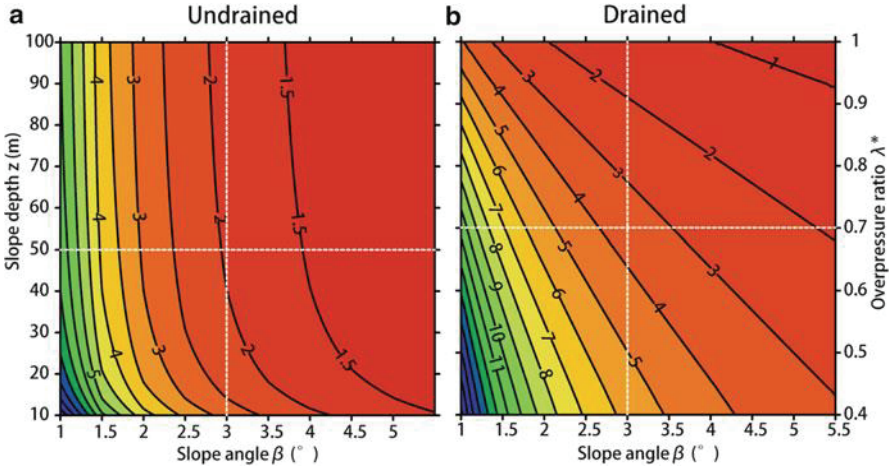

Figure 9.3. Slope stability analysis under undrained (A) and drained (B) conditions for the NTS. *Contour plots* indicate FS values. *Dashed white lines* indicate current mean values of the parameters in the NTS.

overpressure increases with depth and λ^* ranges from 0.24 to 0.77. Drained direct shear tests indicate that sediments from 28 to 45 mbsf have somewhat lower angle of internal friction (approx. 20°) compared to one sample from shallow depth (approx. 30°). Values of the effective cohesion intercept (c'), range from 0 to 30 kPa for granular to clay-rich sediments.

9.4.2 Slope stability analysis

Factor of safeties for four different cases were calculated using Eqs. 9.3, 9.4, 9.5, and 9.6 with two parameters changing within a certain range and other parameters keeping at constant value (*Table 9.1* and *Figures 9.3* and *9.4*). According to the parameters of current situation, the factor of safeties of static undrained and drained cases can be constrained (*Figure 9.3*). Horizontal acceleration coefficients in earthquake undrained and drained cases were back-calculated using Eqs. 9.5 and 9.6 while $FS = 1$. The slope appears to be presently stable both under static undrained and drained conditions. The depth of the failure surface shows less influence on FS compared to slope angle in the undrained slope stability analysis. Overpressure ratios $\lambda^* \geq 0.93$ are required to fail a drained slope at an angle of 5.5°. Pseudo-static analysis indicates that slope is vulnerable in undrained earthquake case. Horizontal acceleration coefficient $k = 0.02$ is need to trigger slope failure in undrained earthquake case, while higher horizontal acceleration coefficient ($k = 0.053$) is required to trigger slope failure ($FS = 1$) at current mean values of the slope angle (3°) in drained earthquake case.

9.5 Discussion

9.5.1 Preconditioning factors

Generally factors such as high sedimentation rate, slope steepening and the presence of intrinsically weak layer scan greatly reduce the factor of safety of slope under static loading conditions. High sedimentation (≥m/ka) of low permeability sediments (permeability ≤10^{-16} m²) can generate overpressure, a condition known as under consolidated (Dugan and Sheahan, 2012).Undrained shear tests and consolidation tests presented here suggest the sediments are strongly under consolidated ($OCR = 0.27 - 0.77$). The state of overpressure in the Gela basin most likely results from deposition of fine-grained sediments with high sedimentation rates. Based on seismostratigraphic interpretation and shallow cores a high sedimentation rate (0.3–0.6 m/ka) was proposed since the Last Glacial Maximum at 18–24 ka B.P. (Minisini and Trincardi, 2009). Kuhlmann

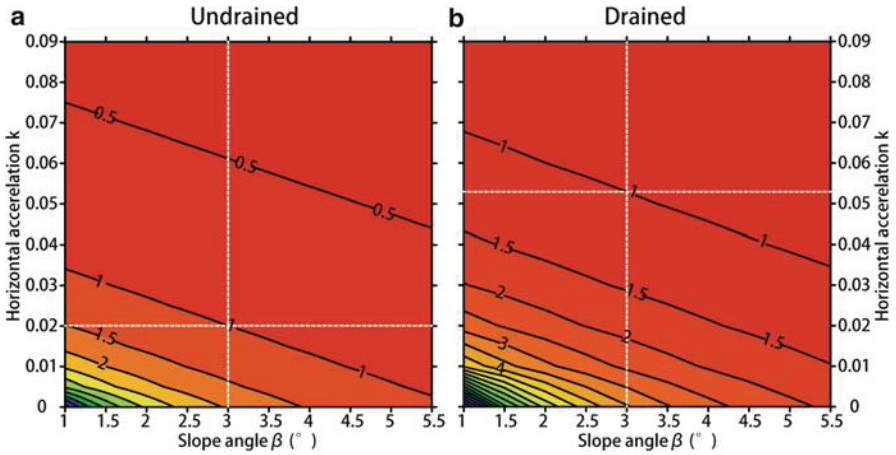

Figure 9.4. Back-calculation of pseudostatic horizontal acceleration ratio showing FS as a function of slope angle and pseudostatic horizontal acceleration ratio under undrained A and drained B conditions for the NTS. *Contour plots* indicate FS values. *Dashed white lines* indicate the value of pseudostatic horizontal acceleration required to trigger slope failure (FSD1) at current mean value of the slope angle.

et al. (2014) estimate the sedimentation rate was ~0.5 m/ka during MIS 1 and ~1 m/ka during MIS 3 according to results from the MeBo core recovered in the undisturbed slope apron of the NTS. Based on our oedometer experiments, the coefficient of permeability of sediment is on the order of 10^{-10} m/s (permeability $\leq 10^{-16}$ m²). Such a low permeability may inhibit fluid seepage and thereby induce the overpressure buildup (Dugan and Sheahan, 2012).

The slope stability analysis suggests the slope angle has a larger influence on the FS than on depth of failure plane. Since FS decreases with increasing slope angle, one possible mechanism for failure could be rapid wedge-shaped sediment accumulation during sea level low stand (Minisini et al., 2007) or bottom currents leading to net erosion and undercutting the toe of slope (Bennett and Nelsen, 1983). Both mechanisms have been hypothesized to occur in the study area (Minisini et al., 2007; Verdicchio and Trincardi, 2008). Based on low internal friction angle derived from direct shear test, sediments from 28 to 45 mbsf appear to be weaker, potentially forming a preferential slip plane for future slope failure. Slope stability analysis further suggests the slope is stable in static conditions. To reach $FS = 1$ or lower, an overpressure ratio of 0.93 at slope angle of 5.5° would be required, which is not observed at present. Hence additional triggers are needed to generate slope failure.

9.5.2 Triggering factors

Pseudostatic slope stability analysis suggests that pseudostatic horizontal acceleration in the order of 0.02–0.053 g is required to fail the slope (FSD1) in undrained as well as drained conditions. Strasser et al. (2011), based on the principles by Seed and Idriss (1971) and Seed (1979), suggested that the pseudostatic horizontal acceleration only represent ~65 % of the effective earthquake peak ground acceleration ($PGA = 0.03 - 0.08\ g$). In order to explore plausible scenarios for earthquake events, which might induce seismic shaking in this intensity range and thus could trigger slope failure of the NTS, PGA is estimated using empirical attenuation equations after Bindi et al. (2011) that depend on the combination of magnitude and source distance of earthquake (*Figure 9.5*). The Sicily channel show slow seismic activity (*Figure 9.5a*). Over the last 40 year, only small earthquakes occurred, which are too low to trigger instabilities (*Figure 9.5b*). The attenuation relationship combined with the critical threshold condition for instability, as revealed from our analysis, indicates that moderate earthquakes with

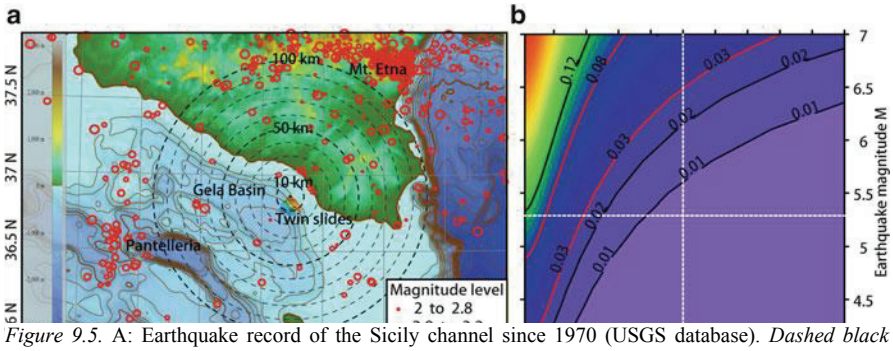

Figure 9.5. A: Earthquake record of the Sicily channel since 1970 (USGS database). *Dashed black circles* indicate the distance to the study area. *Red circles* indicate magnitude levels of earthquakes. B: PGA estimation using empirical attenuation equations after Bindi et al. (2011) that depends on combination of magnitude and source distance of earthquake. *Contour plots* indicate the PGA. *Red lines* indicate the PGA values are required to trigger slope failure. *Dashed white lines* indicate the largest and closest earthquake in the study area during last 40 year.

magnitudes $M = 4.0–4.8$ near or at the location of the study area, or strong ($M = 7$), far-field events in epicentral distance <20–80 km are required to trigger the slope failure. Past landslide occurrence in the study area indicates that over a longer time scale, larger magnitude earthquakes than those recorded during the instrumental period may have occurred. We propose that moderate seismic triggers may have been responsible for NTS formation and could also cause mass wasting in the future.

9.6 Conclusions

In summary, we have demonstrated geotechnical properties of sediments and slope stability analysis of the Gela Basin. Strongly under consolidation of the sediments in the study area are mainly attributed to rapid sedimentation in fine sediments. Despite of the high overpressure presented in the sediments, the stability analysis suggests the slope is stable under static conditions. Slope failure may be triggered by moderate earthquake (M4.0–M4.8) in the study area, or even strong events if farther away. Additional studies of in-situ pore pressure measurement and pore pressure change during the seismic loading are needed in order to further investigate the dynamic response and better assess the slope stability.

Acknowledgements

We thank the captain and crew of the RV Meteor for their support during the cruise MSM15/3.Matthias Lange is thanked for outstanding technical assistance with the geotechnical laboratory devices. This study has been funded through DFG-Research Center/Cluster of Excellence “The Ocean in the Earth System”. We also like thank reviewers Brandon Dugan and Vasilios Lykousis for their constructive remarks.

References

Argnani, A., Cornini, S., Torelli, L., Zitellini, N.,1986. Neogene-quaternary foredeep system in the strait of Sicily. Memoreie Società Geologica Italiana 36,123–130.

ASTM, 2004a. Standard test methods for one-dimensional consolidation properties of soils using incremental loading (Standard D2435-04). ASTM International, West Conshohocken, p. 10.

ASTM, 2004b. Standard test method for direct shear test of soils under consolidated drained conditions (Standard D3080-04). ASTM International, West Conshohocken, p. 7.

Bennett, R.H., Nelsen, T.A., 1983. Seafloor characteristics and dynamics affecting geotechnical properties at shelf breaks. SEPM Special Publications 33, 333–355.

Bindi, D., Pacor, F., Luzi, L., Puglia, R., Massa, M., Ameri, G., Paolucci, R., 2011. Ground motion prediction equations derived from the Italian strong motion database. Bulletin for Earthquake Engineering 9(6), 1899–1920. doi: 10.1007/s10518-011-9313-z.

Blum, P., 1997. Physical properties handbook: a guide to the shipboard measurement of physical properties of deep-sea

cores. ODP Technical Note 26, Ocean Drilling Program, College Station.

Casagrande, A., 1932. Research on the Atterberg limits of soil. Public Roads 13(8), 121–136.

Casagrande, A., 1936. The determination of the pre-consolidation load and its practical significance. In: Proceedings of the 1st international conference of soil mechanics and foundation engineering 3, p. 60–64.

Dugan, B., Sheahan, T.C., 2012. Offshore sediment overpressures of passive margins: mechanisms, measurement, and models. Reviews of Geophysics 50(3), RG3001. doi: 10.1029/2011rg000379.

Emeis, K., Robertson, A., Richter, C., 1996. Site 963. Proceedings ODP, Initial Report 160, p. 55–84.

Flemings, P.B., Long, H., Dugan, B., Germaine, J., John, C.M., Behrmann, J.H., Sawyer, D., Scientists, I.E., 2008. Pore pressure penetrometers document high overpressure near the seafloor where multiple submarine landslides have occurred on the continental slope, offshore Louisiana, Gulf of Mexico. Earth and Planetary Science Letters 269(3–4), 309–325. doi: 10.1016/j.epsl.2007.12.005.

Grasso, M., 1993. Pleistocene structures along the Ionian side of the Hyblean Plateau (SE Sicily): implications for the tectonic evolution of the Malta Escarpment. In:Max MD, Colantoni P (eds) Geological development of the Sicilian-Tunisian platform, vol 58, UNESCO report marine science. UNESCO, Paris, p. 49–54.

Kuhlmann , J., Asioli, A., Strasser, M., Trincardi, F., Huhn, F., 2013. Integrated stratigraphic and morphological investigation of the Twin Slide complex offshore southern Sicily. In: Krastel, S., Behrmann, J.-H., Völker, D., Stipp, M., Berndt, C., Urgeles, R., Chaytor, J., Huhn, K., Strasser, M., Harbitz, C.B. (eds.) Submarine mass movements and their consequences. Springer, Heidelberg, p. 583-594.

Lamb, T.W., Whitman, R.V., 1969. Soil mechanics. Massachusetts Institute of Technology, Cambridge, MA.

Locat, J., Lee, H.J., 2002. Submarine landslides: advances and challenges. Canadian Geotechnical Journal 39(1),193–212. doi: 10.1139/t01-089.

Løseth, T.M., 1999. Submarine massflow sedimentation: computer modelling and basin-fill stratigraphy. Springer, New York.

Masson, D.G., Harbitz, C.B., Wynn, R.B., Pedersen, G., Løvholt, F., 2006. Submarine landslides: processes, triggers and hazard prediction. Philos Trans R Soc A Math Phys Eng Sci 364(1845):2009–2039. doi: 10.1098/rsta.2006.1810.

Minisini, D., Trincardi, F., 2009. Frequent failure of the continental slope: the Gela Basin (Sicily Channel). Journal of Geophysical Research 114(F3), F03014. doi: 10.1029/2008jf001037.

Minisini, D., Trincardi, F., Asioli, A., Canu, M., Foglini, F., 2007. Morphologic variability of exposed mass-transport deposits on the eastern slope of Gela Basin (Sicily channel). Basin Research 19(2), 217–240. doi: 10.1111/j.1365-2117.2007.00324.x.

Morgenstern, N.R., 1967. Submarine slumping and the initiation of turbidity currents. In: Richards, A.F. (ed,) Marine Geotechnique. University of Illinois Press, Urbana, p. 189–210.

Seed, H.B., 1979. Considerations in earthquake-resistant design of earth and rock-fill dams. G´eotechniques 29, 215–263.

Seed, H.B., Idriss, I.M., 1971. Simplified procedure for evaluating soil liquefaction potential. Journal of the Soil Mechanics and Foundations Division. Proceedings of the American Society of Civil Engineers 97(9), 1249–1273.

10 Conclusions

The wide diversity of environmental settings along the continental margins of the world provide a broad range of distinctive factors and processes that not only shape their depositional and, hence, morphological appearance, but as well govern the occurrence of submarine landslides. Despite the replete research on individual mechanisms affecting slope stability, it may hence be argued that current knowledge on the driving forces is rather inconclusive on several occasions (e.g., Camerlenghi et al., 2007; Cochonat et al., 2007). As a consequence, this thesis was set out to explore the specific constellation of predisposing factors and triggering mechanisms at the landslide-prone continental slope of Gela Basin in the Strait of Sicily and sought to answer questions about:

(1) the role of climatically induced environmental changes in shaping continental slope and outer shelf stratal architecture and providing preferential surfaces of failure,

(2) the mechanisms involved in failure, and

(3) the timing and recurrence of landslide events, especially with regard to the governing environmental conditions.

The main findings culminating from this investigative effort are chapter-specific and will be synthesized in the following sections.

10.1 Climatic imprint on slope architecture and depositional processes

A principal relationship between climatic forcing and depositional architecture has been acknowledged on many continental margins around the world. However, sea level fluctuations tend to manifest in individual system tracts (TST, HST, FSST, LST) with site-specific dimensions and preservations states that are characteristic to the prevailing environmental conditions (Lobo and Ridente, 2014, and references therein). The centennial- to millennial-scale multi-methodological chronologic framework proposed in this thesis, along with sequence-stratigraphic interpretations, allowed to disentangle these complex interactions and relate paleoclimatic fluctuations to the depositional continental margin architecture at Gela Basin (chapter 6). Where the sedimentary succession is not truncated by the presence of landslide scars, it resolves a composite record of Milankovitch-type (100-ka/20-ka) and sub-Milankovitch (D/O-scale) climatic oscillations that are captured in a peculiar pattern of systems tracts (chapter 6). While 100-ka (eccentricity-related) cyclicity is recorded by progradational sequences that are proximally bounded by regional erosional surfaces, the 20-ka (precession-related) cyclicity predominantly manifests in alternating HST/FSST

deposits during MIS 5 and MIS 3-2 and displays a suborbital LST wedge during MIS 4 (chapter 6). These cyclic variations induce the formation of key stratigraphic surfaces (i.e., erosional or onlap/downlap surfaces), which invoke a change in the sediment-physical properties as a response to variations in lithology, sediment accumulation rate, or compaction and alteration processes (chapter 7, 8). It was shown that these surfaces act as preferential zones of failure, which could be linked to multiple failure events of translational character within the study area (chapter 7, 8).

Contrasting many other continental settings, where sediment accumulation ratios peak during glacials, the bulk of sediment deposited in Gela Basin during the last glacial-interglacial cycle relates to the highstand units of MIS 5 (chapter 6). This circumstance is thought to origin from (1) hyperpycnal discharges during river floods, and (2) a favourable setting of Levantine Intermediate Water (LIW) strength and pathways distributing sediment in the study area (chapter 6). Both mechanisms may add to the destabilization of the continental slope through rapid deposition and burial of underlying sediments, thus provoking successive generation of excess pore water pressure, as indicated by the presence of contouritic deposits (chapter 8). Additionally, hyperpycnal flows are speculated to cause undulated sediment features emplaced during these intra-MIS 5 highstand units (HST), which do not appear to originate from landslide processes (chapter 6).

10.2 Slide mechanisms and timing of failure

The mechanisms of failure in the study area may be divided into two groups. The first involves the translational movement of disintegrative mudflows along sub-horizontal weak layers (chapter 8), while the latter involves the presence of rotational components and is represented by the *Northern Twin Slide* (chapter 7, 8). In case of the translational motion of the mudflows, glide planes are usually associated with key stratigraphic surfaces relating to climatic oscillations (chapter 6). However, one glideplane recovered in borehole GeoB14401 displays an organic-rich layer enriched with volcanoclastic material of higher grain sizes, indicating a mechanically weaker layer with regard to the surrounding material (chapter 8). Evidence of shear in this layer encompasses the presence of small deformation bands, along which mud clasts show preferential elongation in the direction of motion (chapter 8).

Generally, headwall failure appears to take place along sub-vertical normal faults and through reactivation of paleo-headscarps (i.e. from *Father Slide* event). MTDs involving relatively greater sediment volumes (e.g., *Twin Slides*) tend to cannibalize pre-existing MTDs resulting in extremely complex depositional geometries (chapter 7).

With regard to the timing of failure, eight individual mass transport deposits could be identified that relate to the time span of the last ~90 ka (chapter 8). Within this timespan the *Father Slide* deposits, interpreted as a debris avalanche, comprise the oldest discernible event with an estimated age of 87 ka. The subsequently emplaced MTDs encompass mudflows and date at 59 ka, 40-45 ka, 30 ka, 24 ka, and 8.5 ka (chapter 8). Further sliding, though on a more localized and smaller scale, is related

to a highstand (HST) interval at 70-87 ka. However, the majority of the recognised mudflows are linked to conditions of sea level fall or lowstand (chapter 8).

10.3 Predisposing factors and trigger mechanisms

The study area shows a combination of multiple causing factors that are thought to significantly add to the overall instability in this region, including (1) rapid loading and associated generation of excess pore water pressure (chapter 8, 9), (2) the presence of weak stratigraphic layers associated to abrupt climatic variability (chapter 6) as well as intercalated volcanoclastic material (chapter 8), and (3) recurrent seismic activity (8,9).

10.4 Outlook

This study showed to a large extend the special value of core control on sedimentary successions, especially with regard to the analysis of failure timing and recurrence rates as well as the investigation of the material involved in landslide processes (e.g., through thin section analysis). However, in order to adequately acknowledge the micromechanisms at work in such a glideplane in a muddy setting, the recovery of the same stratigraphic unit in both disturbed and undisturbed masses is desirable. With regard to additional research on this project, the following options are key:

- A high-resolution analysis of the sedimentary succession related to MIS 3 units on the upper slope of Gela Basin using CT scanning and grain size measurements: high sediment accumulation rates (SAR ~ 2 m/ka) and a good preservation state of these units relating to the general sea level fall during MIS 3 may allow to directly observe short-lived (millennial-scale) sea level fluctuations as indicated by the seismo-stratigraphic record (chapter 6). Sedimentologically, these fluctuations should be recorded by multiple condensed layers with relatively coarser material related to low SAR during rapid sea level rises.
- A comprehensive provenance analysis to reveal the origin of sediments relating to MIS 5 highstand units and to test the hypothesis of additional sedimentary input from hyperpycnal flows.
- A high-resolution study of the sapropel equivalent deposited during MIS 5: the thick and continuous sedimentary record of NE Gela Basin provides a type setting to investigate not only the formation of sapropels in general, but as well the environmental changes associated to intra-sapropel depositional variability.
- Tracing of undulated sediment features on the modern highstand units: the peculiar setting with SW-dipping sediments at Gela Basin provides an ideal opportunity to compare morphology and genesis of these undulated features occurring in the highstand units of two different glacial cycles, during MIS 1 and MIS5.

- X-Ray analysis of selected core sections to reveal potential turbiditic/contouritic deposition from hyperpycnal flows and thermohaline contour-parallel circulation, especially during sedimentary units relating to MIS 5.

11 Acknowledgements

This work would not exist without the support and help from many people.

First and foremost, I very much thank my supervisor Prof. Dr. Katrin Huhn for the opportunity to participate in this research project in the framework of my doctoral thesis at MARUM. I am very grateful for your support and complaisant guidance during the last years, including those preceding this work. Thank you for the considerable advice, constructive suggestions and the freedom of finding my own way throughout the last three years.

Sincere thanks go to Dr. Fabio Trincardi for the second review of this work, especially in consideration of your numerous responsibilities as director of the ISMAR institute. I benefited greatly from the various constructive meetings and fruitful discussions during my research stay in Italy and your invaluable scientific input to this project.

In this context, I am very much obliged to Dr. Alessandra Asioli, who not only did a great job on evaluating foraminiferal assemblages and teaching me the basics of micropaleontology, but above all has been a wonderful host during my time at the Istituto di Geoscienze e Georisorse (CNR-UOS) in Padova, Italy. Thank you for all your advice, the good food and the daily walks and talks.

Special thanks are given to my thesis committee members and co-authors Dr. Andreas Klügel for his support in the identification and geochemical analysis of volcanic tephra and Dr. Michael Strasser for his always encouraging and motivating thoughts and fruitful comments.

I owe many thanks to all my colleagues and fellow Ph.D. students at MARUM as well as the student helpers of our working group. Especially Frau Linux and Gerry are thanked for their frequent scientific input, their supportive nature as well as their diverting and amiable company during the last years.

At this point, I would like to thank Vera Lukies, Dr. Ursula Röhl, Walter Hale, Alex Wülbers, Dr. Vera Bender, Dr. Jürgen Pätzold, Dr. Monika Segl, Birgit Meyer-Schack and Dr. Jürgen Titschack as well as Dr. Tim Freudenthal and the MeBo team for the support in the MARUM laboratories and their help with regard to retrieved cores.

All memers of the GLOMAR team are thanked for the opportunity to benefit from educational advancement and scientific discussions in an international and interdisciplinary environment.

Last but not least, my deepest thanks and utter love goes to my family and close friends for their continuous assistance during all phases of my life: to my parents for raising the most lovely potpourri of little rascals I am blessed to call family; my sisters, brother-in-laws, niece and nephews for their ability to instantly cheer me up, sooth my mind and make me feel at ease; team Lurs, the Bremer flodders, Tante Emely, Brendlix, die Keilers, Mathi and Stalo, the schnutzies, Matze, Hedi, Gesa, Max and the entire White Castle, Doggy and everyone else that I cannot spent enough time with.

12 Bibliography

Accaino, F., Catalano, R., Di Marzo, L., Giustiniani, M., Tinivella, U., Nicolich, R., Sulli, A., Valenti, V., Manetti, P., 2011. A crustal seismic profile across Sicily. Tectonophysics 508(1-4), 52-61.

Ai, F., Kuhlmann, J., Huhn, K., Strasser, M., Kopf, A., 2014. Submarine slope stability assessment of the central Mediterranean continental margin: the Gela Basin. In: Krastel, S., Behrmann, J.-H., Völker, D., Stipp, M., Berndt, C., Urgeles, R., Chaytor, J., Huhn, K., Strasser, M., Harbitz, C.B. (eds.) Submarine mass movements and their consequences. Springer, Heidelberg, pp. 225-236.

Allen, J.R.M., Brandt, U., Brauer, A., Hubberten, H.-W., Huntley, B., Keller, J., Kraml, M., Mackensen, A., Mingram, J., Negendank, J.F.W., Nowaczyk, N.R., Oberhänsli, H., Watts, W.A., Wulf, S., Zolitschka, B., 1999. Rapid environmental changes in southern Europe during the last glacial period. Nature 400, 740-743.

Andersen, K.K., Svensson, A., Johnsen, S.J., Rasmussen, S.O., Bigler, M., Röthlisberger, R., Ruth, U., Siggaard-Andersen, M.L., Steffensen, J.P., Dahl-Jensen, D., Vinther, B.M., Clausen, H.B., 2006. The Greenland Ice Core Chronology 2005, 15-42 ka. Part 1: constructing the time scale. Quaternary Science Reviews 25, 3246-3257.

Argnani, A., 1990. The Strait of Sicily rift zone: Foreland deformations related to the evolution of a back-arc basin. J Geodyn 12, 311-331. doi: 10.1016/0264-3707(90)90028-S.

Asioli, A., Trincardi, F., Lowe, J.J., Aritzegui, D., Langone, L., Oldfield, F., 2001. Sub-millennial climatic oscillations in the Central Adriatic during the last deglaciation: paleocceanographic implications. Quaternary Science Reviews 20, 33-53.

Asioli, A., Trincardi, F., Consolaro, C., Ariztegui, D., Canu, M., 2002. High resolution paleoceanographic record for the last deglaciation in the Central Mediterranean: integration with the sequence stratigraphy to detect major intervals of the sea-level rise. EMMMM'2002 Congress (Environmental Micropaleontology, Microbiology and Meiobenthology), September 1-6, Vienna, Austria, p. 45-46.

Assier-Rzadkiewicz, S., Heinrich, P., Sabatier, P.C., Savoye, B., Bourillet, J.F., 2000. Numerical modelling of a landslide-generated tsunami: the 1979 Nice event. Pure and Applied Geophysics 157, 1707-1727. doi: 10.1007/PL00001057.

ASTM, 2004a. Standard test methods for one-dimensional consolidation properties of soils using incremental loading (Standard D2435-04). ASTM International, West Conshohocken, p. 10.

ASTM, 2004b. Standard test method for direct shear test of soils under consolidated drained conditions (Standard D3080-04). ASTM International, West Conshohocken, p. 7.

Astraldi, M., Balopulos, S., Candela, J., Font, J., Gacic, M., Gasparini, G.P., Manca, B., Theocharis, A., Tintoré, J., 1999. The role of straits and channels in understanding the characteristics of Mediterranean circulation. Prog. Oceanogr. 44, 65-108.

Astraldi , M., Gasparini, G.P., Gervasio, L., 2001. Dense water dynamics along the Strait of Sicily (Mediterranean Sea). J. Phys. Oceanogr. 31, 3457-3475.

Banfield, L.A., Anderson, J.B., 2004. Late Quaternary evolution of the Rio Grande delta: complex response to eustasy and climate change. In: Anderson, J.B., Fillon, R.H. (eds.) Late Quaternary Stratigraphic Evolution of the Northern Gulf of Mexico Margin, SEPM Special Publication, 79, pp 289-306.

Barberi, F., Civetta, L., Gasparini, P., Innocenti, F., Scandone, R., Villari, L., 1974. Evolution of a section of the Africa-Europe plate boundary; paleomagnetic and volcanological evidence from Sicily. Earth Planet Sci Lett 22(2), 123-132.

Barnes, P.M., Lewis, K.B., 1991. Sheet slides and rotational failures on a convergent margin: the Kidnappers Slide, New Zealand. Sedimentology 38, 205-221.

Bea, R.G., Wright, S.G., Sircar, P., Niedoroda, A.W., 1983. Wave-induced slides in South Pass Block 70, Mississippi Delta. Journal of Geotechnical Engineering 109(4), 619-644. doi: 10.1061/(ASCE)0733-9410(1983)109:4(619).

Béranger, K., Mortier, L., Gasparini, G.-P., Gervasio, L., Astraldi, M., Crépon, M., 2004. The dynamics of the Sicily Strait: a comprehensive study from observations and models. Deep-Sea Res. II 51, 411-440.

Bennett, R.H., Nelsen, T.A., 1983. Seafloor characteristics and dynamics affecting geotechnical properties at shelf breaks. SEPM Special Publications 33, 333–355.

Berné, S., Vagner, P., Guichard, F., Lericolais, G., Liu, Z., Yin, P., Trentesaux, A., Yi, H.I., 2002. Pleistocene forced-regressions and tidal sand ridges in the East China Sea. Marine Geology 188(3-4), 293-315.

Bethoux, J.P., 1980. Mean water fluxes across sections in the Mediterranean Sea, evaluated on the basis of water and salt budgets and of observed salinities. Oceanol. Acta 3, 79-88.

Bickert, T., Mackensen, A., 2004. Last glacial to Holocene changes in South Atlantic deep water circulation. In: Wefer, G., Mulitza, S., Ratmeyer, V. (Eds) The South Atlantic in the Late Quaternary. Springer, Berlin, p. 599-620.

Bindi, D., Pacor, F., Luzi, L., Puglia, R., Massa, M., Ameri, G., Paolucci, R., 2011. Ground motion prediction equations derived from the Italian strong motion database. Bulletin for Earthquake Engineering 9(6), 1899–1920. doi: 10.1007/s10518-011-9313-z.

Blaauw, M., Christen, J.A., 2011. Flexible paleoclimate age-depth models using an autoregressive gamma process. Bayesian Analysis 6(3), 457-474. doi: 10.1214/11-BA618.

Blaauw, M., 2012. Out of tune: the dangers of aligning proxy archives. Quaternary Science Reviews 36, 38-49. doi: 10.1016/j.quascirev.2010.11.012.

Blum, P., 1997. Physical properties handbook: a guide to the ship board measurement of physical properties of deep-sea cores. ODP Tech Note 26, College Station, Tex.

Bohannon, R.G., Garnder, J.V., 2004. Submarine landslides of San Pedro Escarpment, southwest of Long Beach, California. Marine Geology 203, 261-268. doi: 10.1016/S0025-3227(03)00309-8.

Bond, G., Showers, W., Cheseby, M., Lotti, R., Almasi, P., deMenocal, P., Priore, P., Cullen, H., Hajdas, I., Bonani, G., 1997. A pervasive millennial-scale cycle in North Atlantic Holocene and glacial climates. Science 278, 1257-1266. doi: 10.1126/science.278.5341.1257.

Bornhold, B.D., Prior, D.B., 1990. Morphology and sedimentary processes on the subacqueous Noeick river delta, British Columbia, Canada. In: Colella, A., Prior, D.B. (eds.) Coarse-grained Deltas, Spec Publ 10 Int Assoc of Sedimentol, UK, pp 169-184.

Bouma, A.H., 1962. Sedimentology of some Flysch deposits: a graphic approach to facies interpretation. Elsevier, Amsterdam. 168 pp.

Bourrin, F., Friend, P.L., Amos, C.L., Manca, E., Ulses, C., Palanques, A., Durrieu de Madron, X., Thompson, C.E.L., 2008. Sediment dispersal from a typical Mediterranean flood: The Têt River, Gulf of Lions. Continental Shelf Research 28, 1895-1910.

Bourne, A.J., Lowe, J.J., Trincardi, F., Asioli, A., Blockley, S.P.E., Wulf, S., Matthews, I.P., Piva, A., Vigliotti, L., 2010. Distal tephra record for the last ca 105,000 years from core PRAD 1-2 in the central Adriatic Sea: implications for marine tephrostratigraphy. Quaternary Science Reviews 29, 3079-3094.

Brown, R.J., Orsi, G., de Vita, S., 2008. New insights into Late Pleistocene explosive volcanic activity and caldera formation on Ischia (southern Italy). Bulletin of Volcanology 70, 583-603. doi: 10.1007/s00445-007-0155-0.

Bryn, P., Solheim, A., Berg, K., Lien, R., Forsberg, C.F., Haflidason, H., Ottesen, D., Rise, L., 2003. The Storegga slide complex: repeated large scale landsliding in response to climatic cyclicity. In: Locat, J., Mienert, J. (eds.) Submarine mass movements and their consequences. Kluwer Academic Publishers, Dordrecht, Netherlands. p. 215-222.

Bryn, P., Berg, K., Forsberg, C.F., Solheim, A., Kvalstad, T.J., 2005. Explaining the Storegga slide. Marine and Petroleum Geology 22, 11-19. doi: 10.1016/j.marpetgeo.2004.12.003.

Butler, R.W.H., Grasso, M., LaManna, F., 1992. Origign and deformation of the Neogene-Recent Maghrebian foredeep at the Gela Nappe, SE Sicily. J Geol Soc (Lond) 149: 547-556.

Çağatay, M.N., Eris, K., Ryan, W.B.F., Sancar, Ü., Polonia, A., Akcer, S., Biltekin, D., Gasperini, L., Görür, N., Lericolais, G., Bard, E., 2009. Late Pleistocene-Holocene evolution of the northern shelf of the Sea of Marmara. Marine Geology 265(3-4), 87-100.

Cacchione, D.A., Schwab, W.C., Noble, M.A., Tate, G.B., 1988. Internal tides and sediment movement on Horizon Guyot, Mid-Pacific Mountains. Geo-Marine Letters 9(1), 11-17.

Camerlenghi, A., Urgeles, R., Ercilla, G., Brückman, W., 2007. Scientific ocean drilling behind the assessment of geo-hazards from submarine landslides. Scientific Drilling 4, 45-47.

Camerlenghi, A., Urgeles, R., Fantoni, L., 2010. A database on submarine landslides of the Mediterranean Sea. In: Mosher, D.C., Shipp, C., Moscardelli, L., Chaytor, J., Baxter, C., Lee, H., Urgeles, R. (eds) Submarine Mass Movements and Their Consequences, Springer Netherlands, p. 503-513. doi: 10.1007/978-90-481-3071-9_41.

Canals, M., Lastras, G., Urgeles, R., Casamor, J.L., Mienert, J., Cattaneo, A., De Batist, M., Haflidason, H., Imbo, Y., Laberg, J.S., Locat, J., Long, D., Longova, O., Masson, D.G., Sultan, N., Trincardi, F., Bryn, P., 2004. Slope failure dynamics and impacts from seafloor and shallow sub-seafloor geophysical data: case studies from the COSTA project. Marine Geology 213, 9-72.

Cane, T., Rohling, E.J., Kemp, A.E.S., Cooke, S., Pearce, R.B., 2002. High-resolution stratigraphic framework for Mediterranean sapropel S5: defining temporal relationships between records of Eemian climate variability. Palaeogeography, Palaeoclimatology, Palaeoecology 183, 87– 101.

Capotondi, L., Borsetti, A.M.,Morigi, C., 1999. Foraminiferal ecozones, a high resolution proxy for the late Quaternary biochronology in the central Mediterranean Sea. Marine Geology 153(1–4), 253–274.

Caress, D.W., Chayes, D.N., 2006. MB-System: Mapping the Seafloor. http://www.mbari.org/data/mbsystem, http://www.ldeo.columbia.edu/res/pi/MB-System.

Carter, R.M., Fulthorpe, C.S., Naish, T.R., 1998. Sequence concepts at seismic and outcrop scale: the distinction of physical and conceptual stratigraphic surfaces. Sedimentary Geology 122(1-4), 165-179. doi: 10.1016/S0037-0738(98)00104-3.

Casagrande, A., 1932. Research on the Atterberg limits of soil. Public Roads 13(8), 121–136.

Casagrande, A., 1936. The determination of the pre-consolidation load and its practical significance. In: Proceedings of the 1st international conference of soil mechanics and foundation engineering 3, p. 60–64.

Casas, D., Ercilla, G., Baraza, J., Alonso, B., Maldonado, A., 2003. Recent mass-movement processes on the Ebro continental slope (NW Mediterranean). Marine and Petroleum Geology 20(5), 445-457. doi: 10.1016/S0264-8172(03)00078-3.

Cattaneo, A., Correggiari, A., Marsset, T., Thomas, Y., Marsset, B., Trincardi, F., 2004. Seafloor undulation pattern on the Adriatic shelf and comparison to deep-water sediment waves. Marine Geology 213(1-4), 121-148.

Chiessi, C.M., Mulitza, S., Paul, A., Pätzold, J., Groeneveld, J., Wefer, G., 2008. South Atlantic interocean exchange as the trigger for the Bølling warm event. Geology 36, 919-922. doi: 10.1130/g24979a.1.

Chiocci, F.L., Esu, F., Tommasi, P., Chiappa, V., 1996. Stability of the submarine slope of the Tiber River delta. In: Senneset, K., (ed.). Landslides. Balkema, The Netherlands, pp 521-526.

Chiocci, F.L., 2000. Depositional response to Quaternary fourth-order sea-level fluctuations on the Latium margin (Tyrrhenian Sea, Italy). In: Hunt, D., Gawthorpe, R.L. (eds.) Sedimentary Responses to Forced Regressions. Geological Society Special Publication, 172, p. 271-289.

Ciappa, A. C., 2009. Surface circulation patterns in the Sicily Channel and Ionian Sea as revealed by MODIS chlorophyll images from 2003 to 2007. Continental Shelf Research 29, 2099-2109.

Civile, D., Lodolo, E., Accettella, D., Geletti, R., Ben-Avraham, Z., Deponte, M., Faccin, L., Ramella, R., Romeo, R., 2010. The Pantelleria graben (Sicily Channel, Central Mediterranean): An example of intraplate 'passive' rift. Tectonophysics 490, 173-183.

Clark, P.U., Archer, D., Pollard, D., Blum, J.D., Rial, J.A., Brovkin, V., Mix, A.C., Pisias, N.G., Roy, M., 2006. The middle Pleistocene transition: characteristics, mechanisms, and implications for long-term changes in atmospheric pCO_2. Quaternary Science Reviews 25, 3150-3184.

Cochonat, P., Dürr, S., Herzig, P., Mevel, C., Mienert, J., Schneider, R., Weaver, P.P.E., Winkler, A., 2007. The deep-sea frontier: Science challenges for a sustainable future,

Colantoni, P., 1975. Note di geologia marina sul Canale di Sicilia. Giornale Geol 40(1), 181-207.

Correggiari, A., Trincardi, F., Langone, L., Roveri, M., 2001. Styles of failure in late Holocene highstand prodelta wedges on the Adriatic shelf. Journal of Sedimentary Research 71: 218-236.

Costanza, R., Farley, J., 2007. Ecological economics of coastal disasters: Introduction to the special issue. Ecological Economics 63, 249-253.

Coulomb, C.A., 1773. Sur une application des regles de maximis et minimis a quelques problems de statique, reltifs a l'architecture. Mémoires de Mathematique et de Physique. Royal Academy of Sciences 7, 343-387.

Cunningham, A.P., Barker, P.F., 1996. Evidence for westward-flowing Weddell Sea Deep Water in the Falkland Trough, western South Atlantic. Deep Sea Research Part I: Oceanographic Research Papers 43(5): 643-654.

Curry, W.B., Oppo, D.W., 2005. Glacial water mass geometry and the distribution of $\delta^{13}C$ of ΣCO_2 in the western Atlantic Ocean. Paleoceanography 20, Pa1017. doi: 10.1029/2004pa001021.

Dadson, S., Hovius, N., Pegg, S., Dade, B., Horng, M.J., Chen, H., 2005. Hyperpycnal river flows from an active mountain beld. Jornal of Geophysical Research 110, F04016. doi: 10.1029/2004JF000244.

Dansgaard, W., Clausen, H.B., Gundestrup, N., Hammer, C.U., Johnsen, S.J., Kristindottir, P.M., Reeh, N., 1982. A new Greenland deep ice core. Science 218, 1273-1277.

Dansgaard, W., Johnsen, S.J., Clausen, H.B., Dahl-Jensen, D., Gundestrup, N.S., Hammer, C.U., Hvidberg, C.S., Steffensen, J.P., Sveinbjörnsdottir, A.E., Jouzel, J., Bond, G., 1993. Evidence for general instability of past climate from a 250-kyr ice-core record. Nature 364, 218-220.

De Rijk, S., Troelstra, S.R., Rohling, E.J., 1999. Benthic foraminiferal distribution in the Mediterranean Sea. Journal of Foraminiferal Research 29(2), 93–103.

De Stigter, H. C., Jorissen, F. J., Van der Zwaan, G.J., 1998. Bathymetric distribution and microhabitat partitioning of live (Rose Bengal stained) benthic foraminifera along a shelf to deep sea transect in the southern Adriatic Sea. Journal of Foraminiferal Research 28(1), 40–65.

Di Stefano, E., Infuso, S., Scarantino, S., 1993. Plio-Pleistocene sequence stratigraphy of southwestern offshore Sicily from well logs and seismic sections in a high-resolution calcareous plankton biostratigraphic framework. In: Max, M.D., Colantoni, P. (eds.) UNESCO Technical Report in Marine Sciences 58, 105-110.

Di Stefano, E., 1998. Calcareous nannofossil quantitative biostratigraphy of Holes 963E and 963B (Eastern Mediterranean). In: Emeis, K.-C., Robertson, A.H.F., Richter, C., Camerlenghi, A. (eds.) Proceedings of the Ocean Drilling Program, Scientific Results 160, 99-112.

Díaz, J.I., Ercilla, G., 1993. Holocene depositional history of the Fluviá-Muga prodelta, northwestern Mediterranean Sea. Marine Geology 111: 83-92.

Dilek, Y., Sandvol, E., 2009. Seismic structure, crustal architecture and tectonic evolution of the Anatolian-African plate boundary and the Cenozoic orogenic belts in the eastern Mediterranean region. In: Murphy, J.B., Keppie, J.D., Hynes, A.J. (eds) Ancient Orogens and Modern Analogues. Geological Society, London, Special Publications 327, 127-160. doi: 10.1144/SP327.8.

Ducassou, E., Capotondi, L., Murat, A., Bernasconi, S.M., Mulder, T., Gonthier, E., Migeon, S., Duprat, J., Giraudeau, J., Mascle, J., 2007. Multiproxy Late Quaternary stratigraphy of the Nile deep-sea turbidite system — Towards a chronology of deep-sea terrigenous systems. Sedimentary Geology 200(2007), 1–13.

Dugan, B., Sheahan, T.C., 2012. Offshore sediment overpressures of passive margins: mechanisms, measurement, and models. Reviews of Geophysics 50(3), RG3001. doi: 10.1029/2011rg000379.

Emeis, K.C., Robertson, A.H.F., Richter, C., et al., 1996. 4. Site 963. Proceedings of the ODP, Initial Reports 160, 55-84.

Emiliani, C., 1955. Pleistocene temperatures. Journal of Geology 63, 538-578.

Ercilla, G., Farrán, M., Alonso, B., Diáz, J.I., 1994. Pleistocene progradational growth pattern of the northern Catalonia continental shelf (northwestern Mediterranean). Geo-Marine Letters 14(4), 264-271.

Ercilla, G., Díaz, J.I., Alonso, B., Farrán, M.,1995. Late Pleistocene-Holocene sedimentary evolution of the northern Catalonia continental shelf (northwestern Mediterranean Sea). Coninental Shelf Research 15: 1435-1451.

Ercilla, G., Wynn, R.B., Alonso, B., Baraza, J., 2002. Initiation and evolution of turbidity current sediment waves in the Magdalena turbidite system. Marine Geology 192(1-3): 153-169.

Evans, H.B., 1965. GRAPE - A device for continuous determination of material density and porosity. In: Proceedings of 6th Annual SPWLA Logging Symposium. Society of Petrophysicists and Well-Log Analysts.

Fine, I.V., Rabinovich, A.B., Bornhold, B.D., Thomson, R.E., Kulikov, E.A., 2005. The Grand Banks landslide-generated tsunami of November 18, 1929: preliminary analysis and numerical modelling. Marine Geology 215, 45-57. doi: 10.1016/j.margeo.2004.11.007.

Finetti, I., 1984. Geophysical studies of the Sicily Channel rift zone. Bol Geofis Teor Appl 26, 3-28.

Flemings, P.B., Long, H., Dugan, B., Germaine, J., John, C.M., Behrmann, J.H., Sawyer, D., Scientists, I.E., 2008. Pore pressure penetrometers document high overpressure near the seafloor where multiple submarine landslides have occurred on the continental slope, offshore Louisiana, Gulf of Mexico. Earth and Planetary Science Letters 269(3–4), 309–325. doi: 10.1016/j.epsl.2007.12.005.

Flemming, B.W., 1981. Factors controlling shelf sediment dispersal along the Southeast African continental margin. Marine Geology 42(1-4), 259-277.

Freudenthal, T., Wefer, G., 2007. Scientific drilling with the sea floor drill rig MeBo. Sci. Drill. 5, 63-66.

Freudenthal, T., Wefer, G., 2013. Drilling cores on the sea floor with the remote-controlled sea floor drilling rig MeBo. Geosci. Intrum. Method. Data Syst. 2, 329-337, doi: 10.5194/gi-2-329-2013.

Frigola, J., Canals, M,. Cacho, I., Moreno, A., Sierro, F.J., Flores, J.A., Berné, S., Jouet, G., Dennielou, B., Herrera, G., Pasqual, C., Grimalt, J.O., Galavazi, M., Schneider, R., 2012. A 500 kyr record of global sea-level oscillations in the Gulf of Lion, Mediterranean Sea: new insights into MIS 3 sea-level variability. Climate of the Past 8, 1067-1077.

Gámez, D., Simó, J.A., Lobo, F.J., Barnolas, A., Carrera, J., Vázquez-Suné, E., 2009. Onshore-offshore correlation of the Llobregat deltaic system, Spain: Development of deltaic geometries under different relative sea-level and growth fault influences. Sedimentary Geology 217(1-4), 65-84.

Gallup, C.D., Edwards, R.L., Johnson, R.G., 1994. The timing of high sea levels over the past 200,000 years. Science 263(5148), 796-800.

Gardiner, W., Grasso, M., Sedgeley, D., 1993. Plio-Pleistocene stratigraphy and fault movement of the Malta Platform. In: Max, M.D., Colantoni, P. (eds.) Geological Development of the Sicilan-Tunusian Platform. UNESCO Tech Rep Mar Sci 58, 111-116.

Gee, M.J.R., Uy, H.S., Warren, J., Morley, C.K., Lambiase, J.J., 2007. The Brunei slide: A giant submarine landslide on the North West Borneo margin revealed by 3D seismic data. Marine Geology 246, 9-23.

Goldfinger, C., Kulm, L.V.D., McNeill, L.C., Watts, P., 2000. Super-scale failure of the southern Oregon Cascadia margin. Pure Applied Geophysics 157, 1189-1226.

Grant, K.M., Rohling, E.J., Bar-Matthews, M., Ayalon, A., Medina-Elizalde, M., Bronk Ramsey, C., Satow, C., Roberts, A.P., 2012. Rapid coupling between ice volume and polar temperature over the past 150,000 years. Nature 491, 744-747

Grasso, M., 1993. Pleistocene structures along the Ionian side of the Hyblean Plateau (SE Sicily): Implications for the tectonic evolution of the Malta Escarpment. In: Max, M.D., Colantoni, P. (eds.) Geological Development of the Sicilan-Tunusian Platform. UNESCO Tech Rep Mar Sci 58, 49-55.

Greene, H.G., Maher, N.M., Paull, C.K., 2002. Physiography of the Monterey Bay national Marine Sanctuary and implications about continental margin development. Marine Geology 181, 55-82.

Gutmacher, C.E., Normark, W.R., 1993. Sur submarine landslide, a deep-water sediment slope failure. In: Schwab, W.C., Lee, H.J., Twichell, D.C. (eds.) Submarine landslides: selected studies in the U.S. Exclusive Economic Zone. USGS Bulletin 2002, p. 158-166.

Haflidason, H., Sejrup, H.P., Berstad, I.M., Nygard, A., Richter, T., Lien, R., Berg, K., 2003. A weak layer feature on the northern Storegga slide escarpment. In: Mienert, J., Weaver, P.P.E. (eds.) European margin sediment dynamics. Springer, Berlin, Germany. p. 55-62.

Haflidason, H., Sejrup, H.P., Nygård, A., Mienert, J., Bryn, P., Lien, R., Forsberg, C.F., Berg, K., Masson, D., 2004. The Storegga Slide: Architecture, geometry and slide development. Marine Geology (COSTA Special Issue) 213, 201-234.

Hampton, M.A., Lee, H.J., Locat, J., 1996. Submarine landslides. Reviews of Geophysics 34(1), 33-59.

Harders, R., Kutterolf, S., Hensen, C., Moerz, T., Brueckmann, W., 2010. Tephra layers: A controlling factor on submarine translational sliding? Geochemistry, Geophysics, Geosystems 11(5), Q05S23. doi: 10.1029/2009GC002844.

Hays, J.D., Imbrie, J., Shackleton, N.J., 1976. Variations in the Earth's orbit: Pacemaker of the ice ages. Science 194, 1121-1132. doi: 10.1126/science.194.4270.1121.

Heezen, B.C., Ewing, M., 1952. Turbidity currents and submarine slumps, and the 1929 Grand Banks Earthquake. American Journal of Science 250(12), 849-873. doi: 10.2475/ajs.250.12.849.

Heidarzadeh, M., Pirooz, M.D., Zaker, N.H., Yalciner, A.C., Mokhtari, M., Esmaeily, A., 2008. Historical tsunami in the Makran Subduction Zone off the southern coasts of Iran and Pakistan and results of numerical modelling. Ocean Engineering 35(8-9), 774-786.

Hemleben, C., Spindler, M., Anderson, O.R., 1989. Modern Planktonic foraminifera. Springer-Verlag, New York. p. 1–363.

Herbaut, C., Codron, F., Crépon, M., 1998. Separation of a coastal current at a strait level: case of the Strait of Sicily. J. Phys. Oceanogr. 28, 1346-1362.

Hernández-Molina, F.J., Somoza, L., Lobo, F., 2000. Seismic stratigraphy of the Gulf of Cádiz continental shelf: a model for Late Quaternary very high-resolution sequence stratigraphy and response to sea-level fall. In: Hunt, D., Gawthorpe, R.L. (eds.) Sedimentary Responses to Forced Regressions. Geological Society Special Publication, 172, p. 329-362.

Hernández-Molina, F.J., Llave, E., Stow, D.A.V., García, M., Somoza, L., Vázquez, J.T., Lobo, F.J., Maestro, A., Díaz del Rio, V., León, R., Medialdea, T., Gardner, J., 2006. The contourite depositional system of the Gulf of Cádiz: A sedimentary model related to the bottom current activity of the Mediterranean outflow water and its interaction with the continental margin. Deep-Sea Research II 53, 1420-1463.

Hiscott, R.N., 2001. Depositional sequences controlled by high rates of sediment supply, sea-level variations, and growth faulting: the Quaternary Baram Delta of north-western Borneo. Marine Geology 175(1-4), 67-102.

Holcomb, T., Searle, R.C., 1991. Large landslides from oceanic volcanoes. Marine Geotechnology 10(1-2), 19-32. doi: 10.1080/10641199109379880.

Hübscher, C, Spieß, V., 2005. Forced regression systems tracts on the Bengal Shelf. Marine Geology 219(4), 207-218.

Hughen, K.A., 2007. Radiocarbon dating of deep-sea sediments. In: Hillaire-Marcel, C., De Vernal, A. (eds.) Proxies in Late Cenozoic Paleoceanography. Developments in Marine Geology 1, 185-210.

Hughes Clarke, J.E., 1990. Late stage slope failure in the wake of the 1929 Grand Banks earthquake. Geo-Marine Letters 10, 69-79.

Huhn, K., Kock, I., Kopf, A., 2006. Comparative numerical and analogue shear box experiments and their implications for the mechanics along the failure plane of landslides. Norwegian Journal of Geology 86, 209-220.

Hunt, D., Tucker, M.E., 1992. Stranded parasequences and the forced regressive wedge systems tract: deposition during base-level fall. Sedimentary Geology 81, 1-9.

Ilstad, T., Elverhøi, A., Issler, D., Marr, J.G., 2004. Subaqueous debris flow behaviour and its dependence on the sand/clay ratio: a laboratory study using particle tracking. Marine Geology 213, 415-418. doi: 10.1016/j.margeo.2004.10.017.

Imbrie, J., Hays, J.D., Martinson, D., McIntyre, A. Mix, A., Morley, J., Pisias, N., Prell, W., Shackleton, N.J., 1984. The orbital theory of Pleistocene climate: Support from a revised chronology of the marine $\delta^{18}O$ record. In: Berger, A., et al. (eds.) Milankovitch and climate, Part 1. Hingham, Massachusetts, D. Reidel, p. 269-305.

Incarbona, A., Di Stefano, E., Sprovieri, R., Bonomo, S., Censi, C., Dinarès-Turell, J., Spoto, S., 2008. Variability in the vertical structure of the water column and paleoproductivity reconstruction in the central-western Mediterranean during the Late Pleistocene. Marine Micropaleontology 69, 26–41.

Incarbona, A., Di Stefano, E., Sprovieri, R., Bonomo, S., Pelosi, N., Sprovieri, M., 2010. Millennial-scale paleoenvironmental changes in the central Mediterranean during the last interglacial: Comparison with European and North Atlantic records. Geobios 43, 111–122.

Ismail, S.B., Sammari, C., Gasparini, G.P., Béranger, K., Brahim, M., Aleya, L., 2012. Water masses exchanged through the Channel of Sicily: Evidence for the presence of new water masses on the Tunisian side of the channel. Deep-Sea Research I 63, 65-81.

Jarosewich, E., Nelen, J.A., Norberg, A., 1980. Reference Samples for Electron Microprobe Analysis. Geostandards Newsletter 4(1), 43-47.

Jenny, S., Goes, S., Giardini, D., Kahle, H.-G., 2006. Seismic potential of Southern Italy. Tectonophysics 415, 81-101.

Jochum, K.P., Dingwell, D.B., Rocholl, A., Stoll, B., Hofmann, A.W., Becker, S., Besmehn, A., Bessette, D., Dieze, H.-J., Dulski, P., Erzinger, J., Hellebrand, E., Hoppe, P., Horn, I., Janssens, K., Jenner, G.A., Klein, M., McDonough, W.F., Maetz, M., Mezger, K., Müker, C., Nikogosian, I.K., Pickhardt, C., Raczek, I., Rhede, D., Seufert, H.M., Simakin, S.G., Sobolev, A.V., Spettel, B., Straub, S., Vincze, L., Wallianos, A., Weckwerth, G., Weyer, S., Wolf, D., Zimmer, M., 2000. The preparation and preliminary characterisation of eight geological MPI-DING reference glasses for in-situ microanalysis. Geostandards and Geoanalytical Research 24(1), 87-133.

Johnsen, S.J., Dansgaard, W., Clausen, H.B., Langway Jr., C.C., 1972. Oxygen isotope profiles through the Antarctic and Greenland ice sheets. Nature 359, 311-313.

Jorissen FJ, Asioli A, Borsetti AM, Capotondi L, De Visser JP, Hilgen FJ, Rohling EJ, van der Borg K, Vergnaud-Grazzini C, Zachariasse WJ (1993) Late quaternary central mediterranean biochronology. Mar Micropaleontol 21: 169-189

Jorissen, F.J., Fontanier, C., Thomas, E., 2007. Paleoceanographical proxies based on deep-sea benthic foraminiferal assemblage characteristics. In: Hillaire-Marcel, C., De Vernal, A. (eds.) Proxies in Late Cenozoic Paleoceanography. Developments in Marine Geology 1, 263-325.

Jorstad, F.A., 1968. Waves generated by landslides in Norwegian fjords and lakes. Norwegian Geotechnical Institute Publication 79. Oslo, Norway. p. 13-31.

Kayen, R.E., Lee, H.J., 1991. Pleistocene slope instability of gas hydrate-laden sediment on the Beaufort Sea margin. Marine Geotechnology 10(1-2), 125-141. doi: 10.1080/10641199109379886.

Keller, J., Ryan, W.B.F., Ninkovich, D., Altherr, R., 1978. Explosive volcanic activity in the Mediterranean over the past 200,000 yr as recorded in deep-sea sediments. Geological Society of America Bulletin 89(4), 591-604.

Kennett, J.P., 1982. Marine Geology. Prentice-Hall, Englewood Cliffs, N.J. 813 p.

Kitamura, A., Matsui, H., Oda, M., 2000. Constraints on the timing of systems tract development with respect to sixth-order (41 ka) sea level changes: an example from the Pleistocene Omma Formation, Sea of Japan. Sedimentary Geology 131 (1-2), 67-76. doi: 10.1016/S0037-0738(99)00126-8.

Kock, I., Huhn, K., 2006. Influence of particle shape on the frictional strength of sediments – a case study. Sedimentary Geology 196, 217-233. doi: 10.1016/j.sedgeo.2006.07.011.

Kraml, M., 1997. Laser-40Ar/39Ar-Datierungen an distalen marinen Tephren des jung-quartären mediterranen Vulkanismus (Ionisches Meer, METEOR-Fahrt 25/4). PhD Thesis, University of Freiburg, 216 pp.

Kucera, M., 2007. Planktonic foraminifera as tracers of past oceanic environments. In: Hillaire-Marcel, C., De Vernal, A. (eds.) Proxies in Late Cenozoic Paleoceanography. Developments in Marine Geology 1, 213-263.

Kuhlmann, J., Asioli, A., Strasser, M., Trincardi, F., Huhn, K., 2014. Integrated stratigraphic and morphological investigation of the Twin Slide complex offshore southern Sicily. In: Krastel, S., Behrmann, J.-H., Völker, D., Stipp, M., Berndt, C., Urgeles, R., Chaytor, J., Huhn, K., Strasser, M., Harbitz, C.B. (eds.) Submarine mass movements and their consequences. Springer, Heidelberg, pp. 583-594.

Kuhlmann, J., Asioli, A., Trincardi, F., Klügel, A., Huhn, K., 2014b. Sedimentary response to Milankovitch-type climatic oscillations and formation of sediment undulations: evidence from a shallow-shelf setting at Gela Basin on the Sicilian continental margin. In review with Quaternary Science Reviews.

Kulikov, E.A., Rabinovich, A.B., Thomson, R.E., Borhnhold, B.D., 1996. The landslide tsunami of November 3, 1994 Skagway harbour, Alaska. Journal of Geophysical Research 101, 6609-6615.

Kvalstad, T.J., Andresen, L., Forsberg, C.F., Berg, K., Bryn, P., Wangen, M., 2005. The Storegga slide: evaluation of triggering sources and slide mechanics. Marine and Petroleum Geology 22, 245-256.

Laberg, J.S., Camerlenghi, A., 2008. The significance of contourites for submarine slope stability. Developments in Sedimentology 60, 537-556. doi: 10.1016/S0070-4571(08)10025-5.

Lamb, T.W., Whitman, R.V., 1969. Soil mechanics. Massachusetts Institute of Technology, Cambridge, MA.

Langer, M. R., 1993. Epiphytic foraminifera: Marine Micropaleontology 20, 235–265.

Lascaratos, A., Roether, W., Nittis, K., Klein, B., 1999. Recent changes in deep water formation and spreading in the eastern Mediterranean Sea: a review. Progress in Oceanography 44(1), 5-36. Doi: 10.1016/S0079-6611(99)00019-1.

Lastras, G., Canals, M., Ampblas, D., Ivanov, M., Dennielou, B., Droz, L., Akhametzhanov, A., 2006. Eivissa slides, western Mediterranean Sea: morphology and processes. Geo-Marine Letters 26, 225-233.

Lay, T., Kanamor, H., Ammon, C.J., Nettles, M., Ward, S.N., Aster, R.C., Beck, S.L., Bilek, S.L., Brudzinski, M.R., Butler, R., DeShon, H.R., Ekström, G., Satake, K., Sipkin, S., 2005. The great Sumatra-Andaman earthquake of 26 December 2004. Science 308(5725), 1127-1133.

Le Bas, M.J., Le Maitre, R.W., Streckeisen, A., Zanettini, B., 1986. A chemical classification of volcanic rocks based on the Total Alkali-Silica diagram. Journal of Petrology 27, 745-750. doi: 10.1093/petrology/27.3.745.

Lea, D.W., Martin, P.A., Pak, D.K., Spero, H.J., 2002. Reconstructing a 350 ky history of sea level using planktonic Mg/Ca and oxygen isotope records from a Cocos Ridge core. Quaternary Science Reviews 21(1-3), 283-293.

Lebreiro, S.M., McCave, N.I., Weaver, P.P.E., 1997. Late Quaternary turbidite emplacement on the Horseshoe abyssal plain (Iberian Margin). Journal of Sedimentary Research 67, 856-870.

Lee, H.J., 2005. Undersea landslides: extent and significance in the Pacific Ocean, an update. Natural Hazards and Earth System Sciences 5, 877-892.

Lee, H.J., Locat, J., Desgagnés, P., Parsons, J.D., McAdoo, B.G.. Orange, D.L., Puig, P., Wong, F.L., Dartnell, P., Boulanger, E., 2007. Submarine mass movements on continental margins. In: Nittrouer, C.A., Austin, J.A., Field, M.E., Kravitz, J.H., Syvitski, J.P.M., Wiberg, P.L. (eds.). Continental Margin Sedimentation: From Sediment Transport to Sequence Stratigraphy, Wiley-Blackwell, UK, 213-274.

Lee, H.J., 2009. Timing of occurrence of large submarine landslides on the Atlantic Ocean margin. Marine Geology 264. 53-64.

Lermusiaux, P.F.J., Robinson, A.R., 2001. Features of dominant mesoscale variability, circulation patterns and dynamics in the Strait of Sicily. Deep-Sea Res. I 48, 1953-1997.

Leynaud, D., Mienert, J., Vanneste, M., 2009. Submarine mass movments on glaciated and non-glaciated European continental margins: A review of triggering mechanisms and preconditions to failure. Marine and Petroleum Geology 26, 618-632. doi: 10.1016/j.marpetgeo.2008.02.008.

Lipman, P.W., Normark, W.R., Moore, J.G., Wilson, J.B., Gutmacher, C.E., 1988. The giant submarine Alika debris slide, Mauna Loa, Hawaii. Journal of Geophysical Research 93, 4279-4290.

Lirer, F., Sprovieri, M., Ferraro, L., Vallefuoco, M., Capotondi, L., Cascella, A., Petrosino, P., Insinga, D.D., Pelosi, N., Tamburrino, S., Lubritto, C., 2013. Integrated stratigraphy for the Late Quaternary in the eastern Tyrrhenian Sea. Quaternary International 292, 71-85.

Lisiecki, L.E., Raymo, M.E., 2005. A Pliocene-Pleistocene stack of 57 globally distributed benthic d18O records. Paleoceanography 20, PA1003. doi: 10.1029/2004PA001071.

Liu, J., Saito, Y., Kong, X., Wang, H., Wen, C., Yang, Z., Nakashima, R., 2010. Delta development and channel incision during marine isotope stages 3 and 2 in the western South Yellow Sea. Marine Geology 278(1-4), 54-76.

Liu, Z.-X., Berne, S., Saito, Y., Lericolais, G., Marsset, T., 2000. Quaternary seismic stratigraphy and paleoenvironments on the continental shelf of the East China Sea. Journal of Asian Earth Sciences 18(4), 441-452.

Liquete, C., Canals, M., De Mol, B., De Batist, N., Trincardi, F., 2008. Quaternary stratal architecture of the Barcelona prodeltaic continental shelf (NW Mediterranean). Marine Geology 250(3-4), 234-250.

Løseth, T.M., 1999. Submarine massflow sedimentation: computer modelling and basin-fill stratigraphy. Springer, New York.

Lobo, F.J., Hernández-Molina, F.J., Somoza, L., Díaz del Río, V., Dias, J.M.A., 2002. Stratigraphic evidence of an upper Pleistocene TST to HST complex on the Gulf of Cádiz continental shelf (south-west Iberian Peninsula). Geo-Marine Letters 22(2), 95-107.

Lobo, J., Ridente, D., 2014. Stratigraphic architecture and spatio-temporal variability of high-frequency (Milankovitch) depositional cycles on modern continental margins: An overview. Marine Geology 352, 215-247. doi: 10.1016/j.margeo.2013.10.009.

Locat, J. Norem, H., Schieldrup, N., 1990: Modélisation de la dynamique des glissements sous-marines. In: Proceedings of the 6th Congrss of the International Association of Engineering Geology. Amsterdam. P. 2849-2855.

Locat, J., Lee, H.J., 2002. Submarine landslides: advances and challenges. Canadian Geotechnical Journal 39(1), 193-212. doi: 10.1139/T01-089.

Locat, J., Martin, F., Levesque, C., Locat, P., Leroueil, S., Konrad, J.-M., Urgeles, R., Canals, M., Duchesne, M.J., 2003. Submarine mass movments in the upper Saguenay Fjord (Quebec, Candada) triggered by an earthquake. In: Locat, J., Mienert, J. (eds.) Submarine mass movments and their consequences. Advances in natural and technological hazards research 19. Kluwer, Dordrecht, p. 509-519.

Locat, J., Mienert, J., 2003. Submar1ine mass movements and their consequences. Advances in natural and technological hazards research 19. Kluwer, Dordrecht, 540.

Lourens, L.J., 2004. Revised tuning of Ocean Drilling Program Site 964 and KC01B (Mediterranean) and implications for the $\delta^{18}O$, tephra, calcareous nannofossil, and geomagnetic reversal chronologies of the past 1.1. Myr. Paleoceanography 19, PA3010. doi: 10.1029/2003PA000997.

Lowe, D.J., 2011. Tephrochronology and its application: A review. Quaternary Geochronology 6, 107-153.

Lykousis, V., Roussakis, G., Alexandri, M., Pavlakis, P., Papoulina, I., 2002. Marine Geology 186(3-4), 281-298.

Malouta, D.N., Gorsline, D.S., Thornton, S.E., 1981. Processes and rates of recent (Holocene) basin filling in an active transform margin: Santa Monica Basin, California continental borderland. Journal of Sedimentary Research 51(4), 1077-1095.

Marsset, T., Xia, D., Berné, S., Liu, Z., Bourillet, J.-F., Wang, K., 1996. Stratigraphy and sedimentary environments during the Late Quaternary, in the Eastern Bohai Sea (North China Platform). Marine Geology 135(1-4), 97-114.

Martin, R.G., Bouma, A.H., 1982. Active diapirism and slope steepening, northern Gulf of Mexico continental slope. Marine Geotechnology 5(1), 63-91. doi: 10.1080/10641198209379837.

Martinson, D.G., Pisias, N.G., Hays, J.D., Imbrie, J., Moore, T.C., Shackleton, N.J., 1987. Age dating and the orbital theory of the ice ages: Development of a high-resolution 0 to 300,000-year chronostratigraphy. Quaternary Research 27, 1-29. doi: 10.1016/0033-5894(87)90046-9.

Martrat, B., Grimalt, J.O., Lopez-Martinez, C., Cacho, I., Sierro, F.J., Abel Flores, J., Zahn, R., Canals, M., Curtis, J.H., Hodell, D.A., 2004. Abrupt temperature changes in the western Mediterranean over the past 250,000 years. Science 306, 1762-1765.

Maslin, M., Mikkelsen, N., Vilela, C., Haq, B., 1998. Sea-level and gas-hydrate-controlled catastrophic sediment failures of the Amazon fan. Geology 26, 1107-1110.

Maslin, M., Owen, M., Day, S., Long, D., 2004. Linking continental-slope failures and climate changes: Testing the clathrate gun hypothesis. Geology 32, 53-56.

Massari, F., Sgavetti, M., Rio, D., D'Alessandro, A., Prosser, G., 1999. Composite sedimentary record of falling stages of Pleistocene glacio-eustatic cycles in a shelf setting (Crotone basin, south Italy). Sedimentary Geology 127 (1-2), 85-110. doi: 10.1016/S0037-0738(99)00025-1.

Masson, D.G., 1996. Catastrophic collapse of the flank of El Hierro about 15,000 years ago, and the history of large flank collapses in the Canary islands. Geology 24, 231-234. doi: 10.1130/0091-7613(1996)024<0231:CCOTVI>2.3.CO;2.

Masson, D.G., Canals, M., Alonso, B., Urgeles, R., Hühnerbach, V., 1998. The Canary debris flow: source area morphology and failure mechanisms. Sedimentology 45, 411-432. doi: 10.1046/j.1365-3091.1998.0165f.x.

Masson, D.G., Watts, A.B., Gee, M.R.J., Urgeles, R., Mitchell, N.C., Le Bas, T.P., Canals, M., 2002. Slope failures on the flanks of the western Canary islands. Earth-Science Reviews 57(1-2), 1-35. doi: 10.1016/S0012-8252(01)00069-1.

Masson, D.G., Harbitz, C.B., Wynn, R.B., Pedersen, G., Løvholt, F., 2006. Submarine landslides: processes, triggers and hazard prediction. Philosophical Transactions of the Royal Society A 364, 2009-2039. doi: 10-1098/rsta.2006.1810.

Max, M.D., Kristensen, A., Michelozzi, E., 1993. Small-scale Plio-Quaternary sequence stratigraphy and shallow geology of the west-central Malta Plateau. In: Max, M.D., Colantoni, P. (eds.) Geological development of the Sicilian-Tunusian Platform. UNESCO Technical Report in Marine Sciences 58, 117-122.

McAdoo, B.G., Pratson, L.F., Orange, D.L., 2000. Submarine landslide geomorphology, US continental slope. Marine Geology 169, 103-136.

McCrea, J.M., 1950. On the isotopic chemistry of carbonates and a paleotemperature scale. Journal of Chemical Physics 18, 849-857. doi: 10.1063/1.747785.

Melki, T., Kallel, N., Jorrissen, F.J., Guichard, F., Dennielou, B., Berné, S., Labeyrie, L., Fontugne, M. 2009. Abrupt climate change, sea surface salinity and paleoproductivity in theWestern Mediterranean (Gulf of Lion) during the last 28 kyr. Palaeogeography, Palaeoclimatology, Palaeocology 279, 96–113.

Milankovitch, M., 1930. Mathematische Klimalehre und astronomische Theorie der Klimaschwankungen. In: Köppen, W., Geiger, R. (eds.), Handbuch der Klimatologie, 1(A). Berlin, Gebrüder Borntraeger, 1-176.

Milliman, J.D., Meade, R.H., 1983. World-wide delivery of river sediment to the ocean. Journal of Geolgoy 91, 1-21.

Milliman, J.D., Syvitski, J.P.M., 1992. Geomorphic/tectonic control of sediment discharge tot he ocean: the importance of mountainous rivers. Journal of Geology 100, 525-544.

Milliman, J.D., Farnsworth, K.L., 2011. River discharge tot he coastal ocean: a global synthesis. Cambridge University Press.

Millot, C., 1999. Circulation in the Western Mediterranean Sea. Journal of Marine Systems 20, 423-442.

Millot, C., Taupier-Letarge, I., 2005. Circulation in the Mediterranean Sea. In: Saliot, A. (ed.) The Mediterranean Sea, Handbook of Environmental Chemistry. Springer Berlin Heidelberg, p. 29-66. Doi: 10.1007/b107143.

Minisini, D., Trincardi, F., Adioli, A., Canu, M., Foglini, F., 2007. Morphologic variability of exposed mass-transport deposits on the eastern slope of Gela Basin (Sicily channel). Basin Research 19, 217-240.

Minisini, D., Trincardi, F., 2009. Frequent failure of the continental slope: The Gela Basin (Sicily Channel). Journal of Geophysical Research 114, F03014, doi: 10.1029/2008JF001037.

Mitchum, R.M.J., Van Wagoner, J.C., 1991. High-frequency sequences and their stacking patterns: sequence-stratigraphic evidence of high-frequency eustatic cyclces. Sedimentary Geology 70(2-4), 131-160. doi: 10.1016/0037-0738(91)90139-5.

Mix, A.C., Bard, E., Schneider, R., 2001. Environmental processes of the ice age: land, oceans, glaciers (EPILOG). Quaternary Science Reviews 20, 627-657.

Moore, J.G., Clague, D.A., Holcomb, R.T., Lipman, P.W., Normark, W.R., Torresan, M.E., 1989. Prodigious submarine landslides on the Hawaiian Ridge. Journal of Geophysical Research 94, 17465-17484.

Morgenstern, N.R., Price, V.E., 1965. The analysis of the stability of general slip surfaces. Géotechnique 15(1), 79-93. doi: 10.1680/geot.1965.15.1.79.

Morgenstern, N.R., 1967. Submarine slumping and the initiation of turbidity currents. In: Richards, A.F. (ed,) Marine Geotechnique. University of Illinois Press, Urbana, p. 189–210.

Mosher, D.C., Moscardelli, L., Shipp, R.C., Chaytor, J.D., Baxter, C.D.P., Lee, H.J., Urgeles, R., 2010. Submarine mass movements and their consequences IV. Advances in Natural and Technological Hazards Series 28. Springer, p. 1-8.

Muir Wood, D., 1991. Soil behaviour and critical state soil mechanics. Cambridge University Press. 488 p.

Mulder, T., Cochonat, P., 1996. Classification of offshore mass movements. Journal of Sedimentary Research 66(1), 43-57.

Mulder, T., Alexander, J., 2001. The physical character of subaqueous sedimentary density flows and their deposits. Sedimentology 48, 269-299.

Murty, T.S., 1979. Submarine slide-generated water waves in Kitimat inlet, British Columbia. Journal of Geophysical Research 84, 7777-7779.

Nakajima, T., Satoh, M., 2001. The formation of large mudwaves by turbidity currents on the levees of the Toyama deep-sea channel, Japan Sea. Sedimentology 48, 435-463.

Narcisi, B., Vezzoli, L., 1999. Quaternary stratigraphy of distal tephra layers in the Mediterranean – an overview. Global and Planetary Change 21, 31-50.

Negri, A., Capotondi, L., Keller, J., 1999. Calcareous nannofossils, planktonic foraminifera and oxygen isotopes in the late Quaternary sapropels of the Ionian Sea. Marine Geology 157, 89–103.

Nittrouer, C.A., 1999. STRATAFORM: overview of its design and synthesis of its results. Marine Geolgoy 154: 3-12.

Norem, H., Locat, J., Schieldrop, B., 1990. An approach to the physics and the modelling of submarine landslides. Marine Geotechnology 9(2), 93-111. doi: 10.1080/10641199009388233.

Normark, W.R., Piper, D.J.W., 1991. Initiation processes and flow evolution of turbidity currents: implications for the depositional record. In: Osborne, R.H. (ed.) From shoreline to abyssal. Special Publication 46, Society of Economic Paleontologists and Mineralogists. p. 207-230.

Normark, W.R., Hess, G.R., Stow, D.A.V., Bow, A.J., 1980. Sediment waves on the Monterrey fan levee: a preliminary physical interpretation. Marine Geology 42: 201-232.

Normark, W.R., Moore, J.G., Torresan, M.E., 1993. Giant volcano-related landslides and the development of the Hawaiian Islands. In: Schwab, W.C., Lee, H.J., Twichell, D.C. (eds.) Submarine Landslides: Selected Studies in the U.S. Exclusive Economic Zone. U.S. Geologcial Survey Bulletin, 2002, 184-196.

North Greenland Ice Core Project Members, 2004. High-resolution record of Northern Hemisphere climate extending into the last interglacial period. Nature 431, 147-151.

O'Leary, D.W., 1991. Structure and morphology of submarine slab slides: clues to origin and behavior. Marine Geotechnology 10(1-2), 53-69. doi: 10.1080/10641199109379882.

Onken, R., Robinson, A.R., Lermusiaux, PF.J., Haley Jr., P.J., Anderson, L.A., 2003. Data-driven simulations of synoptic circulation and transports in the Tunisia-Sardinia-Sicily region. J. Geophys. Res. 108, 8123-8136.

Osterberg, E.C., 2006. Late Quaternary (marine isotope stages 6-1) seismic sequence stratigraphic evolution of the Otago continental shelf, New Zealand. Marine Geology, 229(3-4), 159-178.

Palanques, A., Puig, P., Guillén, J., Jiménez, J., Gracia, V., Sánchez-Arcilla, A., Madsen, O., 2002. Near-bottom suspended sediment fluxes on the microtidal low-energy Ebro continental shelf (NW Mediterranean). Continental Shelf Research 22: 285-303.

Patacca, E. scandone, P., Giunta, G., Liguori, V., 1979. Mesozoic paleotectonic evolution of the Ragusa zone (Southeastern Sicily). Geol Romana 18: 331-369.

Paterne, M., Guichard, F., Labeyrie, J., 1988. Explosive activity of the south Italian volcanoes during the past 80,000 years as determined by marine tephrochronology. Journal of Volcanology and Geothermal Research 34, 153-172.

Pérez-Folgado, M., Sierro, F.J., Flores, J.A., Cacho, I., Grimalt, J.O., Zahn, R., Shackleton, N., 2003. Western Mediterranean planktonic foraminifera events and millennial climatic variability during the last 70 kyr. Marine Micropaleontology 48, 49-70.

Petit, J.R., Jouzel, J., Raynaud, D., Barkov, N.I., Barnola, J.-M., Basile, I., Bender, M., Chappellaz, J., Davis, M., Delaygue, G., Delmotte, M., Kotlyakov, V.M., Legrand, M., Lipenkov, V.Y., Lorius, C., Pépin, L., Ritz, C., Saltzman, E., Stievenard, M., 1999. Climate and atmospheric history of the past 420,000 years from the Vostok ice core, Antarctica. Nature 399(6735), 429-436. doi: 10.1038/20859.

Pierini. S., Rubino, A., 2001. Modeling the oceanic circulation in the area of the Strait of Sicily: the remotely forced dynamics. Journal of Physical Oceanography 31, 1397-1412.

Pinardi, N., Masetti, E., 2000. Variability of the large scale general circulation of the Mediterranean Sea from observations and modelling: a review. Palaeogeography Palaeoclimatology Palaeoecology 158(3/4), 153-173.

Piper, D.J.W., Shor, A.N., Hughes-Clarke, J.E., 1988. The 1929 Grand Banks earthquake, slump and turbidity current. In: Clifton, H.E. (ed.) Sedimentologic consequences of convulsive geologic events. Geological Society of America, Special Paper 229. P. 77-92.

Piper, D.J.W., Aksu, A.E., 1992. Architecture of stacked Quaternary deltas correlated with global oxygen isotopic curve, Geology 20(5), 415-418.

Piper, D.J.W., Pirmez, C., Manley, P.L., Long, D., Flood, R.D., Normark, W.R., Showers, W., 1997. Mass-transport deposits of the Amazon fan. In: Flood, R.D., Piper, D.J.W., Klaus, A., Peterson, L.C. (eds.) Proceedings of the Ocean Drilling Program, Scientific Results 155, p. 109-146.

Piper, D.J.W., Cochonat, P., Morrison, M.L., 1999. The sequence of events around the epicenter of the 1929 Grand Banks earthquake: initiation of debris flows and turbidity current inferred from sidescan sonar. Sedimentology 46, 79-97.

Piper, D.J.W., Mosher, D.C., Gauley, B.-J., Jenner, K., Campbell, D.C., 2003. The chronology and recurrence of submarine mass movments on the continental slope off southeastern Canada. In: Locat, J., Mienert, J. (eds.) Submarine mass movements and their consequences. Kluwer Academic Publishers, the Netherlands, p. 299-306.

Piva, A., Asioli, A., Schneider, R.R., Trincardi, F., Andersen, N., Colmenero-Hidalgo, E., Dennielou, B., Flores, J.-A., Vigliotti, L., 2008. Climatic cycles as expressed in sediments of the PROMESS1 borehole PRAD1-2, Central Adriatic, for the last 370 ka, 1: integrated stratigraphy. Geochemistry, Geophysics, Geosystems 9(1), Q01R01. doi: 10.1029/2007GC001713.

POEM group, 1992. General circulation of the Eastern Mediterranean. Earth Science Reviews 32, 285-309.

Popenoe, P., Schmuck, E.A., Dillon, W.P., 1993. The Cape Fear landslide: slope failure associated with salt diapirism and gas hydrate decomposition. In: Schwab, W.C., Lee, H.J., Twichell, D.C. (eds.) Submarine landslides: selected studies in the U.S. Exclusive Economic Zone. USGS Bulletin 2002, 40-53.

Prior, D.B., Coleman, J.M., 1978. Disintegrating retrogressive landslides on very-low-angle subaqueous slopes, Mississippi delta. Marine Geotechnology 3(1), 37-60. doi: 10.1080/10641197809379793.

Prior, D.B., Coleman, J.M., 1982. Active slides and flows in underconsolidated marine sediments on the slope of the Mississippi delta. In: Saxov, S., Nieuwenhuis, J.K. (eds.) Marine slides and other mass movements. Plenum Press, New York. p. 21-49.

Prior, D.B., Bornhold, B.D., Johns, M.W., 1984. Depositional characteristics of a submarine debris flow. Journal of Geology 92, 707-727.

Puig, P., Palanques, A., Gullién, J., 2001. Near-bottom suspended sediment variability caused by storms and near-inertial internal waves on the Ebro mid continental shelf (NW Mediterranean). Marine Geology 178(1-4): 81-93.

Puig, P., Ogston, A.S., Guillén, J., Fain, A.M.V., Palanques, A., 2007. Sediment transport processes from the topset to the foreset of a crenulated clinoform (Adriatic Sea). Continental Shelf Research 27: 452-474.

Pujol, C., Vergnaud Grazzini, C., 1995. Distribution patterns of live planktic foraminifera as related to regional hydrography and productive systems of the Mediterranean Sea. Marine Micropaleontology 25, 187–217.

Rabineau, M., Berné, S., Aslanian, D., Olivet, J.L., Joseph, P., Guillocheau, F., Bourillet, J.F., Le Drezen, E., Grangeon, D., 2005. Sedimentary sequences in the Gulf of Lion: a record of 100,000 years climatic cycles. Marine and Petroleum Geology 22(6-7), 775-804.

Radhakrishnamurty, C., Likhite, S.D., Amin, B.S., Somayajulu, B.L.K., 1968. Magnetic susceptibility stratigraphy in ocean sediment cores. Earth and Planetary Science Letters 4, 464-468. doi: 10.1016/0012-821x(68)90025-3.

Ravelo, C., Hillaire-Marcel, C., 2007. The use of oxygen and carbon isotopes of foraminifera in paleoceanography. In: Hillaire-Marcel, C., De Vernal, A. (eds.) Proxies in Late Cenozoic Paleoceanography. Developments in Marine Geology 1, 735-764.

Raymo, M.E., 1997. The timing of major climate terminations. Paleoceanography 12(4), 577-585. doi: 10.1029/97PA01169.

Rebesco, M., Neagu, R.C., Cuppari, A., Muto, A., Accettella, D., Dominici, R., Cova, A., Romano, C., Caburlotto, A., 2009. Morphobathymetric analysis and evidence of submarine mass movements in the western Gulf of Taranto (Calabria margin, Ionian Sea). International Journal of Earth Sciences 98(4), 791-805.

Reimer, P.J., Bard, E., Bayliss, A., Beck, J.W., Blackwell, P.G., Bronk Ramsey, C., Buck, C.E., Cheng, H., Edwards, R.L., Friedrich, M., Grootes, P.M., Guilderson, T.P., Haflidason, H., Hajdas, I., Hatté, C., Heaton, T.J., Hoffman, D.L., Hogg, A.G., Hughen, K.A., Kaiser, K.F., Kromer, B., Manning, S.W., Niu, M., Reimer, R.W., Richards, D.A., Scott, E.M., Southon, J.R., Staff, R.A., Turney, C.S.M., van der Plicht, J., 2013. IntCal13 and Marine13 radiocarbon age calibration curves 0-50,000 years cal BP. Radiocarbon 55(4), 1869-1887.

Richter, T.O., van der Gaast, S., Koster, R., Vaars, A., Gieles, R., de Stigter, H.C., de Haas, H., van Weering, T.C.E., 2006. The AVAATECH XRF Core Scanner: Technical description and applications to NE Atlantic sediments. In: Rothwell, R.G. (ed.) New Techniques in sediment core analysis. Special Publications of the Geological Society 267, p. 39-50.

Ridente, D., Trincardi, F., 2002. Eustatic and tectonic control on deposition and lateral variability of Quaternary regressive sequences in the Adriatic basin. Marine Geology 184(3-4), 273-293.

Ridente, D., Trincardi, F., Pica, A., Asioli, A., Cattaneo, A., 2008. Sedimentary response to climate and sea level changes during the past ~ 400 ka from borehole PRAD1-2 (Adriatic margin). Geochemistry Geophysics Geosystems 9(Q09R04).

Ridente, D., Trincardi, F., Piva, A., Asioli, A., 2009. The combined effect of sea level and supply during Milankovitch cyclicity: evidence from shallow-marine $\delta^{18}O$ records and sequence architecture (Adriatic margin). Geology 37(11), 1003-1006.

Robb, J.M., 1984. Spring sapping on the lower continental slope, offshore New Jersey. Geology 12(5), 278-282.

Robinson, A.R., Golnaraghi, M., 1994. The physical and dynamical oceanography of the Mediterranean. In: Malanotte-Rizzoli, P., Robinson, A.R. (Eds.), Ocean Processes in Climate Dynamics: Global and Mediterranean Examples. Kluwer Academic Publishers, The Netherlands, p. 255-306.

Robinson, A.R., Sellschopp, J., Warn-Varnas, A., Leslie, W.G., Lozano, C.J., Haley Jr., P.J., Anderson, L.A., Lermusiaux, P.F.J., 1999. The Atlantic Ionian Stream. J. Mar. Syst. 20, 129-156.

Rodero, J., Pallares, L., Maldonado, A., 1999. Late Quaternary seismic facies of the Gulf of Cadiz Spanish margin: depositional processes influenced by sea-level change and tectonic controls. Marine Geology 155(1-2), 131-156.

Rohling E.-J., Gieskes, W.W.C., 1989. Late Quaternary changes in Mediterranean lntermediate Water density and formation rate. Paleoceanography 4, 531-545.

Rohling, E.-J., Hayes, A., De Rijk, S., Kroon, D., Zachariasse, W.-J., Eisma, D., 1998. Abrupt cold spells in the Northwest Mediterranean. Paleoceanography 13, 316–322.

Rohling, E., Cooke, S., 2003. Stable oxygen and carbon isotopes in foraminiferal carbonate shells. In: Sen Gupta, B. (ed) Modern foraminifera. Springer Netherlands, p. 239-258.

Rouis-Zaragouni, I., Turon, J.-L., Londeix, L., Essallami, L., Kallel, N., Sicre, M.-A., 2010. Environmental and climatic changes in the central Mediterranean Sea (Siculo–Tunisian Strait) during the last 30 ka based on dinoflagellate cyst and planktonic foraminifera assemblages. Palaeogeography, Palaeoclimatology, Palaeoecology 285, 17–29.

Sánchez-Cabeza, J.A., Masqué, P., Ani-Ragolta, I., Merino, J., Alvisi, F., Palnques, A., Puig, P., 1999. Sediment accumulation rates in the southern Barcelona continental margin (NW Mediterranean Sea) derived from 210Pb and 137Cs chronology. Progress in Oceanography 44, 313-332.

Sammari, C., Millot, C., Taupier Letage, I., Stefani, A., Brahim, M., 1999. Hydrological characteristics in the Tunisia-Sardinia-Sicily area during spring 1995. Deep-Sea Res. I 46, 1671-1703.

Sbaffi, L., Wezel, F.C., Kallel, N., Paterne, M., Cacho, I., Ziveri, P., Shakleton, N., 2001. Response of the pelagic environment to paleoclimatic changes in the central Mediterranean Sea during the late Quaternary. Marine Geology 178, 39-62.

Schefuß, E., Kuhlmann, H., Mollenhauer, G., Prange, M., Pätzold, J., 2011. Forcing of wet phases in southeast Africa over the past 17,000 years. Nature 480, 509-512. doi: 10.1038/Nature10685.

Schmiedl, G., de Bovée, F., Buscail, R., Charrière, B., Hemleben, C., Medernach, L., Picon, P., 2000. Trophic control of benthic foraminiferal abundance and microhabitat in the bathyal Gulf of Lions, western Mediterranean Sea. Marine Micropaleontology 40(3), 167– 188.

Schröder, C.J., Scott, D.B., Medioli, F.S., 1987. Can smaller benthic foraminifera be ignored in paleoenvironmental analyses? Journal of Foraminiferal Research 17(2), 101-105.

Schwab, W.C., Danforth, W.W., Scanlon, K.M., 1993. Tectonic and stratigraphic control on a giant submarine slope failure: Puerto Rico insular slope. In: Schwab, W.C., Lee, H.J., Twichell, D.C. (eds.) Submarine landslides: selected studies in the U.S. Exclusive Economic Zone. USGS Bulletin 2002, p. 60-68.

Schwarzacher, W., 2000. Repetitions and cycles in stratigraphy. Earth-Science Reviews 50(1-2), 51-75. doi: 10.1016/S0012-8252(99)00070-7.

Seed, H.B., 1979. Considerations in earthquake-resistant design of earth and rock-fill dams. G´eotechniques 29, 215–263.

Seed, H.B., Idriss, I.M., 1971. Simplified procedure for evaluating soil liquefaction potential. Journal of the Soil Mechanics and Foundations Division. Proceedings of the American Society of Civil Engineers 97(9), 1249–1273.

Shackleton, N.J., 1967. Oxygen isotope analyses and Pleistocene temperatures re-assessed. Nature 215, 15-17. doi: 10.1038/215015a0.

Shackleton, N.J., Opdyke, N.D., 1973. Oxygen isotope and palaeomagnetic stratigraphy of equatorial Pacific core V28-238: Oxygen isotope temperatures and ice volumes on a 105 year and 106 year scale. Quaternary Research 3, 39-55. doi: 10.1016/0033-5894(73)90052-5.

Shanmugam, G., 2000. 50 years of the turbidite paradigm (1950s-1990s): deep-water processes and facies models – a critical perspective. Marine and Petroleum Geology 17, 285-342.

Siani, G., Paterne, M., Arnold, M., Bard, E., Métivier, B., Tisnerat, N., Bassinot, F., 2000. Radiocarbon reservoir ages in the Mediterranean Sea and Black Sea. Radiocarbon 42, 271-280.

Siani, G., Paterne, M., Colin, C. 2010. Late glacial to Holocene planktic foraminifera bioevents and climatic record in the South Adriatic Sea. Journal of Quaternary Science 25(5): 808-821.

Sierro, F.J., Andersen, N., Bassetti, M.A., Berné, S., Canals, M., Curtis, J.H., Dennielou, B., Abel Flores, J., Frigola, J., Gonzalez-Mora, B., Grimalt, J.O., Hodell, D.A., Jouet, G., Pérez-Folgado, Schneider, R., 2009. Phase relationship between sea level and abrupt climate change. Quaternary Science Reviews 28, 2867-2881.

Siddall, M., Rohling, E.J., Almogi-Labin, A., Hemleben, Ch, Meischner, D., Schmelzer, I., Smeed, D.A., 2003. Sea-level fluctuations during the last glacial cycle. Nature 423, 853-858.

Siddall, M., Rohling, E.J., Thompson, W.G., Waelbroeck, C., 2008. Marine Isotope Stage 3 sea level fluctuations: data synthesis and new outlook. Reviews of Geophysics 46, RG4003. doi: 10.1029/2007RG000226.

Solheim, A., Berg, K., Forsberg, C.F., Bryn, P., 2005a. The Storegga Slide comples: Repetitive large-scale sliding with similar cause and development. Marine and Petroleum Geology 22(1-2), 97-107.

Solheim, A., Bryn, P., Sejrup, H.P., Mienert, J., Berg, K., 2005b. Ormen Lange – and integrated study for the safe development of a deep-water gas field within the Storegga Slide complex, NE Atlantic continental margin; executive summary. Marine and Petroleum Geology 22(1-2), 1-9.

Somoza, L., Hernández-Molina, F.J., De Andrés, J.R., Rey, J., 1997. Continental shelf architecture and sea-level cycles: Late Quaternary high-resolution stratigraphy of the Gulf of Cádiz, Spain. Geo-Marine Letters 17(2), 133-139.

Sorgente, R., Drago, A.F., Ribotti, A., 2003. Seasonal variability in the Central Mediterranean Sea circulation. Annales Geophysicae 21, 299-322.

Sprovieri, R., Di Stefano, E., Incarbona, A., Gargano, M.E., 2003. A high resolution record of the last deglaciation in the Sicily Channel based on foraminifera and calcareous nannofossil quantitative distribution. Palaeogeography, Palaeoclimatology, Palaeoecology 2002, 119-142.

Sprovieri, R., Di Stefano, E., Incarbona, A., Oppo, D.W., 2006. Suborbital climate variability during Marine Isotopic Stage 5 in the central Mediterranean basin: evidence from calcareous plankton record. Quaternary Science Reviews 25, 2332-2342.

Stansfield, K., Gasparini, G.P., Smeed, D., 2003. High-resolution observations of the path of the overflow from the Sicily Strait. Deep-Sea Research I 50, 1129-1149.

Stow, D.A.V., Mayall, M., 2000. Deep-water sedimentary systems: New models for the 21st century. Marine and Petroleum Geology 17, 125-135.

Stuiver, M., Reimer, P.J., 1993. Extended 14C database and revised CALIB radiocarbon calibration program. Radiocarbon 35, 215-230.

Sultan, N., Cochonat, P., Foucher, J.P., Mienert, J., Haflidason, H., Sejrup, H.P., 2003. Effect of gas hydrates dissociation on seafloor slope stability. In: Locat, J., Mienert, J. (eds.) Submarine mass movments and their consequences. Kluwer Academic Publishers, Dordrecht, Netherlands. p. 103-111.

Sultan, N., Cochonat, P., Canals, M., Cattaneo, A., Dennielou, B., Haflidason, H., Laberg, J.S., Long, D., Mienert, J., Trincardi, F., 2004. Triggering mechanisms of slope instability processes and sediment failure on continental margins: a geotechnical approach. Marine Geology 213, 291-321.

Sun, S.-S., McDonough, W.F., 1989. Chemical and isotopic systematics of oceanic basalts: implications for mantle composition and processes. Geological Society, London, Special Publications 42, 313-345. doi: 10.1144/GSL.SP.1989.042.01.19.

Svensson, A., Andersen, K.K., Bigler, M., Clausen, H.B., Dahl-Jensen, D., Davies, S.M., Johnsen, S.J., Muscheler, R., Parrenin, F., Rasmussen, S.O., Röthlisberger, R., Seierstad, I., Steffensen, J.P., Vinther, B.M., 2008. A 60000 year Greenland stratigraphic ice core chronology. Climate of the Past 4, 47-57.

Sydow, J., Roberts, H.H., 1994. Stratigraphic framework of a late Pleistocene shelf-edge delta, northeast Gulf of Mexico. American Association of Petroleum Geologists Bulletin 78(8), 1276-1312.

Synolakis, C.E., Bardet, J.P., Borrero, J.C., Davies, H.L., Okal, E.A., Sweet, S., Tappin, D.R., 2002. The slump origin of the 1998 Papua New Guinea Tsunami. Proceedings of the Royal Society London A 485, 763-789. doi: 10.1098/rspa.2001.0915.

Tahchi, E., Urgeles, R., Hübscher, C., Benkhelil, J., 2010. Mass wasting at the easternmost Cyprus arc, off Syria, Eastern Mediterranean. In: Mosher, D.C., Shipp, C., Moscardelli, L., Chaytor, J., Baxter, C., Lee, H., Urgeles, R. (eds.) Submarine mass movements and their consequences IV. Advances in Natural and Technological Hazards Serie 28. Springer, p. 323-334.

Talling, P.J., 2014. On the triggers, resulting flow types and frequencies of subaqueous sediment density flows in different settings. Marine Geology 352, 155-182. doi: 10.1016/j.margeo.2014.02.006.

Tappin, D.R., Watts, P., McMurtry, G.M., Lafoy, Y., Matsumoto, T., 2001. The Sissano, Papua New Guinea tsunami of July 1998 – offshore evidence on the source mechanism. Marine Geology 175, 1-13.

Tappin, D.R., Watts, P., Grilli, S.T., 2008. The Papua New Guinea tsunami of 17 July 1998: anatomy of a catastrophic event. Natural Hazards Earth System Sciences 8, 243-266.

Terzaghi, K., 1943. Theoretical soil mechanics. John Wiley & Sons, New York. 510 pp.

Tesson, M., Posamentier, H.W., Gensous, B., 2000. Stratigraphic organization of late Pleistocene deposits of the western part of the Golfe du Lion shelf (Languedoc shelf), western Mediterranean Sea, using high-resolution seismic and core data. American Association of Petroleum Geologists Bulletin 84(1), 119-150.

Thornalley, D.J.R., Elderfield, H., McCave, I.N., 2010. Intermediate and deep water paleoceanography of the northern North Atlantic cover the past 21,000 years. Paleoceanography 25, PA1211. doi: 10.1029/2009PA001833.

Thunell, R.C., 1978. Distribution of recent planktonic foraminifera in surface sediments of the Mediterranean Sea. Marine Micropaleontology 3, 147–173.

Tinti, S., Maramai, A., Graziani, L., 2001. A new version of the European tsunami catalogue: updating and revision. Natural Hazards and Earth System Sciences 1, 255-262.

Tomlinson, E.L., Albert, P.G., Wulf, S., Brown, R.J., Smith, V.C., Keller, J., Orsi, G., Bourne, A.J., Menzies, M.A., 2014. Age and geochemistry of tephra layers from Ischia, Italy: constraints from proximal-distal correlations with Lago Grande di Monticchio. Journal of Volcanology and Geothermal Research 287: 22-39.

Trincardi, F., Argnani, A., 1990. Gela submarine slide: a major basin-wide event in the Plio-Quaternary foredeep of Sicily. Geo-Marine Letters 10, 13-21.

Trincardi, F., Normark, W.R., 1988. Sediment waves on the Tiber prodelta slope. Geo-Marine Letters 8, 149-157.

Trincardi, F., Correggiari, A., 2000. Quaternary forced regression deposits in the Adriatic basin and the record of composite sea-level cycles. In: Hund, D., Gawthorpe, R.L.G. (eds.) Sedimentary responses to forced regressions. Geological Society, London, Special Publications, p. 245-269.

Trincardi, F., Cattaneo, A., Correggiari, A., Mongardi, S., Breda, A., Asioli, A., 2003. Submarine slides during sea level rise: Two examples from the eastern Tyrrhenian margin. In: Locat, J., Mienert, J. (eds.) Submarine mass movements and their consequences. Kluwer Academics, Dordrecht, the Netherlands. p. 469-478.

Ulug, A., Duman, M., Ersoy, S., Özel, E., Avci, M., 2005. Late Quaternary sea-level change, sedimentation and neotectonics of the Gulf of Gökova: Southeastern Aegean Sea. Marine Geology 221(1-4), 381-395.

UNEP (United Nations Environment Programme), 2003. Riverine transport of water, sediments and pollutants to the Mediterranean Sea. MAP Technical Reports Series 141, Athens, 111 pp

Urgeles, R., De Mol, B., Liquete, C., Canals, M., De Batist, N., Hughes-Clarke, J.E., Amblás, D., Arnau, P.A., Calafat, A.M., Casamor, J.L., Centella, V., De Rycker, K., Fabrés, J., Frigola, J., Lafuerza, S., Lastras, G., Sànchez, A., Zuniga, D., Versteeg, W., Willmott, V., 2007. Sediment undulations on the Llobregat prodelta: Signs of early slope instability or bottom current activity? Journal of Geophysical Research 112, Art. No. B05102.

Urgeles, R., Cattaneo, A., Puig, P., Liquete, C., De Mol, B., Amblàs, D., Sultan, N., Trincardi, F., 2011. A review of undulated sediment features on prodeltas: distinguishing sediment transport from sediment deformation. Marine Geophysical Research 32: 49-69.

Van der Zwaan, G.J., Jorissen, F.J., 1991. Biofacial patterns in river-induced shelf anoxia. In: Tyson, R.V., Pearson, T.H. (eds.) Modern and Ancient Continental Shelf Anoxia. Geological Society Special Publication 58. p. 65-82.

Van Kessel, T., Kranenburg, C., 1998. Wave-induced liquefaction and flow of subaqueous mud layers. Coastal Engineering 34, 109-127.

Vanneste, M., Mienert, J., Bünz, S., 2006. The Hinlopen Slide: a giant, submarine slope failure on the northern Svalbard margin, Arctic Ocean. Earth and Planetary Science Letters 245, 373-388.

Vanneste, M., Sultan, N., Garziglia, S., Forsberg, C.F., L'Heureux, J.-S., 2014. Seafloor instabilities and sediment deformation processes: The need for integrated, multi-disciplinary investigations. Marine Geology 352, 183-214.

Vanoudheusden, E., Sultan, N., Cochonat, P., 2004. Mechanical behaviour of unsaturated marine sediments: experimental and theoretical approaches. Marine Geology 213, 323-342.

Varnes, D.J., 1958. Lanslide types and processes. In: Eckel, E.D. (ed.) Landslides and Engineering Practice. Special Report 29. Highway Research Board, Washington, DC. p. 20-47.

Varnes, D.J., 1978. Slope movement types and processes. In: Schuster, R.L., Krizek, R.J. (eds.) Lanslides – Analysis and Control. Special Report 176. Transportation and Road Research Board, National Academy of Science, Washington, DC. p. 11-33.

Verdicchio, G., Trincardi, F., 2008. Mediterranean shelf-edge muddy contourites: examples from the Gela and South Adriatic basins. Geo-Marine Letters 28, 137-151. doi: 10.1007/s00367-007-0096-9.

Waelbroeck, C., Labeyrie, L., Michel, E., Duplessy, J.C., McManus, J.F., Lambeck, K., Balbon, E., Labracherie, M., 2002. Sea-level and deep water temperature changes derived from benthic foraminifera isotopic records. Quaternary Science Reviews 21, 295-305. doi: 10.1016/s0277-3791(01)00101-9.

Ward, S.N., Day S.J., 2001. Cumbre Vieja volcano – potential collapse and tsunami at La Palma, Canray Islands. Geophysical Research Letters 28, 3397-3400.

Warrick, J.A., Xu, J., Noble, M.A., Lee, H.J., 2008. Rapid formation of hyperpycnal sediment gravity currents offshore of a semi-arid California river. Continental Shelf Research 28, 991-1009.

Watts, W.A., Allen, J.R.M., Huntley, B., 1996. Vegetation history and palaeoclimate of the last glacial period at Lago Grande di Monticchio, southern Italy. Quaternary Science Reviews 15, 133-153.

Weaver, P.P.E., Kuijpers, A., 1983. Climatic control of turbidite deposition on the Madeira Abyssal plain. Nature 306, 360-363. doi: 10.1038/306360a0.

Weltje, G.J., Tjallingii, R., 2008. Calibration of XRF core scanners for quantitative geochemical logging of sediment cores: Theory and application. Earth and Planetary Science Letters 274, 423-438.

Wessel, P., Smith, W. H. F., 1998. New, improved version of Generic Mapping Tools released. EOS Trans. Amer. Geophys. U. 79, p. 579.

Wheatcroft, R.A., Sommerfield, C.K., Drake, D.E., Borgeld, J.C., Nittrouer, C.A., 1997. Rapid and widespread dispersal of flood sediment on the northern California margin. Geology 25, 163-166. doi: 10.1130/0091-7613(1997)025<0163:RAWDOF>2.3.CO;2.

Wheatcroft, R.A., Borgeld, J.C., 2000. Oceanic flood deposits on the northern California shelf: large-scale distribution and small-scale physical properties. Continental Shelf Research 20, 2163-2190.

Wilson, C.K., Long, D., Bulat, J., 2004. The morphology, setting and processes of the Afen slide. Marine Geology 213-149-167. doi: 10.1016/j.margeo.2004.10.005.

Winkelmann, D., Geissler, W., Schneider, J., Stein, R., 2008. Dynamics and timing of the Hinlopen/Yermak Megaslide north of Spitsbergen, Arctic Ocean. Marine Geology 250, 34-50.

Wulf, S., Kraml, M., Brauer, A., Keller, J., Negendank, J.F.W., 2004. Tephrochronology of the 100 ka lacustrine sediment record of Lago Grande di Monticchio (southern Italy). Quaternary International 122, 7-30. Doi: 10.1016/j.quaint.2004.01.028.

Wynn, R.B., Stow, D.A.V., 2002. Classification and characterization of deep-water sediment waves. Marine Geology 192, 7-22.

Wynn, R.B., Talling, P.J., Masson, D.G., Stevenson, C.J., Cronin, B.T., Le Bas, T.P., 2010. Investigating the timing, processes and deposits of one of the world's largest submarine gravity flows: the 'Bed 5 event' off northwest Africa. In: Mosher, D.C., Shipp, C., Moscardelli, L., Chaytor, J., Baxter, C., Lee, H., Urgeles, R. (eds.) Submarine

mass movements and their consequences IV. Advances in Natural and Technological Hazards Series, Springer, p. 463-474.

Yokoyama, Y., Lambeck, K., De Deckker, P., Johnson, P., Fifield, K., 2000. Timing for the maximum of the Last Glacial constrained by lowest sea-level observations. Nature 406, 713-716.

Zachos, J.C., Röhl, U., Schellenberg, S.A., Sluijs, A., Hodell, D.A., Kelly, D.C., Thomas, E., Nicolo, M., Raffi, I., Lourens, L.J., McCarren, H., Kroon, D., 2005. Rapid acidification of the ocean during the Paleocene-Eocene thermal maximum. Science 308, 1611-1615. doi: 10.1126/science.1109004.